Bulletin 38
Part 2
(of 3 Parts)

THE SHOCK AND VIBRATION BULLETIN

AUGUST 1968

A Publication of
THE SHOCK AND VIBRATION
INFORMATION CENTER
Naval Research Laboratory, Washington, D.C.

Office of
The Director of Defense
Research and Engineering

Bulletin 38
Part 2
(of 3 Parts)

THE SHOCK AND VIBRATION BULLETIN

AUGUST 1968

A Publication of
THE SHOCK AND VIBRATION
INFORMATION CENTER
Naval Research Laboratory, Washington, D.C.

The 38th Symposium on Shock, Vibration and Associated Environments was held in St. Louis, Missouri, on 1-2 May 1968.

Office of
The Director of Defense
Research and Engineering

SYMPOSIUM MANAGEMENT

THE SHOCK AND VIBRATION INFORMATION CENTER

William W. Mutch, Director
Henry C. Pusey, Coordinator
Rudolph H. Volin, Coordinator
Katherine G. Jahnel, Administrative Secretary

Bulletin Production

Graphic Arts Branch, Technical Information Division,
Naval Research Laboratory

CONTENTS

PART 2

Structural Analysis

Mechanical Impedance

PAPERS APPEARING IN PART 1

Vibration Analysis

*This paper appears in Shock and Vibration Bulletin 38, Supplement.

PAPERS APPEARING IN PART 3

Damping

*This paper appears in Shock and Vibration Bulletin 38, Supplement.

Isolation

STRUCTURAL ANALYSIS

AN OVERALL VIEW OF STRUCTURAL DYNAMICS

Robert M. Maine
Department of Civil and Environmental Engineering
Washington University
St. Louis, Missouri

The problems of structural dynamics are discussed in the context of the entire operation, beginning with consideration of the purposes of a dynamic analysis and carrying through to the question of what action to take as a result of the findings. Much attention has previously been given to the processes of computation and the details of how to perform them. Because of this and because the first time through is invariably a long and tedious learning, programming, and debugging operation, it is not uncommon that the analysis calculations are considered to be the whole job, instead of the smaller part of it. A proper effort in the planning and strategy of the analysis pays off in shorter, simpler computations. Dynamic analysis results that have not been evaluated against performance criteria are incomplete, and unless the performance evaluation is translated into action of some sort, then the effort has amounted only to wheel spinning.

PLANNING AND STRATEGY

The most important part of structural dynamics work occurs in the beginning when the planning is being done and the strategy for the analysis is being devised. The purpose of the analysis is established at this time, and it usually falls somewhere within the following categories:

A. To investigate behavior before hardware is built:

1. To obtain design data (balance requirements, loads for small items, stress levels)
2. To predict response to some expected environment
3. To head off failure or malfunction
4. To discover design errors in time to change

B. To investigate behavior after hardware is built:

1. To predict behavior in some previously unchecked environment
2. To determine the cause of a failure or malfunction
3. To devise a fix
4. To evaluate the effect of a proposed design change

C. To satisfy a specification requirement:

1. Shipboard shock
2. Hardened base shock
3. Earthquake shock
4. Flight (or launch) vibration

Once the purpose is clear, then it is necessary to consider what moves, how it moves, and what forces are acting. A study of these items leads to consideration of what could malfunction or fail as a result of the motions and forces. At this stage of the planning, performance criteria must be established and allowable limits on motion, or stress, or degradation of function must be developed. It is particularly important that these allowable limits be set in advance of the calculation so that a fair judgment of requirements is not clouded by knowledge of the results of the calculation. It may be necessary to modify the allowable limits after the calculation, but it should be done only for clear and sound reasons. In this way the problem of having obtained effective forces on masses for answers, when stresses in members are the criterion for acceptance can be avoided.

The next consideration is that of size. How many coordinates are needed to describe the motions so that all of the performance criteria can be applied and properly evaluated? Any coordinates in excess of the number required for the application of performance criteria must be justified by a saving in man time, or machine time, or by an improvement in quality of the result. The inclusion of more and more details, because the program can handle them, leads to confusion and obscuring of the purpose of the analysis. The larger the number of coordinates, the more trouble with round-off and calculation difficulties.

When the number of coordinates simply must be larger than available programs can handle, it is helpful to consider whether symmetry can be used to reduce the problem size, or whether subsystem black boxes must be used. Symmetry helps by permitting the solution of two half-size problems, or four quarter-size problems, instead of the full problem. Details on symmetry and black boxes are given in the Appendices.

As a final consideration in planning, it is helpful if the problem is linear, because this is a considerable simplification. If the problem is not linear, it is desirable to consider whether the nonlinear parts can be approximated satisfactorily with linear functions, or whether a piece-wise linear relationship can be used. If neither of these is possible, then a direct numerical method may be the only way to obtain a solution.

STRUCTURAL CALCULATIONS

The structural calculations are made to establish the relationship between force, deformation, and stress in each member; a member is that piece of structure that connects two coordinate stations. For the simpler elements, such as prismatic beams and right circular cylinders, the calculations are straightforward and give well-verified results. In almost every problem, though, there are some elements which do not fall into the well-known category, and which may be uncalculable by any known analysis. The structural relationships for such elements are best obtained by the measurement of models. Properly made models, with properly made measurements, are far superior to calculations for elements that are not in the well-known category. A prototype element makes the best model, but scaled models of easy-to-work material can give good results.

At the end of the analysis, it is helpful to be able to check statics and see that spring forces and inertial forces balance properly. Whether this can be done is determined, at the beginning of the analysis, by the precision of the interrelationships between the various parts of the element stiffness matrix. If the ratio between moment stiffness and shear stiffness is supposed to be $\ell^2/3$, then an element stiffness which has this ratio correct to one in 250 cannot be expected to produce a statics balance at the end of the computation that will be as good as one in 250. Figure 1 summarizes the structural relationships for a cantilever beam of prismatic shape.

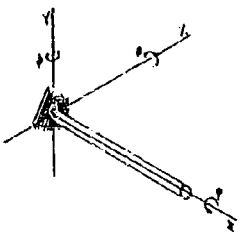

$$f_{11} = \frac{\ell^3}{3EI_z} + \frac{A\ell}{GA} \qquad f_{66} = \frac{\ell}{EI_x}$$

$$f_{55} = \frac{\ell^3}{3EI_y} + \frac{A\ell}{GA} \qquad f_{15} = \frac{\ell^2}{2EI_y} \qquad f_{44} = \frac{\ell}{EI_y}$$

$$f_{51} = \frac{\ell^2}{2EI_y} \qquad f_{45} = \frac{\ell^2}{2EI_x}$$

$$f_{33} = \frac{\ell}{EA} \qquad f_{22} = \frac{\ell}{GJ}$$

Fig. 1. Structural relationships -- cantilever beam

Because an analysis model frequently has coordinate stations that are spaced no farther apart then the lateral dimensions of the beam element between them, it is important to include shear deformations. The deformation from shear is often larger than the deformation from bending. Torsional flexibility needs also to be considered, because a proper stress criterion needs to be related to maximum shear stress [1] (or shear strain energy), rather than just tensile yield stress.

When all of the element stiffness data are complete, the compilation of the system stiffness matrix can be made. This compilation is now routine, and consists of rotation, translation, and assembly operations on the element stiffness matrices [2]. Up to this point, the structural calculations are done in the same way as for a static analysis for the thermal stress, as an example.

For dynamic analysis, an additional calculation must be made that is not done for static

analysis. This calculation is to determine the mass matrix, as the selection of discrete coordinate stations requires the mass to be lumped at these coordinates. There are some attempts to be analytical about this calculation, and to determine a "consistent mass" matrix [3]. These are so far not consistent, and are effective only for dynamic modes that are nearly the same shape as the static deflection shape used in deriving the mass values. The achievement of off-diagonal mass terms is not in itself a virtue, and may be incorrect. For example, if the stiffness, model matrix and eigenvalue matrix were known in the equation

$$Mx_0\omega_0^2 = Kx_0 \tag{1}$$

in which

K = stiffness matrix

x_0 = modal matrix (by columns)

ω_0^2 = eigenvalue matrix (diagonal)

M = mass matrix,

then one can solve for the mass matrix as

$$M = Kx_0\omega_0^{-2}x_0^T \tag{2}$$

as

$$x_0^T x_0 = I \quad \text{(orthonormality)} \tag{3}$$

and

$$x_0^{-1} = x_0^T. \tag{4}$$

Equation (2) provides a means whereby an "effective mass" matrix can be calculated for a discrete mass system when the solution for the equivalent distributed mass system can be made. A study of various known solutions might lead to a generalization of how properly to lump the masses in a system, but at present a good analyst's eyeball is still the best method.

Another calculation not ordinarily made for static analysis is the determination of the damping matrix. When specific damping devices are included in the system, the compilation of the damping matrix is relatively easy. When the only damping is from material hysteresis, joint friction, and aerodynamic drag, the problem becomes more difficult. Some analysts favor a damping matrix derived from the stiffness matrix, and others prefer to associate damping with mass. The author uses a formulation analogous to critical damping in a single element system, but modified to suit matrix analyses:

$$C = 2\zeta\,[M^{1/2}KM^{1/2}]^{1/2} \tag{5}$$

in which

C = damping matrix

ζ = critical damping ratio

and the square roots are a term-by-term operation. There is no attempt to justify this formulation mathematically, but when it has been used, the results compared favorably with measured values.

DYNAMIC RESPONSE CALCULATIONS

For linear problems, a number of choices are available according to the purpose of the calculations. The dynamic equation is

$$M\ddot{x} + C\dot{x} + Kx = f(t) \tag{6}$$

in which the new terminology is $f(t)$ = forcing function. The equation

$$M\ddot{x} + Kx = 0 \tag{7}$$

can be solved to give x_0 = normal modes (eigenvectors), ω_0^2 = normal frequencies (eigenvalues), which are useful in many ways, especially when x_0 is normalized so that

$$x_0^T M x_0 = I \tag{8}$$

which then requires that

$$x_0^T K x_0 = \omega_0^2. \tag{9}$$

Now let $x = x_0 y$ in Eq. (6) and premultiply by x_0^T to get

$$I\ddot{y} + 2\zeta\omega_0\dot{y} + \omega_0^2 y = x_0^T f(t) \tag{10}$$

which is convenient as all the terms on the left are diagonal matrices, and the system is decoupled. (This requires that $2\zeta\omega_0 = x_0^T C x_0$ which is not necessarily so, but it is convenient.) Next Laplace transform Eqs. (8) and (10) to get

$$(Ms^2 + Cs + K)\,x(s) = f(s) \tag{11}$$

$$(Is^2 + 2\zeta\omega_0 s + \omega_0^2)\,y(s) = x_0^T f(s); \tag{12}$$

let

$$Z_c = Ms^2 + Cs + K \tag{13}$$

and

$$Z_u = Is^2 + 2\zeta\omega_0 s + \omega_0^2 \tag{14}$$

so that Eqs. (11) and (12) become

$$Z_c \cdot x(s) = f(s) \text{ (coupled system)} \tag{15}$$

$$Z_u = y(s) = x_0^T f(s) \text{ (uncoupled system)} \quad (16)$$

The inverse transforms of Eqs. (15) and (16) gives

$$x(t) = \mathcal{L}^{-1} Z_c^{-1}(s)\, f(s) \quad \text{(coupled system)} \quad (17)$$

$$x(t) = x_0 \mathcal{L}^{-1} Z_u^{-1}(s)\, x_0^T f(s) \text{ (uncoupled system)} \quad (18)$$

If a step velocity shock, A, is used for f(t) in Eq. (6), then Eq. (18) becomes

$$x_{amp} = x_0 * \omega_0^{-1} \underbrace{\left[x_0^T M\right]}_{n \times n} * \underbrace{\left[-A\right]}_{\text{scalar}} \quad (19)$$

in which x_{amp} = modal amplitude (undamped), A = step velocity magnitude, and $\left[x_0^T M\right]$ is diagonalized after multiplication, and is the same as the "participation factor" in Navy shock analysis terms. If the $x_0^T M$ product is not diagonalized, then all of the modal amplitudes are summed and the separate modal contributions are lost. As the mode shapes are all subject to an arbitrary multiplier of ±1, summing them with the (chance) signs they have from the eigenvalue routine has no meaning.

The solution for a step velocity applied to Eq. (17) is a tedious and lengthy numerical computation, but it can be done. Such a solution does avoid the chance sign of the normal modes and is the preferred computation when a crucial analysis is to be made. It requires the calculation of the inverse complex impedance at a number of discrete frequencies and the associated complex frequency response. As the complex response preserves phase relationships, the inverse transformation is a proper time function and does not suffer from the chance sign problem as normal modes do.

The untransformed Eqs. (6) and (10) can be time-step integrated in Runge-Kutta fashion as another solution to the problem. This approach is best when nonlinear functions are involved and other methods do not apply. It is helpful to include the nonlinear items on the right-hand side of the equation in case an iterative procedure is needed.

Response to random excitation is only describable in statistical terms, as the forcing function is so described. The relationship is

$$\left[x(i\omega)\right]^2 = \left[Z^{-1}(i\omega)\right]^2 * F(i\omega) \quad (20)$$

in which $[x(i\omega)]^2$ = mean square response density [(units)²/cycle], $[Z(i\omega)]^2$ = square of modulus of complex impedance (in units suitable to change F into X), and $F(i\omega)$ = mean square spectral density [(units)²/cycle]. The results of calculations from Eq. (20) can presently be evaluated only if one frequency is strongly dominant, so that damage evaluation can proceed essentially the same as if the response were sinusoidal. Insufficient data exist to evaluate damage from a random stress, for example.

Once the motion responses to dynamic load have been calculated, it is necessary to translate them into terms of forces, or stresses, or other items suitable for performance evaluation. This translation should be relatively routine, though tedious, if the planning of the analysis has properly anticipated this step.

PERFORMANCE EVALUATION

At this stage of the operation, dynamic analysis has been completed, and the problem is to interpret the results in the light of the performance criteria established in the planning stage of operations. Three kinds of criteria are usual: motion limits, stress or strain limits, or functional degradation limits. The motion limits are commonly on displacement, on collision of elements, on velocity, on acceleration, or on jerk (time derivative of acceleration). The stress-strain limits are usually on: stress level to avoid brittle fracture, low-cycle fatigue for transient responses, high-cycle fatigue for vibration responses, or damage accumulation [1] for mixed varieties of loading such as thermal and pressure cycles. Malfunction criteria are widely variable and tend to be different for each element of a system, as well as for different systems. Malfunction limits have been applied to gyro precession, noise generation in a circuit, false signals, dropped bits (in a computer), permanent deformation, hunting of a control loop, zero drift, and almost any other phenomenon.

The weighing and judging of dynamic analysis results against performance criteria is at the same time the most difficult and the most important part of the whole task. The outcome of this weighing and judging governs what subsequent action shall be taken: to accept, to fix, or to scrap. The choice cannot be left to a machine, and a proper discussion of various possibilities needs a large book instead of a short paper.

TRANSLATION INTO ACTION

The determination of what action to take as a result of the evaluation of a dynamic analysis requires the participation of the designer, the analyst, the manufacturer, and the client. This is the time to consider —

1. Whether the loads were really right as used.

2. Whether the structural relationships were too approximate or need to be improved.

3. Whether the masses were reasonable as used.

4. Whether the damping used was reasonable.

5. Whether computational checks were all OK.

6. Whether there was evidence of round-off trouble.

If all of these considerations are satisfactory, then additional detail calculations may be needed that were not included in the main run, such as bolt and weld stresses, stress concentration effects, and points of special interest (gyro mounts, sensor locations, and the like). These detail problems may be known only to the designer, as he made decisions about them in the process of design, and no other person is likely to anticipate all of them.

After all of this, the question may well remain as to how to alter the design to change a behavior, lower a stress, or reduce an excursion. Various alterations that might be considered would include changing stiffness, changing damping, changing mass, adding local reinforcement, modifying connections, or altering symmetry. Which change to make is a matter for individual consideration. Sometimes the effect of a change is readily predictable, and sometimes a complete rerun of the analysis is required. The latter case is avoided whenever possible because of the expense.

TIME AND COST

The various pie slices in Fig. 2 will probably average out to roughly equal times and costs over a variety of problems. The structural and dynamic response calculations all too often consume 80 to 90 percent of time and cost, to the detriment of the overall operation. This may be because these calculations seem to be definite, and prodigious quantities of eight-figure numbers are generated. In reality, the definiteness and accuracy are only apparent, because the assumptions involved in the input are frequently such as to require a ±20 or 30 percent on the numbers. (The modulus of elasticity of steel, for example, is no better than ±10 percent.) The performance evaluation operation is the real meat of the whole task, and it merits top-caliber attention and appreciable time. Inadequate planning at the outset can lead to a result that is meaningless, because the numbers cannot be translated into performance measures.

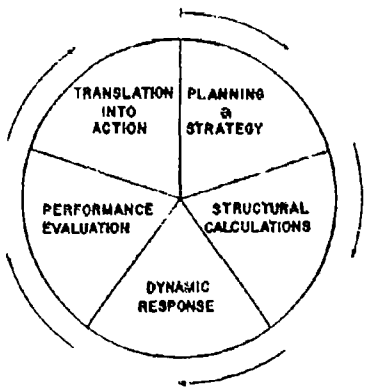

Fig. 2. Pie chart of the structural dynamics problem

These statements about time and cost presume that computer programs are checked out and running, that the crew has performed similar analyses before and knows the ropes, and that no difficult error indicators appear. Generating new programs, training new personnel, or hunting wayward decimals can greatly distort the picture. It can take 6 months to find a mispunched exponent on an input card, and then it may only be discovered by chance. The larger the problems become, the more likely that errors exist that are either unrecognized or are not to be found.

REFERENCES

1. "Structural Design Basis for Reactor Pressure Vessels and Associated Components," U.S. Dept. of Commerce PB151987 (old number)

2. R. M. Maine, "The Practical Problems of Generating Large Stiffness or Flexibility Matrices," ASME Paper 63 WA 209

3. J. S. Archer, "Consistent Mass Matrix for Distributed Mass Systems," EM 13-4, TRW Space Tech. Lab., Feb. 1963

4. R. M. Maine, "The Application of Mechanical Impedance Techniques to a Shipboard Vibration Absorber," Shock and Vibration Bull. 33, Part 4, Mar. 1964

Appendix A

SYMMETRY CONSIDERATIONS

Consider the stiffness matrix and displacement vectors for the symmetric structure of Fig. A-1. This would be

$$\begin{bmatrix} K_{11} & K_{12} & 0 \\ K_{21} & K_{22} & K_{23} \\ 0 & K_{32} & K_{33} \end{bmatrix} \begin{bmatrix} v_1 \\ v_2 \\ v_3 \end{bmatrix} \qquad \text{(A-1)}$$

in which each K represents a 6×6 matrix and each v represents a 6×1 vector. Now symmetry about the x-y plane requires that

$$\left.\begin{array}{llll} x_1 = +x_3 & \theta_1 = -\theta_3 & \theta_2 = 0 \\ y_1 = +y_3 & \phi_1 = -\phi_3 & \phi_2 = 0 \\ \psi_1 = +\psi_3 & Z_1 = -Z_3 & Z_2 = 0 \end{array}\right\}. \qquad \text{(A-2)}$$

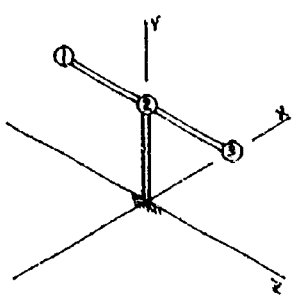

Fig. A-1. Single-plane symmetry

If in matrix Eq. (A-1) column 3 is added to column 1 and row 3 to row 1, then

$$\begin{bmatrix} (K_{11} + K_{33}) & (K_{12} + K_{32}) \\ (K_{21} + K_{23}) & K_{22} \end{bmatrix} \begin{bmatrix} v_1 \\ v_2 \end{bmatrix} \qquad \text{(A-3)}$$

and in the off-diagonal matrices the x, y, ψ terms add, while the θ, ϕ, Z terms cancel.

Further,

$$K_{11} + K_{33} = 2K_{11}$$

$$K_{12} + K_{32} = 2K_{12}$$

for the terms that do not cancel. The net result of the foregoing process is

$$\begin{bmatrix} 2K_{11} & 2\bar{K}_{12} \\ 2\bar{K}_{21} & \bar{K}_{22} \end{bmatrix} \begin{bmatrix} v_1 \\ v_2 \end{bmatrix} \qquad \text{(A-4)}$$

in which the $\bar{K}$ and v terms have had the columns and rows for θ, ϕ, Z eliminated.

In structural dynamics, the homogeneous matrix equation is

$$(-\omega^2 M + K)v = 0 \qquad \text{(A-5)}$$

in which M is a mass matrix (usually diagonal) and ω is a frequency. If the mass matrices had been included in Eq. (A-1), then the same set of operations would have produced, in Eq. (A-4),

$$\begin{bmatrix} 2(-\omega^2 M_{11} + K_{11}) & 2\bar{K}_{12} \\ 2\bar{K}_{21} & (-\omega^2 \bar{M}_{22} + \bar{K}_{22}) \end{bmatrix} \begin{bmatrix} v_1 \\ v_2 \end{bmatrix}. \qquad \text{(A-6)}$$

The usual eigenvalue problem (normal modes and frequencies) then consists of setting Eq. (A-6) equal to zero and solving for ω_j.

Multiplying Eq. (A-6) by a constant would not change any of the eigenvalues or eigenvectors.

If the structure of Fig. A-1 is turned so that the 1-2-3 element is parallel to the X axis, the structure is now symmetric about the y-z plane. Symmetry about the y-z plane requires that

$$\left.\begin{array}{lll} y_1 = y_3 & x_1 = -x_3 & x_2 = 0 \\ Z_1 = Z_3 & \phi_1 = -\phi_3 & \phi_2 = 0 \\ \theta_1 = \theta_3 & \psi_1 = -\psi_3 & \psi_2 = 0 \end{array}\right\}. \qquad \text{(A-7)}$$

Rows and columns can be added just as before, except that in Eqs. (A-4) and (A-6) a different set of rows and columns have been eliminated.

For a structure with two planes of symmetry, as in Fig. A-2, the operations of adding some rows and columns and eliminating some others can be done in sequence. The result would be

$$\begin{bmatrix} 4\bar{K}_{11} & 2\bar{K}_{12} & 2\bar{K}_{14} & 0 \\ 2\bar{K}_{21} & 2\bar{K}_{22} & 0 & 2\bar{K}_{25} \\ 2\bar{K}_{41} & 0 & 2\bar{K}_{44} & 2\bar{K}_{45} \\ 0 & 2\bar{K}_{52} & 2\bar{K}_{54} & \hat{K}_{55} \end{bmatrix} \begin{bmatrix} v_1 \\ v_2 \\ v_4 \\ \hat{v}_5 \end{bmatrix} \qquad \text{(A-8)}$$

in which $\bar{K}$ and v denote one set of coordinates eliminated, and $\hat{K}$ and $\hat{v}$ denote two sets of coordinates eliminated.

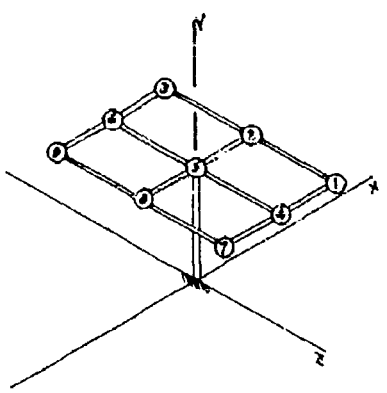

Fig. A-2. Two-plane symmetry

Antisymmetry is the opposite of symmetry, so for antisymmetry the condition of Eq. (A-2) becomes

$$\left.\begin{array}{lll} x_1 = -x_3 & \theta_1 = \theta_3 & x_2 = 0 \\ y_1 = -y_3 & \phi_1 = \phi_3 & y_2 = 0 \\ \psi_1 = -\psi_3 & Z_1 = Z_3 & \psi_2 = 0 \end{array}\right\} \qquad \text{(A-9)}$$

and Eq. (A-7) becomes

$$\left.\begin{array}{lll} y_1 = -y_3 & x_1 = x_3 & y_2 = 0 \\ Z_1 = -Z_3 & \phi_1 = \phi_3 & Z_2 = 0 \\ \theta_1 = -\theta_3 & \psi_1 = \psi_3 & \theta_2 = 0 \end{array}\right\}. \qquad \text{(A-10)}$$

Now for antisymmetry Eqs. (A-4), (A-6), and (A-8) are the same as they were for symmetry except that different coordinates have been eliminated on the plane of symmetry, and different off-diagonal elements cancel.

This process of taking advantage of symmetry and antisymmetry is direct and can be done by machine for problems small enough to permit the matrix manipulations within the machine. Usually, one wishes to take advantage of symmetry because otherwise the matrices are too large for the machine. Fortunately, the difficulty can be minimized by compiling the stiffness matrix for only one-half or one-fourth of the structure at the outset. This has the effect of dividing Eqs. (A-4) and (A-6) by 2, and Eq. (A-8) by 4. The rules to follow then are –

1. Compile stiffnesses up to and including members lying in a plane of symmetry. Do not include stiffnesses past the plane of symmetry.

2. Compile stiffnesses and masses for members lying in a plane of symmetry at one-half magnitude.

3. Compile stiffnesses and masses for members lying on the intersection of two planes of symmetry at one-fourth magnitude.

The resulting eigenvalues and eigenvectors (normal modes and frequencies) will be correct, structural distortions will be correct for forces divided by 2 or 4 as in rules (2) and (3) above, shears and moments will be half-size in planes of symmetry, and stresses will be correct as distortions are.

Appendix B

IMPEDANCE BLACK BOXES

The division of a system into subsystems allows the subsystems to be treated in more detail than would otherwise be possible. Eventually, however, the subsystems must be put back together, and the impedance formulation of relationships is most convenient for this. In Fig. B-1, x_1 and f_1 are the motions and forces at the input coordinates; x_2 and f_2 are the motions and forces at the output coordinates; and x_3 and f_3 are the motions and forces at internal points of interest (for force, stress, or motion reasons) that do not connect with another impedance box. These forces and motions are conveniently related by

$$\begin{bmatrix} f_1 \\ f_3 \\ f_2 \end{bmatrix} = \begin{bmatrix} Z_{11} & Z_{13} & Z_{12} \\ Z_{31} & Z_{33} & Z_{32} \\ Z_{21} & Z_{23} & Z_{22} \end{bmatrix} \begin{bmatrix} x_1 \\ x_3 \\ x_2 \end{bmatrix} \qquad \text{(B-1)}$$

or

$$f = Zx \qquad \text{(B-2)}$$

in which

$$Z = (-\omega^2 M + K) \qquad \text{(B-3)}$$

arranged in the order required by Eq. (B-1).

A variety of conditions for Eq. (B-1) are of interest for use in connecting the subsystem into a system. For example, f_3 is frequently zero, so that x_3 can be eliminated to give

$$\begin{bmatrix} f_1 \\ f_2 \end{bmatrix} = \begin{bmatrix} \bar{Z}_{11} & \bar{Z}_{12} \\ \bar{Z}_{21} & \bar{Z}_{22} \end{bmatrix} \begin{bmatrix} x_1 \\ x_2 \end{bmatrix} \qquad \text{(B-4)}$$

in which

$$\left.\begin{aligned} \bar{Z}_{11} &= Z_{11} - Z_{13}\, Z_{33}^{-1}\, Z_{31} \\ \bar{Z}_{12} &= Z_{12} - Z_{13}\, Z_{33}^{-1}\, Z_{32} \\ \bar{Z}_{21} &= Z_{21} - Z_{23}\, Z_{33}^{-1}\, Z_{31} \\ \bar{Z}_{22} &= Z_{22} - Z_{23}\, Z_{33}^{-1}\, Z_{32} \end{aligned}\right\} . \qquad \text{(B-5)}$$

This provides a means for starting with a larger subsystem than is needed for insertion into the overall system, but which permits the determination of the subsystem behavior in as much detail as desired, after the overall system response has been obtained. It adds to the computation required, but if the information is needed, it can be done.

If damping is to be included, then Z in Eq. (B-3) must be made double size, as

$$Z = \begin{bmatrix} (-\omega^2 M + K) & (+\omega C) \\ (-\omega C) & (-\omega^2 M + K) \end{bmatrix} \qquad \text{(B-6)}$$

to keep the imaginary terms, $(i\omega C)$, separated in the computer. This is a nuisance in computation with complex numbers, but it is necessary for the additional information on phase relationships.

To combine subsystems already in the form of Eq. (B-4) in series, see Fig. B-2, for which

$$\begin{bmatrix} f_{12} \\ f_{21} \end{bmatrix} = \begin{bmatrix} Z_{122} & Z_{12} \\ Z_{21} & Z_{221} \end{bmatrix} \begin{bmatrix} x_1 \\ x_2 \end{bmatrix} \cdot \qquad \text{(B-7) (Cont.)}$$

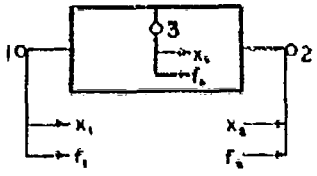

Fig. B-1. Impedance black box

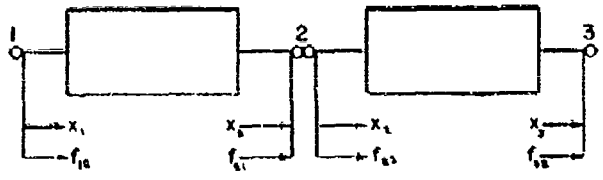

Fig. B-2. Series addition of impedances

$$\begin{bmatrix} f_{2a} \\ f_{2c} \end{bmatrix} = \begin{bmatrix} Z_{22a} & Z_{23} \\ Z_{32} & Z_{33c} \end{bmatrix} \begin{bmatrix} x_2 \\ x_3 \end{bmatrix} \quad \text{(B-7)}$$

Connection of the two subsystems at interface 2 requires that

$$\left.\begin{aligned} f_{2a} + f_{2c} &= f_2 \quad \text{if external forces are applied at 2, or} \\ &= 0 \quad \text{if there are no external forces} \end{aligned}\right\} \quad \text{(B-8)}$$

The application of Eq. (B-8) to (B-7) gives

$$\begin{bmatrix} f_{1a} \\ f_2 \\ f_{3c} \end{bmatrix} = \begin{bmatrix} Z_{11a} & Z_{12} & 0 \\ Z_{21} & Z^*_{22} & Z_{23} \\ 0 & Z_{32} & Z_{33c} \end{bmatrix} \begin{bmatrix} x_1 \\ x_2 \\ x_3 \end{bmatrix} \quad \text{(B-9)}$$

in which

$$Z^*_{22} = Z_{22a} + Z_{22c}$$

If $f_2 = 0$, then

$$\begin{bmatrix} f_{1a} \\ f_{3c} \end{bmatrix} = \begin{bmatrix} Z'_{13} & Z_{13} \\ Z_{31} & Z_{33} \end{bmatrix} \begin{bmatrix} x_1 \\ x_3 \end{bmatrix} \quad \text{(B-10)}$$

in which

$$\left.\begin{aligned} Z_{11} &= Z_{11a} - Z_{12} Z^{*-1}_{22} Z_{21} \\ Z_{13} &= 0 - Z_{12} Z^{*-1}_{22} Z_{23} \\ Z_{31} &= 0 - Z_{32} Z^{*-1}_{22} Z_{21} \\ Z_{33} &= Z_{33c} - Z_{32} Z^{*-1}_{22} Z_{23} \end{aligned}\right\} \quad \text{(B-11)}$$

This combination of subsystems can be continued for as many subsystems as desired, subject to the limitation that roundoff errors accumulate and eventually destroy accuracy. If the number of coordinates at each interface is of the order of 40 (or 20 if complex Z is used), then about 5 subsystems represent a practical limit.

To combine subsystems in parallel, refer to Fig. B-3, for which

$$\begin{bmatrix} f_{1a} \\ f_{2c} \end{bmatrix} = \begin{bmatrix} Z_{11a} & Z_{12a} \\ Z_{21a} & Z_{22a} \end{bmatrix} \begin{bmatrix} x_{1a} \\ x_{2c} \end{bmatrix} \quad \text{(B-12) (Cont.)}$$

$$\begin{bmatrix} f_{1b} \\ f_{2d} \end{bmatrix} = \begin{bmatrix} Z_{11b} & Z_{12b} \\ Z_{21b} & Z_{22b} \end{bmatrix} \begin{bmatrix} x_{1b} \\ x_{2d} \end{bmatrix} \quad \text{(B-12)}$$

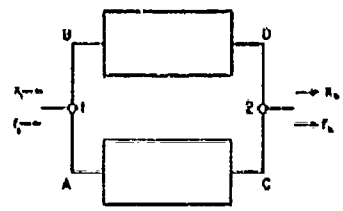

Fig. B-3. Parallel combination of impedances

If A and B are attached at 1, and C and D are attached at 2, then

$$\left.\begin{aligned} x_{1a} &= x_{1b} = x_1 \\ x_{2c} &= x_{2d} = x_2 \end{aligned}\right\} \quad \text{(B-13)}$$

and by statics

$$\left.\begin{aligned} f_{1a} + f_{1b} &= f_1 \\ f_{2c} + f_{2d} &= f_2 \end{aligned}\right\}. \quad \text{(B-14)}$$

Now by simple addition,

$$\begin{bmatrix} f_1 \\ f_2 \end{bmatrix} = \begin{bmatrix} (Z_{11a} + Z_{11b}) & (Z_{12a} + Z_{12b}) \\ (Z_{21a} + Z_{21b}) & (Z_{22a} + Z_{22b}) \end{bmatrix} \begin{bmatrix} x_1 \\ x_2 \end{bmatrix} \quad \text{(B-15)}$$

or

$$\begin{bmatrix} f_1 \\ f_2 \end{bmatrix} = \begin{bmatrix} Z_{11} & Z_{12} \\ Z_{21} & Z_{22} \end{bmatrix} \begin{bmatrix} x_1 \\ x_2 \end{bmatrix} \quad \text{(B-16)}$$

The cases for B not attached at 1, $f_{1b} \neq 0$, and for $f_{1b} = 0$ can be solved algebraically to represent the situation of adding stiffness, damping, or mass to the subsystem. With one end not attached and not loaded, the case of the vibration absorber is solved [4].

The series and parallel additions in suitable combinations are the means for studying large systems in the most effective way. The computation scheme can be kept flexible and the analyst can keep the physical sense of what he is doing.

DISCUSSION

R. E. Dobson (G. E. Co.): Would you give us a brief comparison of the state of the art with regard to the work in underwater shock and in the missile and aircraft industries? There seems to be considerable difference in the methods of approach and the criteria of failure. The methodology in general appears to be a little more advanced in the missile and spacecraft industries than in the naval aspects.

Dr. Mains: To answer that question properly would require the rest of the morning. I can't agree that the state of the art in the aircraft and missile business is more advanced. The naval shipboard scheme for shock analysis is based on an extensive history of measurement and field experiment. The correlation between the way the calculations are done and the results are measured is good. I once did a turbine analysis using the usual Navy approach. There were some 40 coordinates involved. We later put gages on these calculation stations and took the ship out, shot at it, and measured the results. None of the measured points was off more than 30 percent from the calculation, and most of them were within 10 or 15 percent. The calculation was on the conservative side. This is pretty good. Now the aircraft style of analysis seems to be more sophisticated because it is done with Laplace transforms or with something other than the relatively straightforward matrix manipulations we use in Navy shock; but this is only appearance — I don't think it is really more sophisticated.

* * *

DYNAMIC SUBSTRUCTURES METHOD FOR SHOCK ANALYSIS

Michael Pakstys, Jr.
General Dynamics
Electric Boat Division
Groton, Connecticut

The objective of this paper is to describe a dynamic substructure method for finite element, normal mode analysis and its applicability to shock analysis of complex structures. The basic concepts of the dynamic substructure method are reviewed and its relationship to the static substructure method is indicated. The application to dynamic analysis of shipboard equipment is outlined in some detail and illustrated by an analysis of three-dimensional frame structures. The advantages of the use of the dynamic substructure solution vs a direct solution are enumerated.

INTRODUCTION

The finite element analysis method has proven to be a valuable tool for solving complex static and dynamic structural mechanics problems by the use of modern digital computers. However, even the use of most sophisticated computer programs and most modern computer hardware does not eliminate the possibility of errors that may creep in the complicated process of the analysis. The errors could be generally of three types: computer, program, and human.

Human errors that are introduced in computerized finite element analysis generally fall into the following groups:

1. The mathematical model fails to properly idealize the structure that is to be analyzed.

2. The mathematical model results in numbers that can not be adequately handled by numerical processes prescribed by the computer software and hardware.

3. The input data contains errors that are not picked up by the program.

The detection and location of these errors is difficult, as the use of computerized finite element analysis tremendously increased the complexity of problems that can be solved on a routine basis; but it also resulted in the analyst's losing the "feel" for the results that he could expect from the analysis.

However, the analyst still wants and must have some verification that the large amount of numbers that the complex computer programs generate are reasonable and accurate.

One technique that offers at least a partial resolution of the above problems, in addition to offering other advantages, is the substructure method. Briefly, in the substructure method, unlike the usual direct method, the complete solution is obtained by parts rather than directly as a whole. The advantages of substructure method for static analysis have been well established by the active application to "production" analysis of a large number of complex structures.

This paper describes a dynamic substructure method for normal mode analysis and specifically examines its application and advantages in the currently specified Dynamic-Design-Analysis Method (DDAM) for shock analysis of shipboard components and foundations.

BASIC CONCEPTS

Static Analysis

In 1963, Przemieniecki [1], proposed a substructure method for static, finite element, displacement type of analysis of structures.

A computer routine using this method was coded at the author's firm and applied to static analysis of a number of complex structures. One such analysis is described in Ref. [2].

The basic steps in the procedure are:

1. Draw up a finite element mathematical model which closely represents the behavior of the actual structure.

2. Partition the whole mathematical model into a number of substructures. The joints on the boundaries of the substructure are called boundary joints and all joints inside the substructure are called internal joints.

3. With all the boundary joints displacements completely fixed, $\{u_b^F\} = \{0\}$, analyze each substructure separately to determine its displacement of internal joints $\{u_i^F\}$ and reactions for each substructure at the boundary joints. (The symbol $\{\ \}$ in this paper designates a column matrix, while the symbol $[\ ]$ designates a rectangular matrix.)

4. Relax the boundary joints and obtain the displacements at the boundary joints $\{u_b^R\}$, and, after finding these, calculate the displacement at internal joints $\{u_i^R\}$ owing to this relaxation of the in boundary joints.

5. Obtain the total displacements of the structure $\{u\}$ by a superposition of the displacements for the fixed and relaxed conditions

$$\{u\} = \{u^F\} + \{u^R\} \tag{1}$$

or

$$\begin{Bmatrix} u_i \\ u_b \end{Bmatrix} = \begin{Bmatrix} u_i^F \\ u_b^F \end{Bmatrix} + \begin{Bmatrix} u_i^R \\ u_b^R \end{Bmatrix}. \tag{1a}$$

Note that $\{u_b^F\} = \{0\}$ by definition in step 3.

Dynamic Analysis

The substructures method for normal mode dynamic analysis described in this paper follows the same basic concepts outlined for the static analysis, and its implementation is based on the general techniques advocated by Hurty [3].

In the dynamic analysis case, steps (1) and (2) are the same as in the static analysis case except that a dynamic mathematical model accounting for mass as well as elastic properties is used. For an example, see Fig. 1, which shows the lumped mass beam mathematical model, partitioned into four substructures.

The solution for the whole structure is obtained by combining the solutions obtained by parts using Eq. (1).

Step (3) is similar to the static case in that all boundary joints are completely fixed $\{u_b^F\} = \{0\}$ and the normal modes of each substructure are obtained for these boundary conditions. The displacement of internal joints can be written in terms of the substructure normal modes as

$$\{u_i^F\} = [\Pi]\{p_s\} \tag{2}$$

where $\{p_s\}$ is a column matrix of the generalized coordinate of each substructure and $[\Pi]$ is a matrix of normal mode shapes.

In step (4) the boundary joints are relaxed 1 degree of freedom (DOF) at a time (6 DOF's in case of a three-dimensional structure) by allowing a unit displacement at that degree of freedom.

The process is illustrated in the bottom part of Fig. 1. The displacements caused by the relaxation modes can be expressed as

$$\begin{Bmatrix} u_i^R \\ u_b^R \end{Bmatrix} = \begin{matrix} [G] \\ [I] \end{matrix} \{p_R\} \tag{3}$$

where $\{p_R\}$ are generalized coordinates of the relaxation modes, $[G]$ is matrix representing displacements of internal joints owing to unit displacements at boundary joints, and $[I]$ is identity matrix.

Using Eq. (1)

$$\begin{Bmatrix} u_i \\ u_b \end{Bmatrix} = \begin{Bmatrix} u_i^F \\ 0 \end{Bmatrix} + \begin{Bmatrix} u_i^R \\ u_b^R \end{Bmatrix} = \begin{Bmatrix} [\Pi]\{p_s\} \\ \{0\} \end{Bmatrix} + \begin{Bmatrix} [G]\{p_R\} \\ [I]\{p_R\} \end{Bmatrix}$$

or by designating matrix

$$[R] = \begin{bmatrix} [\Pi] & [G] \\ 0 & [I] \end{bmatrix} \tag{4}$$

$$\{u\} = [R]\{p\}$$

Thus $[R]$ is the transformation matrix which transforms the generalized coordinates into actual coordinates.

APPLICATION TO DDAM

Review of Direct Solutions

The DDAM procedure, which is currently specified by the Navy for shock analysis of

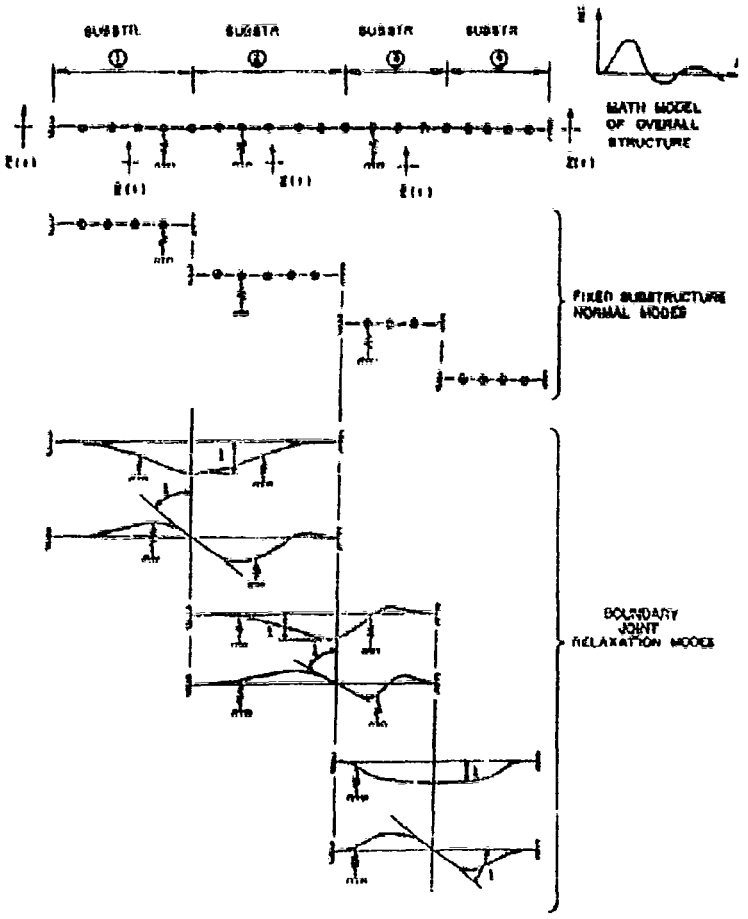

Fig. 1. Planar example

shipboard equipment and foundations, can be described as a finite element, lumped mass, normal mode method [4,5]. The shock inputs, which represent a certain intensity of underwater explosion attack on the ship, are given in terms of design shock spectra for a uniform shock motion of all support of the equipment systems. The design shock spectra vary as a function of the modal frequencies, modal weights, and location in the ship.

A DDAM analysis of a typical shipboard component is described in some detail in Ref. [6]. Once the mathematical model is established, the major steps in the DDAM procedure are:

1. Formation of the equations of motion including the determination of the stiffness or flexibility matrix and mass or weight matrix.

2. Free vibration analysis to determine the modal frequencies and mode shapes.

3. Calculation of the major shock response quantities such as modal weight, inertial force, and joint displacement matrices.

4. Detailed force and stress analysis of each member of the structure.

For example, the equations of motion for the usual direct solution for the mathematical model, shown in Fig. 1, are given in Eq. (5) in matrix form

$$[m]\{\ddot{u}\} + [k]\{u\} = -[m]\{v\}\,\ddot{z}(t) \qquad (5)$$

where $[m]$ is mass matrix, $[k]$ is stiffness matrix, $\{v\}$ is direction cosine matrix between

the DOF and the direction shock motion of the supports, and $\ddot{z}(t)$ is shock motion of supports in terms of acceleration.

Substructure Solution

To derive the equations of motion for a substructure solution, we substitute Eq. (4) for $\{u\}$ in Eq. (5) and premultiply by $[R]^T$, obtaining Eq. (6),

$$[R]^T[m][R]\{\ddot{p}\} + [R]^T[k][R]\{p\} = -[R]^T[m]\{v\}\ddot{z}(t). \tag{6}$$

If we shorten the notation for the transformed mass and stiffness matrices, we have the equations of motion in the substructures solution format,

$$[M]\{\ddot{p}\} + [k]\{p\} = -[R]^T[m]\{v\}\ddot{z}(t). \tag{6a}$$

For the free vibrations case, we drop the right-hand side of Eq. (6a) to obtain

$$[M]\{\ddot{p}\} + [k]\{p\} = \{0\}. \tag{7}$$

Some interesting properties of the mass and stiffness matrices of the combined system can be observed if they are separated into the fixed substructures modes and the relaxation modes, designated by subscripts S and R, respectively:

$$[M] = \left[\begin{array}{c|c} [M_{SS}] & [M_{SR}] \\ \hline [M_{RS}] & [M_{RR}] \end{array}\right]$$

$$[k] = \left[\begin{array}{c|c} [k_{SS}] & 0 \\ \hline 0 & [k_{RR}] \end{array}\right].$$

Note that $[M_{SS}]$ is diagonal matrix containing the generalized mass of each substructure mode considered, $[M_{RR}]$ is a matrix representing the mass effective at the boundary joints, $[k_{SS}]$ is a diagonal general stiffness matrix of fixed substructure modes, and $[k_{RR}]$ is the stiffness matrix of the substructure boundary joints.

The flexibility formulation of the free vibration is given by

$$[\Delta][M]\{\ddot{p}\} + \{p\} = \{0\} \tag{8}$$

where $[\Delta] = [k]^{-1}$ is called the flexibility matrix.

The flexibility formulation for constrained structures is more desirable because it determines the lower modes first and the mass matrix (which is a full matrix here) does not need to be inverted for the frequency equation given below:

$$\left|[\Delta][M] - \frac{1}{\omega^2}[I]\right| = 0. \tag{9}$$

Using Eq. (9), we can find all the frequencies (ω) and the mode shape matrix $[\theta]$ for the system, using the usual methods for solving the eigenvalue problems.

The mode shape matrix $[\phi]$ for the actual mass coordinates of the substructures is

$$[\phi] = [R][\theta]. \tag{10}$$

At this stage we are ready to calculate the shock response quantities, which can be calculated using exactly the same equations as for the direct solution.

Once the modal inertial loads and modal displacements of the joints are calculated, we can perform a detail force and stress analysis of each member of the structure by one of the following methods:

1. Equivalent static analysis of each substructure for each set of modal inertial forces at the internal mass joints and modal boundary joint displacement.

2. Equivalent static analysis of the total structure for each set of the inertial loads at all the mass joints.

EXAMPLE PROBLEM

General

The following example problem will illustrate the application of the dynamic substructure method to shock analysis of a three-dimensional frame structure. The structure will be solved using the common direct method as well as the substructure method to compare results. The mathematical model of the structure is shown in Fig. 2. The structure was given 33 dynamic degrees of freedom in the global (X, Y, Z) coordinate system according to the following manner:

1. Three translatory DOF's each for joints AB, AC, AD, AF, AG, AI, and AJ.

2. All 6 DOF's each for joints AE and AH. (The additional rotation degrees were assigned to these joints to compare the direct and the

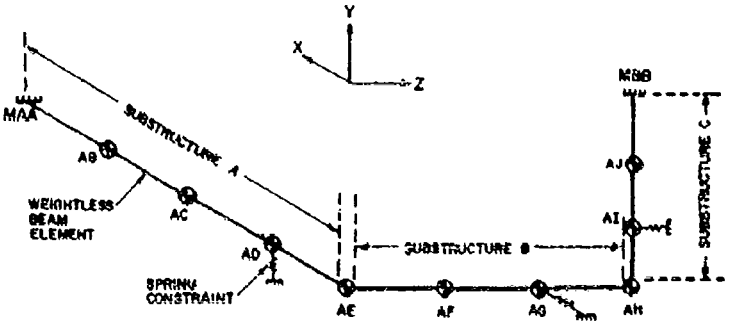

Fig. 2. Mathematical model of 3-D frame

substructure methods on the basis of the same size of matrices for the equations of motion.)

The shock loading for the structure was specified in terms of a shock spectrum value representing uniform shock motion in z direction. The specific acceleration shock spectrum value used in this analysis was 1 g for all the normal modes.

Actually four types of analysis were performed for the math model shown in Fig. 2:

1. Substructure — all modes

2. Substructure — reduced number of modes

3. Direct — all dynamic degrees of freedom

4. Direct — reduced dynamic degrees of freedom.

For all the four analyses, the following normal mode quantities were calculated using a UNIVAC 1107 computer:

1. Frequencies and mode shapes

2. Inertial loads

3. Modal weights.

Substructures Analyses — All Modes

The mathematical model shown in Fig. 2 was partitioned into three substructures, A, B, and C, separated by the boundary joints AE and AH. In the dynamic substructure notation this resulted in the following breakup of modes:

Substructure Modes:

Substructure A — nine modes

Substructure B — six modes

Substructure C — six modes

Relaxation Modes:

Joint AE — six modes

Joint AH — six modes

The following were the major steps in the analysis:

1. Calculation of eigenvalues $[\lambda]$ and frequencies $[\Omega]$ for each of the substructures using the Electric Boat Division General Structures computer program [7,8]. The mode shapes for substructure A were normalized in such manner as to give $[H_A]^T [w_A] [H_A] = [I]$, where $[w_A]$ is a diagonal weight matrix for substructure.

2. Calculation of the $[G]$ matrix representing the displacement of the substructure degrees of freedom caused by unit displacement of the degrees of freedom at the boundary joints AE and AH. This can be calculated by either direct static or substructure static methods of solution.

3. Calculation of the $[f]$ matrix, which describes the flexibility of the boundary joints, representing the displacement of the degrees of freedom of the boundary joints owing to the applied unit loads at these joints. This also can be calculated by direct static or substructures static methods of solution.

4. Formation of the $[R]$ matrix using the $[\Omega]$ and $[G]$ matrices. Figure 3 presents a block diagram for the formation of the $[R]$

matrix. Note that once the order for the degrees of freedom and the modes of the substructure and the boundary joints is assumed in forming [R] matrix, it must be adhered to in the following steps.

5. Calculation of the weight matrix [W] for the composite structure by $[W] = [R]^T [w] [R]$, where [w] is the weight matrix for all dynamic degrees of freedom of the whole structure arranged in the same order as the [R] matrix. This operation results in a matrix shown in Fig. 4.

6. Formation of the [Δ] matrix from the [λ] matrices of the three substructures and the [F] for the boundary joints. Figure 5 gives the format for the [Δ] matrix.

7. Forming the frequency equation, Eq. (9), from the [Δ] and [W] matrices and solution for frequencies [ω] and mode shapes [θ] for all normal modes of the structure.

8. The mode shapes in the actual coordinate system are given as $[\phi] = [R][\theta]$.

Henceforth the calculations can be performed in the same manner as in the direct solution.

Reduction of Substructure Modes

One of the major advantages of the dynamic substructure method is that it provides a rational method for reducing the number of normal modes yet accounting for all the dynamic degrees of freedom. The modes which can be eliminated are the substructures modes, especially the higher ones, that are inherently approximate because of the mass lumping. For a general three-dimensional structure, six relaxation modes must be retained for each boundary joint to allow all the possible normal modes of the composite structure.

In this example problem, a reduced mode substructure analysis was performed by retaining only the following substructure modes:

Substructure A — four lowest modes

Substructure B — three lowest modes

Substructure C — three lowest modes

All the 12 relaxation modes were retained.

The calculation steps were the same as outlined under previous sections for the modes analysis. This reduction of modes resulted in 33 × 22 [R] matrix as shown in Fig. 3, and in

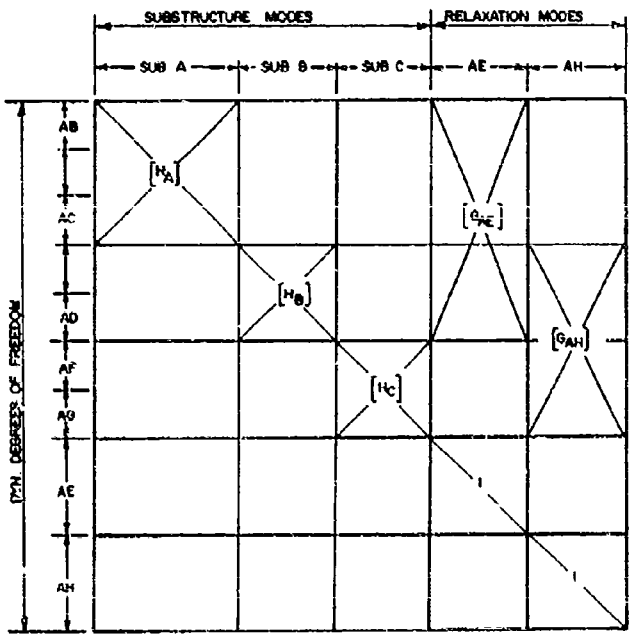

Fig. 3. [R] matrix for substructure analysis

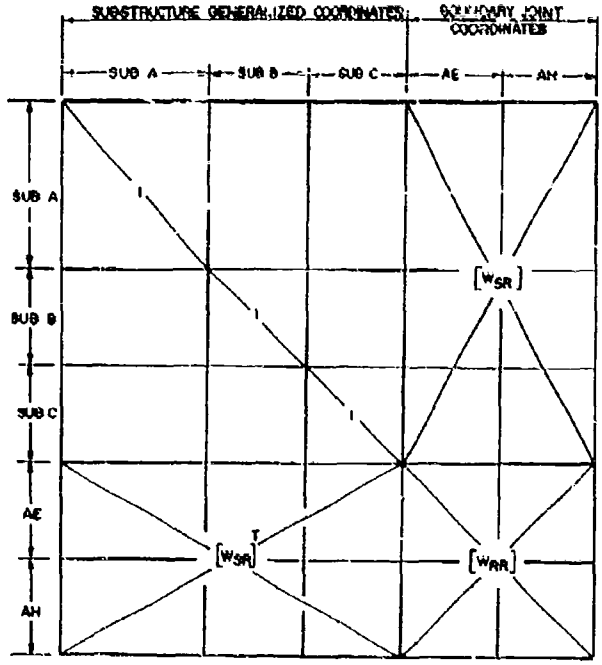

Fig. 4. [W] matrix for substructure analysis

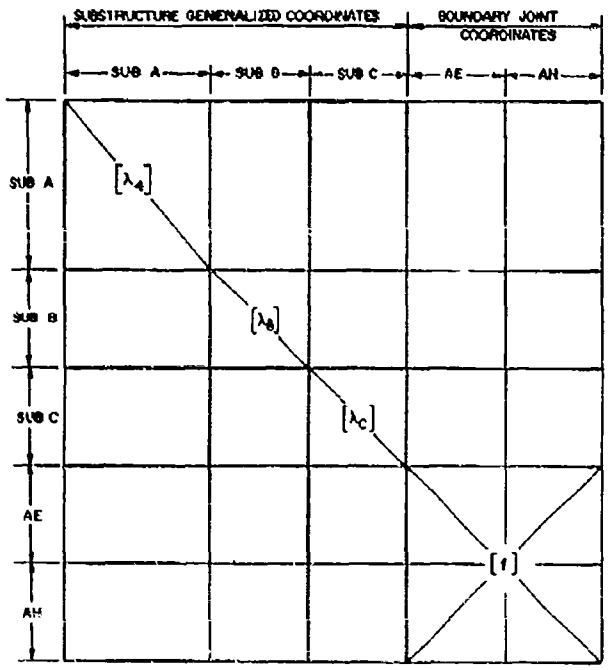

Fig. 5. [Λ] matrix for substructure analysis

22×22 [Φ] and [Δ] matrices as shown in Figs. 4 and 5, respectively.

The calculated frequency matrix (ω) was 22×1 and the untransformed mode shape matrix was 22×22. The transformed (ϕ) is a 33×22 matrix, and this contains the mode shapes for each degree of freedom of the 22 modes. The modal weights for this reduced substructure analysis is shown in Table 1.

Direct Analysis—All Degrees of Freedom

The analysis obtained a direct solution for all the 33 degrees of freedom of the structure shown in Fig. 2. The frequencies and mode shapes and modal weights for 33 normal modes were obtained using the computer program described in the substructures analysis in step (1) for calculating the fixed substructure modes.

Reduced Number of Degrees of Freedom

A reduction technique for direct analysis, proposed by Guyan in Ref. (9), was applied to the mathematical model shown in Fig. 2. This technique, which amounts to elimination of degrees of freedom, rather than normal modes as is the case in the substructure analysis, is more arbitrary and less rational than the latter.

TABLE 1
Modal Weights for Z Direction Shock (in lb)

Mode No.	Direct All DOF	Substructure All Modes	Substructure Reduced	Direct Reduced
1	77.65	77.43	77.13	78.71
2	198.58	200.21	199.95	199.10
3	6.64	4.81	4.85	5.60
4	0.0	0.15	0.15	0.00
5	20.33	20.55	20.50	23.40
6	5.56	5.56	5.64	5.59
7	9.90	4.44	4.64	
8	6.95	12.27	12.50	
9	0.00	0.14	0.08	0.97
10	1.69	1.71	1.64	0.06
		0.03		
11	0.00	0.01	0.00	
12	1.08		0.00	
13	2.60	2.60	0.26	3.02
		1.12		
14	0.00	0.00		0.31
15	46.41	46.41	47.31	45.58
16	0.15	0.15	0.15	0.13
17	0.00	0.00	0.00	
18	1.05	1.05	0.50	2.26
				0.00
19	0.00	0.00	0.00	0.15
20	0.00			0.03
21	0.11	0.11	2.15	0.00
22	0.00	0.00		0.01
23	0.00	0.00	0.00	
24	0.00	0.00		0.27
25	0.16	0.15		
26	0.22	0.22		
27	0.00	0.00		0.00
28	26.63	26.63		
29	0.00			
30	0.00	0.00	0.00	
31	0.00	0.00		
32	0.00	0.00	2.15	2.15
33	0.22	0.22		
		0.0		
Total	406.00	405.97	379.50	367.32

In this example problem, all the degrees of freedom associated with joints AB, AD, AF, and AI were eliminated. This reduced the number of degrees of freedom from 33 to 21. The following were the basic steps in procedure:

1. The 33 × 33 stiffness matrix of the original composite system was arranged in a manner that grouped the retained and eliminated degrees of freedom (see Fig. 6).

2. The 33 × 21 transformation matrix was formed

$$[T] = \frac{[I]}{[-C]^{-1}[B]^T}$$

where [C] and [B] are defined in Fig. 6.

3. The reduced 21 × 21 weight matrix [W] was found by

$$[W] = [T]^T [w][T] .$$

4. The reduced 21 × 21 stiffness matrix was found by

$$[K] = [T]^T [k][T] .$$

5. The flexibility matrix was found by

$$[K]^{-1} = [\Delta]$$

6. The 21 frequencies (ω) and the associated mode shapes $[\theta]$ were found using Eq. (9).

7. The expanded mode shapes for all the 33 degrees of freedom were found by

$$[\phi] = [T][\theta] .$$

Further calculations for inertial loads and modal weights were performed in the same manner for all the previous analyses.

Comparison of Results

Of the four analyses the easiest results to compare are the natural frequencies as they represent only one number for each mode. The mode shapes and inertial forces are harder to compare because they involve 33 numbers for each mode. Fortunately the mode shapes and inertial loads can be indirectly compared by comparing the modal weights that, for a given shock direction, are represented by only one number in each mode. The modal weights are also valuable for checking solutions in that their summation must equal the total weight assigned for all the lumped mass degrees of freedom oriented in the shock-input direction.

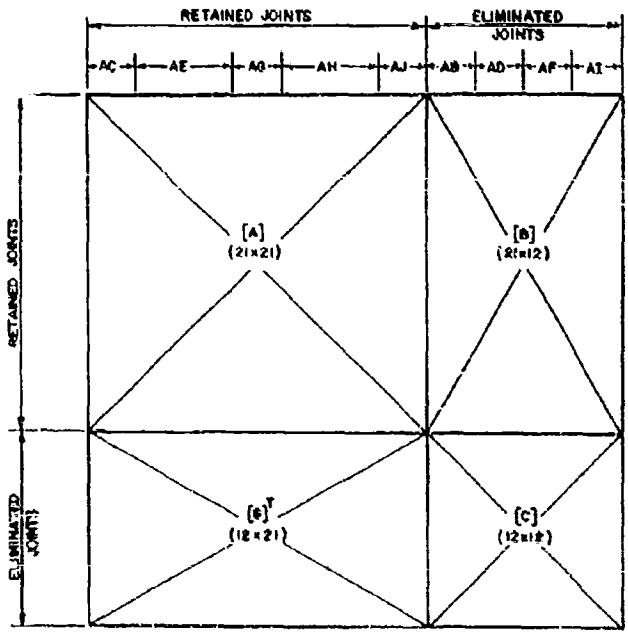

Fig. 6. [k] matrix for reduced direct analysis

In this problem the total weight assigned to the degrees of freedom in the Z shock direction was equal to 406 lb.

The frequencies and modal weights for the four analyses are shown in Tables 2 and 1, respectively. The modal frequencies and modal weights that appeared to belong to the same normal mode were arranged in the same row in these tables.

Let us first examine the results of the direct (all degrees of freedom) analysis and the substructure (all modes) analysis. Both analyses must be inherently theoretically exact for the assumed lumped mass model; any differences must be attributed to the different numerical processes used in the two methods to obtain the solution.

The comparison reveals the following:

1. The summation modal weights for both solutions are almost exactly 406.00 lb.

2. Most modal frequencies correspond within 0.5 percent.

3. The frequencies of modes 4, 7, 8, 9, and 12 and 13 are different by up to 5 percent.

4. Three modal frequencies and mode shapes for both analyses are totally different but none of the modes represents significant responses under the assumed Z loading.

TABLE 2
Modal Frequencies (Hertz)

Mode No.	Direct All DOF	Substructure All Modes	Substructure Reduced	Direct Reduced
1	53.27	53.27	53.28	53.64
2	71.50	71.55	71.57	72.26
3	89.22	88.88	88.94	89.79
4	101.79	99.94	100.03	102.58
5	129.00	128.97	129.13	133.83
6	149.30	149.39	149.45	154.42
7	204.15	190.59	191.02	
8	242.12	228.61	229.37	
9	285.88	275.40	276.06	281.83
10	304.30	304.27	304.47	304.13
		314.09		
11	318.06	318.38	318.08	
12	333.70		326.70	
13	369.59	360.38	362.18	346.02
		380.42		
14	409.84	409.86		435.62
15	523.69	523.60	523.66	523.40
16	590.42	590.42	609.47	607.02
17	641.98	642.11	641.86	
18	747.96	748.02	762.92	717.49
				898.20
19	910.77	911.02	1065.20	916.52
20	1006.59			980.86
21	1328.23	1328.24	1257.29	1057.78
22	1391.51	1391.52		1411.43
23	1539.41	1539.41	1543.25	
24	1554.59	1554.60		1597.74
25	1653.48	1653.48		
26	1694.84	1694.84		
27	1706.07	1706.07		1707.95
28	1774.66	1774.66		
29	1776.26			
30	1993.41	1992.61	1967.74	
31	2106.77	2105.00		
32	2442.36	2442.37	2446.97	2414.28
33	2544.66	2544.67		
		6347.01		

5. There is no concrete basis for deciding whether the direct or the substructure analysis represents a more accurate solution.

Next let us examine results of two reduced analyses – substructure and direct. The results of the substructure analysis for both frequencies and modal weights indicate better correlation to the full analyses results. The reduced direct analysis missed some of the more important modes, such as modes seven and eight altogether. Although no general conclusion can be based on the results of this one example, it is expected that the reduced substructure method should give equivalent or better accuracy than the reduced direct method for the same size matrices, simply because the substructure reduction is an inherently more rational and dynamic method for reduction of matrices describing the equations of motion.

CONCLUSIONS

A dynamic substructure method for finite element, normal mode analysis was described and its application to DDAM shock analysis was demonstrated on a three-dimensional frame structure. The following conclusions can be drawn when the substructure method is compared with the usual direct method of dynamic shock analysis:

1. As in the direct method, considering all the degrees of freedom, the dynamic substructures method, considering all the substructure modes results in a theoretically exact solution for a lumped mass, finite element mathematical mode, although the two methods involve different numerical methods for solving the equations of motion.

2. Dynamic substructure method provides a more rational procedure than the direct method for reducing the number of equations to reduce the size of the matrices to be handled in the computer calculations. The main reason for the rationality is that in the substructure method the reduction involves the elimination of some of the higher substructure modes that can be considered more optimum coordinates than the dynamic degrees of freedom involved in the reduction by the direct method.

A method for estimating the errors in frequencies and mode shapes resulting from elimination of some of the substructure modes is available in Ref. [10].

3. As the substructures method involves a solution by parts, a systematic check of correctness of the results of each step, or trouble shooting for errors, can be made more easily. For example, the static equilibrium can be checked for each substructure before the composite matrices are formed. The frequencies and mode shapes of a substructure that constitutes only a portion of a large structure can also be more easily displayed and checked than those of the whole large structure.

4. The substructure method allows different analysts and computer facilities to work separately on solutions to the individual substructures, before and after obtaining the solution for the composite structure.

5. The substructure method allows for a less time consuming and less costly modification of parts of structures (contained in one or more substructures) than the direct method of solutions which would involve a completely new computer rerun.

6. Using the dynamic substructure method, any dynamic experimental data on one or more substructures, which is usually in terms of frequencies and mode shapes, would be directly input into the analysis.

7. The dynamic substructures method can accommodate the dynamic analysis of a continuous as well as a lumped mass mathematical model, or even a hybrid continuous-lumped mass model, because the equations of motion can be written in terms of the substructure normal mode coordinates.

8. The application of the dynamic substructure method does not necessarily require a new computer program if the user has presently available a direct dynamic analysis program and standard matrix operation computer program routines.

ACKNOWLEDGMENTS

The study described in this paper was performed as a task in the Electric Boat Division of General Dynamics Research and Development program. The author wishes to acknowledge the assistance provided by Mr. B. A. Bott and Mr. D. A. Dutton in computer programing and computer solution of the example problem.

REFERENCES

1. J. S. Przemieniecki, "Matrix Structural Analysis of Substructures," AIAA Journal, 1:139-147 (Jan. 1963)

2. R. F. Sammataro, "Final Report – Substructure Method Analysis of the SS(N)637 Engine Room Compartment One-Third Scale Model," Electric Boat Division Rept. No. U411-67-013, July 21, 1967

3. W. C. Hurty, "Dynamic Analysis of Structural Systems Using Component Modes," AIAA Journal, 3:678-685 (Apr. 1965)

4. R. O. Belsheim and G. J. O'Hara, "Shock Design of Shipboard Equipment," NAVSHIPS 260-423-30, May 1961

5. G. J. O'Hara and P. F. Cunniff, "Elements of Normal Mode Theory," NRL Rept. 6002, Nov. 1963

6. M. Pakstys, "Application of Matrix Techniques to Analysis of Complex Structures," Proc. for Short Course on Normal Modes, Shock and Vibrations, Pa. State Univ., July 1966

7. L. H. Chen, J. E. Cadoret, and C. E. Aldrich, "A Matrix Method for Analysis of Complex Structures," Electric Boat Division Rept., Feb. 1959

8. P. A. Roy et al., "General Structures Program Manual," General Dynamics, Electric Boat Division, Spring 1966

9. R. J. Guyan, "Reduction of Stiffness and Mass Matrices," AIAA Journal (Feb. 1965)

10. W. C. Hurty, "A Criterion for Selecting Realistic Natural Modes of Structure," JPL Tech. Memo 33-364, Nov. 1, 1967

DISCUSSION

R. Mustain (McDonnell Douglas Corp.): Has a program of your complexity been verified by actual test?

Mr. Pakstys: Yes, we were involved in three submarine tests. We made a pretest analysis and made predictions. We then put instrumentation at the locations of major response, obtained the data, and reduced it. It was evaluated and was, in most cases, within 30 percent.

* * *

IDENTIFICATION OF COMPLEX STRUCTURES USING NEAR-RESONANCE TESTING

J. P. Raney
NASA Langley Research Center
Langley Station, Hampton, Virginia

A recent innovation for determining the set of governing differential equations of motion of a complex structure is described in this paper. Numerical values for the mass, stiffness, and damping coefficients of the dynamical equations associated with a particular input response or transmission path are computed from the data usually obtained in conventional vibration tests of a structure. The theory is based on the dynamic properties of multi-degree-of-freedom linear systems. The method requires the steady response (acceleration, velocity, displacement, or stress) and the driving sinusoidal force input for transmission paths of interest to be experimentally determined for a few frequencies near each major structure resonance. Application of the method is illustrated by determining from experimental data the equations of motion of 1/10- and 1/40-scale models of the Apollo/Saturn V launch vehicle. Transient responses computed using the identified equations for the 1/40-scale model are shown to agree favorably with experimental results.

INTRODUCTION

The purpose of this paper is to present a simple technique for experimentally determining an acceptable set of equations of motion for a space vehicle structure. This system identification approach, while yielding the equations of motion, does not involve a detailed analysis or physical idealization of the structure. It relies solely on the experimental determination of the steady-state response of the structure to a sinusoidally varying input force for a few frequencies near each important structural resonance, and on the usual assumptions regarding the behavior of lightly damped, linear structures.

NOMENCLATURE

$[M]$ System mass matrix (symmetric, positive definite)

$[C]$ System viscous damping matrix (symmetric, nonnegative definite)

$[K]$ System stiffness matrix (symmetric, nonnegative definite)

$\{F(t)\}$ System forcing function vector

$\{X\}$ System coordinate vector

x_k kth system coordinate (an element of $\{X\}$)

X_k Amplitude of steady-state displacement response at k

$\{X\}^{(i)}$ System coordinate vector owing only to response in the ith mode

$x_k^{(i)}$ kth element of $\{X\}^{(i)}$

$[\Psi]$ Matrix of modal vectors $\{\varphi\}^{(i)}$ as columns

$\{\varphi\}^{(i)}$ Modal vector obtained from $[K] - \lambda_i [M]\{X\} = 0$

$\varphi_i^{(i)}, \varphi_j^{(i)}$ The ith and kth elements of $\{\varphi\}$

$[\bar{M}]$ Diagonal modal mass matrix

$[\bar{C}]$ Diagonal modal damping matrix

$[\bar{K}]$ Diagonal modal stiffness matrix

$\{q\}$ Normal coordinates defined by $\{X\} = [\Psi]\{q\}$

q_j	jth element of {q}
m_j, c_j, k_j	jth modal mass, damping, and stiffness
$F_i(t)$	Arbitrary external point force applied at i
F_i	Amplitude of $F_i \sin \omega t$
$m_{ik}^{(j)}, c_{ik}^{(j)}, k_{ik}^{(j)}$	Effective mass, damping, and stiffness for the i-k input-output path in the jth mode
θ_{ik}	Phase angle between response and input force for the i-k path
$\mu_{ik}^{(j)}$	Effective percent of critical damping in the jth mode
ω	Circular frequency
ω_j	jth resonant circular frequency
Units	Units used in this paper are lb, in., sec

THEORY

The starting point for the development of the identification technique of this paper is in the mechanics of lightly damped, linear systems. The class of structures for which the technique is proposed is assumed to possess the following, somewhat qualitative features that are stated in the form of assumptions and are basic to the ensuing development:

1. Light damping typical of a space vehicle with no damping specifically designed into the structure.

2. The modes of interest are sufficiently uncoupled in the velocity terms and separated in frequency so that a single degree-of-freedom analysis is adequate to represent the steady response above the half-power point in a mode of interest.

These basic assumptions are designed to imply that the steady response in each vibration mode of interest is not significantly affected by any other mode, and that each mode can be isolated and individually exploited as discussed in Refs. [1] through [4].

With the above assumptions as a background, the proposed identification technique and the supporting analytical arguments are now developed.

General

The equations of motion for the system may be written [5]

$$[M]\{\ddot{x}\} + [C]\{\dot{x}\} + [K]\{x\} = \{F(t)\} \qquad (1)$$

The transformation

$$\{X\} = [\Psi]\{q\} \qquad (2)$$

where

$$x_k = \sum_j \psi_k^{(j)} q_j \qquad (3)$$

is assumed to produce uncoupled equations in terms of the normal coordinates, q, so that

$$[\bar{M}]\{\ddot{q}\} + [\bar{C}]\{\dot{q}\} + [\bar{K}]\{q\} = [\Psi]^T\{F(t)\} \qquad (4)$$

where

$$[\bar{M}] = [\Psi]^T[M][\Psi]$$

$$[\bar{C}] = [\Psi]^T[C][\Psi]$$

$$[\bar{K}] = [\Psi]^T[K][\Psi]$$

The equation for the jth normal coordinate is

$$m_j\ddot{q}_j + c_j\dot{q}_j + k_j q_j = \sum_i \psi_i^{(j)} F_i(t). \qquad (5)$$

For only one external forcing function applied at i, Eq. (5) becomes

$$m_j\ddot{q}_j + c_j\dot{q}_j + k_j q_j = \psi_i^{(j)} F_i(t). \qquad (6)$$

Near Resonant Response

Equation (2) may be written

$$\{X\} = \sum_j \{\psi\}^{(j)} q_j$$

so that the response in the jth mode is

$$\{X\}^{(j)} = \{\psi\}^{(j)} q_j \qquad (7)$$

or

$$x_k^{(j)} = \psi_k^{(j)} q_j \qquad (8)$$

and

$$q_j = \frac{x_k^{(j)}}{\psi_k^{(j)}}. \qquad (9)$$

Substituting Eq. (9) into Eq. (6) and dividing by $\phi_i^{(j)}$,

$$\left(\frac{m_j}{\phi_i^{(j)} \tau_k^{(j)}}\right) \ddot{x}_k^{(j)} + \left(\frac{c_j}{\phi_i^{(j)} \tau_k^{(j)}}\right) \dot{x}_k^{(j)} + \left(\frac{k_j}{\phi_i^{(j)} \tau_k^{(j)}}\right) x_k^{(j)} = F_i(t) \quad (10)$$

or

$$m_{ik}^{(j)} \ddot{x}_k^{(j)} + c_{ik}^{(j)} \dot{x}_k^{(j)} + k_{ik}^{(j)} x_k^{(j)} = F_i(t) \quad (11)$$

The significance of Eq. (11) is that it represents the system dynamics for response at point k owing to forcing at point i. Also, the derivation of Eq. (11) has not placed any restrictions on the forcing function at i. $F_i(t)$ is, in fact, an arbitrary, external, point forcing function. When $F_i(t) = F_i \sin \omega t$ with $\omega = \omega_j$, only one equation of the form of Eq. (11) is required to represent the system response. It is upon this fact that the identification scheme is based.

Equating the coefficients of Eqs. (10) and (11), it is evident that

$$\left.\begin{aligned} m_j &= m_{ik}^{(j)} \phi_i^{(j)} \tau_k^{(j)} \\ c_j &= c_{ik}^{(j)} \phi_i^{(j)} \tau_k^{(j)} \\ k_j &= k_{ik}^{(j)} \phi_i^{(j)} \tau_k^{(j)} \end{aligned}\right\} \quad (12)$$

Setting i = k

$$m_j = m_{ii}^{(j)} \left[\phi_i^{(j)}\right]^2 \quad (13)$$

from which the modal amplitudes at i and k are found to be given by

$$\left.\begin{aligned} \phi_i^{(j)} &= \sqrt{\frac{m_j}{m_{ii}^{(j)}}} \\ \tau_k^{(j)} &= \frac{m_j}{m_{ik}^{(j)} \phi_i^{(j)}} \end{aligned}\right\} \quad (14)$$

The quantities m_j and $m_{ii}^{(j)}$ are defined to be positive, and hence $\phi_i^{(j)}$ is positive. A negative value for $\tau_k^{(j)}$ implies a negative $m_{ik}^{(j)}$ that is wholly consistent with the facts.

Solutions for m_{ik}, c_{ik}, and k_{ik}

The steady state or particular solution of Eq. (11) with $F_i(t) = F_i \sin \omega t$ is given by

$$x = X \sin (\omega t - \theta) \quad (15)$$

Substituting Eq. (15) into Eq. (11) and solving for the coefficients m_{ik}, c_{ik} and k_{ik} results in

$$k_{ik}^{(j)} = m_{ik}^{(j)} \omega^2 + \frac{F_i}{X_k} \cos \theta_{ik} \quad (16)$$

and

$$c_{ik}^{(j)} = \frac{F_i}{\omega X_k} \sin \theta_{ik} \quad (17)$$

If one set of values of ω, F_i, X_k, and θ_{ik} for Eq. (17) and two sets for Eq. (16) are known, the coefficients of Eq. (11) may be computed.

Response to Arbitrary Force

The total system response at k owing to any time dependent force $F_i(t)$ at i is found by superposition of the solutions of each of the set of the following equations:

$$\left.\begin{aligned} m_{ik}^{(1)} \ddot{x}_k^{(1)} + c_{ik}^{(1)} \dot{x}_k^{(1)} + k_{ik}^{(1)} x_k^{(1)} &= F_i(t) \\ \vdots \qquad\qquad \vdots \qquad\qquad \vdots \qquad\qquad &\vdots \\ m_{ik}^{(j)} \ddot{x}_k^{(j)} + c_{ik}^{(j)} \dot{x}_k^{(j)} + k_{ik}^{(j)} x_k^{(j)} &= F_i(t) \\ \vdots \qquad\qquad \vdots \qquad\qquad \vdots \qquad\qquad &\vdots \\ m_{ik}^{(p)} \ddot{x}_k^{(p)} + c_{ik}^{(p)} \dot{x}_k^{(p)} + k_{ik}^{(p)} x_k^{(p)} &= F_i(t) \end{aligned}\right\} \quad (18)$$

and is given using Eqs. (3) and (8) as

$$x_k = \sum_{j=1}^{p} x_k^{(j)}$$

EXPERIMENTAL PROCEDURE

The Langley 1/10-scale and 1/40-scale models of the Apollo/Saturn V launch vehicle are shown in Figs. 1 and 2, and the coordinate systems for both models are presented in Fig. 3. The 1/10-scale model is fully described in Ref. [6].

Fig. 1. 1/10-scale Apollo/Saturn V model

Fig. 2. 1/40-scale Apollo/Saturn V model

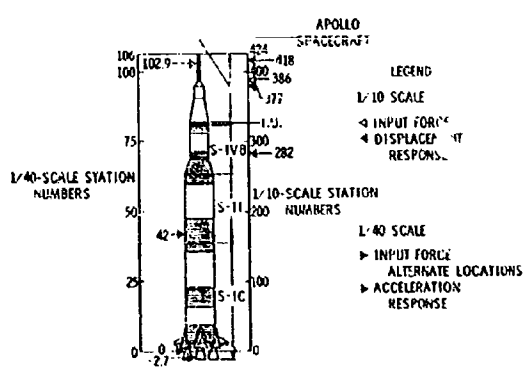

Fig. 3. Schematic of Apollo/Saturn V models

1/10-Scale Model

The 1/10-scale model was complete in the lift-off structural configuration, but was entirely empty of simulated propellants. The boundary conditions were cantilevered-free. A steady frequency, transverse, sinusoidally varying input force was applied in the pitch plane through a strain gage type force gage at station 386 and the displacements at stations 418 (the tip of the escape tower), 377, and 282 were measured using a contacting, cantilever, strain gage beam. The strain gage displacement transducers had natural frequencies in the order of 60 Hz and were used within their flat response regime. The signals from the force and the displacement transducers were processed through a balancing bridge, differential amplifier, dc isolation amplifier and were then recorded together with the calibration signals on an FM analog tape recorder. The selection of both strain gage force and displacement transducers with both signals processed through identical electronics was to assure the accurate determination of phase angle, θ_{1k}, for use in Eqs. (16) and (17).

1/40-Scale Model

The 1/40-scale model was also complete in the lift-off structural configuration. Propellant loading corresponded to first-stage burnout and the boundary conditions simulated were free-free. Steady frequency transverse, sinusoidally varying input force was applied in the

pitch plane, through a crystal type force gage, alternately at stations 0 and 42, and the acceleration responses were measured at model stations 102.9 and -2.7. The crystal transducers were used with this model to evaluate the quality of data produced by the two different instrumentation schemes. The signals from the force gage and accelerometers were processed through similar conditioning equipment to minimize relative phase shift and, together with calibration signals, were recorded on tape.

Data Reduction

The experimental analog data were digitally filtered using a 24-point per cycle Fourier analysis, from which the numerical amplitudes of the fundamental components of the input force and of the displacement and acceleration responses and the input-response phase angles, θ_{ik}, were computed.

IDENTIFICATION PROCEDURE

System Equations

For convenience, Eqs. (18) were written as

$$\left.\begin{aligned} \ddot{x}_k^{(1)} + 2\mu_{ik}^{(1)}\omega_1\dot{x}_k^{(1)} + \omega_1^2 x_k^{(1)} &= \frac{1}{m_{ik}^{(1)}} F_i(t) \\ \vdots \quad\quad \vdots \quad\quad \vdots \quad\quad \vdots \\ \ddot{x}_k^{(p)} + 2\mu_{ik}^{(p)}\omega_p\dot{x}_k^{(p)} + \omega_p^2 x_k^{(p)} &= \frac{1}{m_{ik}^{(p)}} F_i(t) \end{aligned}\right\} \quad (19)$$

and

$$x_k = \sum_{j=1}^{p} x_k^{(j)} \quad (20)$$

Computer Experiments

A controlled computer experiment was conducted in which an exact numerical solution of Eqs. (19) and (20) was generated for an assumed set of typical coefficients. The solution was then corrupted and the coefficients $m_{ik}^{(j)}$, $c_{ik}^{(j)}$, and $k_{ik}^{(j)}$ were computed using Eqs. (16) and (17). The results indicated that errors of up to ±10 percent in F_i/X_k, and ±10 degrees in θ_{ik} can be tolerated by this identifier when applied to systems that satisfy the basic assumptions of this paper. As it was felt that the accuracy of the experimental data fell within these limits, identification of the 1/10-scale and 1/40-scale models was attempted.

Solution for Coefficients

The digitized experimental data, F_i, x_k or $\ddot{x}_k$, θ_{ik} corresponding to a near resonant value of ω were used to determine the values of $m_{ik}^{(j)}$, $c_{ik}^{(j)}$, $k_{ik}^{(j)}$ for each significant mode for each of the selected input-response paths for each model. Four or five frequencies near each resonance were used. The value of $c_{ik}^{(j)}$ for each point was computed using Eq. (17). The values of $m_{ik}^{(j)}$ and $k_{ik}^{(j)}$ were determined by solving Eq. (16) as a pair of simultaneous equations for slightly different near-resonant values of ω. The average value of effective mass, damping, and stiffness for each mode was then determined. Typical first-mode values for station 377 response of the 1/10-scale model are as shown at top of page 28.

The sign of $m_{ik}^{(j)}$ computed using Eq. (16) was very simply verified. The sign was taken to be positive if $\varphi_k^{(j)}$ was in phase (approximately 0 degrees) with $\varphi_i^{(j)}$ and negative if $\varphi_k^{(j)}$ was out of phase (approximately 180 degrees) with $\varphi_i^{(j)}$. The identification results for both models are listed as coefficients of Eq. (19) in Tables 1 and 2.

RESULTS

Comparisons of the identification and experimental frequency responses for the two models are presented in Figs. 4 through 10.

1/10-Scale Results

The results for the 1/10-scale model are shown in Figs. 4 through 6, plotted as the response ratio $|X_k/F_i|$ vs frequency. The particular solutions of Eqs. (19) were obtained for $F_i(t) = \sin \omega t$, i = station 308, for $0 \leq \omega/2\pi \leq 30$ using the coefficients listed in Table 1. The frequency response at stations 418, 377, and 282 were then obtained using Eq. (20). For example,

$$x_{418} = x_{418}^{(1)} + x_{418}^{(2)} + x_{418}^{(3)} .$$

1/40-Scale Results

The results for the 1/40-scale model are shown in Figs. 7 through 10. The frequency

Frequencies		Coefficients of Equations					
f	ω	$m_{ik}^{(i)}$	$c_{ik}^{(i)}$	$k_{ik}^{(i)}$	$2\mu_{ik}\omega_i = \frac{c_{ik}^{(i)}}{m_{ik}^{(i)}}$	$\omega_i^2 = \frac{k_{ik}^{(i)}}{m_{ik}^{(i)}}$	$\frac{1}{m_{ik}^{(i)}}$
4.52	28.39	0.3479	0.1468	304.9	0.4191	876.4	2.87
4.72	29.64	0.3381	0.1615	296.2	0.4777	876.7	2.96
4.99	31.34	0.3311	0.1611	290.1	0.4866	876.2	3.02

TABLE 1
Identified Values of the Coefficients of Eq. (19)
for 1/10-Scale Model
(All Stages Empty, Cantilevered-Free)

Station, k	418			377		282	
Mode, j	1	2	3	1	2	1	2
$2\mu_{ik}^{(j)}\omega_j$	0.472	4.19	15.4	0.477	3.40	0.479	2.85
ω_j^2	877	9240	28,360	876	8860	877	9350
$1/m_{ik}^{(j)}$	3.89	9.01	-4.85	2.95	2.30	1.39	-1.93

TABLE 2
Identified Values of the Coefficients of Eq. (19)
for 1/40-Scale Model
(First Stage Empty, Free-Free)

Force at Station 0						
Station, k	102.9			-2.7		
Mode, j	1	2	3	1	2	3
$2\mu_{ik}^{(j)}\omega_j$	4.09	6.76	13.90	2.76	5.20	60.0
ω_j^2	68,900	288,000	683,000	69,000	288,000	680,000
$1/m_{ik}^{(j)}$	39.0	-28.8	10.1	6.87	3.24	10.2

Force at Station 42								
Station, k	102.9				-2.7			
Mode, j	1	2	3	4	1	2	3	4
$2\mu_{ik}^{(j)}\omega_j$	3.14	4.54	13.71	26.25	4.2	2.68	30.60	20.12
ω_j^2	69,530	289,300	681,160	929,870	69,700	287,100	691,650	933,400
$1/m_{ik}^{(j)}$	-10.1	16.2	-12.2	-11.7	-2.82	-2.25	-1.37	-9.00

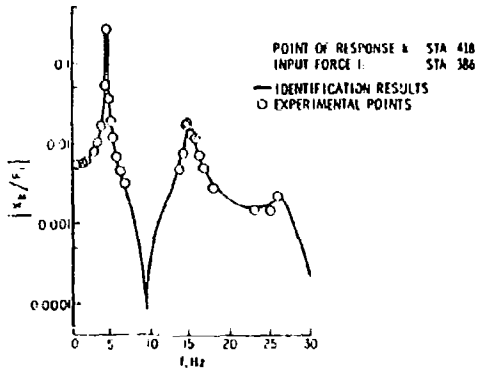

Fig 4. Comparison of identification results with experimental frequency response for 1/10-scale model

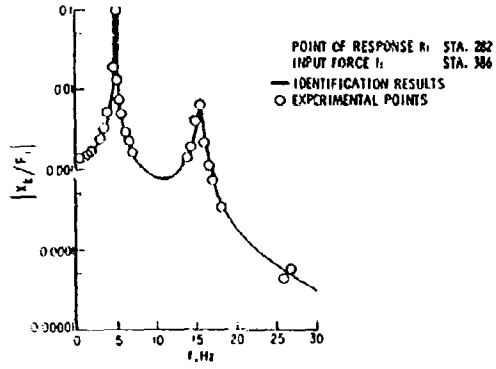

Fig. 6. Comparison of identification results with experimental frequency response for 1/10-scale model

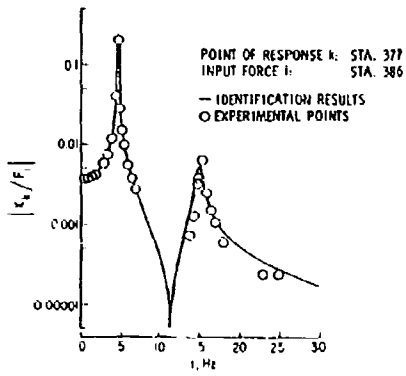

Fig. 5. Comparison of identification results with experimental frequency response for 1/10-scale model

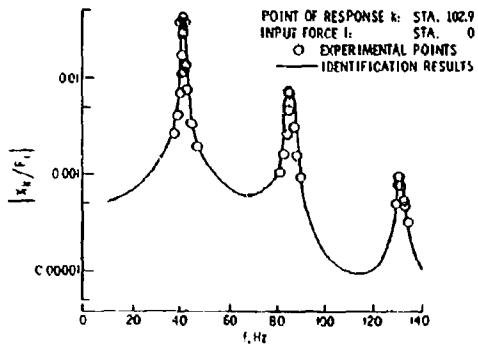

Fig. 7. Comparison of identification results with experimental frequency response for 1/40-scale model

response solutions for forcing first at station 0 and then at station 42 were computed using Eqs. (19) and (20) and the coefficients given in Table 2. For example, for response at station 102.9 owing to forcing at station 42

$$\ddot{x}^{(1)}_{102.9} + 3.14\dot{x}^{(1)}_{102.9} + 69.530x^{(1)}_{102.9} = -10.1 \sin \omega t$$

$$\ddot{x}^{(2)}_{102.9} + 4.54\dot{x}^{(2)}_{102.9} + 289.300x^{(2)}_{102.9} = 16.2 \sin \omega t$$

$$\ddot{x}^{(3)}_{102.9} + 13.71\dot{x}^{(3)}_{102.9} + 681.160x^{(3)}_{102.9} = -12.2 \sin \omega t$$

$$\ddot{x}^{(4)}_{102.9} + 26.25\dot{x}^{(4)}_{102.9} + 929.870x^{(4)}_{102.9} = -11.7 \sin \omega t$$

and

$$x_{102.9} = x^{(1)}_{102.9} + x^{(2)}_{102.9} + x^{(3)}_{102.9} + x^{(4)}_{102.9} .$$

Considerations

The identification results for both models agree quite favorably with the experimental response data. In addition, the associated phase angles

$$\frac{X_k}{F_i} ,$$

also agree, usually to within 5 to 10 degrees.

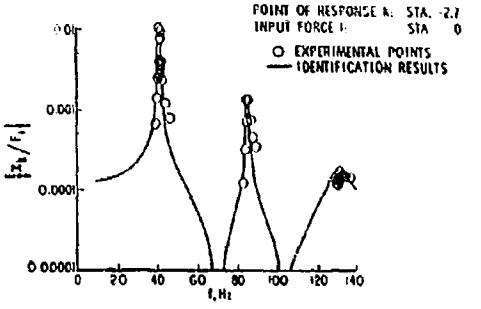

Fig. 8. Comparison of identification results with experimental frequency response for 1/40-scale model

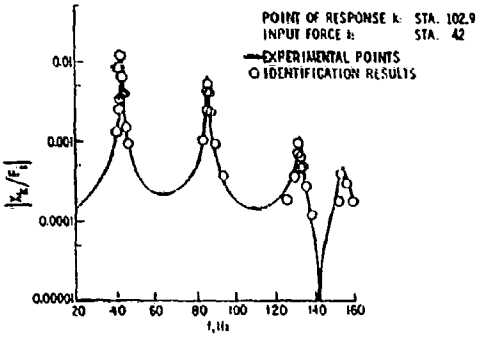

Fig. 9. Comparison of identification results with experimental frequency response for 1/40-scale model

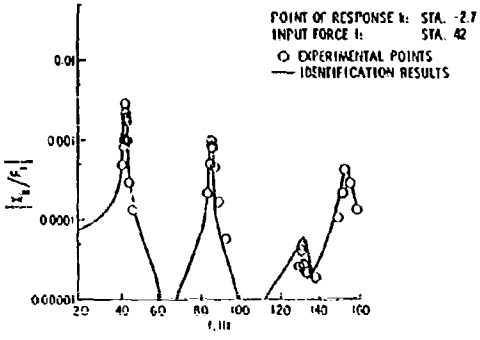

Fig. 10. Comparison of identification results with experimental frequency response for 1/40-scale model

Therefore, it is felt, for both models and for the input-response paths investigated, that systems of equations suitable for computing the response to an arbitrary forcing function have been obtained.

In this connection, the uniqueness of the identified equations has not been rigorously established. It is felt, however, that amplitude agreement as shown in Figs. 4 through 10, together with phase agreement to within 5 to 10 degrees, constitutes sufficient conditions for a system identification adequate for all engineering purposes. The experience thus far also indicates, for the class of systems considered in this paper, that an identifier based on requiring coincidence of frequency response amplitudes only, without regard to phase, will produce basically the same results as if phase information were employed. This fact can be useful, because in general, some obvious small adjustments of the identified parameters to give better results based on amplitude comparison are usually possible. As presented, Figs. 4 through 10 indicate the results that were achieved using the method of this paper without iteration. However, parameters were easily selected to produce perfect coincidence of the amplitude plots of both Figs. 8 and 10, for example. The phase differences were negligible. Therefore, it is felt that refinement of the identified equations to produce perfect amplitude agreement is permissible, if not desirable.

The advantages of using the approach of this paper are that a detailed structural idealization and associated analytical model is not required. The modes that actually contributed to the response were immediately identified as the only ones observable for a given input response path. This obviated the usual concern over the problem of including all of the significant vibratory modes of the structures.

Once the equations of motion for a structure have been identified, the transient response to an arbitrary force can be computed with confidence. In this connection, rigid body modes, if required, can be calculated from model drawings, or experimentally determined. Results thus far of transient tests with the 1/40-scale model have produced excellent agreement between the acceleration response computed, using the identified equations, and the experimental transient acceleration responses. For example, a comparison of identification and experimental transient acceleration and displacement responses for the 1/40-scale model is shown in Fig. 11(a) and (b). The coefficients used in computing the acceleration

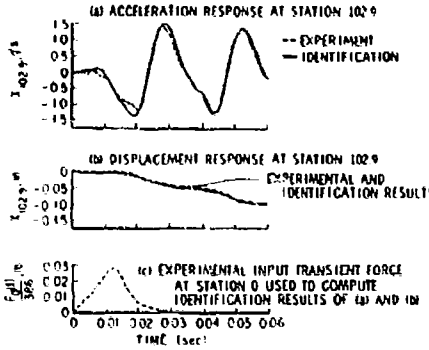

Fig. 11. Comparison of identification and experimental transient response for 1/40-scale model

response as predicted using the system identification results are given in Table 2 for i = 0 and k = 102.9 (see Fig. 7). In addition, the two rigid body modes required for this free-free system were included; this resulted in five equations of motion that were integrated using the measured values of the transient input shown in Fig. 11(c) which was applied at station 0 of the model. The identified equations predict transient acceleration and displacement responses, at station 102.9, that are in good agreement with the experimentally determined response. The results of Fig. 11 are especially important because they demonstrate the ability of the identified equations to predict accurately the response to an input of a different character than was used for their derivation.

CONCLUSIONS

A technique for determining the equations of motion of a complex structure has been presented. Both the number of the essential degrees of freedom and the coefficients of the equations are determined by the procedure, which is applicable to a large class of aerospace and other structures. The procedure requires that good quality experimental frequency response data be obtained for the significant resonances associated with specified input response paths.

For the class of structures considered in this paper, it is felt that coincidence of the identified and experimental frequency response amplitudes constitutes a sufficient condition for a satisfactory identification. This hypothesis, if true, suggests that refinement of the initial identification results to produce perfect amplitude agreement is desirable and may be useful in the formulation of an identifier that does not require explicit experimental phase information.

It is believed that this identification procedure should be advantageous when the dynamical equations of motion for an existing structure are desired. For example, if the available resources are not sufficient to allow the formulation and verification of a detailed analytical model of an existing structure, or if only sinusoidal test equipment is available but transient response data are required, the procedure discussed in this paper may be very useful. In particular, the identified equations were shown to adequately predict the system acceleration response to an arbitrary transient force.

REFERENCES

1. R. Plunkett, "Semi-Graphical Method for Plotting Vibration Response Curves," Proc. 2nd U.S. Cong. Appl. Mech., 1954, pp. 121-126

2. R. P. Thorn, and A. H. Church, "Simplified Vibration Analysis by Mobility and Impedance Methods," reprinted from Machine Design (The Penton Publishing Co.), 1960

3. J. P. Raney, "Analog Computer Solution for Transverse Vibrations of a Uniform Beam with Damped, Flexible, Massive End Restraints," Developments in Theoretical and Applied Mechanics, 1 (Plenum Press), 1963

4. J. T. Howlett, and J. P. Raney, "New Approach for Evaluating Transient Loads for Environmental Testing of Spacecraft," The Shock and Vibration Bull., 36, Pt. 2, Jan. 1967, pp. 97-105

5. T. K. Caughey, and M. E. J. O'Kelley, "Classical Normal Modes in Damped Linear Systems," J. Appl. Mech., 32, Series E (3):583-588, Sept. 1965

6. S. A. Leadbetter, H. Leonard, and E. Brock, Jr., "Design and Fabrication Considerations for a 1/10-Scale Replica Model of the Apollo/Saturn V," NASA TN D-4138, 1967

DISCUSSION

F. Kozin (Midwest Applied Science Corp.): You mentioned that mathematical models are not required; yet you do have the linear equations, so there is some structure being assumed in the actual identification procedure. Exactly what data were taken? Were only acceleration data taken, or were displacement and velocity data taken as well?

Mr. Raney: The answer to the first question is essentially my terminology vs someone elses. When I say no analysis, what I really mean is that the step of taking the drawings of the model and breaking them up into a 1000-degree-of-freedom finite element model, and that type of thing, has been bypassed. So we assume we know quite a bit about the structure. As to the other question, the only things that were measured were the three quantities that I indicated. The phase was not measured. Forces and accelerations were measured. These were recorded on FM tape, digitized, and filtered with a 24-ordinate-per-cycle Fourier system. We looked at all the harmonics as well to be sure we were getting good sinusoidal data. We used only the fundamental of the force and the acceleration response which was all we needed because that was 99.9 percent of what we had. We then determined the phase between those two by numerical means — zero crossing and that type of thing. We had the data all digitized and actually computed the phase without measuring it explicitly. That was the data on which we operated.

M. J. Baruch (Kollsman Instrument Corp.): I notice you had the classical equation of motion which involved K, C, and M. How did you arrive at these coefficients for your equations? Were these modal quantities, modal mass, modal spring constants, or modal damping? I know you had to feed the response back into the equation to add these coefficients. Would you clarify this if possible?

Mr. Raney: It is, I think, totally clarified in the paper. I would characterize these coefficients, as I use them, as effective mass, stiffness, and damping for the particular mode and the particular transmission path. I do not determine modal mass nor have I determined a diagonal mass matrix in terms of modal masses. I have determined an effective mass for a given transmission path for a given mode. That is what those coefficients turn out to be and it is explained more fully in the paper.

Mr. Forkois (NRL): Can you tell us something about the structural and material simulation of your models?

Mr. Raney: If I understand your question correctly, that was not important in this talk. It is a 1/10th-scale replica model of the Apollo/Saturn V launch vehicle. It was originally built for Langley for research related to the Saturn V/Apollo program and not for the program on which my paper is based.

G. C. C. Smith (Bell Aerosystems): Would you agree that the success of the method depends entirely on having well-separated, lightly damped modes?

Mr. Raney: Well, that is the type of system on which it has been successfully used. On the other hand, until I try it in more complicated situations, I do not believe I would like to say that I would agree with that particular proposition. We have evidence that we could deal with systems that behave in a more complex fashion than the system described here; however, I do not want to indicate that I am competing with modal density people where they are up in the very high-frequency ranges either.

R. M. Mains (Wash. Univ.): I would like to say, by way of information, that in exploring this kind of process analytically I did a 24-degree-of-freedom system using all the computed responses. The modes were not all lightly damped and not all well separated. I was able to calculate backwards to get K, C, and M with agreement to around seven figures. It works fine. How well it will work when the data are experimental, I do not know.

Mr. Raney: Having this reference would be very helpful. When I was doing this work it seemed fairly simple to me, but I could find no references where people had actually used experimental data and done very nearly what I presented here. System identification is what you want to make it. It works where it works, and that is it.

* * *

PROPAGATION OF LONGITUDINAL STRESS WAVES IN A COMPLEX BAR-TYPE STRUCTURE

David L. Block
Martin Marietta Corporation
Orlando, Florida

This paper presents results of an analytical investigation on the propagation of longitudinal stress waves in a complex bar-type structure. The analytical investigation presented is simple in concept and yields a procedure for calculating the longitudinal response of a structure which is impact or shock loaded and that can be modeled by a rotationally symmetric nonuniform bar with attached nonstructural masses. An example of such a structure is a missile configuration. Equations are derived for the transmission and reflection of stress waves through elements that account for gradual changes and discontinuities in area and material and that account for rigidly attached masses. The effect of nonelastic waves and wave attenuation is also considered. From the developed equations, the response of the structure at a particular position may be calculated by superimposing the effects of the responses of the various elements at proper time instances. Calculations illustrating the developed procedures are presented for the longitudinal response of a missile configuration excited by a velocity shock. Calculated accelerations are compared with measured acceleration data from a missile configuration and exhibit good agreement considering the complexity of the structure.

INTRODUCTION

To investigate and design structures that are to withstand shock and impact loadings, a theoretical approach is needed that will account for the complexities of the actual structure and yet be simple in concept and procedure. For a structure such as a missile configuration, a configuration with a longitudinal dimension large in comparison with the other two dimensions, a realistic model may be formulated by considering longitudinal responses only. For this type of response two theoretical models may be employed: a lumped parameter type model, or a continuous type model such as a bar or beam. The lumped parameter model can be made to approximate the actual structure by using as many spring and mass parameters as needed [1-3], but this representation is limited in frequency content owing to the necessity of using a finite number of springs and masses in the model. Consequently, the spring mass model is not desirable for obtaining responses owing to stress waves. To obtain the proper wave responses and frequency content a continuous type model is needed.

Therefore, the purpose of this paper is to present a theoretical investigation using a continuous model on propagation of longitudinal stress waves owing to an impact or shock loading in a rotationally symmetric nonuniform bar with attached nonstructural masses. The response at any position is calculated by using the simple concept of a building block technique that superimposes the responses at the proper time instant of the various elements that account for the complexity of the actual structure. Equations are derived for the transmission and reflection of the stress waves through elements which account for gradual changes and discontinuities in area, material, and mass of the bar. The equations for discontinuities and gradual changes in area and material have been previously presented [4-6] and are presented here for completeness; however, the effect of attached nonstructural masses has not been previously considered and allows for the calculation of accelerations. Nonelastic waves and wave attenuation effects are also considered.

Calculations of dynamic response illustrating the developed procedures are presented for a missile configuration that is loaded owing to a velocity shock. Experimental acceleration data are compared with calculated accelerations to evaluate the theoretical results.

NOMENCLATURE

A	Cross sectional area of bar
E	Modulus of elasticity
E_p	Modulus of elasticity for stress after yield stress (see Fig. 3)
N	Nonstructural attached mass
V	Magnitude of step velocity
a	Particle acceleration
c	Velocity of propagation of longitudinal elastic wave, $\sqrt{E/\rho}$
c_p	Velocity of propagation of longitudinal nonelastic wave, $\sqrt{E_p/\rho}$
n	Integer
t	Time
v	Particle velocity
x	Distance wave travels (see Eq. (22))
α, β	Constants defined by Eq. (11)
ρ	Mass density of bar
γ	Internal friction damping factor (see Eq. (22))
σ	Longitudinal stress
σ_y	Yield stress
$U(t - t_0)$	Step function defined by Eq. (13)
Δt	Time increment

Subscripts

i	Incident wave
r	Reflected wave
t	Transmitted wave
$1, 2, 3, \ldots, n$	Integers referring to section of bar (see Fig. 1) or velocity steps (see Fig. 2)

DEVELOPMENT OF BASIC EQUATIONS

To develop the basic equations for the propagation of longitudinal stress waves in a rotationally symmetric nonuniform bar with attached nonstructural masses, the equations governing wave propagation in simple structural elements are derived and used to replace the complex structure by a series of equivalent simple elements and by superimposing their effects. The assumptions to develop the governing equations are: The loading is symmetric about the centerline of the bar; the only waves are plane waves; and the response of each wave is independent of effects of other waves on linear responses so that the principle of superposition is applicable. The elements that are used to represent the complex structure are shown in Fig. 1. These elements will account for discontinuities in area or material, gradual changes in area or material, and attached nonstructural masses, and by suitable combination will represent the considered structure.

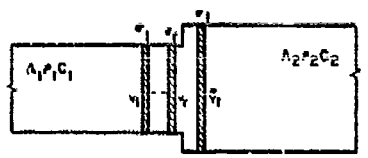

(a) DISCONTINUITY IN AREA AND MATERIAL

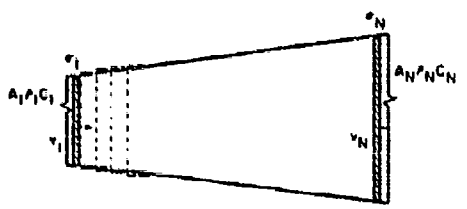

(b) GRADUAL CHANGE IN AREA AND MATERIAL

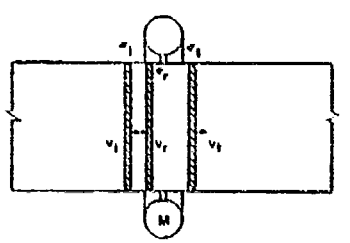

(c) RIGIDLY ATTACHED NONSTRUCTURAL MASS

Fig. 1. Typical structural elements

To derive the relations governing the transmission and reflection of waves in the elements of Fig. 1, the relationship between stress and particle velocity is required. Using the uniform bar solution for a wave traveling in

one direction (one-dimensional wave equation solution) and the one-dimensional stress-strain and displacement-velocity relations, the following equation may be derived [4-6]:

$$\sigma = \rho c v \tag{1}$$

where σ is the longitudinal stress, ρ is the mass density, c is the wave propagation velocity, and v is the particle velocity. Equation (1) gives the relation between stress and velocity and is often referred to as the mechanical counterpart of Ohm's law. Relations may now be obtained for each of the elements of Fig. 1 by using fundamental force equilibrium and displacement compatibility concepts.

Consider first what happens to a wave traveling in a uniform bar that encounters a discontinuity in area and/or material as shown in Fig. 1(a). At the discontinuity there will be transmitted and reflected waves as illustrated in Fig. 1(a). Note that for the sign convention of Fig. 1, the particle velocity and wave velocity are assumed in the same direction. Equality of the forces at the discontinuity gives

$$A_1(\sigma_i + \sigma_r) = A_2\sigma_t . \tag{2}$$

and equality of the particle velocities at the discontinuity gives

$$v_i - v_r = v_t \tag{3}$$

where the subscripts i, r, and t refer to the incident, reflected, and transmitted waves, respectively, and A_1 and A_2 are the areas of the two bars. Equations (2) and (3) are approximate as the stresses and velocities are, in general, not uniformly distributed over the cross-section areas and are valid only for small changes in area. By combining Eqs. (1), (2), and (3), the particle velocity of the transmitted and reflected waves can be determined as

$$v_t = \frac{2A_1\rho_1 c_1}{A_2\rho_2 c_2 + A_1\rho_1 c_1} v_i \tag{4}$$

$$v_r = \frac{A_2\rho_2 c_2 - A_1\rho_1 c_1}{A_2\rho_2 c_2 + A_1\rho_1 c_1} v_i . \tag{5}$$

The corresponding transmitted and reflected stresses are determined from Eq. (1).

Consider next what happens to a traveling wave if there is a gradual change in area and/or material of the bar as shown in Fig. 1(b). For this case assume that the change from one end to the other is brought about in a series of n successive steps as shown by the dashed lines in Fig. 1(b), and that at each of the steps there is no reflected wave. Using Eq. (4), the transmitted particle velocity through the first step is

$$v_2 = \frac{2A_1\rho_1 c_1}{A_2\rho_2 c_2 + A_1\rho_1 c_1} v_1$$

where v_1 is the incident particle velocity at section 1. Similarly, through the proceeding sections

$$v_3 = \frac{2A_2\rho_2 c_2}{A_3\rho_3 c_3 + A_2\rho_2 c_2} v_2$$

$$v_4 = \frac{2A_3\rho_3 c_3}{A_4\rho_4 c_4 + A_3\rho_3 c_3} v_3$$

$$\vdots$$

$$v_n = \frac{2A_{n-1}\rho_{n-1} c_{n-1}}{A_n\rho_n c_n + A_{n-1}\rho_{n-1} c_{n-1}} v_{n-1} .$$

Combining the above equations gives the following:

$$v_n = \frac{\dfrac{A_1\rho_1 c_1}{A_n\rho_n c_n} v_1}{\left(\frac{1}{2} + \frac{1}{2}\frac{A_{n-1}\rho_{n-1}c_{n-1}}{A_n\rho_n c_n}\right) \cdots \left(\frac{1}{2} + \frac{1}{2}\frac{A_2\rho_2 c_2}{A_3\rho_3 c_3}\right)\left(\frac{1}{2} + \frac{1}{2}\frac{A_1\rho_1 c_1}{A_2\rho_2 c_2}\right)} \tag{6}$$

Now, letting the number of steps n become infinite, the denominator of Eq. (6) (for details see Ref. [4]) is reduced to

$$\lim_{n\to\infty}\left(\frac{1}{2} + \frac{1}{2}\frac{A_{n-1}\rho_{n-1}c_{n-1}}{A_n\rho_n c_n}\right) \cdots \left(\frac{1}{2} + \frac{1}{2}\frac{A_2\rho_2 c_2}{A_3\rho_3 c_3}\right) \cdot \left(\frac{1}{2} + \frac{1}{2}\frac{A_1\rho_1 c_1}{A_2\rho_2 c_2}\right) = \sqrt{\frac{A_1\rho_1 c_1}{A_n\rho_n c_n}} . \tag{7}$$

From Eqs. (6) and (7), the equation relating the particle velocity v_1 incident at one end to an element with a gradual change in area or material and the particle velocity v_n transmitted at the other end is

$$v_n = \sqrt{\frac{A_1\rho_1 c_1}{A_n\rho_n c_n}}\, v_1 . \tag{8}$$

Again the stresses may be obtained from Eq. (1). Note that if the gradual change is one of area only, Eq. (8) predicts that the velocity or stress of the wave will vary inversely as the linear dimension of the area. Note also that

the total energy of the wave does not change as it passes through the section.

Consider finally what happens to a traveling wave that is incident to a section that has an attached nonstructural mass as shown in Fig. 1(c). In Fig. 1(c), the mass is shown attached to a uniform element; however, the relations developed below consider the element to have also a discontinuity in area and material at the point of the attached mass. The attached mass is assumed rotationally symmetric, located at a point, and rigidly attached. The rigid attachment allows no relative motion of the mass with respect to the bar. At the point of the attached mass, equality of forces gives

$$A_1(\sigma_i + \sigma_r) = A_2\sigma_t + M\frac{dv_t}{dt} \qquad (9)$$

where M is the total mass, v_t is the transmitted particle velocity, and t is the time. Equation (9) is equivalent to Eq. (2) except for the addition of the mass times acceleration term. Equality of particle velocities gives Eq. (3), and then substitution of Eqs. (1) and (3) into (9) gives the following differential equation governing the transmitted particle velocity:

$$\frac{dv_t(t)}{dt} + \beta v_t(t) = \alpha v_i(t) \qquad (10)$$

where v_i is the incident particle velocity at the attached mass and

$$\beta = \frac{A_1\rho_1c_1 + A_2\rho_2c_2}{M}$$
$$\alpha = \frac{2A_1\rho_1c_1}{M} \qquad (11)$$

Note that the solution of Eq. (10) for the transmitted velocity v_t will be a function of the shape with respect to time of the incident velocity v_i. As the shape of the incident velocity v_i may change with respect to time and as the exact shape may become very complex to describe, an analytical solution of Eq. (10) cannot be obtained for all cases. However, approximate solutions may be obtained in the following manner.

Assume first that the incident particle velocity at the attached mass is in the form of a step velocity at time t_0 as shown by the solid line in Fig. 2(a). This incident velocity can be expressed mathematically as

$$v_i(t) = V_0\,U(t - t_0) \qquad (12)$$

where V_0 is the magnitude of the velocity and $U(t - t_0)$ is a step function defined as

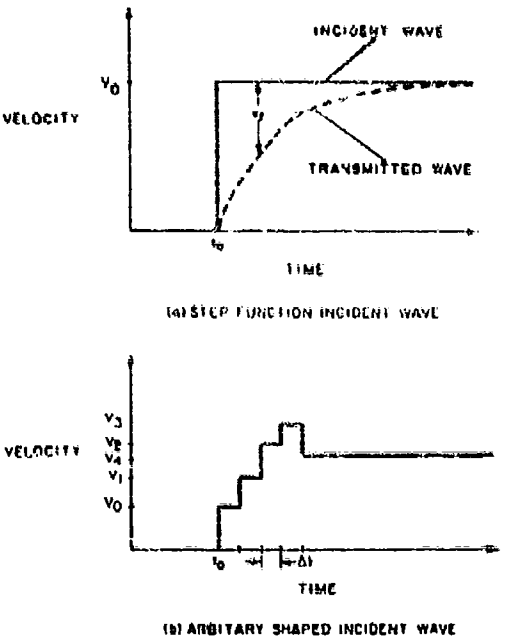

Fig. 2. Incident waveforms at attached nonstructural masses

$$U(t - t_0) = 0 \quad \text{if} \quad t < t_0$$
$$= 1 \quad \text{if} \quad t \geq t_0 \qquad (13)$$

Substituting the incident velocity given by Eq. (12), Eq. (10) can be solved by Laplace transform methods to give, for the transmitted velocity v_t,

$$v_t(t) = \frac{\alpha}{\beta}V_0\left[1 - e^{-\beta(t - t_0)}\right] \quad (t \geq t_0) \qquad (14)$$

and for the transmitted acceleration

$$a_t = \frac{dv_t}{dt}$$
$$a_t(t) = \alpha V_0 e^{-\beta(t - t_0)}\,U(t - t_0) \qquad (15)$$

The reflected velocity is determined from Eq. (3), and the corresponding stresses are determined from Eq. (1). The reflected acceleration is determined by differentiating Eq. (3) and solving. Thus, from Eq. (3)

$$a_r = a_i - a_t \qquad (16)$$

where a_i is the incident acceleration and a_t is the transmitted acceleration. For the case of

the step velocity, the incident acceleration is zero (except at time t_0), and the reflected acceleration equals the negative of the transmitted acceleration. The value of the incident acceleration at time t_0 may be neglected for the type of responses considered here by physical considerations.

If for a bar with an attached mass there is no discontinuity in area or material of the bar ($A_1\rho_1c_1 = A_2\rho_2c_2$), then α equals β, and the solution for the transmitted velocity, Eq. (14), is in a form as shown by the dashed line in Fig. 2(a). Note in Fig. 2(a) and in Eq. (14) that in the limit as t becomes large the transmitted velocity approaches the incident velocity and the reflected velocity approaches zero. If α does not equal β (there is a discontinuity in area or material), the transmitted and reflected velocities approach the values given by Eqs. (4) and (5).

Using the above results, an approximation can be derived for the case where the incident wave has an arbitrary shape as a function of time. An arbitrary shaped incident wave would occur in waves that are produced by variable input forces or by waves that have passed attached masses. To obtain the relations for a wave passing an attached mass, assume that the incident velocity can be approximated by a series of successive velocity step functions separated by equal time increments Δt, as shown in Fig. 2(b). For this representation, the incident velocity v_i can be expressed mathematically as

$$v_i(t) = V_0 U(t - t_0) + (V_1 - V_0) U\left[t - (t_0 + \Delta t)\right] + (V_2 - V_1) U\left[t - (t_0 + 2\Delta t)\right] + \quad (17)$$

where the V's are the magnitudes of the velocities at each time increment and $U(\ )$'s are unit step functions as defined by Eq. (13). The representation of the velocity by Eq. (17) can be made as accurate as needed by taking Δt small. Substituting Eq. (17) for the incident velocity in Eq. (10) and again solving Eq. (10) by Laplace transform methods gives the following for the transmitted velocity:

$$v_t(t) = \frac{\alpha}{\beta}\left[V_0\left(1 - e^{-\beta(t - t_0)}\right) U(t - t_0) + (V_1 - V_0)\left(1 - e^{-\beta(t - t_0 - \Delta t)}\right) U(t - t_0 - \Delta t) + \cdots\right] \quad (18)$$

and for the transmitted acceleration:

$$a_t(t) = \alpha\left[V_0 e^{-\beta(t - t_0)} U(t - t_0) + (V_1 - V_0) e^{-\beta(t - t_0 - \Delta t)} U(t - t_0 - \Delta t) + \cdots\right] . \quad (19)$$

In general, Eqs. (18) and (19) are tedious to evaluate at any time instant. Therefore, recurrence equations were derived that allowed Eqs. (18) and (19) to be evaluated at each time increment Δt from the initial time t_0. The recurrence equations were obtained by evaluating Eqs. (18) and (19) at each time increment and combining the results. Thus, the following recurrence equations are obtained for the transmitted velocity:

$$v_t\left(t_0 + (n+1)\Delta t\right) = \frac{\alpha}{\beta} V_n\left(1 - e^{-\beta\Delta t}\right) + e^{-\beta\Delta t} v_t(t_0 + n\Delta t) \quad (20)$$

and for the transmitted acceleration,

$$a_t\left(t_0 + (n+1)\Delta t\right) = \alpha(V_{n+1} - V_n) + e^{-\beta\Delta t} a_t(t_0 + n\Delta t) \quad (21)$$

where

$$n = 0, 1, 2, 3, \ldots$$

$$v_t(t_0) = 0$$

$$a_t(t_0) = \alpha V_0$$

Equations (20) and (21) give the transmitted particle velocity and acceleration at the point of an attached mass for any time instant from the prior time instant and beginning at time t_0. Equations (1), (3), and (16) are used to calculate the stresses, reflected particle velocity, and reflected particle acceleration, respectively. Equations (20) and (21) are ideally suited for computer computation; therefore, for the calculations presented here, a computer was used to calculate the numerical values of these equations. The accuracy of Eqs. (20) and (21) was examined by making an example calculation in which the exact form of the transmitted velocity and acceleration was known and compared with the values calculated using Eqs. (20) and (21). This comparison resulted in negligible differences between the exact and the approximate values as long as Δt was taken significantly small.

The effect of nonelastic waves may also be considered and included in the present analysis

in a straightforward manner. For an elastic wave the velocity of the wavefront in the material is a constant ($c = \sqrt{E/\rho}$), and the stress is directly proportional to the particle velocity v (Eq. (1)). For an elastic wave, the wavefront does not change with time except when passing an attached mass or if the wave is produced by a variable force input. For a nonelastic wave, the situation is different because the wavefront changes with time. However, a nonelastic wave may be used in the present analysis by the following approximate procedure. Assume that the nonelastic stress-strain relationship can be represented by two straight lines as shown in Fig. 3(a). Straight lines would not have to be used for the nonelastic stress-strain relationship; however, other relationships would complicate the procedure of superimposing the wave effects. For the stress-strain relationship of Fig. 3(a), the first part up to the yield stress is linear and elastic ($\sigma = E\epsilon$ for $\sigma < \sigma_y$), and the second part, after the yield stress, is again linear and related to strain by a reduced modulus denoted E_p ($\sigma = E_p\epsilon + \sigma_y$ for $\sigma > \sigma_y$). For a stress less than or equal to the yield stress, the velocity of the wavefront is constant and is the elastic wave velocity c. Once the stress is greater than yield stress, the velocity of the wavefront is not constant, but may be represented by superimposing the nonelastic wave velocity ($c_p = \sqrt{E_p/\rho}$) on the elastic wave. Thus, the nonelastic wave moves with two velocities that cause a gap, which increases with time, between the elastic and nonelastic wavefronts. This nonelastic wave is illustrated in Fig. 3(b) where stress is plotted against distance of wave travel. The only problem introduced by considering a nonelastic wave in the above manner is that the time relationship of the waves becomes more complex. Further discussion of nonelastic waves may be found in Refs. [4] and [5].

The effect of wave attenuation owing to internal friction of the material may also be considered in the present analysis in the following manner. If the wave does not exceed the elastic limit of the material, the effect of internal friction on reducing a traveling wave may be taken as

$$f(x) = f_0 e^{-\gamma x} \qquad (22)$$

where $f(x)$ is the particle velocity or stress at a distance x from the beginning point of the wave, f_0 is the particle velocity or stress at the beginning ($x = 0$), and γ is a damping factor. The above equation and the damping factor are presented and discussed in Ref. [3], and no attempt is made here to assign numerical values to γ.

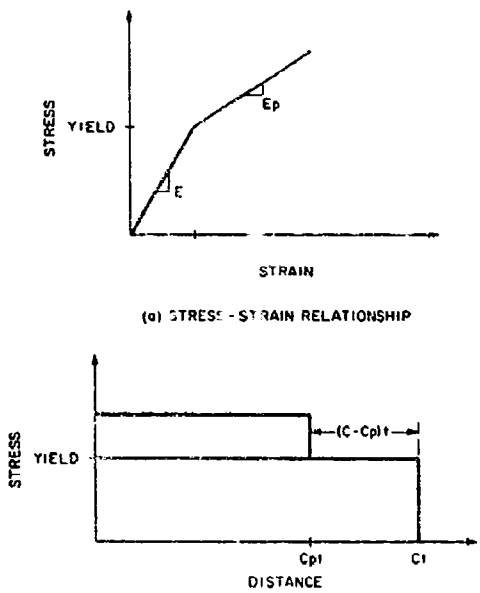

Fig. 3. Elastic-plastic waves

By using Eqs. (1), (3), (4), (5), (8), (16), (20), (21), and (22) and superimposing the effect of each wave, the responses (particle velocity and acceleration) or the stresses at any position and time owing to impact or shock loading can be calculated for a rotationally symmetric nonuniform bar with attached masses. The above governing equations are summarized in Table 1 where the first column gives the text equation number, the second column gives the equation, the third column gives the quantity or quantities that may be determined from the equation, and the fourth column gives the structural element for which the equation is applicable. Note that although the concept is simple, the type of structure to be modeled can be quite complex. An example calculation is presented in the next section to illustrate the application of the developed equations and to present a method of bookkeeping for the superimposed effects of all the waves.

RESULTS

In this section, calculations of the response to an impact loading employing the equations developed here are presented and discussed. A comparison between calculated and measured accelerations is also presented to evaluate the theoretical results. For these calculations, the

TABLE 1
Summary of Governing Equations

Text Equation No.	Equation	Quantity Calculated	Type of Section to Which Equation is Applicable (See Fig. 1)
(1)	$\sigma = \rho c v$	Stress	Any section
(3)	$v_t = v_i - v_r$	Transmitted or reflected velocity	Any section
(4)	$v_t = \frac{2A_1\rho_1 c_1}{A_2\rho_2 c_2 + A_1\rho_1 c_1} v_i$	Transmitted velocity	Discontinuity in area and material
(5)	$v_r = \frac{A_2\rho_2 c_2 - A_1\rho_1 c_1}{A_2\rho_2 c_2 + A_1\rho_1 c_1} v_i$	Reflected velocity	Discontinuity in area and material
(8)	$v_n = \sqrt{\frac{A_1\rho_1 c_1}{A_n\rho_n c_n}}\, v_1$	Velocity	Gradual change in area and material
(16)	$a_r = a_i - a_t$	Reflected acceleration	Any section
(20)	$v_t\left(t_0 + (n+1)\Delta t\right) = \frac{\alpha}{\beta} V_n(1 - e^{-\beta\Delta t}) + e^{-\beta\Delta t}\, v_t(t_0 + n\Delta t)$ $v_t(t_0) = 0$ $n = 0, 1, 2, 3, \ldots$	Transmitted velocity	Rigidly attached mass
(21)	$a_t\left(t_0 + (n+1)\Delta t\right) = \alpha(V_{n-1} - V_n) + e^{-\beta\Delta t}\, a_t(t + n\Delta t)$ $a_t(t_0) = \alpha V_0$ $n = 0, 1, 2, 3, \ldots$	Transmitted acceleration	Rigidly attached mass
(22)	$f(x) = f_0 e^{-\gamma x}$	Attenuated velocity or stress	Any section

structure considered is a complete test missile configuration consisting of an outer shell structure with attached interior sundry packages (nonstructural masses) that would represent electronic devices. The missile configuration is assumed to have longitudinal motion only and to be represented by a rotationally symmetric bar with cross-section areas and attached nonstructural masses as shown in Fig. 4. In Fig. 4, the ordinate is the cross-section area in inches squared of the missile skin configuration and the abscissa is the station along the missile longitudinal axis. The stations are spaced 1 in. apart and station 0 corresponds to the tip of the missile. The attached nonstructural masses are shown as weights in Fig. 4. For the calculations presented here it is assumed that the stress waves are elastic, the material is aluminum, and there is no wave attenuation.

The impact loading is assumed to be an excitation caused by a velocity shock. This impact loading is assumed to produce two step waves, equal in magnitude, that propagate in opposite directions from the point of impact (station 34) at the speed of sound of the material ($c = \sqrt{E/\rho}$ = 200,000 in./sec). The initial magnitude of the particle velocity is assumed

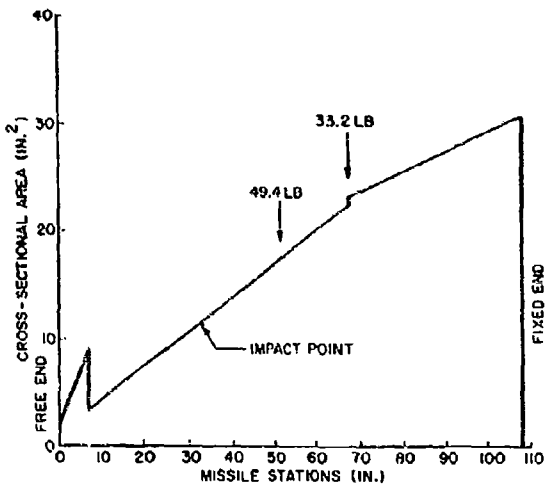

Fig. 4. Geometry of missile configuration

to be 150 in./sec (initial compressive stress = 7600 psi).

The waves beginning at the point of impact propagate and will be reflected at points of discontinuities in area (stations 7 and 68), at points of attached masses (stations 52 and 68), and from the ends (stations 0 and 107). The magnitudes of the responses or stresses in the structure owing to these waves are calculated using the developed equations and may be increased or decreased depending upon the manner in which the reflected and transmitted waves combine together. To develop a bookkeeping procedure to account for each wave, a plot tracing the waves and their reflections is made and is shown in Fig. 5. In Fig. 5, the ordinate is the missile stations, and the abscissa is time (time $t = 0$ corresponds to time of initial impact). In Fig. 5, the slope of lines (slope = $\pm c$) gives the correct distance-time relation of the waves. For example, the time distribution for

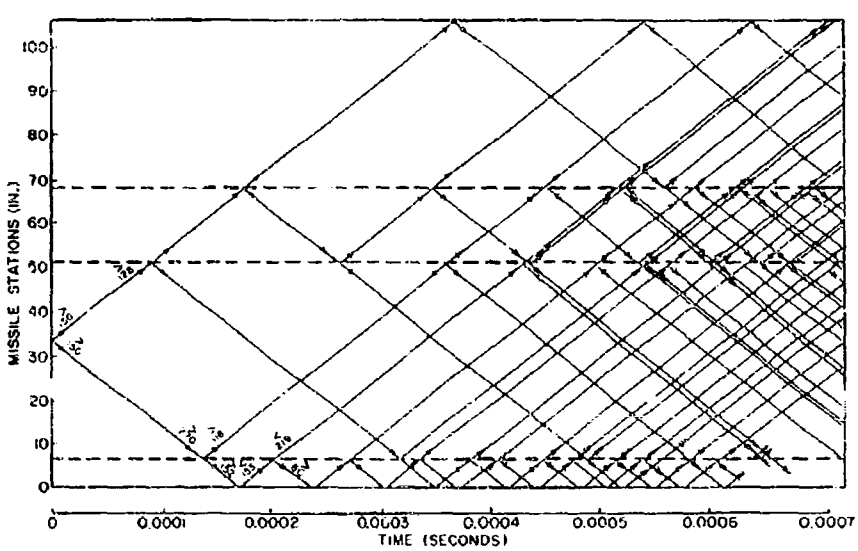

Fig. 5. Stress waves in missile configuration

all of the waves intersecting at station 68 is easily determined from Fig. 5; that is, the first wave intersects at $t = 0.0017$ sec, the second at 0.0035 sec, and so on. Note in Fig. 5 the complexity of the wave pattern as time increases. For this configuration where the modulus of elasticity and the material is a constant, the slope of the lines in Fig. 5 is constant; however, if the modulus of elasticity or the material is not constant throughout the configuration, the slope of the lines would vary accordingly. The direction of the waves (wave propagation velocity sign) is accounted for in Fig. 5 by the arrows on the lines. Knowing the time distribution of the waves from Fig. 5, the magnitude of the particle velocity of each wave is determined by applying the appropriate equations developed in the previous section. For these and the remaining calculations, the particle velocity and acceleration will be the response quantities that are described; however, from the particle velocity the stress may be calculated using Eq. (1). In calculating the stress from the particle velocity, the sign of the wave velocity c (from Fig. 5) must be taken into account.

To calculate the particle velocity and acceleration at a particular station the following procedure is used. Beginning at the point of impact, station 34, and tracing the wave toward the tip station 0, the wave is first reflected at station 7 (see Fig. 5). From station 34 to station 7, the magnitude of the incident wave particle velocity is calculated using Eq. (8), and then the transmittal and reflected particle velocities are calculated using Eqs. (4) and (5). These calculated values of velocities in inches per second are shown at station 7 in Fig. 5, and their directions are shown by the arrow above the numerical value. The first transmitted velocity at station 7 travels to the tip (station 0) where it is reflected from the free end and travels back to station 7. Note that the reflection at the free end reverses the direction of the particle velocity and the wave velocity. At station 7, the wave is again reflected. The magnitudes of these transmitted and reflected velocities are calculated using Eqs. (4) and (5) and are shown on the second wave at station 7 in Fig. 5. The process is repeated.

Tracing the wave in Fig. 5 beginning at the impact point (station 34) and progressing toward station 107, at station 72 a nonstructural attached mass is encountered. At this point, the transmitted particle velocity and acceleration are calculated using Eqs. (20) and (21), respectively, and the incident particle velocity at station 52. The incident particle velocity at station 52 is calculated using Eq. (8) and is shown in Fig. 5. As the transmitted wave travels on from station 52, it encounters another mass at station 68 where, again, Eqs. (20) and (21) are used to calculate the transmitted particle velocity and acceleration. Note that the magnitude of the incident particle velocity at station 68 used in Eqs. (20) and (21) is calculated using the magnitude of the transmitted particle velocity from station 52 and Eq. (8).

Using this procedure, all the waves may be systematically traced throughout the configuration. That is, whenever the wave travels through a region in which there are no discontinuities or masses, Eq. (8) is used to calculate the particle velocity magnitude; at the points of area and material discontinuities, Eqs. (4) and (5) are used to calculate the particle velocity magnitudes; and at the points of attached masses, Eqs. (20), (3), (16), and (21) are used to calculate the particle velocity and acceleration magnitudes. The direction (sign) and the time variation from impact of the velocities and accelerations are determined from Fig. 5.

The final response at a particular station is then determined by superimposing, at the proper time instant, the effect of each wave. This method is illustrated in Fig. 6 where the particle velocity at station 68 is plotted vs time. The dashed lines shown in Fig. 6 are the calculated velocities from Eq. (20) for each wave intersecting station 68. The time variation for each of the waves is determined from Fig. 5. The total particle velocity at station 68 is then determined by adding together the effects of each of the waves and is shown by the solid line in Fig. 6.

In Fig. 7, the calculated total particle velocity at station 52 is shown plotted vs time. These velocities were also calculated using the procedure as illustrated in Fig. 6. From the calculations of particle velocity for Figs. 6 and 7 and from Fig. 5 (sign of wave propagation velocity), the stresses at stations 52 and 68 can be obtained by using Eq. (1).

In Figs. 8 and 9, comparisons of the calculated and experimental accelerations are shown for stations 68 and 52, respectively. The dotted lines shown in Figs. 8 and 9 are accelerations determined from accelerometer data obtained from tests performed at Martin Marietta. These acceleration data were obtained from a test facility that simulates a velocity shock on a test missile configuration. No attempt will be made here to describe the experimental tests as their purpose is only to evaluate the theoretical results. The experiment also determined the magnitude of the initial particle

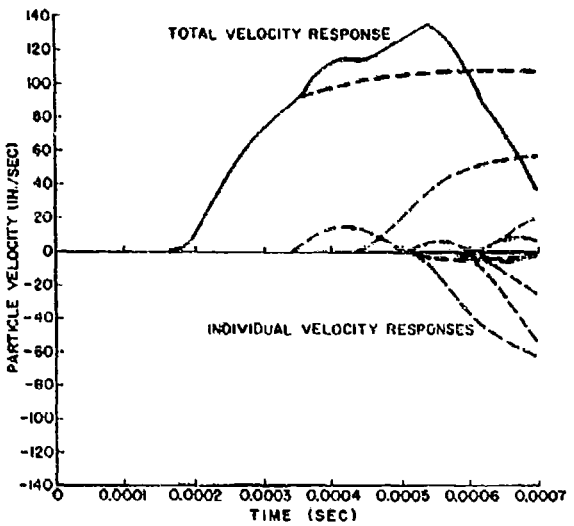

Fig. 6. Calculated particle velocity at station 68

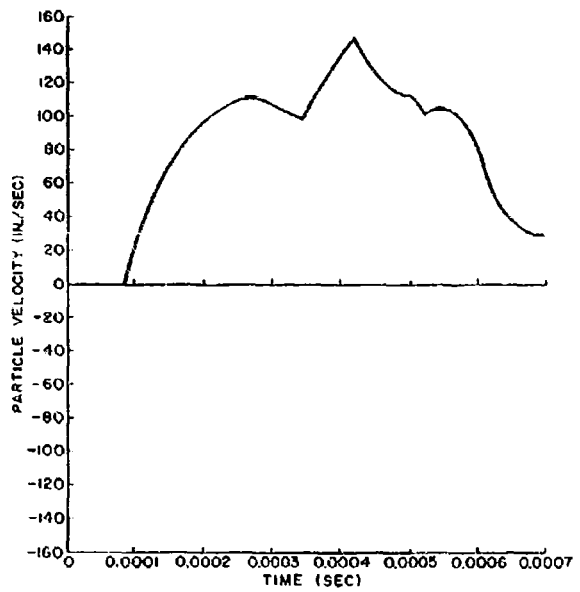

Fig. 7. Calculated particle velocity at station 52

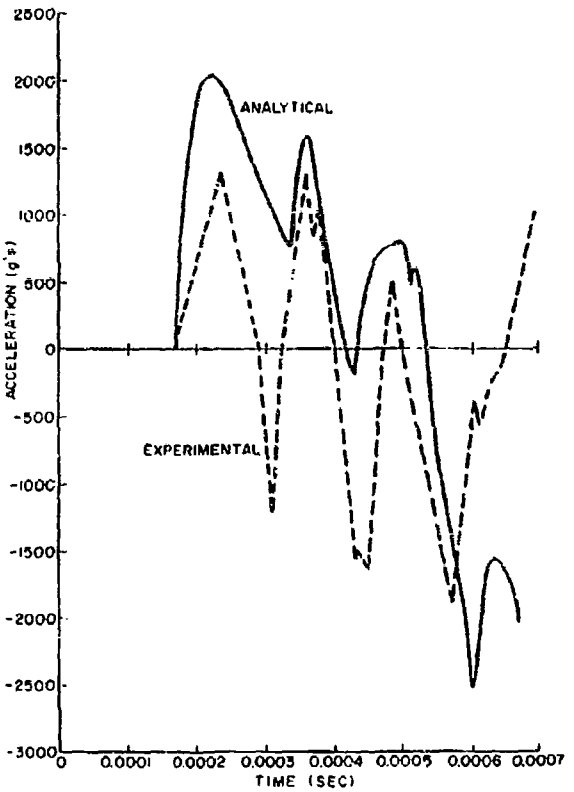

Fig. 8. Calculated and experimental accelerations at station 68

velocity that was used in the theoretical calculations. The theoretical accelerations were calculated using Eq. (21) and were superpositioned according to the time variation of Fig. 5. The total acceleration is shown as the solid lines on Figs. 8 and 9. In Fig. 8, the results comparing calculated and experimental accelerations show good agreement, but in Fig. 9 the results exhibit only fair agreement when comparing the amplitudes of the responses. However, the theoretical results of Figs. 8 and 9 do show remarkably good agreement considering the complexity of the structure examined, and give adequate and reasonable results for design purposes.

A standard industry practice is to describe the response by a shock spectrum or transient response spectrum, but Figs. 8 and 9 completely describe the response by showing its time history. A shock spectrum is a plot of acceleration vs frequency and is derived by considering the maximum response of a single-degree-of-freedom oscillator to a given forcing function. The analytical acceleration time histories of Figs. 8 and 9 and the experimentally measured acceleration time histories were converted into shock spectra. These are shown in Figs. 10 and 11 where the acceleration in gravities is plotted vs frequency in hertz for missile stations 68 and 52, respectively. Again the agreement between theoretical and experimental is better for station 68 than station 52. If the shock spectra of Figs. 10 and 11 were to be used for specification purposes and if a curve is drawn through the peak points of the spectra, then the agreement between the experimental and theoretical spectra would be good.

CONCLUSIONS

An analytical method is presented for calculating responses (particle velocities and accelerations) and stresses owing to longitudinal stress waves in a complex bar-type structure.

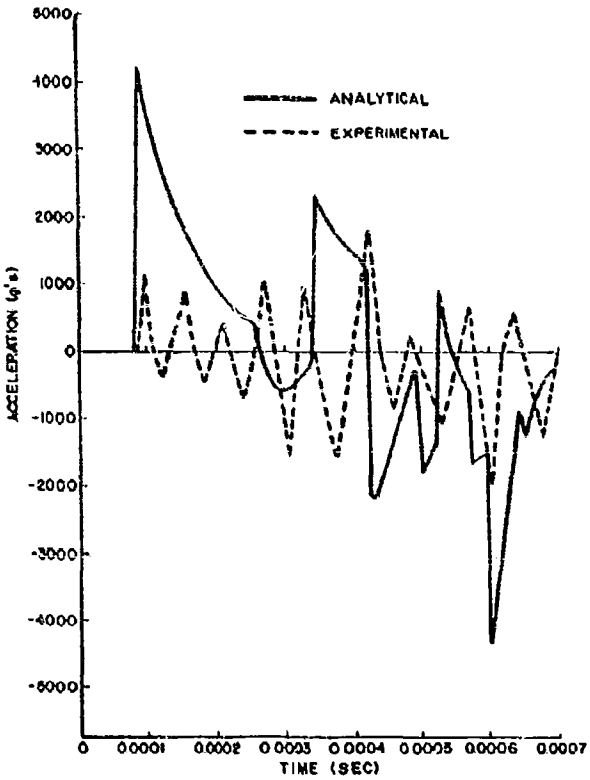

Fig. 9. Calculated and experimental accelerations at station 52

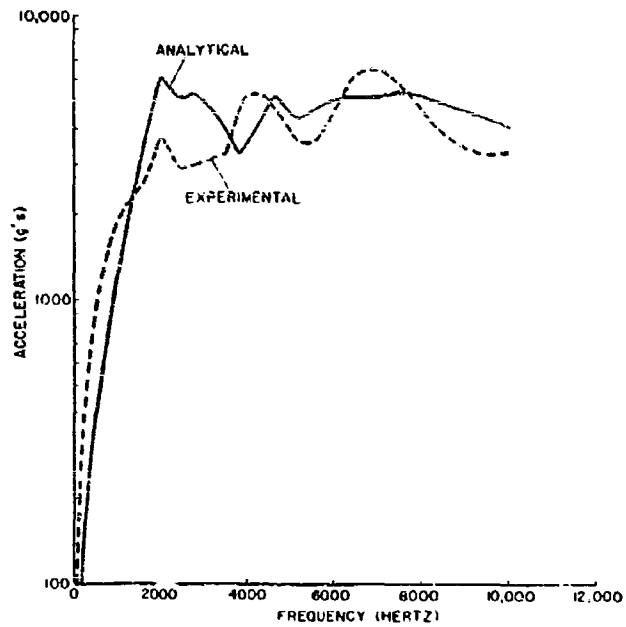

Fig. 10. Calculated and experimental shock spectra at station 68

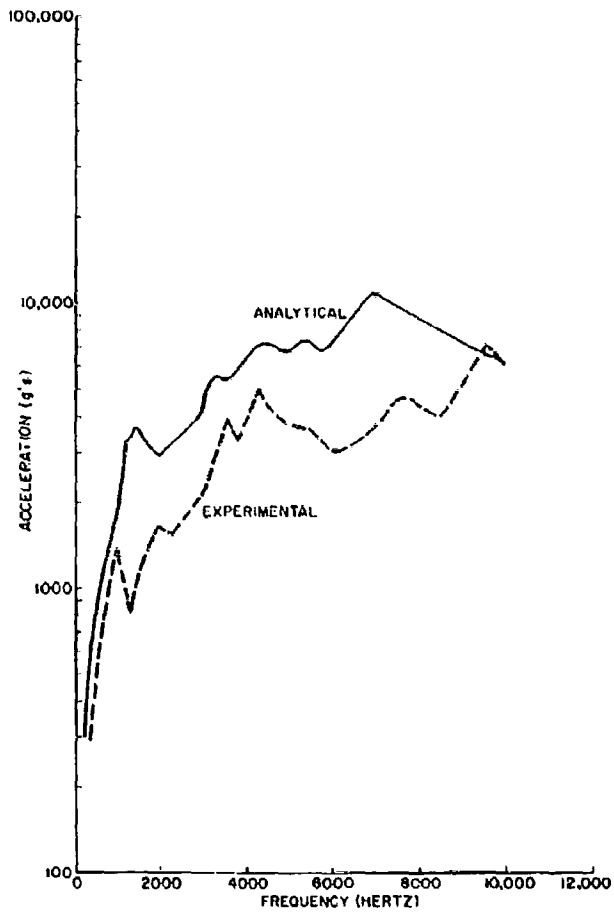

Fig. 11. Calculated and experimental shock spectra at station 52

The method is particular applicable to a structure such as a missile. The method is simple in concept and has the advantage of allowing for realistic consideration of the wave transmission process and of accounting for the effects in the structure of mass, area, and material changes, nonelastic waves, and wave attenuation. The response or stress at any position is calculated by superimposing the response at proper time instants of the elements that account for the complexity of the actual structure.

Results of sample calculations are presented for the longitudinal response of a missile which is impact loaded. For this configuration, the theoretical accelerations are compared with measured experimental results and exhibit good agreement considering the complexity of the missile structure. In addition, as the analysis considers the actual wave pattern, the effects of reflected and combined waves, either detrimental or advantageous, can be considered and could be included in a design application.

REFERENCES

1. J. M. Frankland, "Effects of Impact on Simple Elastic Structures," Proc. Soc. Exptl. Stress Anal., 6(2).7-27, 1948

2. E. A. L. Smith, "Impact and Longitudinal Wave Transmission," Trans. ASME, Aug. 1955, pp. 963-973

3. Harold P. Frisch, "A Spring-Mass Representation of a Free-Free Non-Uniform Bar in Response to Longitudinal Forces," NASA TND-2416, Aug. 1964

4. L. H. Donnell, "Longitudinal Wave Transmission and Impact," Trans. ASME, 52:153-166, 1930

5. H. Kolsky, Stress Waves in Solids (Dover Publications, Inc.), 1963

6. Werner Goldsmith, Impact (Edward Arnold, Ltd.), 1960

DISCUSSION

R. Mustain (McDonnell Douglas Corp.): You did not say how you did your experiment. What was your input force? Was it an explosive type of shock?

Mr. Block: The input was the upper section impacting and latching the lower section. It was a true impact. The lower section is sitting and the upper section moves into it at a known velocity. That would set up the wave that would travel in both directions and actually travel back through that impact point again.

Mr. Mustain: Maybe you have made some kind of a breakthrough for the explosive type shock. I certainly want to read your paper.

Mr. Block: Are you thinking of something like stage separation where there is an explosive cutting charge?

Mr. Mustain: This is true. You are showing high frequencies and up to now we have not been able to do any good prediction work on that.

Mr. Block: If you have a symmetric separation charge all the way around and explode that by some reliable method, knowing the initial particle velocities, you could actually trace the wave throughout the structure to some place in which you are interested.

Mr. Forkois (NRL): Can you tell us what 10,000 g's means in terms of stress?

Mr. Block: The g's do not mean anything in terms of stress. To get the stress you have to go back to the particle velocity. Stress is related to particle velocity and to the material constants, so you are working with the integral of that curve, if you want to look at it that way.

G. Brooks (NASA Langley): When I looked at your next to the last slide, I wondered whether that accelerometer was picking up the stress wave or whether it was just moving relative to the shell. Did you look at that problem?

Mr. Block: The accelerometers were not located on the shell. They were located on a ring and the two I showed were both where there were attached masses. They were located at a ring interior to the shell in the direction of the wave. There would not be lateral motion of the shell, if that is what you mean.

* * *

ALSEP SYSTEM STRUCTURAL DYNAMICS STUDY

M. M. Bahn
The Bendix Corporation
Ann Arbor, Michigan

The dynamics study undertaken by the Aerospace Systems Division of The Bendix Corporation investigated the steady-state response of ALSEP (Apollo Lunar Surface Experiments Package) components, both elastically coupled and uncoupled with the Lunar Module (LM) structure. The results of the analytical study are correlated with the experimental results. The dynamic study resulted in recommendations for design modifications and dynamic interface requirements. A statistical program has been developed that optimizes random vibration flight approval and qualification test specifications. Currently, the common procedure is to take the maximum value of transmissibility within a discrete bandwidth. The optimization of random vibration specifications is based on the axiomatic logic that the transmissibility within a discrete frequency band will be less than a stated reference value based on given confidence and probability.

INTRODUCTION

This systems study of the coupled and uncoupled ALSEP and LM was conducted to develop dynamic interface qualification specifications for experiments selected by the Manned Space Center for lunar scientific exploration. Three distinct and separate structural units form the ALSEP:*

1. Compartment 1, located in the scientific equipment bay of the LM, carries four experiments (ion detector, passive seismic, solar wind, and magnetometer) and the electronic data subsystem.

2. Compartment 2, located in the other scientific equipment bay, carries three experiments: geological tools, drill box, and radioisotope thermal generator.

3. Cask structure supporting the radioactive fuel element, mounted externally to the LM.

The dynamics study computed the steady-state response of the components mounted on the structure, both elastically coupled and uncoupled with the LM structure. A generalized frequency response program was developed to compute the steady-state response of an n-degree-of-freedom system using specified structural damping as an input.

Further eigenvectors and eigenvalues were computed and mode ships plotted using matrix iteration techniques. To check the above frequency-response program, a normal mode frequency program using viscous damping and a generalized forcing matrix was also developed. The dynamic study resulted in a recommendation to govern dynamic interfaces and qualification test criteria, and changes in conceptual design of the ALSEP/LM supporting structure for the experiments.

MATHEMATICAL MODELS

A flexibility influence coefficient matrix was generated for the 43-DOF (degree of freedom) dynamic system when compartments 1 and 2 were added to the LM. The LM landing radar assembly and tilt mechanism base properties were unchanged from those given by Grumman Aircraft Co.

The mass matrices of compartments 1 and 2 were lumped at the center of gravity (cg) of the components. An additional degree of freedom has been added to the compartment 1 model previously described to represent the dynamic effect of the thermal plate assembly (see Fig. 1).

*The present configuration is a modification of the one described here.

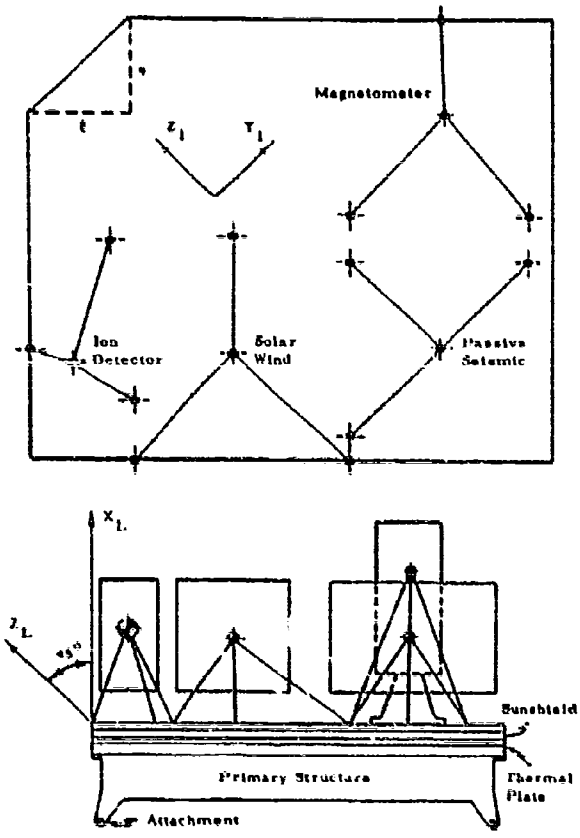

Fig. 1. Compartment 1 model

The composite structure was excited along each of the LM coordinates.

Mathematical Models of Compartments 1 and 2 and the Thermal Plate

Compartment 1 was idealized (see Fig. 1) as follows:

1. The experiments attached to the base plate, also known as the "sunshield," were assumed rigidly connected to their attachment points.

2. The mass of the experiments was assumed to be concentrated at the center of gravity.

3. The "sunshield" plate was assumed to be simply supported all around its edges, and the influence coefficients were calculated for the attachment points of each component.

4. The compartment 1 structure was rigidly attached to the LM.

The model as described is shown in Fig. 1. The attachment points are assumed to move only in the vertical direction, as in-plane deflections of the plate are neglected. This implies that the center of gravity of each attached both has only 3 DOF. The generalized coordinates were thus taken as the three translations of the center of gravity of each box relative to positive LM coordinates.

To use these coordinates, instead of the plate deflections, as generalized coordinates require a rigid body coordinate transformation to obtain influence coefficients in terms of center of gravity displacement. This may be

carried out as follows: The potential energy in terms of plate displacement and stiffness is

$$V = \frac{1}{2} \{d\}^T [C]^{-1} \{d\} \qquad (1)$$

where

$\{d\}$ = the row displacement vector and

$[C]^{-1}$ = the inverse of the influence coefficient matrix.

However, $\{d\}$ is related to $\{D\}$ by a rigid body coordinate transformation, that is,

$$\{d\} = [T]\{D\} \qquad (2)$$

If this is substituted into the potential energy expression, the following is obtained:

$$V = \frac{1}{2} \{D\}^T [T]^T [C]^{-1} [T] \{D\} \qquad (3)$$

Thus, $[[T]^T [C]^{-1} [T]]^{-1}$ is the influence coefficient matrix in terms of displacement of the various component centers of gravity, that is, the d's. Figure 1 shows the locations of the attachment points and the centers of gravity of the experiments.

Compartment 2 was modeled in the same manner as compartment 1. Figure 2 shows the conceptual model used for compartment 2. As the fuel cask is attached externally to a substantially stiffer LM structure, it was analyzed as uncoupled with respect to the LM structure. The analysis of the fuel cask is in itself fairly detailed, and no attempt will be made here to explain it. However, the general method of dynamic analysis was the same as above.

Comments on the Mathematical Models

A general philosophy is involved when attempting to create a meaningful dynamic model to represent an elastic system. The model will usually be some mathematical expression which will describe to the desired accuracy the overall dynamic behavior of a system. Problems associated with obtaining solutions to a large

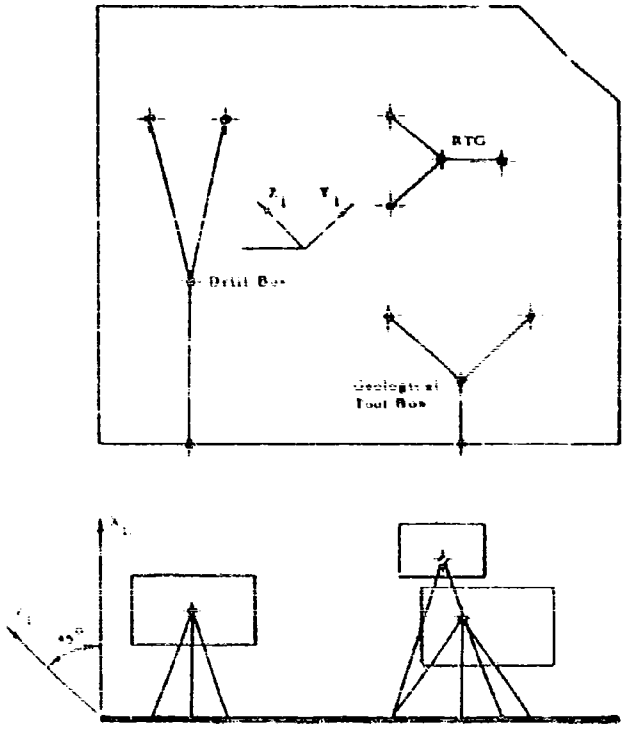

Fig. 2. Compartment 2 model

number of simultaneous differential equations usually tend to limit the complexity of the model chosen. Therefore, the accuracy of the analysis in predicting the behavior of the elastic system depends to a large extent upon how well the mathematical model represents the actual structure.

METHOD OF STRUCTURAL ANALYSIS

Compartment 1 Influence Coefficients

The differential equation for the deflected surface of the thermal plate and sunshield in Fig. 1 is [1]

$$\nabla^4 w = \frac{q}{D} \tag{4}$$

where D = plate flexural rigidity.

Let the loading and deflection functions be represented in the form of a double trigonometric series:

$$q = f(x,y) = \sum_{m=1}^{\infty}\sum_{n=1}^{\infty} A_{mn} \sin\frac{m\pi x}{a} \sin\frac{n\pi y}{b} \tag{5}$$

$$w = f(x,y) = \sum_{m=1}^{\infty}\sum_{n=1}^{\infty} C_{mn} \sin\frac{m\pi x}{a} \sin\frac{n\pi y}{b} . \tag{6}$$

(Solutions with double trigonometric series are due to Navier.) The deflection function satisfies the conditions of zero deflection and zero bending moments along the simply supported edges of the plate.

If the load and deflection functions are placed in the differential equation, the following is obtained:

$$\sum_{m=1}^{\infty}\sum_{n=1}^{\infty} C_{mn}\left(\frac{m^2}{a^2}+\frac{n^2}{b^2}\right)^2 \pi^4 \sin\frac{m\pi x}{a} \sin\frac{n\pi y}{b}$$

$$= \frac{1}{D}\sum_{m=1}^{\infty}\sum_{n=1}^{\infty} A_{mn} \sin\frac{m\pi x}{a} \sin\frac{n\pi y}{b} . \tag{7}$$

Hence, it is found that

$$C_{mn} = \frac{A_{mn}}{\pi^4 D\left(\frac{m^2}{a^2}+\frac{n^2}{b^2}\right)^2} \tag{8}$$

and the deflection becomes

$$w = \frac{1}{\pi^4 D}\sum_{m=1}^{\infty}\sum_{n=1}^{\infty} \frac{A_{mn}}{\left(\frac{m^2}{a^2}+\frac{n^2}{b^2}\right)^2} \sin\frac{m\pi x}{a} \sin\frac{n\pi y}{b} \tag{9}$$

To obtain the coefficient A_{mn}, we turn now to the Fourier formula. It is not difficult to show that the coefficient in the load function can be expressed as

$$A_{mn} = \frac{4P}{ab} \sin\frac{m\pi\xi}{a} \sin\frac{n\pi\eta}{b} \tag{10}$$

where ξ and η are at 45 degrees to the LM Z and Y axes (see Fig. 1). Substituting, we finally obtain the deflection formula of the plate, which is loaded by a concentrated load on the ξ,η coordinates.

$$w = \frac{4P}{\pi^4 abD}\sum_{m=1}^{\infty}\sum_{n=1}^{\infty} \frac{\sin\frac{m\pi\xi}{a} \sin\frac{n\pi\eta}{b}}{\left(\frac{m^2}{a^2}+\frac{n^2}{b^2}\right)^2} \sin\frac{m\pi x}{a} \sin\frac{n\pi y}{b} . \tag{11}$$

Compartment 2 Influence Coefficients

Compartment 2 has four pinned supports. The general method used, namely that of assuming geometrically admissible functions and minimizing potential energy, is outlined by H. L. Langhaar [2].

Solution by Matrices for the Structural Transmissibility of an n-Degree-of-Freedom System

As previously discussed, it is usually possible to express the equations of motion for an undamped lumped parameter system in the matrix form

$$[M]\{\ddot{d}\} + [K]\{d\} = \{F(t)\} \tag{12}$$

where M represents the mass matrix, K the structural stiffness matrix, and d the displacements of the various generalized coordinates. It is usually desirable in response work to introduce a form of energy sink into the equations to account for the structural damping of the system. If g represents such a damping parameter, one way of including such a dissipative effect is shown in Eq. (13), where the complex constant $i = \sqrt{-1}$.

$$[M]\{\ddot{x}\} + [B]\{\dot{x}\} + [K]\{x\} = \{F(t)\} \qquad (13)$$

If the inputs $\{F(t)\}$ are known, it is possible to find the response of the system. Usually, however, the inputs are known only on a statistical basis and thus statistical methods of response computation are required. Fundamental to these calculations is a knowledge of the complex displacement $H_{ij}(\Omega)$ which is defined below. If an input to the system is written as

$$\{F(t)\} = \{A\} e^{i\Omega t}$$

after a sufficient period of time the transients will have died out because of damping. The solution will be of the form

$$\{x\} = \{H(\Omega)\} e^{i\Omega t} \qquad (14)$$

A solution for the displacement $H(\Omega)$ as defined by Eq. (14) might be carried out as shown below. Substituting Eq. (14) into Eq. (13) yields

$$-\Omega^2[M]\{H\} + (Ig)[K]\{H\} = \{A\} \qquad (15)$$

where the factor $\exp(i\Omega t)$ has been removed, as Eq. (13) is to be an identity for all time. We break up H and A into their complex components,

$$\begin{aligned} \{H(\Omega)\} &= \{H_R\} + i\{H_I\} \\ \{A\} &= \{A_R\} + i\{A_I\} \end{aligned} \qquad (16)$$

If Eq. (16) is substituted into Eq. (15) and real and imaginary parts are equated, the following pair of matrix equations are obtained:

$$\begin{aligned} [E]\{H_R\} - g[K]\{H_I\} &= \{A_R\} \\ g[K]\{H_R\} + [E]\{H_I\} &= \{A_I\} \end{aligned} \qquad (17)$$

where the matrix E is defined by

$$[E] = [K] - \Omega^2[M] . \qquad (18)$$

It may be noted that E is the matrix that yields the natural modes and frequencies of the dynamic system. Solution of the pair of equations in Eq. (17) may be effected as follows. The second equation of Eq. (17) may be solved for the column vector H_R:

$$\{H_R\} = \frac{1}{g}[K^{-1}]\{A_I\} - \frac{1}{g}[K^{-1}][E]\{H_I\} \qquad (19)$$

This may then be substituted back into the first equation of Eq. (17) to solve explicitly for H_I. The following is obtained:

$$\{H_I\} = \left[[E][K^{-1}][E] + g^2[K]\right]^{-1} \cdot \left[[E][K^{-1}]\{A_I\} - g\{A_R\}\right] . \qquad (20)$$

Substitution of the result (Eq. (20)) back into Eq. (19) would then yield part of the response vector H.

Comments on LM/ALSEP Dynamic Analysis

A comparison of the results of dynamic modes of compartments 1 and 2 with test results is shown in Table 1.

In attempting to describe a system with infinite degrees of freedom representing a continuous structure, by a system with only a finite degree-of-freedom system has only a finite number of natural frequencies, it may respond only to excitation in these degrees of freedom. It is apparent, then, that the response of such a model to excitations with frequency spectra greatly above its own natural frequency range must be inherently in error owing to the higher frequency contributions which the finite degree-of-freedom model ignores. The contribution of these higher modes may be ignored if the model is well chosen and a realistic value of damping is included in the system.

The results are very sensitive to the choice of the structural damping coefficient. This choice depends upon comparison with similar structures, and also reflects the skill of the modeler.

Figures 3 and 4 show the analytically obtained plots of the frequency response of the center of gravity of compartment 1 along X, Y, Z directions (X axis forcing) for the following cases:

1. Considering LM and ALSEP mass and flexibility matrices assembled (Fig. 3).

2. Considering LM flexibility matrix only, the masses of ALSEP compartments 1 and 2 are assumed to be concentrated at their respective centers of gravity (Fig. 4).*

The effect of adding additional degrees of freedom of ALSEP to a complex structure like LM results in altering the center-of-gravity response. The additional degrees of freedom act to impose perturbations in the center-of-gravity response, even though the substructure is very small compared with the combined structure. However, as may be seen from Figs. 3 and 4,

*The plots of vibration responses of the LM structure shown in Fig. 4 have been obtained from Grumman Aircraft [3].

TABLE 1
Comparison of Dynamic Models of Compartments 1 and 2 with Test Reports

Compartment 1 (without LM — 12 Degrees of Freedom)

a. Natural Frequencies:

Theoretical (Hz)	Test (Hz)
35	38
69	67
102	95
157	150
242	250
267	290
303	310
477	500
725	650
1475	1200
1775	—
1975	—

b. Peak Transmissibilities: Theoretical - 10.1 g/g
Test - 11.0 g/g

Compartment 2 (without LM)

The theoretical analysis assumes 9-degree-of-freedom mathematical model.

a. Natural Frequencies:

Theoretical (Hz)	Test (Hz)
11.5	5.0
30.5	30.5
59.0	52.0
83.0	75.0
112.5	110.0
137.5	180.0
232.7	220.0
307.5	280.0
625.0	450.0

b. Peak Transmissibilities: Theoretical - 8.0 g/g
Test - 10.3 g/g

no drastic change in the magnitude of the response of the center of gravity resulted.

RANDOM VIBRATION SPECIFICATIONS ANALYSIS

A random vibration spectrum is represented by a plot of acceleration power spectral density vs frequency (g^2_{rms}/Hz vs Hz). This plot, whether generated by test or analysis, is a nightmare of "wiggly lines." To conduct a vibration test using this as an input would be nearly impossible. The power spectral density plot must be approximated by a series of constant slope power density lines. Herein lies the problem of what level of constant transmissibility should be used to represent the "wiggly lines" in discrete frequency intervals.

One set of output data that is of interest is the transmissibility of the test article. It might also be expressed as the square root of the ratio of the output random vibration level (in g^2/Hz) to the input random vibration level (in g^2/Hz). A procedure commonly used is to draw an envelope over the peaks of transmissibilities. The resulting curve is then multiplied by the

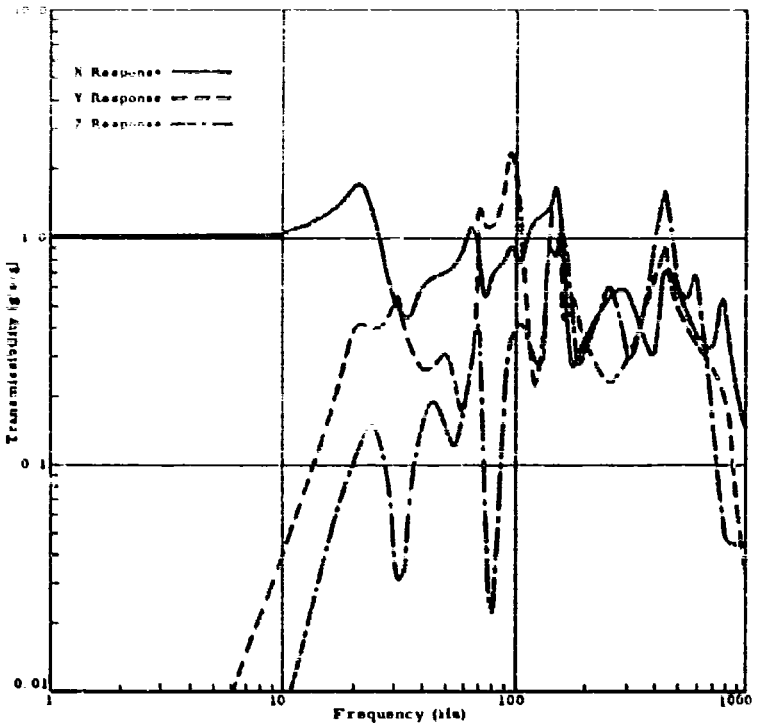

Fig. 3. Composite structure LM/ALSEP translational transmissibility at the center of gravity of compartment 1

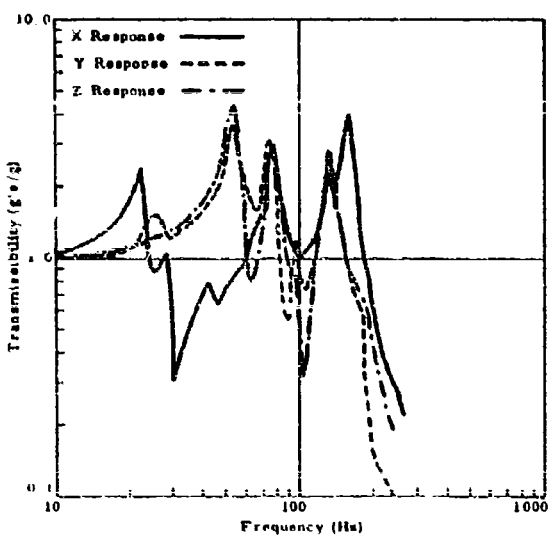

Fig. 4. Scientific equipment shelves translational transmissibility in X, Y, Z directions from LM primary structure to shelves

square of some arbitrary number (for example, 1.3^2) to generate the qualification level. It is believed by the writer that the results would be highly conservative and probably would cause an unnecessary burden in design and schedules. Bendix Aerospace Systems Division has developed a "statistical test criteria" program which assigns a probability and a confidence level to the approximation of the "wiggly lines" in the discrete frequency interval by a constant level of g_{rms}. It is believed that more reasonable test levels will be generated this way and the resulting conservatism can be controlled by statistical inference.

Exponential Distribution of Vibration Responses

If a variable, X, is attributed to the individuals of response data points, the distribution function of X, denoted $F(x)$, may be defined as the number of all data points having an $X < x$ divided by the total number of data points.

This function also gives the probability, P, of choosing at random a discrete response having a value of X equal to or less than x and thus we have

$$P(X \leq x) = F(x) \tag{21}$$

To derive a general form for the distribution, the distribution function may be written in the form

$$F(x) = 1 - e^{\phi(x)} \tag{22}$$

The advantage of this formal transformation depends on the relationship

$$(1 - P)^n = e^{-n\phi(x)} \tag{23}$$

where P is the probability of a single observation. The probability of n successes in n events can be expressed as

$$1 - P_n = (1 - P)^n \tag{24}$$

or

$$P_n = 1 - (1 - P)^n$$

and

$$P_n = 1 - e^{-n\phi(x)} \tag{25}$$

For the resulting function to be a distribution function, the only necessary condition $\phi(x)$ has to satisfy is to be a positive, nondecreasing function vanishing at a value X_u which is not necessarily equal to zero. X_u can also be defined as a minimum independent variable location parameter. The most simple function satisfying this condition is

$$\frac{(X - X_u)^m}{X_o} \tag{26}$$

where

X_o = relative magnitude scale parameter (units) and

X_u = minimum independent variable location parameter (units).

Thus, we have from Eqs. (22) and (26)

$$F(x) = 1 - e^{-\frac{(X - X_u)^m}{X_o}} \tag{27}$$

From Eq. (21) the probability that a randomly selected observation X will not exceed x is

$$P(x) = 1 - e^{-\frac{(X - X_u)^m}{X_o}} \tag{28}$$

where

X = the response at any frequency (independent variable),

$P(x)$ = the probability of occurrence of a discrete response, and

m = the shape parameter (no units),

$$1 - P(x) = e^{-\frac{(X - X_u)^m}{X_o}} \tag{29}$$

According to Weibull [4], Eq. (29) satisfies the observations better than other known distributions.

To fit the observed data to the distribution of Eq. (29), the data may be linearized by taking logarithms:

$$\ln \frac{1}{1 - P(x)} = \frac{(X - X_u)^m}{X_o} \tag{30}$$

or

$$\ln \ln \frac{1}{1 - P(x)} = -\ln X_o + m \ln (X - X_u) \tag{31}$$

The following nomenclature may be convenient.

[illegible]

[illegible]

and

[illegible]

(See Ref. [illegible])

A typical computer output will provide the following information for the above equation:

1. Fifty percent Confidence Line,

$$Y = L + m(X - X_o)$$

(the computer programs call the subroutine "Least Squares Polynomial Fit")

2. X_o

3. L

4. Slope m

5. Sum of the square deviations about item (4), above.

The value of m indicates the type of distribution; m = 1 indicates exponential distribution, or

$$PG_c = 1 - P(x) = e^{-\frac{(X - X_o)^m}{X_o}} \qquad (32)$$

Comments on Random Vibration Specifications Analysis

Of particular interest in optimizing a random vibration spectrum is the probability that at a given confidence level and probability the equipment transmissibility within a given frequency band will exceed or be less than a stated reference level. The guideline in the present analysis calls for the severity of any applied environment for the qualification program to be set on a statistical basis. The noteworthy difference is the criterion of distribution function. In random vibration analysis of aircraft structures, normal distribution is commonly assumed and the qualification test level is taken as the 3σ level. However, the present random vibration specifications computer program at Bendix computes the form of the distribution function, and derives the equation of the polynomial defining the probability of a certain value of transmissibility as a function of the exponential parameter, m, that can also be interpreted as the distribution function. The exponential in ALSEP specification analysis results varies from 0.7 to 3.6, signifying distribution functions ranging from nearly exponential to nearly normal distributions.

The basis for assigning probabilities is a combination of "axiomatic" logic and a priori argument. From the guidelines of the ALSEP-Qualification Test Plan, the qualification test criterion for normal distribution is 3σ or 99.9 percent. Inasmuch as the Exponential Distribution and Rayleigh Distribution are far more conservative than the Normal distribution (M = 3.5), we can with reasonable certainty allocate lower values of probabilities for distributions ranging from M = 0.7 to M = 3. A typical ALSEP component random vibration spectrum obtained by statistical analysis of transmissibilities is shown in Fig. 5. Superimposed on the figure is the same spectrum obtained by enveloping transmissibilities and multiplying by a factor of $(1.3)^2$. It is obvious that the qualification random vibration spectrum based on statistical analysis is more realistic than the spectrum based on enveloping of peak transmissibilities.

ACKNOWLEDGMENTS

The author wishes to thank the ALSEP Program Management at the Manned Space Center and Bendix Aerospace Systems Division for their support in publishing the paper.

Acknowledgments are also made to the management of the Engineering Directorate and the Flight Systems Department at Bendix for their cooperation.

REFERENCES

1. S. Timoshenko and S. Woinowsky-Krieger, Theory of Plates and Shells, 2nd ed., p. 108, McGraw-Hill, New York, 1959

2. H. L. Langhaar, Energy Methods in Applied Mechanics (John Wiley & Sons, Inc., New York), 1962

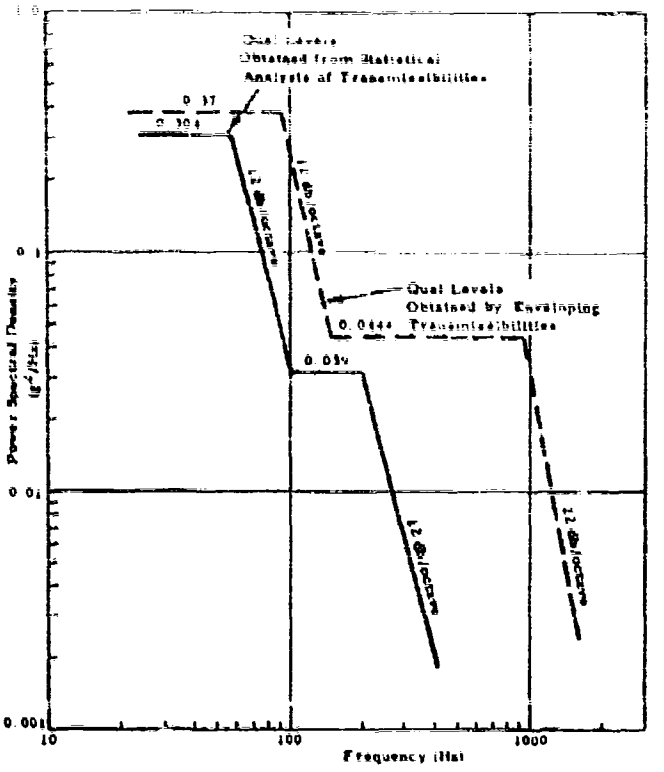

Fig. 5. Random vibration qualification spectra-passive seismic Z-axis (forcing Z-axis)

3. L. Mitchell, "Vibration Amplification Factors of the LM Scientific Equipment Shelves," LM0-520-250B, Grumman Aircraft Engineering Corp., Oct. 1965

4. Walodi-Weibull, "A Statistical Distribution Function of Wide Applicability," Trans. ASME, Appl. Mech. Div., Nov. 25-30, 1951

5. H. W. Beatty, Jr., "Three Parameter Exponential Distribution," Bendix Aerospace Systems Div., 1966

BIBLIOGRAPHY

Bahn, M., et al., ALSEP Dynamics Rept. ATR-16, Bendix Aerospace Systems Div., 1966

* * *

REDUCING THE NUMBER OF MASS POINTS IN A LUMPED PARAMETER SYSTEM

[illegible]
Dynamic Science
Monrovia, California

A method is presented for reducing the number of mass points in a lumped parameter system. The basis for the reduction procedure is that the work done on the original lumped parameter system by the inertial forces, during a free vibration, is equal to the work done on the reduced system.

Several examples are presented, and for these examples, a dynamical equivalence is established. The procedure is recommended for problems in which a base acceleration is the input.

INTRODUCTION

A method commonly used for studying the dynamics of complex elastic structures is to replace the structure by a lumped parameter system (that is, a system consisting of a set of discrete mass points, springs, and dash pots). The location and number of mass points entering the system will be determined by considerations such as the physical appearance of the structure, the number of modes desired, the effects of rotary inertia, shear, and the lumping of appendage masses with main masses. See Refs. [1] through [3] for examples.

The lumped parameter method usually yields reliable results for the first [illegible] modal characteristics of the real structure if at least [illegible] mass points are used [1]. In a number of problems the first [illegible] modes of the real structure are desired. However, owing to the considerations mentioned above, it is necessary to introduce [illegible] mass points, where [illegible]. The use of [illegible] mass points, as opposed to [illegible], where [illegible], will, in most cases, only slightly improve the results for the first [illegible] modal characteristics; therefore, it would be more desirable to treat the system consisting of only [illegible] mass points. Situations may also arise in which no more than [illegible] mass points can be used. An example is the dynamics of a truss type structure. For the formulation it is advantageous to locate a mass point at each truss joint. However, depending on the size of the truss, the number of modes desired, and the possible interaction of the truss to an adjoining structure, locating a mass point at each truss joint may make the problem too cumbersome to handle efficiently.

The purpose of this paper is to present a procedure that will reduce the number of mass points of the lumped parameter system and yield reliable results for the modes of interest. The procedure is presented for systems in which each mass point is allowed a single degree of freedom. The basis for the reduction procedure is that the work done on the reduced system is equal to the work done on the original system by the inertial forces during a free vibration.

Several examples are presented, and the validity of the reduced system is established for these examples by demonstrating a dynamic equivalence between the original and reduced systems. Dynamic equivalence is defined here as demonstrating a "closeness" in natural frequencies and summed effective (modal) weights between the reduced and original systems. Consideration of effective weight is of importance for problems in which a base acceleration is the input as it is the 1-g base reaction [1].

REDUCTION PROCEDURE

Consider an undamped, linearly elastic system consisting of [illegible] discrete mass points connected by springs. Each mass point is allowed

a single degree of freedom. The work, W_n, done on the system during a free vibration is given by

$$W_n = \frac{1}{2} \sum_{i=1}^{n} \quad (1)$$

where the α_{ij}'s denote the influence coefficients (that is, displacements at points i owing to a unit load at point j), and $\ddot{x}_i$ denotes the acceleration of the ith mass point, m_i.

Consider dividing the n mass points into r groups. Each group may or may not contain the same number of mass points. For the present, the subdivision into the r groups is assumed to be an arbitrary process. For each group, replace the mass points of the original system entering the group by a single mass point located at the center of mass of the group, and equal to the sum of the masses entering the group. For example, for the kth group, introduce the mass M_k, defined as

$$M_k = \sum_{i=s+1}^{s+t} m_i \quad (2)$$

where $(t-s)$ denotes the number of mass points of the original system entering the group. The r M_k's defined by Eq. (2) are the mass points of the reduced system. A method for connecting these mass points is required such that the reduced system is dynamically equivalent (as previously defined) to the original system.

Considering the reduced system, the work, W_k, done on the system during a free vibration is given by

$$W_k = \frac{1}{2} \sum_{p=1}^{r} \sum_{q=1}^{r} \bar{\alpha}_{pq} M_p M_q \ddot{X}_p \ddot{X}_q \quad (3)$$

where the $\bar{\alpha}_{pq}$'s denote the as yet unknown influence coefficients, and $\ddot{X}_p$ denotes the acceleration of the pth mass point, M_p.

The criterion to be used for determining the $\bar{\alpha}_{pq}$'s is that the work done on any mass point, M_p, of the reduced system during a free vibration is equal to the work done on all the mass points that make up the mass M_p of the original system. This implies that the total work done on each system is the same. (The converse would not necessarily be true.) Assume that there are "s" mass points in the first of the r groups, $(t-s)$ in the second, ..., $(t-k)$ in the pth, ..., and finally, $(n-u)$ in the rth. The work W_p done on the $(t-k)$ mass points that make up the pth group is obtained from Eq. (1) as

$$W_p = \frac{1}{2} \sum_{i=k+1}^{t} \sum_{j=k+1}^{t} \quad (4)$$

The work done on the pth mass point of the reduced system is obtained from Eq. (3) as

$$W_p = \frac{1}{2} \sum_{q=1}^{r} \bar{\alpha}_{pq} M_p M_q \ddot{X}_p \ddot{X}_q \quad (5)$$

It will be convenient to rewrite Eqs. (4) and (5) in the forms

$$W_p = \frac{1}{2} \sum_{i=k+1}^{t} \left\{ \sum_{j=1}^{s} \quad + \sum_{j=s+1}^{k} \quad + \sum_{j=k+1}^{t} \quad + \sum_{j=t+1}^{u} \quad + \sum_{j=u+1}^{n} \quad \right\} \quad (6)$$

and

$$W_p = \frac{1}{2} M_p \ddot{X}_p \left\{ \bar{\alpha}_{p1} M_1 \ddot{X}_1 + \bar{\alpha}_{p2} M_2 \ddot{X}_2 + \cdots + \bar{\alpha}_{pp} M_p \ddot{X}_p + \cdots + \bar{\alpha}_{pr} M_r \ddot{X}_r \right\} \quad (7)$$

where

$$\bar{\alpha}_{pq} = \alpha_{ij} \quad (8)$$

Note that the third term in Eq. (6) denotes the work that would be done on the group of $(t-k)$ mass points if these points were isolated from the remainder of the system. The remaining terms in Eq. (6) correspond to the work contribution owing to the other mass points. Similarly, the third term in Eq. (7) denotes the work that would be done on the mass point M_p had M_p been isolated, while the remaining terms denote the work contribution owing to the other mass points.

Assume that the accelerations of the mass points of the reduced system are such that the inertia forces of the reduced system are related to the inertia forces of the original system through the relation

$$M_i \ddot{X}_i \ddot{X}_k = \frac{\sum_{p=1}^{r} \sum_{q=1}^{r} \quad}{\sum_{p=1}^{r} \sum_{q=1}^{r} \quad} \quad (9)$$

where the sums on i and j are extended over the original system mass points that have x_i, M_i, and M_j, and n and m denote the number of original mass points associated with each of these sums.

Using Eq. (9), Eq. (6) may be rewritten in the form

$$\left[\begin{array}{c}\\ \\ \\ \\ \\ \end{array}\right] M_1 X_1 + \left[\begin{array}{c}\\ \\ \\ \\ \\ \end{array}\right] M_2 X_2 + \left[\begin{array}{c}\\ \\ \\ \\ \\ \end{array}\right] M_p X_p + \left[\begin{array}{c}\\ \\ \\ \\ \\ \end{array}\right] M_j X_j \qquad (10)$$

Requiring that $\bar{x}_p = x_p$ (that is, equating the right hand sides of Eqs. (7) and (10)), and noting that the X_i's are linearly independent, gives the unknown α_{ij}'s as functions of the known β_{ij}'s. These relations are

$$\left[\begin{array}{c}\\ \\ \\ \\ \\ \end{array}\right] \qquad \left[\begin{array}{c}\\ \\ \\ \\ \\ \end{array}\right] \qquad (11)$$

For any other group the corresponding relations are obtained by appropriately adjusting the indices p, i, and j. Equations (2) and (11) specify the physical properties of the reduced system in terms of the physical properties of the original system.

To demonstrate the application of the procedure presented above and the validity of the use of the reduced system, several examples are presented. For each example presented, the original system is examined and then the reduced system, so that a dynamic equivalence may be demonstrated. A dynamic equivalence is established when the natural frequencies, ω_i, and summed effective weights,

$$\left[\begin{array}{c}\\ \\ \\ \\ \\ \end{array}\right]$$

of the reduced system are "close" to the natural frequencies, ω_i, and summed effective weights,

$$\left[\begin{array}{c}\\ \\ \\ \\ \\ \end{array}\right]$$

of the original system. The kth mode effective weight is defined through the equation

$$\left[\begin{array}{c}\\ \\ \\ \\ \\ \end{array}\right] \qquad (12)$$

where g denotes the gravitational acceleration, and $\phi_i^{(k)}$ the kth mode shape associated with the ith mass point, m_i.

Example 1

To demonstrate the reduction procedure, consider the two-mass model shown in Fig. 1(a). This model was selected because of its proximity to the panel point model for vertical motion of the simple truss shown in Fig. 1(b). The parameter γ in the two-mass model is left open to account for a variable stiffness ratio between the vertical member and upper chords of the simple truss. The dynamic characteristics of interest will be obtained for the original system first and then for the reduced (single-mass) system shown in Fig. 1(c), using the procedure outlined above. A physically meaningful range for the parameter γ will be obtained by considering the relation of the two-mass model to the simple truss.

The stiffness, K_{ij}, and mass, M_{ij}, matrices for the two-mass model are given by

$$\left[\begin{array}{c}\\ \\ \\ \\ \\ \end{array}\right] \qquad (13)$$

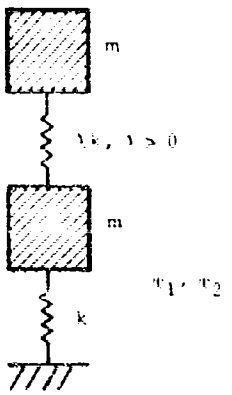

(a) Original system

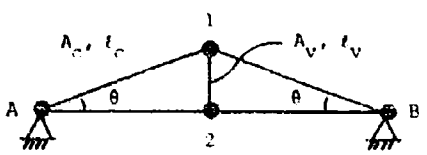

(b) Simple truss

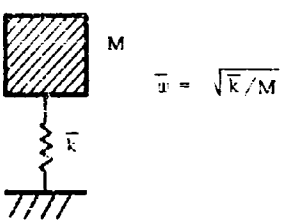

(c) Reduced system

Figure 1

$$M_{11} = m\begin{bmatrix} 1 & 0 \\ 0 & 1 \end{bmatrix} \quad (14)$$

Solving the associated eigenvalue problem, the lowest natural frequency is

$$\omega_1 = \left[1 - \frac{\gamma}{2} - \sqrt{1 - \gamma + \gamma^2}\right]^{1/2} \left(\frac{k}{m}\right)^{1/2} \quad (15)$$

and the first mode amplitude ratio is

$$\frac{A_2}{A_1} = \frac{2}{\gamma - 1 + \sqrt{1 - \gamma + \gamma^2}} \quad (16)$$

To obtain the natural frequency, $\bar{\omega}$, of the reduced system, invert the stiffness matrix, S_{11}, to obtain the influence coefficient matrix

$$\begin{bmatrix} \cdot & \cdot \\ \cdot & \cdot \end{bmatrix} \quad (17)$$

Using Eqs. (11) and (17), obtain the influence coefficient for the reduced system

$$\frac{1}{\bar{k}} = \sum_{i=1}^{2} \left(1 + \frac{A_i}{A_1}\right)^2 \frac{1}{k} \quad (18)$$

so that

$$\bar{\omega} = \left[\sum_{i=1}^{2} \left(1 + \frac{A_i}{A_1}\right)^2\right]^{-1/2} \left(\frac{k}{m}\right)^{1/2} \quad (19)$$

To establish a dynamic equivalence between the original and reduced systems, compare the frequencies $\bar{\omega}$ and ω_1, and the first mode effective weight, $\bar{M}_1$, of the original system with $\bar{M}_1 = M$ of the reduced system.

Before proceeding with this comparison, examine the simple truss of Fig. 1(b) to obtain a range of physical interest for the parameter γ. Requiring that the loaded members of the truss be equally stressed when the truss is subjected to equal concentrated vertical loads at joints 1 and 2, the area ratio of the upper chord to the vertical member is found to be

$$\frac{A_c}{A_v} = \frac{1}{\sin^2\theta} \quad (20)$$

The stiffness of joint 1 to ground (joints A and B), for vertical motion, is given by

$$k_c = 2\left(\frac{A_c E}{\ell_c}\right)\sin^2\theta \quad (21a)$$

The stiffness between joints 1 and 2, for vertical motion, is given by

$$k_v = \frac{A_v E}{\ell_v} \quad (21b)$$

Combining Eqs. (20) and (21b), and noting the geometry, Eq. (21b) may be rewritten in the form

$$k_v = \frac{A_c E}{\ell_c} \quad (21c)$$

The stiffnesses k and k given above correspond respectively to k and k of the two-mass model. Hence,

$$k = \frac{1}{2}\left(\quad\right) \tag{22}$$

The dynamic characteristics of the original and reduced systems will now be compared for values of $= 1/2$. The comparison between $_1$ and ^{1} is presented in Fig. 2. It is seen that the error in ^{1} approaches a maximum value of 6.7 percent as approaches 0.5 from above. This error decreases rapidly as increases. For $= 1$ the error is 2.3 percent, and for $= 2$ the error is less than 1 percent, decreasing to zero as continues to increase.

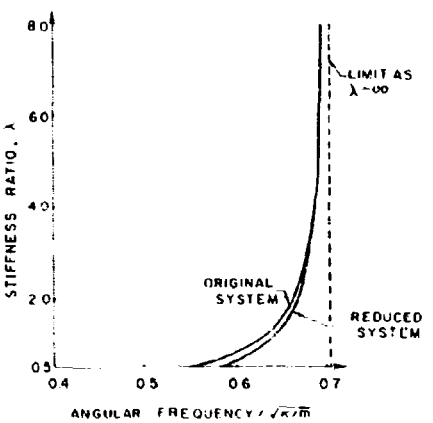

Fig. 2. Frequency comparison

The second characteristic to be compared is the first mode effective weight of the original system, $_1$, with that of the reduced system, ^{1}. For the original system $_1$ is given by

$$_1 = \left(\quad\right)^2 \left(\quad\right)^{-1} \left(\quad\right) \tag{23}$$

and for the reduced system,

$$^1 = M_r \left(\quad\right)^2 \tag{24}$$

The comparison between $_1$ and ^{1}, for $= 1/2$ is presented in Fig. 3. It is seen that the error in ^{1} approaches a maximum value of 17 percent as approaches 0.5 from above. This error decreases rapidly as increases. For $= 1$ the error is 5.3 percent, and for $= 2$ the error is less than 1.5 percent, decreasing to zero as continues to increase. Hence, a complete dynamic equivalence, to within 5.3 percent, is established between the original and reduced systems for $= 1$. In terms of the simple truss of Fig. 1(b), values of $= 1$ are attained for truss angles $= 45$ degrees.

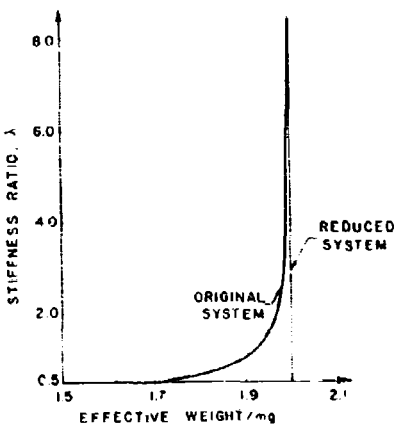

Fig. 3. Effective weight comparison

The preceding example was presented to demonstrate the reduction procedure. The examples to be considered next are more complex and consequently warrant, from a practical viewpoint, the use of the reduction procedure.

Example 2

The truss shown in Fig. 4(a) has a span-to-height ratio of 10, and was so proportioned that each of its elements would be equally stressed to 20,00 psi when a 30,000-lb vertical load is placed at each joint. Using a material density = 0.283 lb/in.^{3}, and assuming a uniform weight distribution, the weight per mass point is 4093 lb. The influence coefficient matrix, $_{ij}$, for vertical deformation is given in Table 1. This matrix was obtained by first formulating the stiffness matrix allowing for both X and Y deformations. The stiffness matrix was then inverted using a digital computer), and the elements corresponding to deformations in the X direction deleted. The

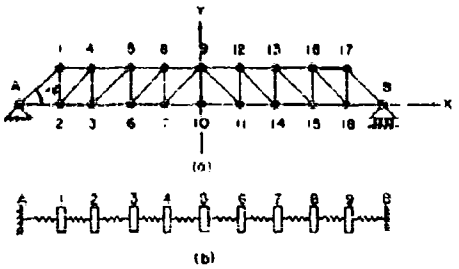

Fig. 4. (a) Truss (original system), and (b) reduced system

influence coefficient matrix, a_{ij}, and the weight matrix were substituted into the DTMB Program 2262 [4] to find the eigenvalues and modal characteristics. The results of this computation, for the parameters of interest (ω_i, μ_i) are presented in Tables 2 and 3, respectively, for the first nine modes.

Using the influence coefficient matrix given in Table 1 and Eq. (11), the influence coefficient matrix, a_{ij}, for the reduced (nine-mass-point) system shown in Fig. 4(b) is obtained. This matrix is presented in Table 4. Replacing the mass points lying on the same truss vertical by a single mass point, and using Eq. (2), the weight per mass point is 8106 lb. Again, employing the DTMB program, the parameters of interest (ω_i, μ_i) were obtained and are presented in Tables 2 and 3, respectively, for the system's nine modes.

The errors that would be incurred if the reduced system were used in place of the original system are also given in Tables 2 and 3. It is seen from Table 2 that the first seven natural frequencies are reproduced to within

TABLE 1
Influence Coefficient Matrix for Vertical Deformation of the Truss Shown in Fig. 4(a) (in./lb)

4.7	4.6	6.0	6.1	6.7	6.5	6.3	6.6	5.5	5.5	4.4	4.1	3.1	3.3	2.2	7.1	1.0	1.1
4.6	5.5	6.8	6.9	7.4	7.2	6.9	7.2	6.0	6.0	4.8	4.5	3.4	3.6	2.4	2.3	1.1	1.2
6.0	6.8	13.2	12.2	14.5	14.1	13.5	14.1	11.7	11.7	9.4	8.8	6.6	7.0	4.7	4.5	2.2	2.4
6.1	6.9	12.2	12.5	13.7	13.3	12.7	13.4	11.1	11.1	8.9	8.3	6.2	6.6	4.5	4.2	2.1	2.3
6.7	7.4	14.5	13.7	20.1	19.5	18.7	19.7	16.4	16.4	13.2	12.2	9.2	9.8	6.6	6.2	3.1	3.4
6.5	7.2	14.1	13.3	19.5	20.9	19.9	20.9	17.4	17.4	14.0	13.0	9.8	10.4	7.0	6.6	3.3	3.6
6.3	6.9	13.5	12.7	18.7	19.9	26.9	24.9	23.5	23.5	18.9	17.5	13.2	14.0	9.4	8.9	4.4	4.8
6.6	7.2	14.1	13.4	19.7	20.9	24.9	26.3	21.8	21.8	17.5	16.2	12.2	13.0	8.8	8.3	4.1	4.5
5.5	6.0	11.7	11.1	16.4	17.4	23.5	21.8	29.1	29.1	23.5	21.8	16.4	17.4	11.7	11.1	5.5	6.0
5.5	6.0	11.7	11.1	16.4	17.4	23.5	21.8	29.1	39.1	23.5	21.8	16.4	17.4	11.7	11.1	5.5	6.0
4.4	4.8	9.4	8.9	13.2	14.0	18.9	17.5	23.5	23.5	26.9	24.9	18.7	19.9	13.5	12.7	6.3	6.9
4.1	4.5	8.8	8.3	12.2	13.0	17.5	16.2	21.8	21.8	24.9	26.3	19.7	20.9	14.1	13.4	6.6	7.2
3.1	3.4	6.6	6.2	9.2	9.8	13.2	12.2	16.4	16.4	18.7	19.7	20.1	19.5	14.5	13.7	6.7	7.4
3.3	3.6	7.0	6.6	9.8	10.4	14.0	13.0	17.4	17.4	19.9	20.9	19.5	20.9	14.1	13.3	6.5	7.2
2.2	2.4	4.7	4.5	6.6	7.0	9.4	8.8	11.7	11.7	13.5	14.1	14.5	14.1	13.2	12.2	6.0	6.8
2.1	2.3	4.5	4.2	6.2	6.6	8.9	8.3	11.1	11.1	12.7	13.4	13.7	13.3	12.2	12.5	6.1	6.9
1.0	1.1	2.6	2.1	3.1	3.3	4.4	4.1	5.5	5.5	6.3	6.6	6.7	6.5	6.0	6.1	4.7	4.6
1.1	1.2	2.4	2.2	3.4	3.6	4.8	4.5	6.0	6.0	6.9	7.2	7.4	7.2	6.8	6.9	4.6	5.5

$\times 10^{-6}$

TABLE 2
Frequency Comparison (Uniform Weight Distribution)

Mode	ω_i (rad/sec)	$\bar{\omega}_i$ (rad/sec)	Percent Error
1	20.6	20.6	0
2	45.0	45.1	0.2
3	68.4	70.2	2.6
4	102.8	104.4	1.6
5	104.8	111.7	6.6
6	151.4	157.8	4.5
7	156.8	161.1	2.7
8	188.6	227.7	20.7
9	220.4	227.8	3.4

TABLE 3
Effective Weight Comparison (Uniform Weight Distribution)

Mode (m)	$\sum_{i=1}^{m} w_i$ (lb)	$\sum_{i=1}^{m} w_i$ (lb)	Percent Error[a]
1	63,576	63,678	0.2
2	63,576	63,678	0.2
3	68,067	68,678	0.9
4	70,708	68,678	2.9
5	70,708	71,213	0.7
6	72,450	71,213	1.7
7	72,450	72,669	0.3
8	72,661	72,669	0
9	72,661	73,675[b]	1.4

[a]To nearest tenth of a percent.
[b]Total truss weight = 73,675 lb.

TABLE 4
Influence Coefficient Matrix for Vertical Deformation of the Model Shown in Fig. 4(b) (in./lb)

$$\begin{bmatrix} 4.9 & 6.5 & 7.0 & 6.8 & 5.8 & 4.5 & 3.4 & 2.3 & 1.1 \\ 6.5 & 12.5 & 13.9 & 13.4 & 11.4 & 8.9 & 6.6 & 4.5 & 2.3 \\ 7.0 & 13.9 & 20.0 & 19.8 & 16.9 & 13.1 & 9.8 & 6.6 & 3.4 \\ 6.8 & 13.4 & 19.8 & 25.8 & 22.7 & 17.5 & 13.1 & 8.9 & 4.5 \\ 5.8 & 11.4 & 16.9 & 22.7 & 31.6 & 22.7 & 16.9 & 11.4 & 5.8 \\ 4.5 & 8.9 & 13.1 & 17.5 & 22.7 & 25.8 & 19.8 & 13.4 & 6.8 \\ 3.4 & 6.6 & 9.8 & 13.1 & 16.9 & 19.8 & 20.0 & 13.9 & 7.0 \\ 2.3 & 4.5 & 6.6 & 8.9 & 11.4 & 13.4 & 13.9 & 12.5 & 6.5 \\ 1.1 & 2.3 & 3.4 & 4.5 & 5.8 & 6.8 & 7.0 & 6.5 & 4.9 \end{bmatrix} \times 10^{-6}$$

6.6 percent accuracy. It is seen from Table 3 that the sum of effective weights (up to and including the mode of interest) are reproduced to within 2.9 percent accuracy.

Example 3

The truss of Fig. 4(a) was treated in example 2 under the assumption of a uniform weight distribution. The same problem is treated here dropping this assumption. The weight distribution used is obtained by assigning to each mass point (truss joint) one-half the sum of the weights of the truss members entering each joint. From the geometry of the structure it is seen that this is a realistic assumption. The diagonal weight matrix is presented in Table 5.

The weight distribution for the reduced system is obtained, as in example 2, by replacing the mass points lying on the same truss vertical by a single mass point, and using Eq. (2). This diagonal weight matrix is presented in Table 6.

The DTMB program was again employed imputing the matrices given in Tables 1 and 5 for the original system, and the matrices given in Tables 4 and 6 for the reduced system. The resulting dynamic characteristics of interest are presented in Tables 7 and 8.

From these tables it is seen that the results for the first seven natural frequencies are reproduced to within 6.1 percent accuracy, and the sum of effective weights (up to and including the mode of interest) is reproduced to within 2.6 percent accuracy.

CONCLUSIONS

A method for reducing the number of mass points in a lumped parameter system has been presented, and several examples demonstrating the procedure have been considered. For the examples considered, a dynamic equivalence has been established between the original and reduced systems. This consists of demonstrating a "closeness" in natural frequencies

TABLE 5
Weight Matrix for Truss Shown in Fig. 4(a) (lb)
(Nonuniform Weight Distribution, Total Weight = 73,675 lb)

2671																								
	4254																							
		4721																						
			3454																					
				3910																				
					4774																			
						4673																		
							4072																	
								4059																
									4558															
										4673														
											4072													
												3910												
				(0)									4774											
														4721										
															3454									
																2671								
																	4254							

TABLE 6
Weight Matrix for the Model Shown in Fig. 4(b) (lb)
(Nonuniform Weight Distribution, Total Weight = 73,675 lb)

6925																								
	8175																							
		8684																						
			8745																					
				8617																				
					8745																			
			(0)									8684												
														8175										
															6925									

TABLE 7
Frequency Comparison (Nonuniform Weight Distribution)

Mode	ω_i (rad/sec)	$\bar{\omega}_i$ (rad/sec)	Percent Error
1	20.6	20.1	0.5
2	44.4	44.5	0.2
3	66.7	69.4	4.0
4	100.8	104.0	3.2
5	104.3	110.7	6.1
6	150.9	159.3	5.6
7	156.0	160.9	2.0
8	188.4	234.7	24.6
9	224.2	237.2	5.8

TABLE 8
Effective Weight Comparison (Nonuniform Weight Distribution)

Mode (m)	$\sum_{i=1}^{m} \bar{w}_i$ (lb)	$\sum_{i=1}^{m} \bar{w}_i$ (lb)	Percent Error[a]
1	64,521	64,561	0.1
2	64,521	64,561	0.1
3	68,416	66,975	0.8
4	70,636	68,975	2.6
5	70,836	71,203	0.5
6	72,388	71,203	1.6
7	72,388	72,539	0.2
8	72,526	72,539	0
9	72,526	73,675[b]	1.6

[a]To nearest tenth of a percent.
[b]Total truss weight = 73,675 lb.

and effective weights (summed to the mode of interest) between the reduced and original systems.

Satisfying the dynamic equivalence for frequencies and summed effective weights is of importance for problems in which a base acceleration is the input. For other inputs, higher resolution may be required in the criterion for establishing a dynamic equivalence. This was attempted for the problems considered above by requiring, in addition to the frequency comparisons, a comparison of the generalized displacements (reciprocal of the product of generalized mass and frequency squared) for each of the normal modes considered. Agreement to within 5 percent accuracy was attained between the generalized displacements of the original and reduced systems for the first two modes only. The higher modes showed a marked loss in accuracy, demonstrating the possible limitations of the procedure to inputs more complex than a base acceleration.

REFERENCES

1. R. O. Belsheim and G. J. O'Hara, "Shock Design of Shipboard Equipment, Dynamic Design - Analysis Method," NavShips 250-423-30, May 1961

2. R. L. Harrington and W. S. Vorus, "Dynamic Shock Analysis of Shipboard Equipment," Marine Technology, Oct. 1967, pp. 331-354

3. E. G. Fisher, "Theory of Equipment Design," Shock and Vibration Handbook, 3:42 (McGraw-Hill), 1961

4. J. H. Avila, "Normal Mode Computer Analysis of Structures," David Taylor Model Basin Rept. 2262, Jan. 1967

DISCUSSION

M. Pakstys (General Dynamics/Electric Boat): As I understand it, in reducing the mass all you did was to lump the mass at the center joint. Is this correct?

Mr. Soifer: Not at the center joint, but at the center of mass of the system.

Mr. Pakstys: Have you tried to use a method I described, to reduce the mass matrix which will give a nondiagonal mass matrix? I think that might improve your results.

Mr. Soifer: I have not tried that. I did not see any simplification of the problem in your

method, in the sense that you were reducing the actual number of points used. I see that you are subdividing the system and then analyzing each subdivided system.

Mr. Paksiys: This was the main part of my paper, but the so-called direct reduction that was proposed actually involves the reduction of the mass matrix and the stiffness matrix. It is actually eliminating the degrees of freedom. It is just as you have said here except it also reduces the mass matrix by the same transformation matrix instead of just lumping it at the center.

* * *

LATERAL DYNAMIC RESPONSE OF LARGE SUBSYSTEMS DURING LAUNCH TRANSIENT CONDITIONS*

J. S. Gaffney and P. E. Campos
Atlantic Research Corporation
Costa Mesa, California

The dynamic response of large aerospace vehicles to the launch transient loading in the lateral direction has been the subject of considerable study. For the most part, these analyses have been concerned with body loads and either ignore large flexible subsystems within the vehicle shell or treat them as simple 1- and 2-degree-of-freedom models. The purpose of this paper is to present a comparison of the vehicle/subsystem interaction for several models and to show the advantages of using a multiple-degree-of-freedom subsystem model for certain configurations. The problem originated with the Saturn class boosters and the capacity to carry large auxiliary payloads in the spacecraft adapter area. The objective of the analysis is to provide a better understanding of interaction of large subsystems with the primary vehicle and to obtain a good engineering definition of the resultant dynamic loads.

INTRODUCTION

The method of approach is to write the equations of motion in matrix form with the primary vehicle model coupled with the subsystem model in the equations of motions rather than in the modal analysis. This feature allows the study of the effects of the interface stiffness without resorting to calculation of new system modes. The isolation of this parameter is very important in preliminary design activities.

The subsystem models included in this study are:

1. Flexible subsystem — 20 mass model.

2. Center-of-gravity supported subsystem — rigid-body model with the interface at the center of gravity of the subsystem.

3. Base-supported subsystem -- rigid-body model with the interface lower than the center of gravity of the subsystem.

The attachment springs for the rigid-body models include all structural flexibility between the vehicle shell and the center of gravity of the subsystem.

The main feature of the analysis is the separation of the primary vehicle and subsystem models for the modal calculations and then the coupling of the systems in the equations of motion. This procedure requires that rigid-body equations and modal equations of motion be written for both the vehicle and subsystem; however, the versatility obtained offsets this inconvenience. An important consideration that cannot be overlooked when this method is used is the accuracy with which the motion of the interface can be described. This problem was solved by pinning the subsystem model at the interface and calculating the modes for this model. It is then possible to describe the interface motion with only the rigid-body coordinates of the subsystem. If a free-free subsystem model is used, it becomes almost impossible to describe this motion with the required accuracy.

Comparisons between the vehicle/subsystem interface loads, and loads and accelerations

*The work described in this paper was performed by the authors while employed at North American Aviation.

at a typical vehicle station for the various subsystem configurations are presented. These results show that the loads for the more complete (multiple-degree-of-freedom) model are lower than for other models. Utilization of the method presented in this paper will result in weight savings in addition to providing detailed information for preliminary design trade-off studies.

NOMENCLATURE

- A Area (ft^2)
- A_α Control system angle of attack gain
- A_t Control system rate gain (1/sec)
- C_D Drag coefficient
- F Interface force (lb)
- $\bar{F}$ Wind force (lb)
- I Mass moment of inertia ($lb\text{-}sec^2/in.$)
- L Wind load (lb)
- M Total mass ($lb\text{-}sec^2/in.$)
- m Elemental mass ($lb\text{-}sec^2/in.$)
- Q Modal generalized force (lb)
- q Modal generalized coordinate (in.)
- T Total thrust (lb)
- T_β Gimballed thrust (lb)
- V Wind velocity (fps)
- X Station coordinate (in.)
- Y Rigid-body translation (in.)
- y Sloshing mass displacement (in.)
- β Gimbal angle (rad)
- β_c Command gimbie angle (rad)
- β_t Thrust misalinement (rad)
- ζ Damping coefficient
- ρ Density of air (lb/ft^3)
- θ Rigid-body rotation (in.)
- ϕ Modal generalized displacement (in./in.)
- ϕ' Modal generalized slope (rad/in.)
- ω Natural frequency (rad/sec)

Subscripts

- p Peak
- ss Steady state
- n Body station (general)
- i Mode indicator
- g At the gimbal station
- j Sloshing mass
- cg Center of gravity
- s Refers to subsystem
- m Refers to the rigid body

CONSIDERATIONS

The dynamic response of large aerospace vehicles such as the Saturn and Titan class vehicles to the launch transient loading in the lateral direction has been the subject of considerable study and concern. The first studies of the dynamic loads were limited to relatively simple models of 10 or 20 mass elements and simple descriptions of the aerodynamic loading on the vehicle. Subsequent improvements were directed toward better definition of the body loads. However, these analyses have either ignored large flexible subsystems within the vehicle shell or have used simple 1- and 2-degree-of-freedom rigid-body models of the subsystem. Because the relatively flexible payload region of a large vehicle is especially sensitive to the instantaneous release of the launch pad mechanisms and as the internal payload is located close to the payload, the dynamic interaction of the subsystem with the payload must be considered with sufficient detail to describe the total effects. As secondary payloads that are carried in areas such as the Spacecraft Adapter on the Saturn V for the Apollo Application Program are designed, it becomes necessary to have better definition of the subsystem dynamic response.

One method which will provide better detail is to model the subsystem as a multi-degree-of-freedom system in the same way as the primary vehicle. Details of the mass distribution and subsystems flexibility can then be included. Studies of this nature require digital computers both for the calculation of normal modes of vibration and for the dynamic response calculation. To develop a program that has applicability in both preliminary and detail design it is advantageous to separate the models of the primary vehicle and the subsystem. The model for the primary vehicle can be determined and these modes calculated only one time. As various subsystem configurations are studied, it is necessary only to recalculate the new subsystem modes. It is also possible to study the effects of various attachment schemes as the attachment spring rates are used to determine the interaction forces between the primary vehicle and subsystem.

When the primary vehicle and subsystem models are separated for the modal analysis and coupled in the equations of motion, rigid-body and modal equations of motion are required for both the vehicle and subsystem. An important consideration is the accuracy with which the motion of the interface can be described. If a free-free model of the subsystem is used, it is almost impossible to describe this motion with the required accuracy. This problem is solved by pinning the subsystem model at the interface stations. It is then possible to describe the translational motion of the interface with only the rigid-body coordinates of the subsystem.

LAUNCH LOADING CONDITIONS

Lateral dynamic loads at launch are caused by a combination of ground winds, vehicle deflection, and engine thrust vector misalinement. In all of the large booster programs, the structural design criteria specify a certain percentage ground-wind profile that will not be exceeded during the launch phase. The type of gust, either triangular or 1-minus-cosine, and gust duration are specified. As a result of these criteria two methods for ground-wind loading have been developed for the Saturn class vehicles.

The type of gust for Saturn vehicles is triangular and the period is equal to the period of the first cantilevered bending mode of the vehicle. The first ground-wind method, developed by the NASA at Marshall Space Flight Center, proceeds as follows: the bending moment distribution for steady winds is calculated. An inverted triangular loading (the base at the top of the vehicle) is constructed to have values such that when added to the steady-state loading, the resulting base moment is equal to 1-1/2 times the steady state base bending moment. All details of this rationale are not known to the authors except that it accounts for the effects of wind gusts and vortex shedding as well as the steady-state loading, and reportedly agrees well with wind-tunnel tests.

The second method, developed by Space Division, North American Rockwell, is described as follows: the ground-wind loading is calculated on each segment of the vehicle for steady-state wind, wind gusts, and vortex shedding, and an empirical factor is included to account for the dynamic response of the flexible vehicle to wind gusts.

The loading on any segment for the prelaunch winds is considered simply as drag on a cylinder. Wind-gust velocities are determined by multiplying the steady-state winds by 1.4. For a triangular gust tuned to the first mode frequency of the vehicle the response will be a maximum of 1.0 times the forcing gust load. As it turns out, it makes no practical difference whether the gust is triangular or sinusoidal; the overshoot is approximately 80 percent for both cases. As the load is proportional to the square of the velocity, the peak load is given by

$$L_p = L_{ss} + 1.6\left[(1.4)^2 - 1.0\right] L_{ss}$$

or

$$L_p = 2.54\, L_{ss}$$

The loading owing to vortex shedding has been estimated as 1.25 times the steady-state load. This load is normal to the dragwise load resulting in

$$F_n = \left[(2.54)^2 + (1.25)^2\right]^{1/2} L_{ss}$$

or

$$F_n = 2.83\, L_{ss} \tag{1}$$

The steady-state loading on the segment is written

$$L_{ss} = 1/2\, C_D \rho V_{ss}^2 A \tag{2}$$

The aerodynamic loading on the vehicle, owing to ground winds, and the subsequent deflection of the vehicle constitute the initial conditions at release. Although the loading prior to release may vary with time, for the purposes of loads analysis, release is effected at time of maximum deflection. Investigation of the response for various initial conditions has shown that maximum loads occur for the vehicle at maximum deflection. Figure 1 is a schematic of the vehicle just prior to release. The base shear and bending moment are discontinuous in time at the instant release. This step-release of the launch pad forces is the prime excitation causing the launch dynamic loads. The prelaunch equivalent wind loading is the aerodynamic force caused by steady-state winds, wind gusts, and Von Kármán vortex shedding effects.

The deflection of the vehicle on the launch pad can be calculated by determining the bending moment diagram for the loading as shown in Fig. 1 (notice that the displacement of the weight segment is included in the moment diagram), integrating the moment diagram for the slope, and then integrating the slope curve to obtain the deflection. By starting the integration at the base, the value of the integrals will

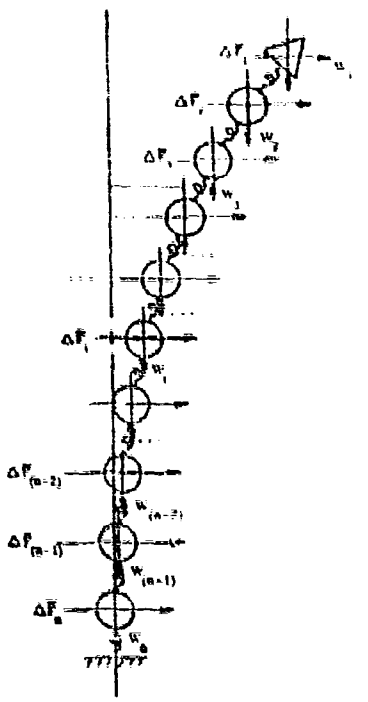

Fig. 1. Loading diagram for static deflection calculation

give the slope and deflection at each mass and the curves can be constructed. The additional effects of the masses when deflected from the rigid-body centerline are taken into account on the second and subsequent iterations. Although the actual number of iterations depends on the weight distribution, three to five iterations are generally required before the additional incremental moment owing to the vehicle weight is negligible. Figure 2 shows the peak and steady-state prelaunch bending moment.

The wind loading after release is caused by the steady-state wind and wind gusts only. The dynamic response and vortex shedding factor are dropped from Eq. (1), yielding

$$F_n = 1.96 L_{ss} \qquad (3)$$

When the vortex shedding term is dropped from the wind-force equation, a shift in the direction of the wind-loading vector occurs. This vector rotation is neglected. It would be possible to include the vector shift by using symmetrical modes. This is not done because the criteria inaccuracies do not justify the formulation and programing difficulties.

EQUATIONS OF MOTION

The equations of motion for the system shown in Fig. 3 are developed below.

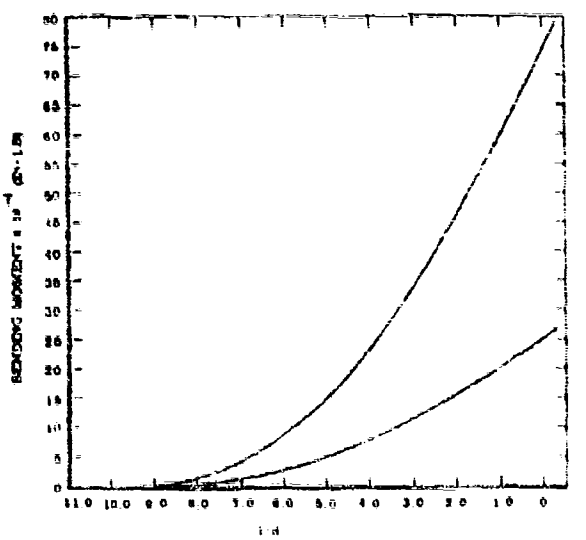

Fig. 2. Steady-state and peak bending moment for ground-wind conditions

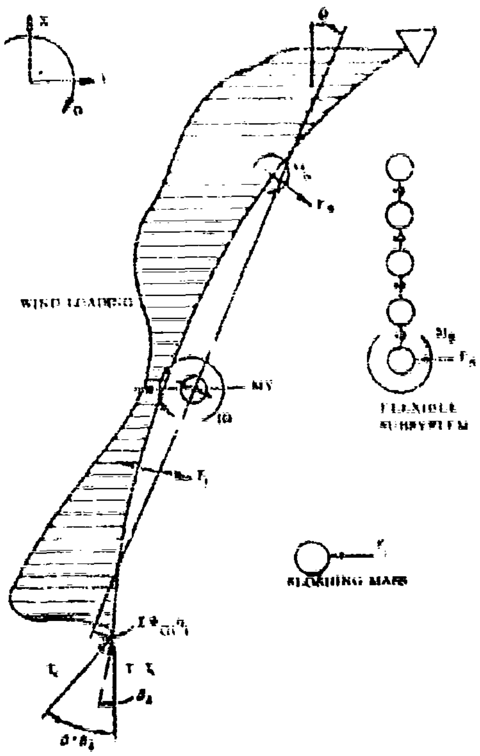

Fig. 3 Loading diagram for in-flight vehicle

Primary Vehicle Equations

Rigid-body translation:

$$M\ddot{Y} = \sum_n F_n + (T - T_c)\left(\theta + \beta_i + \sum_i \phi'_{gi} q_i\right) + T_c\left(\theta + \beta + \beta_c + \sum_i \phi'_{gi} q_i\right) + F_s + \sum_j F_j \quad (4)$$

Rigid-body rotation:

$$I\ddot{\theta} = \sum_n \left[\Delta F_n (X_n - X_{cg})\right] + (T - T_c)\left(\beta_i + \sum_i \phi'_{gi} q_i\right)(X_{cg} - X_g) + T_c\left(\beta + \beta_c + \sum_i \phi'_{gi} q_i\right)(X_{cg} - X_g) + M_s + F_s(X_s - X_{cg}) + \sum_j \left[F_j (X_j - X_{cg})\right] \quad (5)$$

Fuel slosh:

$$\ddot{y}_j + 2\zeta_j \omega_j \dot{y}_j + \omega_j^2 y_j = -\omega_j^2 \left[Y + (X_j - X_{cg})\theta + \sum_i \phi_{ji} q_i\right] - 2\zeta_j \omega_j \left[\dot{Y} + (X_j - X_{cg})\dot{\theta} + \sum_i \phi_{ji} \dot{q}_i\right] \quad (6)$$

A discussion of the method employed to determine the fuel slosh mass and frequency is given in Ref. [1].

Flexible-body equations:

$$M_i \ddot{q}_i + 2\zeta_i \omega_i M_i \dot{q}_i + \omega_i^2 M_i q_i = Q_i \quad (7)$$

The generalized forces, Q_i, are caused by ground winds, engine thrust, and mounted mass and fuel slosh coupling. Taking each item in turn, Q_i is

$$Q_i = \sum_n \Delta F_n \phi_{ni} + \left[(T - T_c)\left(\beta_i + \sum_i \phi'_{gi} q_i\right) + T_c\left(\beta + \beta_c + \sum_i \phi'_{gi} q_i\right)\right]\phi_{gi} + F_s \phi_{si} + M_s \phi'_{si} + \sum_j F_j \phi_{ji} \quad (8)$$

Subsystem Equations

The subsystem equations are formulated for a model that is pin-ended at the station corresponding to the connection station. This allows the absolute displacement of this station to be defined by the rigid-body coordinate. The main advantage of this model is to decouple the accuracy of the interface loads between the subsystem and the primary vehicle from the number of modes used in the equations of motion for the subsystem. As the subsystem modes generally have higher frequencies than the vehicle, a few modes in addition to the rigid-body modes are sufficient to define the subsystem loads using the modal acceleration method. On the other hand, if the subsystem model is free-free, many modes are required to accurately define the displacement at the interface. Then, it is almost impossible to establish the correct initial conditions with free-free subsystem modes. With this short prelude, the equations are —

Rigid-body translation:

$$M_s \ddot{Y}_s = -F_s \quad (9)$$

Rigid-body rotation:

$$I_s \ddot{\theta}_s = -M_s + F_s(X_{scg} - X_{ss}) \quad (10)$$

Flexible body:

$$M_s \ddot{q}_{si} + 2\zeta_{si}\omega_{si} M_s \dot{q}_{si} + \omega_{si}^2 M_s q_{si} = Q_{si} \quad (11)$$

The generalized force Q_{si} is a function of F_s and M_s which, in turn, are functions of the interface spring constants and the relative

deflection and rotation at the interface. For the pin-ended model the contribution of the moment can be calculated by

$$Q_{sm_i} = -M_s \varphi_{ssi} \qquad (12)$$

However, the contribution of the force F_s cannot be determined with a similar expression because the mode shape is zero at the pin joint for all modes. It is therefore necessary to determine this contribution from the inertia forces on each mass.

$$Q_{sf_i} = \sum_n \left\{ m_{sn} \left[Y_s + (X_{sn} - X_{scg}) \ddot{\beta}_s + \sum_i \varphi_{sn_i} q_{si} \right] \varphi_{sn_i} \right\} . \qquad (12a)$$

The total generalized force is given by

$$Q_{s_i} = Q_{sm_i} + Q_{sf_i} \qquad (12b)$$

Interface forces:

$$F_s = -K_s \left[Y + (X_s - X_{cg})\beta + \sum_i \varphi_{si} q_i - Y_s \right] - C_s \left[\dot{Y} + (X_s - X_{cg})\dot{\beta} + \sum_i \varphi_{si} \dot{q}_i - \dot{Y}_s \right] . \qquad (13)$$

$$M_s = -K_\beta \left[\beta + \sum_i \varphi_{si} q_i - \beta_s - \sum_i \varphi_{ssi} q_{si} \right] - C_\beta \left[\dot{\beta} + \sum_i \varphi_{si} \dot{q}_i - \dot{\beta}_s - \sum_i \varphi_{ssi} \dot{q}_{si} \right] . \qquad (14)$$

Control Equations

The control system used for the vehicle just after launch is based on attitude control principles. To avoid unnecessary complexity, only the rigid-body motion is considered in the system gain calculations. Actually, considerable liberty is taken with the simplification of the control system. The peak loads on the vehicle occur within the first 5 sec after launch and the control system has little or no effect on the loads during this time. The gimbal equations are also simplified, assumed to be second order, and of the form

$$\ddot{\beta} + 2\zeta_g \omega_g \dot{\beta} + \omega_g^2 \beta = \omega_g^2 \beta_c \qquad (15)$$

The control equation is

$$\beta_c = A_0 \dot{\theta} + A_1 \theta \qquad (16)$$

Using Eqs. (5), (15), and (16), the open loop transfer function can be determined as

$$\text{OLTF} = \frac{\frac{T_c}{I}\left[(X_{cg} - X_g) A_0 \left(\frac{A_1}{A_0} s + 1\right)\right]}{\omega_g^2 s^2 \left(\frac{s^2}{\omega_g^2} + 2\zeta_g \frac{s}{\omega_g} + 1\right)} \qquad (17)$$

The corresponding closed loop transfer function is

$$\text{CLTF} = \frac{\frac{T_c}{I}\left[(X_{cg} - X_g) A_0 \left(\frac{A_1}{A_0} s + 1\right)\right]}{\omega_g^2 s^2 \left(\frac{s^2}{\omega_g^2} + 2\zeta_g \frac{s}{\omega_g} + 1\right) + \frac{T_c}{I}\left[(X_{cg} - X_g) A_0 \left(\frac{A_1}{A_0} s + 1\right)\right]} \qquad (18)$$

To determine the gains, A_0 and A_1, it is necessary only to choose a rigid-body pitching frequency, ω_m, and the associated damping, ζ_m. These choices define the operating points as shown in Fig. 4.

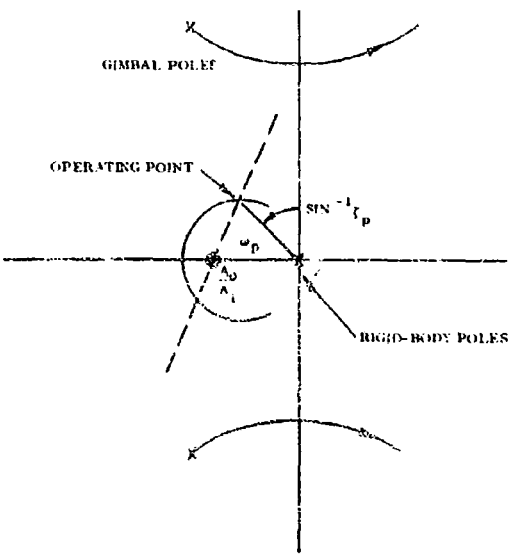

Fig. 4. Root locus of attitude control guidance principle

The relationships for A_0 and A_1 can now be obtained by dividing the equation that describes the rigid-body roots,

$$s^2 + 2\zeta_m \omega_m s + \omega_m^2 = 0 ,$$

into the characteristic equation of the closed loop transfer function, Eq. (18). The resulting expressions for the gains are

$$\frac{T_c(X_{cg} - X_g) + \omega_g^2 A_1}{I} = (\omega_m^2 2\zeta_g\omega_g - 2\zeta_m\omega_m\omega_m^2) - 2\zeta_m\omega_m\left[\omega_g^2 - \omega_m^2 - 2\zeta_m\omega_m(2\zeta_g\omega_g - 2\zeta_m\omega_m)\right], \quad (19)$$

and

$$\frac{T_c(X_{cg} - X_g) + \omega_g^2 A_0}{I} = \omega_g^2 - \omega_m^2 - 2\zeta_m\omega_m(2\zeta_g\omega_g - 2\zeta_m\omega_m)\omega_m^2 \quad (20)$$

As the characteristic equation is the product of all the roots, the quotient of the above operation is the equation for the location of the roots associated with the gimbal poles. This expression is

$$s^2 + (2\zeta_g\omega_g - 2\zeta_m\omega_m)s + \left[\omega_g^2 - \omega_m^2 - 2\zeta_m\omega_m(2\zeta_g\omega_g - 2\zeta_m\omega_m)\right] = 0 \quad (21)$$

The criterion for stability of the vehicle is that the coefficient of the velocity (s term) in Eq. (21) is positive, or that

$$2\zeta_g\omega_g > 2\zeta_m\omega_m \quad (22)$$

EQUATION OF MOTION MATRIX

The equations of motion are grouped in matrix form in Eq. (23), shown on page 74. These equations gives ready reference to the interaction between the various degrees of freedom and the effects of applied forces. The Laplace operator S is used to denote the derivative of the variables with respect to time. This usage is only a convenience. No attempt is made to solve for the steady-state solution through Laplace operations. The solution is obtained by numerical integration of these equations in the sequence shown. The generalized forces for the subsystem are shown as $Q_{s_i}(F)$ and $Q_{s_i}(M)$. It is to be understood that the actual expression for these terms is as given in Eqs. (12) and (12a).

CONCLUSIONS

The loads summarized in Table 1 and the time histories presented in Figs. 5 through 8 are tabulated against a description of the subsystem model. The flexible subsystem, mounted at the base, consists of translational and rotational rigid-body degrees of freedom plus two flexible-body modes. This model was composed of 20 mass elements and was pinned at the base support. The other two models have rigid-body degrees of freedom only. Bending moments are shown for a station on the primary vehicle and for the subsystem/vehicle interface. Accelerations of the subsystem center of gravity and the vehicle station are also presented. The primary vehicle loads are for an especially critical station that is approximately 1-1/2 body diameters forward of the subsystem interface.

The maximum bending moment at the vehicle body station for the flexible subsystem is lower than for the rigid-body subsystem. This difference in loads is caused by the structural dynamic effect of the subsystem model and shows that although the primary vehicle may be many times heavier and more rigid than the subsystem the effect of the type of model can have an appreciable effect on primary vehicle loads. The lateral accelerations which may be used by the stress analyst to determine bending moments between stations that are recorded and loads on local components could result in further errors.

TABLE 1
Maximum Load Comparison

Subsystem Model	Shear × 10^{-3} (lb)	Moment × 10^{-6} (in.-lb)	Acceleration (g)	Location of Load
		Launch		
Flexible	7.7	1.5	0.3	Body station
Cg support	12.0	1.8	0.53	Body station
Base support	9.3	1.8	0.28	Body station
Flexible	3.8	0.275	0.7	Subsystem
Cg support	10.0	0.240	1.8	Subsystem
Base support	5.8	0.360	1.1	Subsystem

$$
\begin{bmatrix}
1 & 0 & 0 & -C_s S - K_s & 0 & 0 & C_s S + K_s & C_s \ell S + K_s \ell & \begin{Bmatrix} C_s \Psi_{si} S \\ + K_s \Psi_{si} \end{Bmatrix}^T & 0 \\
0 & 1 & 0 & 0 & -C_\theta S - K_\theta & \begin{Bmatrix} -C_\theta \psi_{ssi} S \\ -K_\theta \psi_{ssi} \end{Bmatrix}^T & 0 & C_\theta S + K_\theta & \begin{Bmatrix} C_\theta \psi_{si} S \\ + K_\theta \psi_{si} \end{Bmatrix}^T & 0 \\
0 & 0 & \begin{bmatrix} S^2 + \\ 2\zeta_j \omega_j S \\ + \omega_j^2 \end{bmatrix} & 0 & 0 & 0 & \begin{Bmatrix} -2\zeta_j \omega_j S \\ -\omega_j^2 \end{Bmatrix} & \begin{Bmatrix} -2\zeta_j \omega_j \varphi_j S \\ -\omega_j^2 \ell_j \end{Bmatrix} & \begin{bmatrix} -2\zeta_j \omega_j \varphi_{ji} S \\ -\omega_j^2 \varphi_{ji} \end{bmatrix} & 0 \\
1 & 0 & 0 & M_s S^2 & 0 & 0 & 0 & 0 & 0 & 0 \\
-\ell & 1 & 0 & 0 & I_s S^2 & 0 & 0 & 0 & 0 & 0 \\
-Q_{si}(F) & -Q_{si}(M) & 0 & 0 & 0 & \begin{bmatrix} M_s S^2 + \\ 2\zeta_{si} \omega_{si} M_s S \\ + \omega_{si}^2 M_s \end{bmatrix} & 0 & 0 & 0 & 0 \\
-1 & 0 & \left\{ -M_j S^2 \right\}^T & 0 & 0 & 0 & MS^2 & -T & \left\{ T\ell_{Gi} \right\}^T & -T_c \\
-\ell_s & -1 & \left\{ -M_j \ell_j S^2 \right\}^T & 0 & 0 & 0 & 0 & IS^2 & \left\{ -T\ell_G \varphi_{Gi} \right\}^T & -T_c \ell_G \\
\begin{Bmatrix} -\varphi_{si} \end{Bmatrix} & \begin{Bmatrix} -\psi_{si} \end{Bmatrix} & \left[-M_j \varphi_{si} S^2 \right] & 0 & 0 & 0 & 0 & 0 & \begin{bmatrix} MS^2 + \\ 2\zeta_i \omega_i MS \\ + \omega_i^2 M \end{bmatrix} & \left\{ -T_c \varphi_{Gi} \right\} \\
0 & 0 & 0 & 0 & 0 & 0 & 0 & -\omega_G^2 (A_0 - A_1 S) & 0 & \begin{matrix} S^2 + \\ 2\zeta_G \omega_G S \\ + \omega_G^2 \end{matrix}
\end{bmatrix}
\begin{Bmatrix} F_s \\ M_s \\ Y_j \\ Y_s \\ \theta_s \\ q_{si} \\ Y \\ \theta \\ q_i \\ \beta \end{Bmatrix}
=
\begin{Bmatrix} 0 \\ 0 \\ 0 \\ 0 \\ 0 \\ 0 \\ \Sigma_n \Delta F_n + T\delta_s \\ \Sigma_n \Delta F_n \ell_n + T\delta_s \ell_G \\ \begin{Bmatrix} \Sigma_n \Delta F_n \varphi_{ni} \\ + T\delta_s \varphi_{Gi} \end{Bmatrix} \\ 0 \end{Bmatrix}
\tag{23}
$$

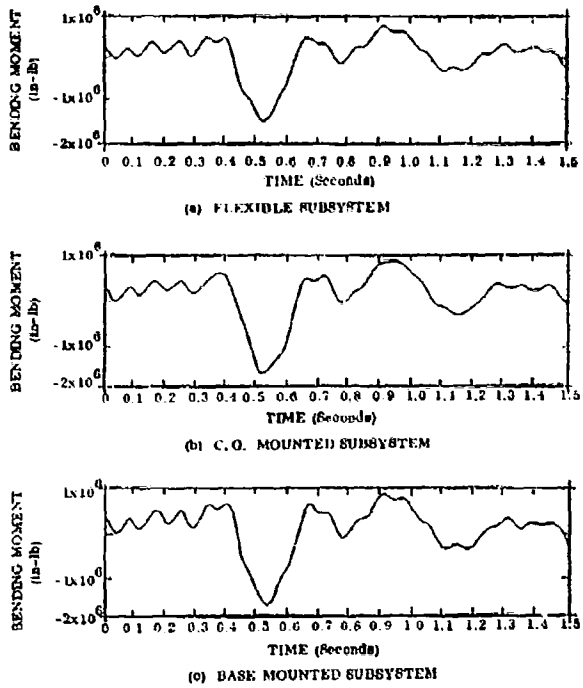

Fig. 5. Bending moment at a typical station on the primary vehicle for several subsystem models

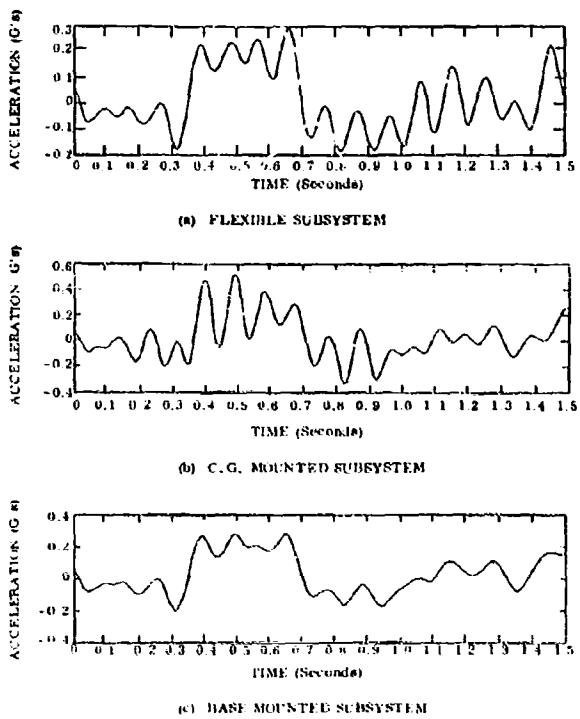

Fig. 6. Lateral acceleration at a typical station on the primary vehicle for several subsystem models

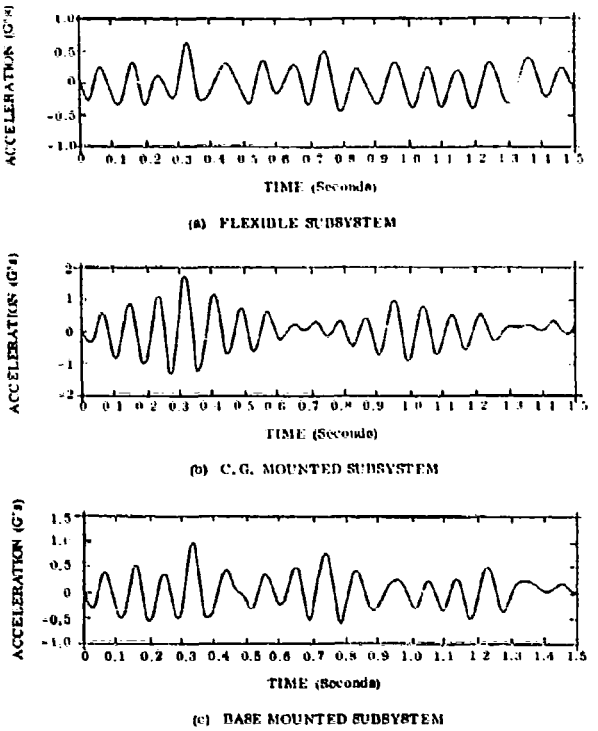

Fig. 7. Lateral acceleration of the subsystem center of gravity for several subsystem models

The subsystem response is, of course, greatly dependent on the model that is used. The maximum bending moment for the center-of-gravity supported subsystem is the lowest because the moment of inertia about the attachment interface of the model is the lowest of the three configurations. If the rigid-body subsystem is supported at its proper base station, the bending moment is increased by 50 percent because all of the bending must take place at the interface and is not distributed throughout the subsystem.

The time histories of bending moment and acceleration show the differences in frequency content that result from the three subsystem models. If components or assemblies mounted in these areas are frequency sensitive, erroneous design will result if simple rigid-body models are used.

Simple rigid-body models of flexible structure are not sufficient to provide design loads or response characteristics for either the subsystem or the primary vehicle. When dynamic interactions as a result of transient loading are a large effect on the loads, an investigation of the dynamic characteristics of the subsystem is necessary. As an example, the loads comparison for the configurations used in this analysis shows variations of up to 50 percent depending on the model. The use of flexible subsystem models will produce a more realistic evaluation of the response of the primary vehicle as well as the subsystem.

REFERENCE

1. H. F. Bauer, "Fuel Oscillations in the Containers of a Space Vehicle and Their Influence Upon Stability," NASA TR R-187, Feb. 1964

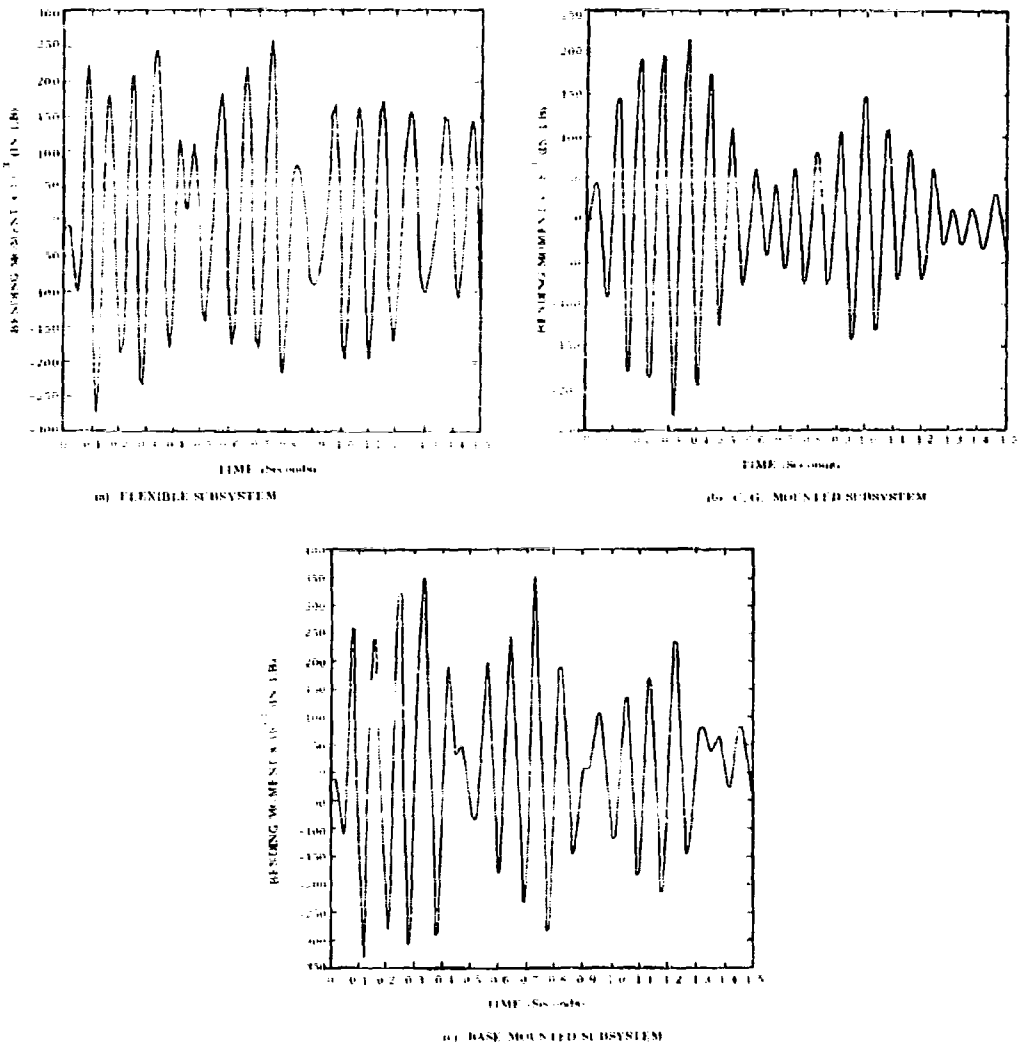

Fig. 8. Bending moment at the subsystem/vehicle interface for several subsystem models

BIBLIOGRAPHY

Norris, C. H., et al., Structural Design for Dynamic Loads, (McGraw-Hill, New York), 1959

Gaffney, J. S. and P. E. Campos, "Lateral Dynamic Response of Large Subsystems During Launch and Stage Separation Transient Conditions," NAA STR 175, July 1967

DISCUSSION

C. Perisho (McDonnell-Douglas Corp.): Was this all theory or has this been verified experimentally?

Mr. Gaffney: No, this is all theory; there is no experimental verification.

A NEW APPROACH TO THE INTERACTION PROBLEMS OF FLUID-FILLED ELASTIC MEMBRANE SHELLS*

Clement L. Fai and Shoichi Uchiyama
North American Rockwell Corporation
Downey, California

A new engineering approach is presented for the computation of natural frequencies and the corresponding mode shapes of the interaction of fluid in elastic tanks. It is assumed that the velocity potential of fluid exists and that the shell motion is based on membrane theory under inertia loading of the shell and the fluid pressure at the interface. The shell displacements are solved analytically. As the velocity potential is represented by a series of infinite terms, each with an unknown coefficient, the free surface boundary condition and the interface condition can only be satisfied approximately. An eigenvalue problem is formulated by minimizing the integrated squared errors for the boundary conditions subject to the constraint that the prescribed radial displacement along the edge of the shell be satisfied. An analytical formulation and solution of the longitudinal vibration of the fluid-filled hemispherical shell is presented as a practical application.

INTRODUCTION

Development of large liquid rockets has created increased interest in the interaction dynamics of fluid in elastic tanks. Several fine papers have been published in the last few years on the investigation of shell vibrations of thin-walled circular cylinders filled with fluid [1-5]. A few of these papers deal, in a cursory manner, with the axisymmetric oscillation of fluid-filled hemispherical shells [6-8]. Nothing has been published on investigations of configurations other than those mentioned above.

The main obstruction to the progress of interaction dynamics for general configurations may be attributed to the very difficult nature of the systems of hydrodynamic equations, shell dynamic equations, and associated boundary conditions that have kept many investigators from reaching any reasonable solutions. The most powerful energy method that has been applied successfully to the fluid-filled cylindrical shells produces a horrendous and lengthy mathematical expression in the treatment of, for instance, an oblate spheroidal shell or a cylinder with an elastic bulkhead.

Under these difficult circumstances, a new engineering approach was developed to compute the natural frequencies and the corresponding mode shapes of the interaction system by using certain simplified assumptions. This approach, which has been successfully applied to the longitudinal vibration of a fluid-filled hemispherical shell, a fluid-filled oblate spheroidal shell, and a fluid-filled cylindrical shell with an inverted conical bulkhead [9], will be described in this paper. A detailed analytical formulation and solution of the longitudinal vibration of the fluid-filled hemispherical shell is presented below as a practical application.

MATHEMATICAL MODEL AND METHOD OF SOLUTION

In this approach, it is assumed that the fluid is inviscid, incompressible, its motion is irrotational, and that the shell motion is based on membrane theory and is under inertial loading and fluid pressure. Under these assumptions, velocity potentials are obtained from the solution of Laplace's equations in coordinates according to the configuration of the different

*The results presented in this paper were drawn from the NASA-sponsored study, Contract NAS8-11490.

parts of the tank. This velocity potential, together with Bernoulli's equation, permits the evaluation of the fluctuating fluid pressure at the interface. By treating the interface pressure as a forcing function in the shell equations, the shell displacement components can be determined analytically.

As the velocity potential in the general case is represented by a series of infinite terms, each with an unknown coefficient, the pressure and shell displacements are also represented in series form. When the series solutions are substituted in the free surface boundary condition and the interface boundary conditions, these conditions can be satisfied only approximately, because these series have to be truncated. The differences between the exact and approximate satisfaction of the boundary conditions are the functional errors. When each functional error is first squared and then integrated over the subscribed boundary surface, the integrated squared error is obtained. The total integrated squared error for the entire free surface and the interface is the sum of the separate squared error multiplied by its weighting factor. If the weighting factor of the functional error of the interface condition is defined as unity, the weighting factor of the functional error of the free-surface condition is the ratio of the order of magnitude between the functional errors of the interface and the free surface.

An eigenvalue problem is formulated from the equations that are obtained by minimizing the total integrated squared errors, with respect to those unknown coefficients, and the equation of constraint that the prescribed radial deflection along the edge of the shell be satisfied. The use of the constrained equation of radial deflection along the edge has a dual purpose. For a complete formulation of Lagrange's constrained minima problem the edge condition of radial deflection is a necessary relation to connect the unknown coefficients that were the outgrowth of the two independent boundary conditions, one at the free surface and the other at the interface. Furthermore, as the radial displacement is obtained from the meridional displacement and its derivative, there is no arbitrary constant involved for the radial displacement solution. This is the consequence of using the membrane shell theory. Therefore, the radial displacement solution precludes the satisfaction of the edge condition and the edge condition imposed on the radial displacement must be treated as a constraint.

The formulated eigenvalue problem is then solved with a digital computer. The method of solution as programed is essentially a systematic trial-and-correction process which searches for frequency until the frequency determinant vanishes.

VELOCITY POTENTIAL FOR HEMISPHERICAL FLUID

The suggested method will be applied to the solution of longitudinal vibrations of a fluid-filled hemispherical shell. We shall consider the shell to be a thin elastic uniform membrane, completely filled with an inviscid and a compressible propellant under irrotational motion. The shell coordinate system is shown in Fig. 1.

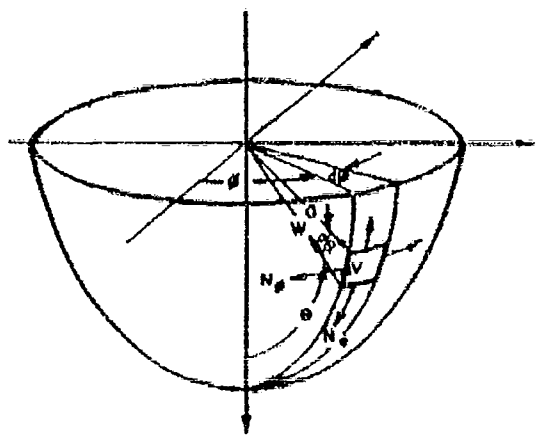

Fig. 1 Hemispherical shell coordinate system

Under the above assumptions, the problem of small-amplitude axisymmetric vibrations of a hemisphere of fluid is reduced to the solution of Laplace's equation, subject to appropriate boundary conditions. In spherical coordinates, for the case of axial symmetry, Laplace's equation takes the form

$$\sin\theta \frac{\partial}{\partial r}\left(r^2 \frac{\partial \Phi}{\partial r}\right) + \frac{\partial}{\partial \theta}\left(\sin\theta \frac{\partial \Phi}{\partial \theta}\right) = 0 \qquad (1)$$

where Φ is the velocity potential, and r, θ are coordinates that denote the distance measured from the origin and the "cone angle" measured from the vertical axis, respectively.

On the free surface of the fluid, the linearized boundary condition [10] is given by

$$-\frac{g}{r}\frac{\partial \Phi}{\partial \theta} = \frac{\partial^2 \Phi}{\partial t^2} \quad \text{at} \quad \theta = \frac{\pi}{2}. \qquad (2)$$

On the interface $r = a$, the radial velocity of the fluid must be equal to the radial velocity of the shell. Thus,

$$\left.\frac{\partial w}{\partial t}\right|_{\text{shell}} = \left.\frac{\partial w}{\partial t}\right|_{\text{fluid}} \quad \text{at} \quad r = a \qquad (3)$$

In the case of simple harmonic motion, the velocity potential may be taken in the form

$$\Phi = \chi(r, \theta) \cos \omega t \qquad (4)$$

where $\chi(r, \theta)$ is the velocity potential for steady flow, ω is the natural frequency of the system, and t is the time. The velocity potential is related to the meridional and radial velocity components of the fluid, respectively, by the relations

$$\left.\frac{\partial w}{\partial t}\right|_{\text{fluid}} = \frac{1}{r}\frac{\partial \Phi}{\partial \theta} \qquad (5a)$$

$$\left.\frac{\partial u}{\partial t}\right|_{\text{fluid}} = \frac{\partial \Phi}{\partial r} \qquad (5b)$$

On substituting Eq. (4) into Eq. (1), a differential equation that is identical in form to Eq. (1) is obtained for $\chi(r, \theta)$. This differential equation for χ can be solved by assuming

$$\chi(r, \theta) = R(r)\,\Theta(\theta) \qquad (6)$$

Upon substituting into Laplace's equation, two ordinary differential equations for determining $R(r)$ and $\Theta(\theta)$ are obtained. They are

$$r^2 \frac{d^2R}{dr^2} + 2r\frac{dR}{dr} - n(n+1)R = 0 \qquad (7)$$

and

$$\frac{d^2\Theta}{d\theta^2} + \cot\theta \frac{d\Theta}{d\theta} + n(n+1)\Theta = 0 \qquad (8)$$

where n is a nonnegative integer.

Equation (7) has as its solution

$$R(r) = Ar^n + Br^{-(n+1)} \qquad (9)$$

where A and B are arbitrary constants. To avoid the singularity at $r = 0$ so that the velocity potential will remain finite, the constant B is assumed 0.

Equation (8) may be transformed into Legendre's equation by introducing a new variable, μ, defined by

$$\mu = \cos\theta. \qquad (10)$$

The result is

$$\frac{d}{d\mu}\left[(1-\mu^2)\frac{d\Theta}{d\mu}\right] + n(n+1)\Theta = 0 \qquad (11)$$

which has the solution

$$\Theta(\mu) = \bar{C} P_n(\mu) + \bar{D} Q_n(\mu) \qquad (12)$$

where $\bar{C}$ and $\bar{D}$ are arbitrary constants, and $P_n(\mu)$ and $Q_n(\mu)$ are Legendre's polynomials of the first and second kind, respectively, of degree n. In a similar fashion, with regard to the constant B in Eq. (9), the constant $\bar{D}$ is assumed 0 because $Q_n(\mu)$ has logarithmic singularities at $\mu = 1$ corresponding to $\theta = 0^\circ$.

With both $R(r)$ and $\Theta(\theta)$ determined, the steady-state velocity potential can be derived immediately from Eq. (6). As each term of degree n is a solution, the most general expression for the velocity potential is given by the sum of all such solutions plus an additional arbitrary constant. For convenience, the radius r is nondimensionalized by dividing it by the radius "a" of the hemisphere. In addition, the constants are redefined so that χ finally takes the form

$$\chi = a^2 \left[C_0 + \sum_{n=1}^{\infty} \frac{C_n}{n}\left(\frac{r}{a}\right)^n P_n(\mu)\right] \qquad (13)$$

where $C_0, C_1, \ldots, C_n$ are nondimensional arbitrary constants. Thus, substituting this expression back into Eq. (4), the velocity potential is

$$\Phi = a^2 \left[C_0 + \sum_{n=1}^{\infty} \frac{C_n}{n}\left(\frac{r}{a}\right)^n P_n(\mu)\right] \cos \omega t \qquad (14)$$

On substituting Eq. (14) into Eq. (2), the following relation for the free surface boundary condition is obtained:

$$\frac{a\omega^2}{g} C_0 + \sum_{n=1}^{\infty} \frac{C_n}{n} \left(\frac{r}{a}\right)^{n-1} \left[\sqrt{1-\mu^2} \frac{d}{d\mu} P_n(\mu) + \frac{a\omega^2}{g} \left(\frac{1}{n}\right) P_n(\mu)\right]_{\mu=\cos\frac{\pi}{2}=0} = 0 \qquad (16)$$

It is seen that this linearized boundary condition cannot be satisfied for each nth-degree term of the Legendre's functions for C_n's different from 0. Hence, the relation will be averaged over the entire series by integrating it over the free surface of the liquid. It is this resulting expression that will be used later in formulating the eigenvalue problem to determine the natural frequencies of the system.

The dynamic fluid pressure can be obtained from the velocity potential through the linearized Bernoulli equation. This relation [10] is given by

$$p = -\rho_0 \frac{\partial \Phi}{\partial t} \qquad (16)$$

where ρ_0 is the fluid density. Inserting the expression for Φ from Eq. (14), we have

$$p = a^2\omega^2\rho_0 \left[C_0 + \sum_{n=1}^{\infty} \frac{C_n}{n} \left(\frac{r}{a}\right)^n P_n(\mu)\right] \sin \omega t. \qquad (17)$$

At the interface where $r = a$, the pressure is

$$p(a,\theta) = a^2\omega^2\rho_0 \left[C_0 + \sum_{n=1}^{\infty} \frac{C_n}{n} P_n(\mu)\right] \sin \omega t \qquad (18)$$

which represents the fluctuating pressure at the interface between the fluid and the hemispherical shell.

EQUATIONS OF MOTION FOR A HEMISPHERICAL SHELL

The equations of equilibrium for a shell of revolution under a symmetrical loading are given in Timoshenko and Woinowsky-Krieger [11]. On specializing these equations to the case of a spherical or hemispherical shell under inertial loading and fluid pressure, they take the form

$$\frac{dN_\theta}{d\theta} + (N_\theta - N_\phi)\cot\theta = \rho h \frac{\partial^2 v}{\partial t^2} \qquad (19a)$$

and

$$N_\theta + N_\phi = \rho h \frac{\partial^2 w}{\partial t^2} + p_0(r=a) \qquad (19b)$$

where N_θ and N_ϕ are the stress resultants in the direction of the meridional and circumferential coordinates, respectively; ρ is the density of the shell material; and h is the shell thickness. The meridional displacement v is taken positively in the direction of increasing θ, where θ is measured from the axis of symmetry, and the radial displacement w is positive in the direction of the inward normal. As the expression for the pressure $p(a,\theta)$ given by Eq. (18) is in terms of the constants C_n's, there is no loss of generality by assuming that it acts in the direction of the outward normal, as was done in Eq. (19b).

Equations (19a) and (19b) may be expressed in terms of the displacements by utilizing the following relations for the stress resultants [11]:

$$N_\theta = \frac{D}{a}\left[\frac{\partial v}{\partial \theta} + v\cot\theta - (1+\nu)w\right] \qquad (20a)$$

and

$$N_\phi = \frac{D}{a}\left[\frac{\partial v}{\partial \theta} + v\cot\theta + (1-\nu)w\right] \qquad (20b)$$

where

$$D = \frac{Eh}{1-\nu^2}.$$

On substituting Eqs. (20a) and (20b) into Eqs. (19a) and (19b) and introducing the nondimensionalized displacement components v and w defined by

$$v = \frac{\rho a^4 \omega^2}{D} \bar{v} \sin \omega t \qquad (21a)$$

and

$$w = \frac{\rho a^4 \omega^2}{D} \bar{w} \sin \omega t \qquad (21b)$$

and the pressure given by Eq. (18), we obtain

$$\frac{d^2\bar{v}}{d\theta^2} + \cot\theta \frac{d\bar{v}}{d\theta} - (\nu + \cot^2\theta - \kappa^2)\bar{v} + (1+\nu)\frac{d\bar{w}}{d\theta} = 0 \qquad (22)$$

and

$$(1+\nu)\left(\frac{d\bar{v}}{d\theta} + \bar{v}\cot\theta + 2\bar{w}\right) + \kappa^2\bar{w} = \frac{\rho_0}{\rho}\left[C_0 + \sum_{n=1}^{\infty} \frac{C_n}{n} P_n(\mu)\right] \qquad (23)$$

where

$$\cdot = \frac{a^2 b}{D}$$

The displacement components in nondimensional form will simply be referred to as displacements or displacement components in the remainder of the paper.

SOLUTION OF MERIDIONAL DISPLACEMENT

Equations (22) and (23) may be decoupled to yield a differential equation expressed in terms of the displacement component v alone. If the expression for $\bar{v}$ from Eq. (23) is substituted into Eq. (22), we obtain

$$\frac{d^2 v}{d\alpha^2} + \cot\alpha \frac{dv}{d\alpha} + (\lambda - \csc^2\alpha)v + \left(\frac{a}{c}\right)\sum_{n=1}^{\infty} \frac{C_n}{n} \frac{d}{d\alpha} P_n(\cos\alpha) = 0 \quad (24a)$$

where

$$\lambda = \frac{2(1+\nu^2) + (1+3\nu)\kappa^2 + \kappa^4}{1 - \nu^2 + \kappa^2} \quad (24b)$$

and

$$\kappa^2 = \frac{1+\nu}{(1-\nu^2) + \kappa^2} \quad (24c)$$

This equation may, in turn, be expressed in terms of independent variable z according to the relation given in Eq. (10). Thus,

$$\frac{d}{dz}\left\{(1-z^2)\frac{dv}{dz}\right\} + \left(\lambda - \frac{1}{1-z^2}\right)v + \left(\frac{a}{c}\right)\sum_{n=1}^{\infty} \frac{C_n}{n}(1-z^2)^{1/2} \frac{d}{dz} P_n(z) = 0 \quad (25)$$

The first two terms of Eq. (25) may be transposed into a hypergeometric equation. To do this, first let

$$v = (1-z^2)^{1/2} F \quad (26)$$

Then Eq. (25) becomes

$$(1-z^2)\frac{d^2F}{dz^2} - 4z\frac{dF}{dz} + (2-\lambda)F + \left(\frac{a}{c}\right)\sum_{n=1}^{\infty} \frac{C_n}{n} \frac{d}{dz} P_n(z) = 0. \quad (27)$$

The introduction of a new variable, x, defined as

$$x = \frac{1}{2}(1-z) \quad (28)$$

into this equation leads to

$$x(1-x)\frac{d^2F}{dx^2} + 2(1-2x)\frac{dF}{dx} - (2-\lambda)F = -\frac{a}{2}\left(\frac{a}{c}\right)\sum_{n=1}^{\infty} \frac{C_n}{n} \frac{d}{dx} P_n(1-2x) \quad (29)$$

The homogeneous part of Eq. (29) is recognized as a hypergeometric differential equation. The analytic solution of this homogeneous differential equation about $x = 0$ is the hypergeometric series and expressed [12] as

$$F_1(\lambda, \lambda, 2, x) = 1 + \frac{\lambda^2}{2}x + \frac{\lambda(\lambda+1)\lambda^2(\lambda+1)^2}{2^2 \times 3}x^2 + \cdots \quad (30a)$$

where

$$\lambda = \frac{1}{2}\left[3 + (1+4\kappa^2)^{1/2}\right] \quad (30b)$$

and

$$\lambda = \frac{1}{2}\left[3 - (1+4\kappa^2)^{1/2}\right] \quad (30c)$$

Thus, the complementary function of Eq. (25) is obtained as

$$\bar{v} = b_0\sqrt{1-z^2}\, F_1\left[\lambda, \lambda, 2, \frac{1}{2}(1-z)\right] \quad (31)$$

The particular integral of Eq. (25) may be assumed as

$$\bar{v} = \sum_{n=1}^{\infty} A_n P_n^1(z) \quad (32)$$

where $P_n^1(z)$ is the associated Legendre's polynomial and expressed as

$$P_n^1(z) = -\frac{dP_n(z)}{dz}\sqrt{1-z^2} = -\frac{dP_n(z)}{d\alpha}\sin\alpha \quad (33)$$

The associated Legendre's polynomial, $P_n^1(z)$ satisfies the differential equation

$$\frac{d^2P_n^1}{d\alpha^2} + \cot\alpha\frac{dP_n^1}{d\alpha} + \left(n(n+1) - \csc^2\alpha\right)P_n^1 = 0 \quad (34)$$

Substituting Eq. (32) into Eq. (24a) gives

$$\sum_{n=1}^{\infty} A_n \left(\frac{d^2 P_n'}{d\phi^2} + \frac{dP_n'}{d\phi} \cot \phi - P_n' \csc^2 \phi + \lambda P_n' \right)$$

$$= \frac{b_o}{2} \sum_{n=1}^{\infty} \frac{C_n}{n} P_n' \qquad (35)$$

Substituting Eq. (34) into Eq. (35) and deleting the sign of summation gives

$$A_n \left[\lambda - n(n+1) \right] = \frac{b_o}{2} \frac{C_n}{n}$$

from which

$$A_n = \frac{\frac{b_o}{2} \frac{C_n}{n}}{\lambda - n(n+1)} \qquad (36)$$

The particular integral of Eq. (25a) is then obtained by substituting Eq. (36) and Eq. (33) into Eq. (32) as

$$\bar{v} = \sum_{n=1}^{\infty} \frac{\frac{b_o}{2} \frac{C_n}{n}}{\lambda - n(n+1)} \sqrt{1 - \mu^2} \frac{dP_n(\mu)}{d\mu} \qquad (37)$$

The complete solution of Eq. (25a) is the sum of the complementary function, Eq. (31) and the particular integral, Eq. (37). Thus

$$\bar{v} = b_o \sqrt{1 - \mu^2} F_1 \left[\alpha, \beta, 2, \frac{1}{2} (1 - \mu) \right]$$

$$+ \frac{b_o}{2} \sqrt{1 - \mu^2} \sum_{n=1}^{\infty} \frac{C_n \frac{dP_n(\mu)}{d\mu}}{n[\lambda - n(n+1)]} \qquad (38)$$

The boundary conditions for $\bar{v}$ are

$$\bar{v} = 0 \quad \text{at} \quad \mu = 1 \qquad (39)$$

and

$$\bar{v} = 0 \quad \text{at} \quad \mu = 0 \qquad (40)$$

Equation (38) automatically satisfies the boundary condition, Eq. (39). The arbitrary constant, b_o of Eq. (22) is determined from the boundary condition, Eq. (40).

$$b_o = -\frac{\frac{b_o}{2}}{F_{1c} \left[\alpha, \beta, 2, \frac{1}{2} \right]} \sum_{n=1}^{\infty} \frac{C_n}{n[\lambda - n(n+1)]} \frac{dP_n(0)}{d\mu} \qquad (41)$$

Hence, the complete solution for meridional displacement is

$$\bar{v} = \frac{b_o}{2} \sqrt{1 - \mu^2} \sum_{n=1}^{\infty} \frac{C_n}{n[\lambda - n(n+1)]}$$

$$\left\{ \frac{dP_n(\mu)}{d\mu} - \frac{F_1 \left[\alpha, \beta, 2, \frac{1}{2} (1 - \mu) \right]}{F_{1c} \left[\alpha, \beta, 2, \frac{1}{2} \right]} \frac{dP_n(0)}{d\mu} \right\} \qquad (42)$$

SOLUTION FOR RADIAL DISPLACEMENT

As $\bar{v}$ is now known, the radial displacement for the hemispherical shell may be obtained directly from Eq. (23). It gives

$$\bar{w} = \frac{1 + \nu}{2(1 + \nu) - \mu^2} \left(\frac{d\bar{v}}{d\phi} + \bar{v} \cot \phi \right)$$

$$= \frac{\frac{b_o}{2}}{2(1 + \nu) - \mu^2} \left[C_o + \sum_{n=1}^{\infty} \frac{C_n}{n} P_n(\mu) \right] \qquad (43)$$

From Eq. (33),

$$\frac{dP_n(\mu)}{d\mu} = \frac{1}{\sqrt{1 - \mu^2}} \frac{dP_n(\mu)}{d\phi} \qquad (44)$$

and

$$\frac{dP_n(0)}{d\mu} = \frac{dP_n(0)}{d\phi}$$

Substituting Eq. (44) into Eq. (42) gives

$$\bar{v} = \frac{b_o}{2} \sqrt{1 - \mu^2} \sum_{n=1}^{\infty} \frac{C_n}{n[\lambda - n(n+1)]}$$

$$\left[\frac{1}{\sqrt{1 - \mu^2}} \frac{dP_n(\mu)}{d\phi} + \frac{F_1}{F_{1c}} \frac{dP_n(0)}{d\phi} \right] \qquad (45)$$

and hence

$$\frac{d\bar{v}}{d\phi} = \frac{b_o}{2} \sum_{n=1}^{\infty} \frac{C_n}{n[\lambda - n(n+1)]}$$

$$\left[\frac{d^2 P_n(\mu)}{d\phi^2} + \frac{F_1}{F_{1c}} \frac{dP_n(0)}{d\phi} \sqrt{1 - \mu^2} + \frac{\frac{dF_1}{d\phi}}{F_{1c}} \frac{dP_n(0)}{d\phi} \right] \qquad (46)$$

From Eq. (44),

$$\frac{d^2 P_n(\mu)}{d\phi^2} = \frac{d}{d\phi} \left(\frac{dP_n(\mu)}{d\mu} \right) \qquad (47)$$

By the aid of Eqs. (44) through (47), the terms inside the first bracket of Eq. (43) have the following expression:

$$\frac{d\bar{V}}{d} + \bar{V}\cot \quad - \cdot \cdot \sum_{n=1}^{} \frac{C_n}{n\lambda - n(n+1)}$$

$$\cdot \left\{ (1 - \cdot^2) \frac{d^2 P_n}{d\cdot^2} - 2\cdot \frac{dP_n}{d\cdot} \right.$$

$$\left. \cdot \left[2\cdot \frac{F_1}{F_{1c}} - (1 - \cdot^2) \frac{\frac{dF_1}{d\cdot}}{F_{1c}} \right] \frac{dP_n(0)}{d\cdot} \right\} \cdot \tag{48}$$

The Legendre polynomial $P_n(\cdot)$ satisfies the differential equation

$$(1 - \cdot^2) \frac{d^2 P_n(\cdot)}{d\cdot^2} - 2\cdot \frac{dP_n(\cdot)}{d\cdot} + n(n+1) P_n(\cdot) = 0. \tag{49}$$

Substituting Eq. (49) into Eq. (48), gives

$$\frac{d\bar{V}}{d} + \bar{V}\cot \quad = \cdot \frac{\cdot_0}{} \sum_{n=1}^{} \frac{C_n}{n\lambda - n(n+1)}$$

$$\cdot \left\{ n(n+1) P_n(\cdot) - \left[2\cdot \frac{F_1}{F_{1c}} - (1 - \cdot^2) \frac{\frac{dF_1}{d\cdot}}{F_{1c}} \right] \frac{dP_n(0)}{d} \right\} \cdot \tag{50}$$

Substituting Eq. (50) into Eq. (43), the solution for radial displacement becomes

$$\bar{w} = \frac{(1+\cdot)\cdot \cdot_0}{2(1+\cdot) - \cdot \cdot^2} \sum_{n=1}^{} \frac{C_n}{n\lambda - n(n+1)} \left\{ n(n+1) P_n(\cdot) \right.$$

$$\left. \cdot \left[2\cdot \frac{F_1}{F_{1c}} - (1 - \cdot^2) \frac{\frac{dF_1}{d\cdot}}{F_{1c}} \right] \frac{dP_n(0)}{d\cdot} \right\} - \frac{\cdot_0}{2(1 - \cdot)\lambda - \cdot^2}$$

$$\cdot \left[C_0 - \sum_{n=1}^{} \frac{C_n}{n} P_n(\cdot) \right] \cdot \tag{51}$$

INVESTIGATION OF SINGULARITY

As a practical interest, the following numerical values are introduced:

$\cdot$ (radius of shell) = 200 (in.)

h (shell thickness) = 0.1 (in.)

$\cdot$ (density of shell) = 2.59×10^{-4} (lb_f-$sec^2/in.^4$)

$\cdot_0$ (density of liquid) = 1.06×10^{-4} (lb_f-$sec^2/in.^4$)

E (Young's modulus) = 10^7 ($lb_f/in.^2$)

Thus, the parameters $\cdot$, λ, and $\cdot$ are evaluated as

$$\cdot = \frac{n^2 h}{D} = \frac{n^2 h}{\frac{Eh}{1 - \cdot^2}} = 0.942 \cdot 10^{-6}$$

$$2\cdot(1+\cdot) - \cdot^2 \cdot 2(1+\cdot) \tag{52a}$$

$$\lambda = \frac{2(1-\cdot^2) + (1+3\cdot)\cdot^2 - \cdot^2\cdot^4}{1 + \cdot^2 - \cdot^2} \cdot 2 \tag{52b}$$

$$\cdot = \frac{1+\cdot}{1 - \cdot^2} \cdot \frac{1}{1-\cdot} \cdot \tag{52c}$$

In this case, the term $1/[\lambda - n(n+1)]$ appearing in Eq. (51) behaves like a singularity at $n = 1$. To avoid such singularity Eq. (51) may be written in the form

$$\bar{w} \quad S_1(\cdot) C_1 + \frac{(1+\cdot)\cdot \cdot_0}{2(1 - \cdot)\lambda - \cdot^2} \sum_{n=2}^{} \frac{C_n}{n\lambda - n(n+1)}$$

$$\left\{ n(n+1) P_n(\cdot) - \left[2\cdot \frac{F_1}{F_{1c}} - (1 - \cdot^2) \frac{\frac{dF_1}{d\cdot}}{F_{1c}} \right] \frac{dP_n(0)}{d\cdot} \right\}$$

$$- \frac{\cdot_0}{2(1 - \cdot)\lambda - \cdot^2} \left[C_0 - \sum_{n=1}^{} \frac{C_n}{n} P_n(\cdot) \right] \tag{53}$$

and $S_1(\cdot)$ will be obtained as follows.

When $\lambda = 2$ and $n = 1$, Eq. (27) may be written as

$$(1 - \cdot^2) \frac{d^2 F}{d\cdot^2} - 4\cdot \frac{dF}{d\cdot} \cdot \frac{\cdot_0}{} C_1 \cdot \tag{54}$$

The above equation can be solved with the aid of boundary conditions, Eq. (39) and Eq. (40). The solution of F is

$$F = \frac{1}{3} \left[\frac{1}{(1 - \cdot)} - n(1 - \cdot) \right] \cdot^n C_1 \cdot$$

$$(\lambda = 2, n = 1) \tag{55}$$

Substituting Eq. (54) into Eq. (26), gives

$$\bar{v} = -\frac{1}{3}\sqrt{1-\mu^2}\left[\frac{\mu}{1+\mu} + \ln(1+\mu)\right]\psi\frac{\rho_o}{\rho}C_1 . \qquad (\chi = 2,\ n = 1) \qquad (56)$$

and

$$\frac{d\bar{v}}{d\theta} + \bar{v}\cot\theta = -\sqrt{1-\mu^2}\,\frac{d\bar{v}}{d\mu} + \frac{\mu}{\sqrt{1-\mu^2}}\,\bar{v} = -\frac{1}{3}\left[3\mu - 2 + 2\mu\ln(1+\mu)\right]\psi\frac{\rho_o}{\rho}C_1 \qquad (\chi = 2,\ n = 1) . \qquad (57)$$

Thus, when $\chi = 2$ and $n = 1$, the value of $S_1(\mu)C_1$ is determined from the first term of Eq. (43).

$$S_1(\mu)C_1 = \frac{1+\nu}{2(1+\nu) - \kappa\omega^2}\left(\frac{d\bar{v}}{d\theta} + \bar{v}\cot\theta\right) = -\frac{(1+\nu)[3\mu - 2 + 2\mu\ln(1+\mu)]}{3[2(1+\nu) - \kappa\omega^2]}\psi\frac{\rho_o}{\rho}C_1 . \qquad (58)$$

Furthermore, for $\chi = 2$, Eq. (30a) gives

$$F_1(\alpha,\beta;2;z) = 1$$
$$F_{1c}\left(\alpha,\beta;2;\frac{1}{2}\right) = 1 \qquad (59)$$

Thus, substituting Eq. (59) and Eq. (52a) into Eq. (53) gives the radial displacement $\bar{w}$ for the case of $\kappa << 1$ as follows:

$$\bar{w} = S_1(\mu)C_1 - \frac{1}{2(1-\nu)}\frac{\rho_o}{\rho}\sum_{n=2}^{\infty}\left[\frac{n+1}{n(n+1)-2}P_n(\mu) - \frac{2}{n[n(n+1)-2]}\frac{dP_n(0)}{d\mu}\right]C_n - \frac{1}{2(1+\nu)}\frac{\rho_o}{\rho}\left[C_n + \sum_{n=1}^{\infty}\frac{C_n}{n}P_n(\mu)\right] \qquad (60)$$

where

$$S_1(\mu) = -\frac{1}{6(1-\nu)}\frac{\rho_o}{\rho}[3\mu - 2 + 2\mu\ln(1+\mu)] .$$

CONDITION OF CONSTRAINT

As the expression for the solution of radial displacement $\bar{w}$ was obtained from the solution of meridional displacement, $\bar{v}$, and its derivative, there are no arbitrary constants involved for the $\bar{w}$ solution. Hence, no boundary conditions can be applied to $\bar{w}$. This is the consequence of using the membrane shell theory in which bending stiffness is neglected. Because of the original stipulation, $\bar{w}$ will satisfy the condition of axial symmetry; by implication, it will not contain any singularity at $\theta = 0°$, as both $\bar{v}$ and $p(\alpha,\theta)$ are regular at this point.

If it is assumed that the hemispherical shell is provided with a rigid ring at the equatorial plane, thus giving the edge simple support, then

$$\bar{w}|_{\mu=0} = 0 . \qquad (61)$$

However, the absence of an arbitrary constant precludes the satisfaction of this condition. Therefore, this, or whatever other boundary conditions may be imposed on $\bar{w}$, must be treated as a constraint.

IMPOSITION OF INTERFACE CONDITION

The interface condition represents the compatibility condition that must exist between the fluid and the shell at their common boundary and that will be applied to couple the system.

In view of Eq. (5b), the condition stipulated by Eq. (3) for compatibility of velocities may be written

$$\frac{\partial w}{\partial t} = -\left.\frac{\partial\Phi}{\partial r}\right|_{r=a} . \qquad (62)$$

The minus sign must be present as the positive radial displacement direction for the shell and the hemisphere of fluid are opposite each other. Substituting from Eqs. (14) and (21b), the foregoing relation becomes

$$\sum_{n=1}^{\infty}C_n P_n(\mu) + \omega^2\frac{a^3\rho_o}{D}\bar{w} = 0 . \qquad (63)$$

FORMULATION OF EIGENVALUE PROBLEM

The eigenvalue problem for determining the natural frequencies and corresponding mode shapes of the coupled fluid-shell system is formulated using three equations that were obtained as a result of imposing the necessary boundary conditions of the problem. These

three equations are the liquid free-surface boundary condition given in Eq. (15), the boundary condition of zero-radial displacement at the equatorial plane given in Eq. (61), and the condition of compatible velocities at the interface given by Eq. (63). The solution of these three equations taken simultaneously will yield the natural frequencies. Other than the trivial case in which all the C_n's are zero, it is apparent that the series in these equations cannot be satisfied term by term. This, together with the complexity of the expressions involved, excludes all possibility of an analytical solution. Hence, some approximate numerical method of solution must be used. The approximate method used herein to formulate the eigenvalue problem is based on the least squared error technique.

Because, from a practical point of view, the series representation for the velocity potential must be truncated, the boundary conditions given by Eqs. (15), (61), and (63) will be satisfied only approximately. However, the intention is to treat the boundary condition for $\bar{w}$ as a constraint so that it will be satisfied exactly within the limitation of using only a finite series representation for the velocity potential.

The difference between the exact and approximate satisfaction of the free-surface boundary condition is denoted by the functional error ε_1. Thus,

$$\varepsilon_1 = \frac{\omega^2}{g} C_o + \sum_{n=1}^{\infty} \frac{C_n}{n} \left(\frac{r}{a}\right)^{n-1} \left[\frac{d}{d\zeta} P_n(0) + \frac{\omega^2}{g} \left(\frac{r}{a}\right) P_n(0)\right] . \quad (64)$$

If this expression is first squared and then integrated over the free surface of the fluid, the integrated squared error ε_1 is obtained. Accordingly,

$$\varepsilon_1 = 2\pi a^2 \int_0^1 \varepsilon_1^2 \left(\frac{r}{a}\right) d\left(\frac{r}{a}\right) . \quad (65)$$

From Eq. (63), the error ε_2 along a meridian, resulting from the truncation of the series expansion in Legendre's polynomials, is

$$\varepsilon_2 = \sum_{n=1}^{N} C_n I_n(\zeta) + \frac{\omega^2 a^2}{D} \bar{w} . \quad (66)$$

Similarly, to obtain the integrated squared error for this case, ε_2 is first squared and then integrated over the surface of the hemisphere so that

$$\varepsilon_2 = 2\pi a^2 \int_0^1 \varepsilon_2^2 \, d\zeta . \quad (67)$$

The total integrated squared error for the entire free surface and the interface is then

$$\varepsilon_T = \varepsilon_1^2 + \varepsilon_2 \quad (68)$$

where ε is introduced as a weighting factor for the difference of order of magnitudes between the functional errors of the interface and the free surface.

Equation (68) contains a total of $N+2$ unknowns. There are $N+1$ unknown C_n's plus the unknown frequency, ω. For the finite series representation of the velocity potential to provide the best possible fit for the satisfaction of the boundary conditions, these $N+1$ unknown C_n's are determined in such a manner as to render ε_T a minimum subject to Eq. (61) treated as a constraint. This is equivalent to minimizing the function

$$\varepsilon = \varepsilon_T + \lambda \bar{w} \, (\mu = 0) \quad (69)$$

where λ is a Lagrangian multiplier. Hence,

$$\left.\begin{aligned} \omega^2 \frac{\partial \varepsilon_1}{\partial C_o} + \frac{\partial \varepsilon_2}{\partial C_o} + \lambda \left.\frac{\partial \bar{w}}{\partial C_o}\right|_{\mu=0} &= 0 \\ \omega^2 \frac{\partial \varepsilon_1}{\partial C_1} + \frac{\partial \varepsilon_2}{\partial C_1} + \lambda \left.\frac{\partial \bar{w}}{\partial C_1}\right|_{\mu=0} &= 0 \\ \cdots\cdots\cdots\cdots\cdots\cdots\cdots\cdots & \\ \omega^2 \frac{\partial \varepsilon_1}{\partial C_n} + \frac{\partial \varepsilon_2}{\partial C_n} + \lambda \left.\frac{\partial \bar{w}}{\partial C_n}\right|_{\mu=0} &= 0 \\ \bar{w}|_{\mu=0} & \end{aligned}\right\} \quad (70)$$

which can be reduced to the following matrix form:

$$\left.\begin{bmatrix} & & \\ f_{mn}(\omega^2) & \vdots & f_m \\ & & \\ \cdots\cdots & & \cdots \\ g_n & & 0 \end{bmatrix} \begin{bmatrix} C_o \\ C_1 \\ \vdots \\ C_n \\ \vdots \\ \lambda \end{bmatrix} \right\} \quad \begin{matrix} 0 \\ m = 0, 1, \ldots, n \\ n = 0, 1, \ldots, n \end{matrix} \quad (71)$$

where $f_{mn}(\omega^2)$ is a quadric of ω^2, and f_m, g_n are known constants. This linear algebraic system of $N+2$ homogeneous simultaneous equations for $N+2$ unknowns, C_o, C_1, ..., C_n, and

λ has a nontrivial solution only if the determinant of the above equation is zero.

The solution of the determinantal equation will yield N + 1 natural frequencies. Only the first few frequencies will have any physical significance, however, as it takes more and more terms, in the series expansion for the fluid pressure, to be able to represent it accurately as the frequency increases.

DETERMINATION OF WEIGHTING FACTOR a

The functional errors at the interface and free surface are defined respectively as

$$\eta_I = \frac{\partial w}{\partial t} + \frac{\partial \phi}{\partial r} \tag{72a}$$

and

$$\eta_s = \frac{1}{g}\frac{\partial^2 \phi}{\partial t^2} + \frac{1}{r}\frac{\partial \phi}{\partial \mu} . \tag{72b}$$

The ratio of η_I to η_s is defined as the weighting factor a; thus,

$$a = \frac{\eta_I}{\eta_s} = \frac{\dfrac{\partial w}{\partial t} + \dfrac{\partial \phi}{\partial r}}{\dfrac{1}{g}\dfrac{\partial^2 \phi}{\partial t^2} + \dfrac{1}{r}\dfrac{\partial \phi}{\partial \mu}} . \tag{73}$$

The magnitude of a may be obtained [13] by comparison of the order of magnitude of the equations of motion for the hemispherical shell, Eqs. (19a) and (19b), and the boundary conditions, Eqs. (72a) and (72b). The results are

$$\begin{aligned} a &= O\left(\frac{\rho_f a^2}{D}\right) && \text{for } \omega \geq 30 \\ a &= O\left(\frac{g}{a\omega^2}\right) && \text{for } 1 \leq \omega < 30 \\ a &= O(1) && \text{for } 0 \leq \omega < 1 \end{aligned} \tag{74}$$

For $D = 10^6$, $a = 200$, $\rho_f \approx 1.06 \quad 10^{-4}$, the numerical value of a is summarized as follows:

a	ω
1.638×10^{-3}	$\omega \geq 34.2$
$g/a\omega^2$	$1.393 \leq \omega < 34.2$
1	$0 \leq \omega < 1.393$

where

$$\frac{g\rho_f a^2}{D} = \frac{g}{a\omega^2} \quad \text{at} \quad \omega = 34.2$$

and

$$\frac{g}{a\omega^2} = 1 \quad \text{at} \quad \omega = 1.393$$

as a must be continuous for ω.

SOLUTION FOR FREQUENCIES

The eigenvalue problem as formulated cannot be solved unless a digital computer is used. The method of solution as programed is essentially a systematic trial-and-correction process that searches for an ω until the frequency determinant vanishes. A modal frequency is assumed that permits the calculation of the hypergeometric function $F_1(\alpha, \beta, 2, z)$ and the displacements $\bar{v}$ and $\bar{w}$ corresponding to this estimated frequency. For the present numerical example, however, the function $F_1(\alpha, \beta, 2, z)$ is very nearly equal to 1, (Eq. (59)), so that it is not included in the frequency equation. The integrals that appear in the expressions for $\bar{v}$ and $\bar{w}$ are evaluated numerically by using the trapezoidal rule. Because the constants C_n's are unknown, only their coefficients are actually calculated at each discrete point used in the numerical process. This calculation requires the arranging of these values in a matrix to facilitate the bookkeeping involved.

With the determination of the displacement $\bar{w}$, numerical values for all the elements appearing in matrix Eq. (71) are calculated. The determinant of the matrix is then evaluated This process is repeated a second time with the frequency incremented to initiate the Newton-Raphson method of root determination, which continues until a zero value for the determinant is obtained within the specified degree of accuracy.

The results of the present analyses are compared with Hwang's [6] and Gossard's [8] results shown on Table 1. The radial mode shapes of the hemispherical shell filled with liquid oxygen for ω = 0.8, 45, 59, and 75 rad/sec, respectively, are shown in Figs. 2 through 5.

CONCLUSIONS

The approach suggested in this paper for the solution of interaction problems is called "engineering" because the fluid motion is based on the existence of velocity potential and the shell motion is based on the membrane theory.

TABLE 1

Authors	Boundary Conditions	Dimension of Tank	Frequencies (Hz)		
			ω_1	ω_2	ω_3
Present Analysis		a = 200 in. h = 0.1 in.	0.13	7.15	9.40
Hwang	$v = 0$ $w = 0$ at	a = 200 in. h = 0.3 in.	0.42	16.14	22.63
Gossard	$\theta = \frac{\pi}{2}$	a = 200 in. h = 0.1 in.	—	8.48	14.04

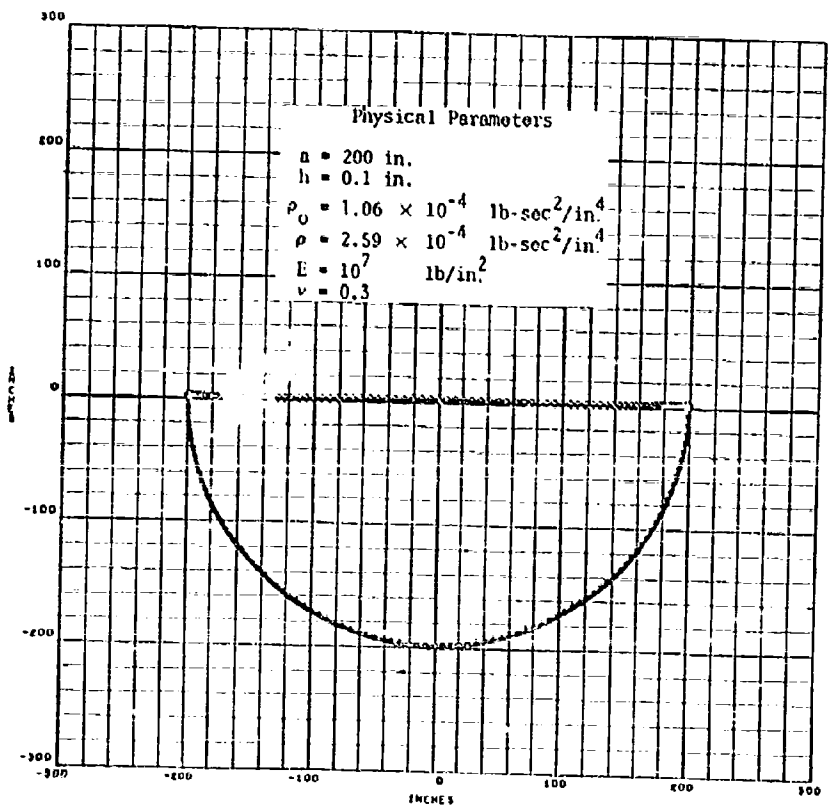

Fig. 2. Radial mode shape for hemispherical shell filled with liquid oxygen, ω = 0.8 rad/sec

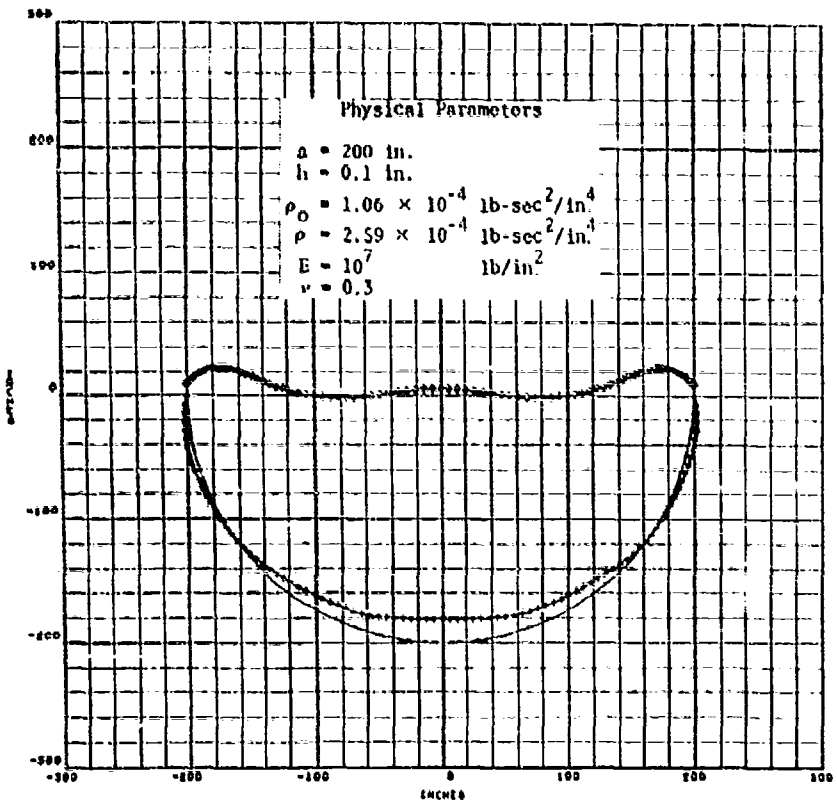

Fig. 3. Radial mode shape for hemispherical shell filled with liquid oxygen, ω = 45 rad/sec

From such assumptions the velocity potential of fluid can be obtained from the Laplace equation and the dynamic displacement of shells can always be solved from the statically determinate membrane equations. The substitution of the velocity potential and shell displacements into the interface boundary conditions insures the compatible and unique relation of the solution. The least squared error technique is adopted to make the best of the selection of the unknown coefficients in the truncated series solution.

There is some resemblance between the suggested approach and the energy method. For instance, the suggested approach uses the least squared error numerical technique and the energy method uses the Rayleigh-Ritz numerical technique. Besides this, the suggested approach is quite different from the energy method. The suggested approach demands the analytical solution of the displacement function first and then the substitution of them into the interface boundary conditions. The energy method takes the assumed displacement functions that have to satisfy the boundary conditions at the beginning. In the suggested approach, the equations of motion are the shell dynamic equations. In the energy approach, the equations of motion are the Lagrange's generalized dynamic equations.

The suggested approach requires a little more analytical work but apparently offers much less numerical complication. The suggested approach might produce a better result because the displacements are obtained from the closed solution. Usually the frequencies given by the Rayleigh-Ritz method are in the higher side. This can be seen from the foregoing comparison. If the thickness of the shell in Hwang's investigation is changed to 0.1 in., the corresponding frequencies are ω_1 = 0.24, ω_2 = 9.33, and 13.10 Hz. Hwang used three modes in his work, Gossard used two modes,

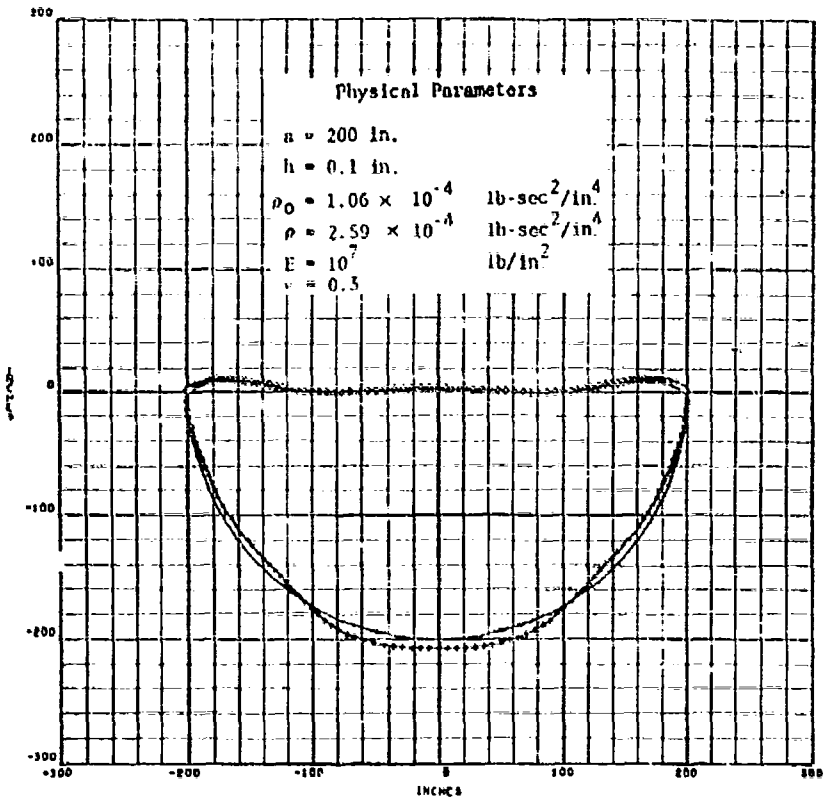

Fig. 4. Radial mode shape for hemispherical shell filled with liquid oxygen, . . 59 rad/sec

and the present analysis used eight terms of the Legendre polynomial. This showed that Gossard had a higher frequency and the present analysis had a lower frequency than Hwang's results.

REFERENCES

1. J. G. Berry and E. Reissner, "The Effect of an Internal Compressible Fluid Column on the Breathing Vibrations of a Thin Pressurized Cylindrical Shell," J. Aero. Sci., 25(5) (May 1958)

2. M. L. Baron and H. Bleich, "The Dynamic Analysis of Empty and Partially Full Cylindrical Tanks," Part I, Frequencies and Modes of Free Vibration and Transient Response by Mode Analysis, DASA No. 1123 A, Defense Atomic Support Agency, May 1959

3. J. S. Mixson and R. S. Kerr, "An Investigation of the Vibration Characteristics of Pressurized Thin-Walled Circular Cylinders Partly Filled with Liquid," NASA TR R-145, 1962

4. W. H. Chu, "Breathing Vibration of a Partially Filled Cylindrical Tank - Linear Theory," J. Appl. Mech. 30, 4 Dec. 1963

5. P. Tong and Y. C. Fung, "The Effect of Wall Elasticity and Surface Tension on the Forced Oscillations of a Liquid in a Cylindrical Container," Fluid Mechanics and Heat Transfer Symposium at Palo Alto, June 1965

6. C. Hwang, "Longitudinal Sloshing of Liquid in a Flexible Hemispherical Tank," J. Appl. Mech., Paper No. 05-APM-14

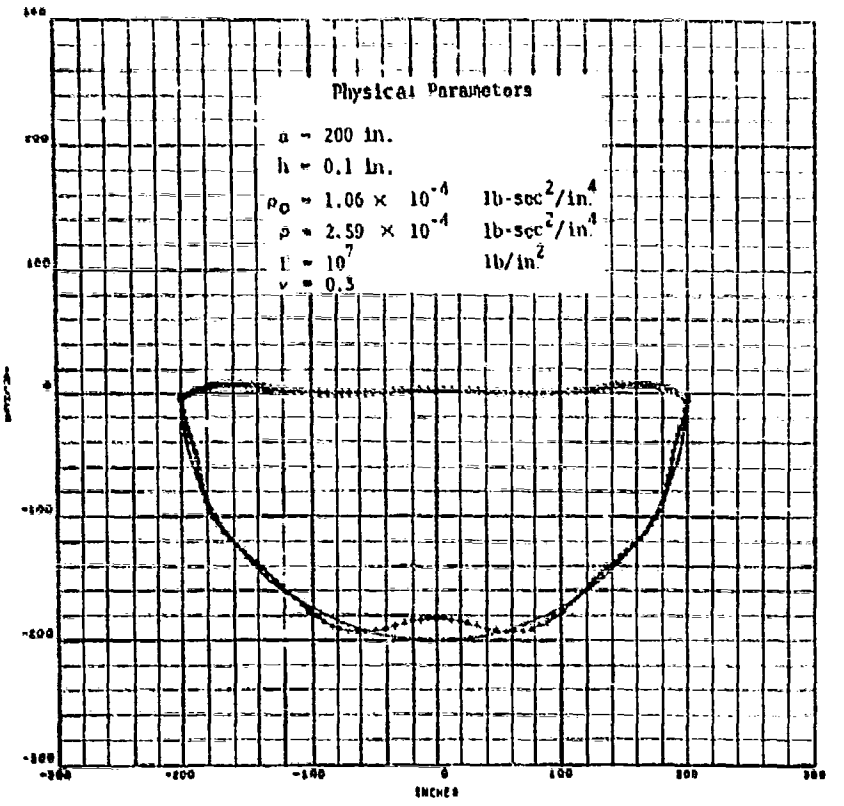

Fig. 5. Radial mode shape for hemispherical shell filled with liquid oxygen, ω = 75 rad/sec

7. C. W. Coale and M. Nagano, "Axisymmetric Modes of an Elastic Cylindrical Hemispherical Tank Partially Filled with a Liquid," AIAA Symposium on Structural Dynamics and Aeroelasticity, Boston, Aug. 1965

8. M. L. Gossard, "Axisymmetric Dynamic Response of Liquid-Filled, Hemispherical, Thin-Walled, Elastic Tanks," AIAA Symposium on Structural Dynamics and Aeroelasticity, Boston, Aug. 1965

9. North American Aviation, Inc., Internal Repts. Nos. SID 66-46-4, Rev. May 1967, SID 66-46-5, and SID 67-212-2 (NASA Contract NAS8-11490)

10. H. Lamb, Hydrodynamics, 6th ed. (Dover Publications), 1932

11. S. Timoshenko and S. Woinowsky-Krieger, Theory of Plates and Shells, 2nd ed. (McGraw-Hill), 1959

12. E. T. Whittaker and G. N. Watson, A Course of Modern Analysis, 4th ed. (Cambridge Univ. Press), 1960

13. C. L. Tai and S. Uchiyama, "Longitudinal Oscillation of a Propellant-Filled Flexible Hemispherical Tank," North American Aviation, Inc., SID 66-46-4, Rev. May 1967

DISCUSSION

Y. K. Liu (Univ. of Mich.): How did you overcome the problem of the fluid having, in a sense, an infinity-to-infinity set of possible frequencies, since, in your shell equation, you have

only an infinite set of equations? How do you take care of this?

Mr. Tai: I presume that the first "infinity" of your statement "an infinity-to-infinity set of possible frequencies" referred to the variable depth of the fluid. In the present paper only the case of full depth is considered. Under the full depth condition, there is only one solution of the fluctuating fluid pressure which is evaluated from the velocity potential. The interface pressure was used as a forcing function in the shell equations.

Mr. Liu: In your least square integrated result, why not something else? Why not the mini-max criteria?

Mr. Tai: You may use something else if you want to. I used the integrated "square" errors because I intended to use Lagrange's constrained minima technique. The error function is a function of the first order of unknown coefficients. The integrated square error function is of the second order. The differentiations of the integrated square error function with respect to the unknown coefficients result in a set of linear equations which is what I am looking for.

C. Smith (Bell Aerosystems Co.): Is there any sort of constant volume restraint imposed upon the solution in the interface problem? This would presumably affect the pressure conditions in the liquid.

Mr. Tai: Yes, the Laplace equation is derived from the conservation of mass. The equilibrium equations of membrane shell are based on the undeformed configuration, and all interface boundary conditions are constructed on the undeformed surfaces. All these imply a constant volume.

Mr. Smith: By a suitable handling of the membrane or the shell stiffness properties, do you see any difficulty in extending this already difficult problem to the case of constant acceleration?

Mr. Tai: With variable thicknesses and a constant forcing function I can see the difficulty lies more in the variable thickness and less in the constant forcing function.

C. Perisho (McDonnell Douglas Corp.): You spoke of the size of the problem. Could you tell me what the running time is for what size problem on what machine?

Mr. Tai: Since the present approach involves more analytical work and less numerical computation, the computer running time is actually a minor part. In the problem of longitudinal vibrations of a fluid-filled hemispherical shell, the running time in IBM 7094 for computing the eight natural frequencies and the corresponding mode shapes takes approximately 4 min.

* * *

STRUCTURAL AND VIBRATION ANALYSIS OF NAVY CLASS HIGH IMPACT, MEDIUM WEIGHT SHOCK TESTS*

W. P. Welch and Paul D. Saunders
Westinghouse Electric Corporation
Sunnyvale, California

Shock testing of equipment in the mediumweight classification (250 to 6000 lb approximately) to MIL-S-901C [1] requires, in some cases, the design of a mounting fixture to simulate the stiffness of the machinery foundation to be used in the ship installation. As the fixture must have sufficient strength, as well as prescribed stiffness, some ingenuity is needed to arrive at a balanced design.

When the weight of the apparatus to be tested approaches the upper limit of the mediumweight classification, the fixture weight becomes a significant burden in limiting the total weight on the anvil table to an acceptable value, especially so because of the introduction of the 30 degrees inclined test mode. Hence, designing for minimum fixture weight becomes an important aspect of this problem.

In this paper statical and dynamical considerations are discussed, and curves are presented that correlate stiffness, inertia loads or accelerations, and weight. With the aid of the formula and curves, dynamically equivalent and adequate mounting fixtures can be designed.

A typical application of the procedure to a class H.I. (High Impact) shock test of a turbine-driven forced-draft blower weighing over 5000 lb is presented. Calculated maximum g-values both for the initial impact and the motion reversal owing to the stops are developed.

INTRODUCTION

The standard Navy shock test for equipment weighing from 250 to 6000 lb is described in MIL-S-901C [1] and utilizes the HI Shock Testing Machine for Mediumweight Equipment. The shock machine consists of a 3000 lb hammer that swings through an arc greater than 180 degrees and strikes an anvil table. The anvil table thereby suddenly acquires a velocity in the upward direction. The equipment under test is mounted to the anvil table on a relatively soft structural adapter that causes the response of the equipment to lag behind the anvil table motion. Consequently the equipment and the anvil table execute an out-of-phase vibration on the stiffness of the mounting adapter. Thus the composite system moves upward with an average velocity plus a severe transient vibration at one or more frequencies. After 1-1/2 or 3 in. of anvil table travel, depending upon the initial setting, the anvil table strikes definite stops and its motion is reversed to the downward direction. Although severe, this stopping impact differs from the initial impact in that no energy is added to the system, there being in fact a moderate loss in the rebound.

The controlling specification, MIL-S-901C [1], requires that the mounting adapters be similar to those shown in the specification or, alternatively, the adapters should simulate the stiffness of the foundation on which the equipment is to be mounted in the ship. The -C revision of the specification introduced the 30 degrees inclined test mode, for the laudable purpose of introducing a transverse component to the shock and thus simulating sidewise or fore and aft shock aboard ship.

The specification limits the weight on the anvil table to approximately 7400 lb, and the

*This paper was not presented at the Symposium.

equipment weight from 250 to 6000 lb. When the equipment approaches the upper end of this weight classification, a challenging design problem is posed in developing mounting fixtures of minimum weight, adequate strength, and controlled stiffness. In the inclined test mode, the problem is compounded by the requirement that the fixture must rotate the equipment mounting surface by 30 degrees with respect to the anvil table surface. The intent of this paper is to develop guidelines and rules based on our experience to enable this design work to be done more easily in the future.

NOMENCLATURE

F_I Maximum force acting on mounting adapter during phase I (lb)

F_{II} Maximum force acting on mounting adapter during phase II (lb)

G_I Maximum acceleration of M_3 during phase I (g)

G_{II} Maximum acceleration of M_3 during phase II (g)

g Acceleration of gravity (in./sec^2)

K Spring rate of mounting adapter (lb/in.)

L Fractional energy loss on impact of M_1 and M_2

M_1 Mass of hammer (lb-sec^2/in.)

M_2 Mass of anvil table (lb-sec^2/in.)

M_3 Mass of equipment (lb-sec^2/in.)

P Ratio M_3/M_2

R Ratio M_2/M_1

t Time from instant that hammer hits anvil (sec)

T Time from instant that anvil hits stops (sec)

t_s Time from instant hammer hits to instant stops are hit (sec)

U Average velocity of M_2 and M_1 during phase I (in./sec)

U_1 Velocity of M_1 the instant after the hammer hits (in./sec)

U_2 Velocity of M_2 the instant after the hammer hits (in./sec)

V_1 Velocity of hammer just before impact (in./sec)

Y_2 Displacement of M_2 after hammer impacts (in.)

$\dot{Y}_2$ Velocity of M_2 after hammer impacts (in./sec)

Y_3 Displacement of M_3 after hammer impacts (in.)

$\dot{Y}_3$ Velocity of M_3 after hammer impacts (in./sec)

Z_2 Displacement of M_2 after stops are hit (in.)

$\dot{Z}_2$ Velocity of M_2 after stops are hit (in./sec)

Z_3 Displacement of M_3 after stops are hit (in.)

$\dot{Z}_3$ Velocity of M_3 after stops (in./sec)

α Velocity of anvil (M_2) just after hitting stops/velocity before hitting stops

ω_n Circular natural frequency of M_2 and M_3 on K (rad/sec)

f_n Natural frequency of M_2 and M_3 on K (Hz)

MATHEMATICAL MODEL

The 3000-lb hammer strikes the 4000-lb anvil table with a controllable upward velocity, V_1, that depends on the height of the drop, and may be as high as 19 ft/sec. The hammer is extremely rigid, and the anvil table is designed with a very rigid central section and stiff ribs and gussets extending outward to the underside of the table. Therefore, we consider both the hammer and anvil table as concentrated masses in simple impact.

The mounting adapter is relatively flexible as compared to the anvil table and equipment or machinery under test, especially in the 5000-lb weight category. An equivalent system of the hammer, M_1, anvil table, M_2, mounting adapter, and equipment under test, M_3, is shown in Fig. 1. This is reasonably correct if the equipment, M_3, is rigid, as is most power machinery, and if damping is assumed to be zero. The assumption of zero damping is reasonable if there is no significant yielding in the structure and no appreciable sliding of bolted joints. Although the model is correct for the normal upright

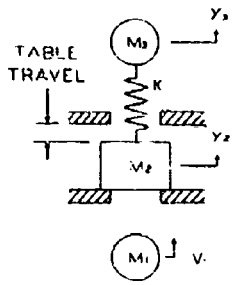

Fig. 1. Mathematical model of shock machine and equipment

mounting position. It is only approximate for the 30 degrees inclined mode as large lateral responses to vertical shock would be present in the subsequent shock motion.

DYNAMICS OF INITIAL IMPACT AND SUBSEQUENT VIBRATION – PHASE I

At initial impact, energy, and momentum are transferred from the striking hammer, M_1, to the anvil table, M_2. The momentum of the system before and after impact remains unchanged as the instantaneous response of the spring, k, is trivial, and is expressed by

$$M_1V_1 = M_1U_1 + M_2U_2 \tag{1}$$

The transfer of energy from M_1 to M_2 is accompanied by a loss, but this is small because of the careful design of the striking surfaces. If L is the fractional loss of energy, the energy transfer equation is

$$\frac{1}{2}M_1V_1^2 = \frac{1}{2}M_1U_1^2 + \frac{1}{2}M_2U_2^2 + L\left(\frac{1}{2}M_1V_1^2\right) \tag{2}$$

Solving Eqs. (1) and (2) for the ratio of the velocity, U_2, of M_2 after impact to the hammer striking velocity V_1, we obtain

$$\frac{U_2}{V_1} = \frac{R + \sqrt{R^2 - L(R^2 + R)}}{R^2 + R} \tag{3}$$

where R is the ratio M_2/M_3, and L is the fractional loss of energy during the impact.

The system consisting of the anvil table, M_2, coupled by the mounting adapter spring, K, to the equipment under test, M_3, is thus started upward by a suddenly applied velocity, U_2, imposed on M_2 at $t = 0$. The subsequent motion is defined by the following equations:

$$\begin{aligned} M_2\ddot{Y}_2 &= K(Y_3 - Y_2) \\ M_3\ddot{Y}_3 &= K(Y_2 - Y_3) \end{aligned} \tag{4}$$

$$\begin{aligned} M_2\ddot{Y}_2 + KY_2 &= KY_3 \\ M_3\ddot{Y}_3 + KY_3 &= KY_2 \end{aligned} \tag{4a}$$

the solution of which is

$$\begin{aligned} Y_2 &= A\sin\omega t + B\cos\omega t + Ut \\ Y_3 &= C\sin\omega t + D\cos\omega t + Ut \end{aligned} \tag{5}$$

With the initial conditions at $t = 0$, $Y_2 = Y_3 = U_2 = 0$, the motion after the initial impact is given by

$$\begin{aligned} Y_2 &= \frac{U_2 - U}{\omega}\sin\omega t + Ut \\ Y_3 &= -\frac{U}{\omega}\sin\omega t + Ut \end{aligned} \tag{6}$$

U_2 is the anvil table initial velocity given by Eq. (3). U is the velocity of the center of gravity of M_2 and M_3, or the average velocity of either. ω is the natural frequency of M_2 and M_3 on K.

The motion of the system then consists of an upward motion of the center of gravity at a velocity U with the two masses M_2 and M_3 executing an accordion-type vibration at the frequency

$$\omega = \sqrt{\frac{(M_2 + M_3)K}{M_2M_3}} \tag{7}$$

The relative amplitude, $y_2 - y_3$, is obtainable from Eq. (6) and is

$$Y_2 - Y_3 = \frac{U_2}{\omega}\sin\omega t \tag{8}$$

The system motion is illustrated by the curves of Fig. 2, which show the sinusoidal motion of the anvil table and the equipment under test, with the average upward velocity being given by

$$U = \frac{M_2}{(M_2 + M_3)}U_2 \tag{9}$$

As the upward travel is limited to 3 in. maximum, the effect of gravity in reducing U is too small to be important.

It is not, however, the steady velocity but the vibration that shock loads the equipment under test. The greatest acceleration on the tested equipment occurs at the 1/4-cycle point in time, and at each 1/2-cycle period thereafter, with the shock forces alternating first

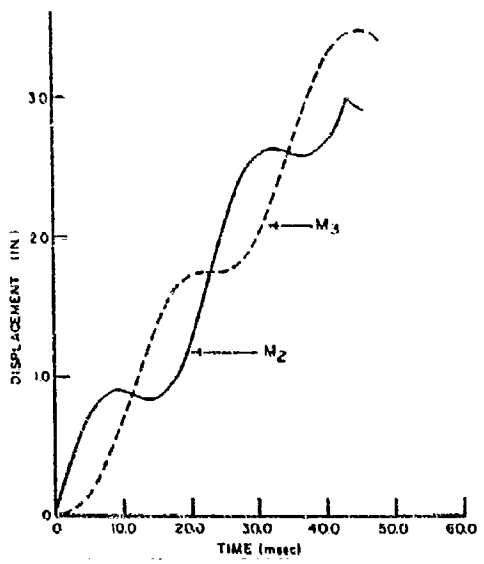

Fig. 2. Anvil table and equipment displacement vs time for a forced-draft blower (DE-1052 Class)

upward and then downward. The force magnitude is $K(Y_2 - Y_3)$ and is

$$F_I = \frac{K}{\omega} U_2 \sin \omega t \qquad (10)$$

with a maximum value of

$$F_{I\,max} = \frac{K}{\omega} U_2 = \omega \frac{M_2 M_3}{M_2 + M_3} U_2 . \qquad (11)$$

The maximum acceleration in g's on the tested equipment, M_3, is

$$G_I = \frac{\omega}{g} \frac{M_2}{M_2 + M_3} U_2 \qquad (12)$$

and if Eq. (7) is substituted in Eq. (12), we get

$$G_I = \sqrt{\frac{K}{g W_3 (1 + W_3/W_2)}}\, U_2 \qquad (13)$$

where g is the acceleration of gravity and W_3 and W_2 are the weights in pounds of M_3 and M_2, respectively.

Equation (7) can be used to find the mounting adapter spring rate necessary to simulate an expected shipboard natural frequency, or conversely it can be used to find the test natural frequency resulting from making the mounting adapter stiffness simulate shipboard mounting stiffness. It is interesting to note that the finite weight of the anvil table prevents both the shipboard frequency and the shipboard spring rate from being duplicated in the shock test.

Equations (12) and (13) can be used for designing the mounting adapter and the equipment to the proper strength levels if the value of U_2 is known. As the amount of energy lost on impact of the hammer is difficult to determine, Eq. (3) cannot be readily used to determine U_2. Accordingly, experimental values of U_2 vs V_1, and the height of the hammer drop [2] are shown in Fig. 3.

Figure 4 is a plot of system natural frequency vs K for equipment weights between 250 and 6000 lb. Figure 5 is a plot of Eq. (12), which gives the maximum acceleration of M_3/initial anvil table velocity U_2, during phase I for various values of ω and W_3/W_2. Figure 6 is a plot of Eq. (13) giving the maximum acceleration of M_3/initial anvil table velocity U_2, during phase I for various values of K and W_3 for an anvil table weight, W_2, of 4000 lb.

DYNAMICS OF IMPACT OF HITTING THE STOPS – PHASE II

After rising 1-1/2 or 3 in., depending upon the initial height setting of the anvil table, the anvil table motion is arrested and rebounds from the stops with a downward velocity that is some fraction a of the striking velocity. Let this occur at time t_s so that the initial conditions for phase II or the "rebound" phase of the shock are at $t = t_s$ and $T = 0$:

$$\begin{aligned} Z_2 &= 0 \\ \dot{Z}_2 &= -a\dot{Y}_{2s} \\ Z_3 &= Y_{3s} - Y_{2s} = \Delta Y_s \\ \dot{Z}_3 &= \dot{Y}_{3s} \end{aligned} \qquad (14)$$

with a new origin of coordinates T and Z being chosen so that time is zero and the anvil table displacement is zero at the onset of rebound.

Two general aspects of the rebound are immediately evident. First, there is no energy added – only a change in momentum – of a degree dependent upon the efficiency of the rebound as expressed by a. Second, there is no immediate effect on the equipment under test (M_3), although its velocity $\dot{Y}_{3s}$ and the stretch of the spring $Y_{3s} - Y_{2s} = Y_s$ at the time of

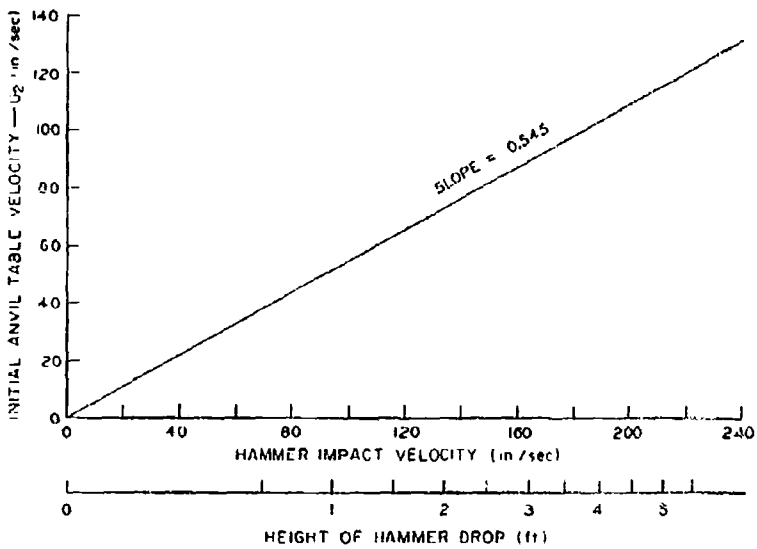

Fig. 3. Initial anvil table motion vs hammer velocity and height of hammer drop

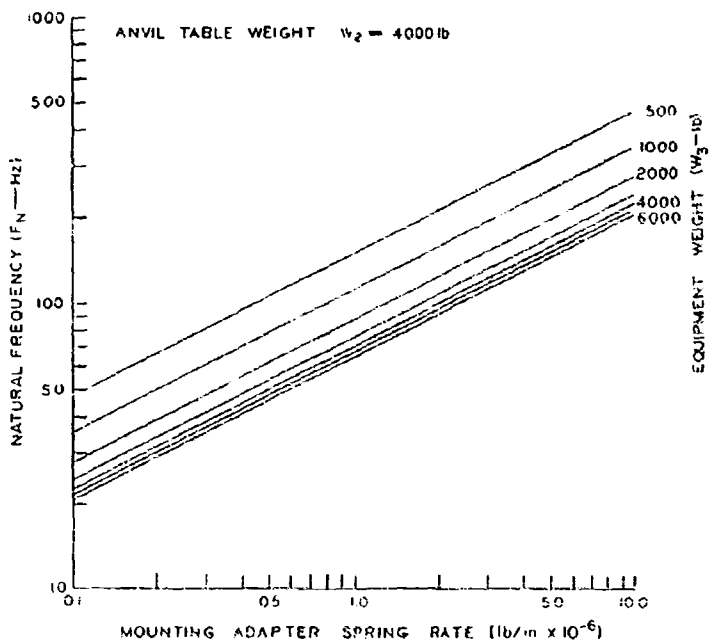

Fig. 4. Natural frequency vs spring rate

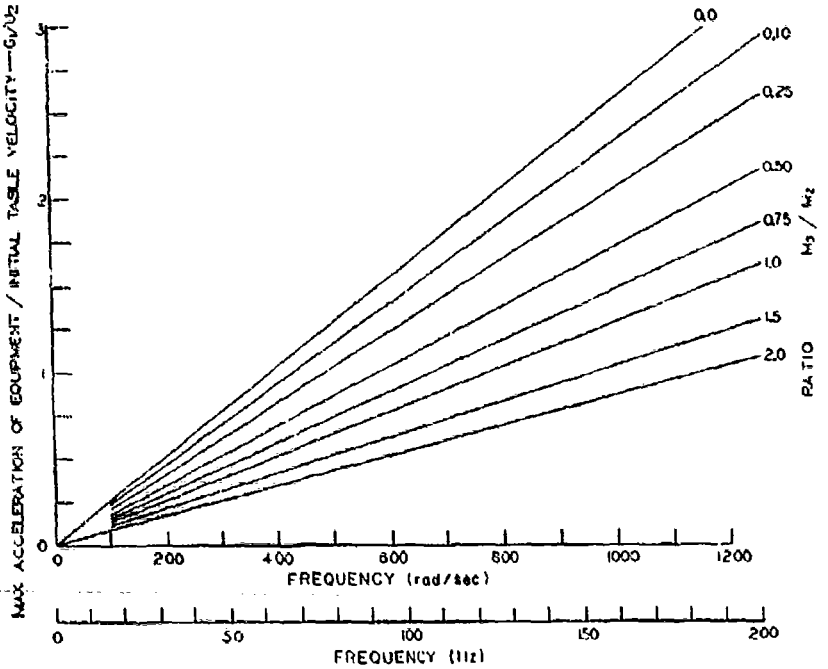

Fig. 5. Maximum phase I acceleration of equipment/initial anvil table velocity vs natural frequency

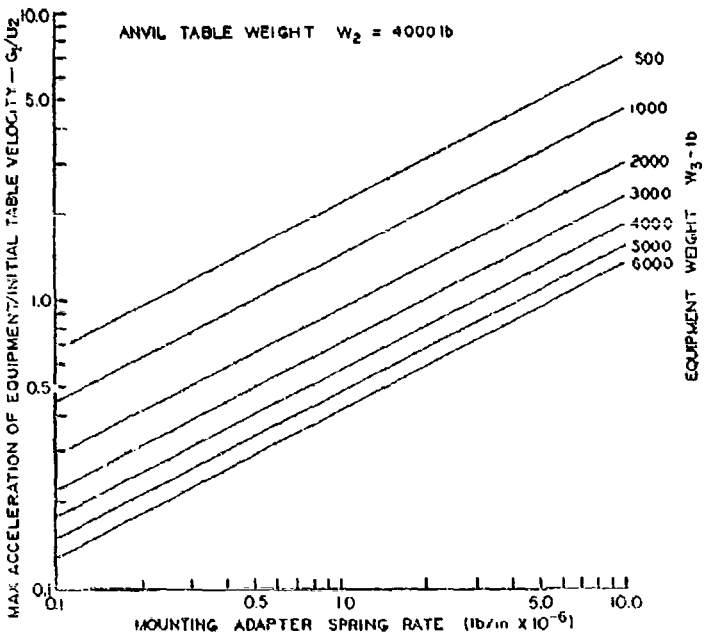

Fig. 6. Maximum phase I acceleration of equipment/initial anvil table velocity vs spring rate for an anvil table weight of 4000 lb

rebound will influence the rebound shock motion.

As the frequency will not change and the average velocity of rebound is of minor interest, only the extension of the spring $Z_2 - Z_3$ and maximum g-loads will be calculated and discussed. Using the above initial conditions and solving Eq. (5), the following is obtained for the maximum value of $Z_2 - Z_3$:

$$(Z_2 - Z_3)_{max} = \sqrt{\left(\frac{\dot{Y}_{2s} - \dot{Y}_{3s}}{\omega}\right)^2 + (Y_s)^2} \quad (15)$$

It is seen that the maximum spring load $K(Z_2 - Z_3)$ during the rebound phase is most dependent on timing — that is, the time of hitting the stops as a function of fractions of a cycle of vibration of M_2 and M_3 on k. The ratio

$$\frac{(Z_2 - Z_3)_{max}}{(Y_2 - Y_3)_{max}} = \frac{F_{II}}{F_I} = \frac{G_{II}}{G_I} \quad (16)$$

both differences being taken as maximum values, is a direct measure of the amplification or attenuation of the phase I force and g levels caused by hitting the stops.

From Eqs. (14) and (6) we get

$$\frac{G_{II\,max}}{G_{I\,max}} = \sqrt{\left[\left(\frac{1-P}{1+P}\right)\cos\omega t_s - \left(\frac{1-P}{1+P}\right)\right]^2 + \left[\sin\omega t_s\right]^2} \quad (17)$$

where P is the ratio of the equipment weight, W_3, to the anvil table weight, W_2.

Equation (17) is used to find the amplification or attenuation of forces on the mounting adapter and g levels on the equipment that occurs after the stops are hit. The rebound efficiency can be determined from plots of anvil table displacement vs time, and may be of the order of 0.6 [3]. The time, t_s, at which the stops are hit can be determined from Eq. (6) by setting Y_2 to 1-1/2 and 3 in. Note that any error in calculating the natural frequency is multiplied by the number of cycles occurring in the initial phase I travel. Therefore for higher frquencies, it is desirable to use the maximum possible shock amplification for designing the adapter and the equipment.

Figures 7, 8, and 9 are plots of Eq. (17) for various values of P, , and fraction of a cycle of when the stops are hit. When M_3 is larger than M_2, the velocity of M_2, $\dot{Y}_2$ is negative for a portion of each cycle of motion in phase I. If the velocity of M_2 is negative, M_2 is moving away from the stops, and no contact can occur.

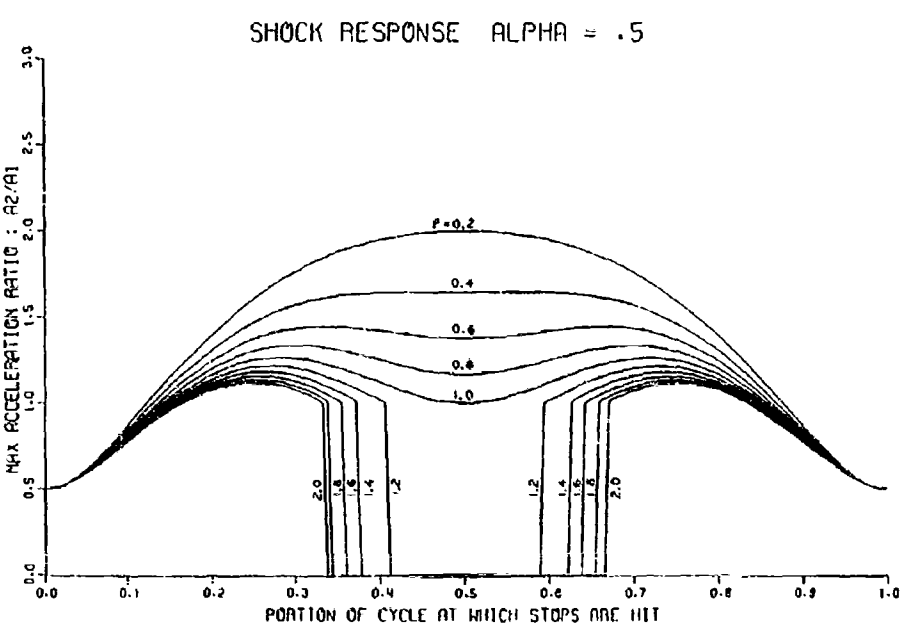

Fig. 7. Ratio of acceleration in phase II to acceleration in phase I vs fraction of a cycle when stops are hit for alpha equals 0.5, $P = W_3/W_2$

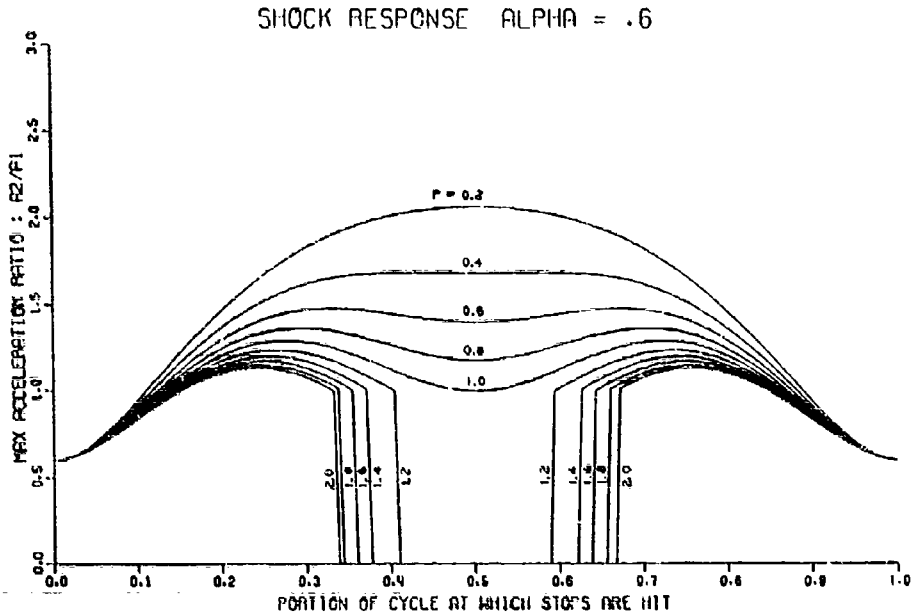

Fig. 8. Ratio of acceleration in phase II to acceleration in phase I vs fraction of a cycle when stops are hit for alpha equals 0.6, $P = W_3/W_2$

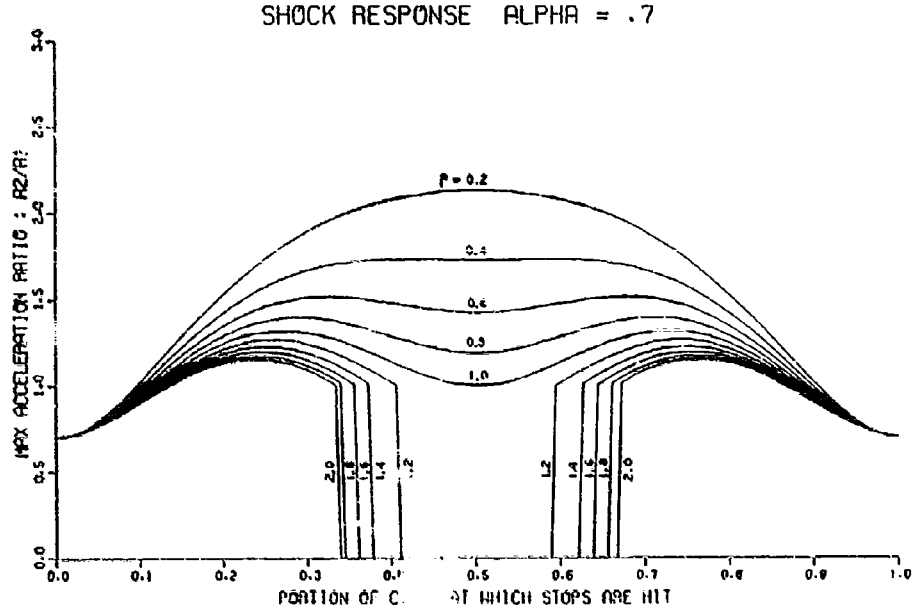

Fig. 9. Ratio of acceleration in phase II to acceleration in phase I vs fraction of a cycle when stops are hit for alpha equals 0.7, $P = W_3/W_2$

This condition is indicated in Figs. 7, 8, and 9 by the areas where the acceleration ratio goes to zero.

From the foregoing it is easily seen that the phase II shock may easily exceed the severity of the shock resulting from the initial impact of the hammer (phase I). The ratio of g-loadings ranges from 0.6 to 2.07 for $\cdot$ = 0.60, depending only on the timing t_2 of the shock reversal and the ratio of W_3 W_2. This phenomenon has been witnessed many times by those experienced in H.I. shock testing; parts will fail "upward" rather than in the downward direction.

APPLICATION TO A FORCED DRAFT BLOWER

This analysis of the Mediumweight Shock Machine was performed in conjunction with designing the mounting adapter and shock testing a DE-1052 Class Forced Draft Blower. The blower weight (M_3) was approximately 5500 lb, and the stiffness of the shipboard mounting was approximately 300,000 lb/in.

In designing the mounting fixture, it soon became apparent that it was not possible to duplicate the shipboard mounting stiffness and still have a fixture that had the required strength and whose weight, when added to the blower weight, did not exceed the specifications weight limit. This problem was especially apparent in the 30 degrees test mode, where the standard 30 degree-adapter of MIL-S-901C [1] weighs approximately 1480 lb. Accordingly a fixture was designed that had a spring constant of approximately 520,000 lb/in. and met the necessary strength and weight requirements. The effect of increasing the spring constant was to increase the g-loading on the blower to about 132 percent of the g-loading that would have resulted if the shipboard stiffness had been duplicated in the fixture. This g-loading is 188 percent of the g-loading that would have resulted if the shipboard natural frequency had been duplicated in the shock test.

Table 1 shows the calculated response of the forced draft blower for a 5-1/2-ft hammer drop. Figure 2 is a plot of the displacements of the anvil table, M_2, and the blower, M_3, vs time. Unfortunately it was not possible to verify any of these values experimentally during the shock test, although the successful completion of the shock test itself, along with the minor damage observed, is an indication that the calculated results were of the right order of magnitude. Figures 10 and 11 show the blower mounted on the shock machine in the horizontal and 30 degrees test modes.

TABLE 1
Shock Response of a Forced Draft Blower (DE-1052 Class)

Weight of blower and part of fixture W_3	5900 lb
Weight of anvil table and part of fixture W_2	5000 lb
Spring constant K	520,000 lb/in.
Natural frequency	43.4 Hz
Height of hammer drop	5.5 ft
Initial anvil table velocity	122 in./sec
Maximum acceleration in phase I	46.6 g
Maximum acceleration in phase II	57.9 g
Portion of cycle when stops are hit	Phase II acceleration
Start of cycle	28.0 g
0.1 of cycle	40.6 g
0.2 of cycle	55.0 g
0.3 of cycle	57.1 g
0.4 of cycle	47.5 g
0.5 of cycle	No impact
0.6 of cycle	47.5 g
0.7 of cycle	57.1 g
0.8 of cycle	55.0 g
0.9 of cycle	40.0 g
1.0 of cycle	28.0 g

Fig. 10. Forced-draft blower (DE-1052) mounted for horizontal shock test

Fig. 11. Forced-draft blower (DE-1052) mounted for 30 degrees inclined shock test

CONCLUSIONS

Considering the terms of Eq. (12), the weight of the equipment is usually well defined, which in turn defines the height of the hammer drop and the starting velocity of the anvil table, V_1. (See Table I of MIL-S-901C.) This means that the g levels experienced during the shock test will be directly proportional to the natural frequency ω_n. Hence it is of the utmost importance that when designing the mounting adapter, proper attention be given to the adapter spring rate, as this defines ω_n. This is contrary to the usual practice of designing mounting adapters with emphasis on high strength and light weight, and with little or no consideration being given to spring rate.

An important secondary aspect of this analysis is that the shipboard mounting natural frequency should be simulated on the shock machine rather than the spring rate, as the shock machine vibration consists of an accordion-like mode of M_1 and M_2 with a node in the spring, K.

It is hoped that this paper has clarified some of the important theoretical aspects of the Mediumweight Shock Machine Test, and that the equations and curves will aid in utilizing the theory in practical applications with a minimum amount of effort.

REFERENCES

1. MIL-S-901C (Navy) "Shock Tests, H.I. (High Impact) Shipboard Machinery, Equipment and Systems, Requirements for," 15 Jan. 1963

2. I. Vigness, "Navy High-Impact Shock Testing Machines for Lightweight and Mediumweight Equipment," NRL Rept. 5618, June 1, 1961, p. 29

3. W. P. Welch, "Mechanical Shock on Naval Vessels," NavShips 250-660-26, March 1946, p. 97

* * *

TRANSIENT RESPONSES OF A LINEAR MECHANICAL SYSTEM BY USE OF EXPERIMENTALLY DETERMINED UNIT IMPULSE RESPONSES*

Victor P. Warkulwiz
General Electric
Missile and Space Division
Philadelphia, Pennsylvania

A numerical technique based on the convolution integral has been developed whereby the transient responses of a linear mechanical system subjected to arbitrary excitations can be determined utilizing the results of a shock or vibration test. The type of test and the type of excitation used in the test are not restricted theoretically but are subject only to practical limitations. This allows the user a wide variety of tests and excitations from which to choose. The numerical technique is applied to the test data by use of an analog-to-digital converter and a digital computer and results in unit impulse responses. The unit impulse responses are then used as inverse transfer functions to determine transient responses caused by arbitrary excitations.

INTRODUCTION

The purpose of this paper is to introduce a method of obtaining the transient responses of a linear mechanical system that may prove to be quicker, cheaper, and more reliable than methods presently used. This method requires a simple shock or vibration test in which an arbitrary excitation is applied to the system and responses are measured. One such test is performed in each of three mutually perpendicular directions or in the appropriate direction if only unidirectional response information is desired. The test data is then processed by an analog-to-digital converter and a digital computer. This processing provides the transfer characteristics of the system in the form of unit impulse responses. These responses are then used to determine the transient responses caused by any given excitation.

Essentially, the technique is a numerical scheme in which the convolution integral is expressed in the form of a matrix equation. This equation is then used to obtain the desired responses.

The discussion will begin with a brief review of the unit impulse function followed by a description of the acceleration transfer equations for lumped linear systems. This enables a background to be developed whereby the full potential of the technique can be realized. The numerical method will then be developed, and additional applications will be introduced. The technique will then be extended to include continuous linear systems. The procedure will be summarized in the form of a flow chart, and an example problem will be presented that will illustrate the use of the technique and provide some information concerning its accuracy. The appendix contains mathematical developments of the various relationships introduced.

THE UNIT IMPULSE FUNCTION

Consider a square pulse of time duration, t_a, and height, $1/t_a$, as shown in Fig. 1. The area under the pulse is equal to unity. Now let t_a approach zero. In the limit the area under the pulse will remain at unity as shown in the following equation:

*This paper was not presented at the Symposium.

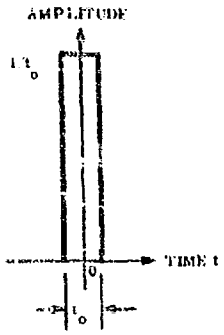

Fig. 1. Pulse used to generate unit impulse

$$\lim_{t_o \to 0} (t_o\, t_c) = 1 \qquad (1)$$

The resulting function is known as the unit impulse function or Dirac delta function. It can be defined loosely as follows:

$$\delta(t) = \infty \quad \text{at} \quad t = 0$$

$$\delta(t) = 0 \quad \text{at} \quad t \neq 0 \qquad (2)$$

$$\int_{-\infty}^{\infty} \delta(t)\, dt = 1$$

The aspect of the unit impulse that will prove to be most important is that the responses of a linear system to this function can be used to characterize vibrational relationships in the system.

ACCELERATION TRANSFER EQUATIONS

If a lumped linear mechanical system (Fig. 2) is initially at rest in its equilibrium position and a force is applied to a mass point, $P_i(x_i, y_i, z_i)$, in the system giving it an acceleration as a function of time, then the acceleration of another mass point, $P_j(x_j, y_j, z_j)$, in the system is related to the acceleration of P_i by the equations

$$\ddot{x}_j(t) = \int_{-\infty}^{t} \ddot{x}_i(\tau)\, h^x_{ij}(t-\tau)\, d\tau \qquad (3a)$$

$$\ddot{y}_j(t) = \int_{-\infty}^{t} \ddot{y}_i(\tau)\, h^y_{ij}(t-\tau)\, d\tau \qquad (3b)$$

and

$$\ddot{z}_j(t) = \int_{-\infty}^{t} \ddot{z}_i(\tau)\, h^z_{ij}(t-\tau)\, d\tau \qquad (3c)$$

where the double dot over a letter indicates the acceleration of the corresponding coordinate. The functions, $h^x_{ij}(t)$, $h^y_{ij}(t)$, and $h^z_{ij}(t)$, are the components of the acceleration of P_j caused by giving P_i a unit impulse acceleration. The superscripts, x, y, and z indicate direction and are not exponents. They will frequently be omitted in the discussion for purposes of generality.

The resultant acceleration of P_j is

$$\ddot{r}_j(t) = \left[\ddot{x}_j^2(t) + \ddot{y}_j^2(t) + \ddot{z}_j^2(t)\right]^{1/2} \qquad (4)$$

where r_j is the distance from the origin of the coordinate system to P_j.

The unit impulse response, $h_{ij}(t)$, is also known as the inverse transfer function because it is the inverse transform of the transfer function H(s) used in the Laplace transform treatment of linear systems. It is dependent only upon the physical characteristics of the system, that is, spring constants, masses, damping coefficients, and configuration.

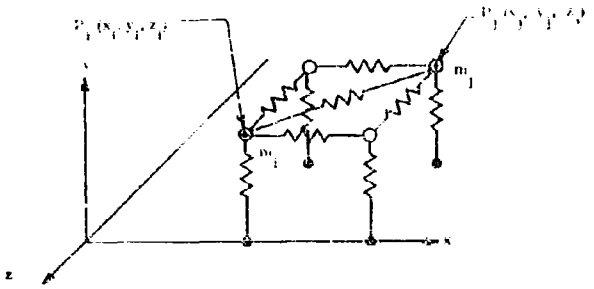

Fig. 2. Representation of a mechanical system in space

The integrals of Eqs. (3a), (3b), and (3c) are in the form of the familiar convolution integral. They reveal the fact that if unit impulse responses are known then the acceleration of P_j caused by other arbitrary accelerations given to P_i can be obtained.

Impulse responses of a system can be determined experimentally by direct testing the system using fast pulses to approximate impulses. The use of fast pulses, however, presents some practical problems that may make testing difficult. Tests of this nature are not required though, because the numerical technique discussed in the next section provides a way to solve Eqs. (3a), (3b), and (3c) for $h_{ij}(t)$, given the acceleration of P_i and the corresponding acceleration of P_j. Therefore, almost any type of shock or vibration test will provide sufficient information to solve for the impulse responses.

NUMERICAL METHOD

Equations (3a), (3b), and (3c) can be solved numerically for the response acceleration of P_j if $h_{ij}(t)$ and the acceleration of P_i are known. Conversely, they can be solved for $h_{ij}(t)$ if the accelerations of P_i and P_j are known. These solutions will be obtained by the use of sampled functions. (A sampled function is one whose value is specified only at particular points in time. A sample corresponding to a given time is the value of the function at that time.)

Figure 3 shows the type of sampled acceleration-time function that will be discussed in this section. It is sampled at constant time intervals, T, with the first sample at $t = 0$. The reciprocal of T is the sampling rate in samples per second. Sampling rate is sometimes expressed in the same terms as frequency, for example, 100 kHz means 100,000 samples per second.

Consider now the following general form of Eqs. (3a), (3b), and (3c):

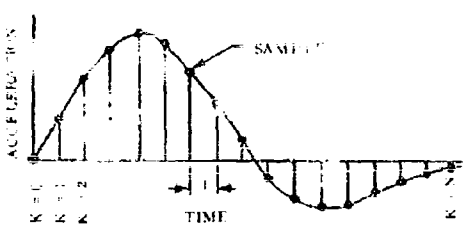

Fig. 3. Sampled acceleration - time function

$$f_j(t) = \int_0^t f_i(\tau)\, h_{ij}(t-\tau)\, d\tau = f_i(t) * h_{ij}(t)^{\dagger} \qquad (5)$$

where $f_j(t)$, $f_i(t)$, and $h_{ij}(t)$ designate a response function, an input function, and a unit impulse response, respectively.† By replacing $d\tau$ by the sampling time increment T and substituting nT for τ, we can approximate Eq. (5) by the summation

$$f_j(t) = T \sum_{n=0}^{K} f_i(nT)\, h_{ij}(t-nT) \qquad (6)$$

for $KT \le t < (K+1)T$ where $n = 0, 1, 2, \ldots, K$.

If the samples of $f_j(t)$ are to be calculated only at points of time KT, then Eq. (6) can be written

$$f_j(KT) = T \sum_{n=0}^{K} f_i(nT)\, h_{ij}\left[(K-n)T\right]. \qquad (7)$$

The meaning of K is illustrated in Fig. 3. For any particular value of K, Eq. (7) can be written as the product of a row matrix whose elements are the samples $f_i(nT)$, a column matrix whose elements are the samples $h_{ij}[(K-n)T]$, and the sampling time increment T. A column matrix of $f_j(KT)$ for all K up to a given value, N, can therefore be written as

$$\begin{Bmatrix} f_j(0) \\ f_j(T) \\ \vdots \\ f_j(NT) \end{Bmatrix} = T \begin{bmatrix} f_i(0) & 0 & 0 & \cdots & 0 \\ f_i(T) & f_i(0) & 0 & \cdots & 0 \\ \vdots & & & & \\ f_i(NT) & f_i[(N-1)T] & f_i[(N-2)T] & \cdots & f_i(0) \end{bmatrix} * \begin{Bmatrix} h_{ij}(0) \\ h_{ij}(T) \\ \vdots \\ h_{ij}(NT) \end{Bmatrix}. \qquad (8)$$

†The asterisk notation for convolution will be used throughout the rest of this paper.

If $f_i(0) \neq 0$, Eq. (8) can be transposed to yield the sampled unit impulse response.

$$\begin{Bmatrix} h_{ij}(0) \\ h_{ij}(T) \\ \vdots \\ h_{ij}(NT) \end{Bmatrix} = \frac{1}{T} \begin{bmatrix} f_i(0) & 0 & 0 & \cdots & 0 \\ f_i(T) & f_i(0) & 0 & \cdots & 0 \\ \vdots & \vdots & & & \\ f_i(NT) & f_i[(N-1)T] & f_i[(N-2)T] & \cdots & f_i(0) \end{bmatrix}^{-1} \cdot \begin{Bmatrix} f_j(0) \\ f_j(T) \\ \vdots \\ f_j(NT) \end{Bmatrix}. \quad (9)$$

If $f_i(0) = 0$, then the $f_i(KT)$ matrix is singular and cannot be inverted. This problem can be overcome by noting that $h_{ij}(0) = f_j(0) = 0$ always, because in a real physical system an acceleration cannot be transmitted instantaneously, that is, no physical system is infinitely rigid. Under these conditions Eq. (8) then reduces to

$$\begin{Bmatrix} f_j(2T) \\ f_j(3T) \\ \vdots \\ f_j[(N+1)T] \end{Bmatrix} = T \begin{bmatrix} f_i(T) & 0 & 0 & \cdots & 0 \\ f_i(2T) & f_i(T) & 0 & \cdots & 0 \\ \vdots & \vdots & & & \\ f_i(NT) & f_i[(N-1)T] & f_i[(N-2)T] & \cdots & f_i(T) \end{bmatrix} \cdot \begin{Bmatrix} h_{ij}(T) \\ h_{ij}(2T) \\ \vdots \\ h_{ij}(NT) \end{Bmatrix} \quad (10)$$

with $f_i(T) = f_i(0) = 0$. If $f_i(T) = 0$, Eq. (10) can then be transposed to give

$$\begin{Bmatrix} h_{ij}(T) \\ h_{ij}(2T) \\ \vdots \\ h_{ij}(NT) \end{Bmatrix} = \frac{1}{T} \begin{bmatrix} f_i(T) & 0 & 0 & \cdots & 0 \\ f_i(2T) & f_i(T) & 0 & \cdots & 0 \\ \vdots & \vdots & & & \\ f_i(NT) & f_i[(N-1)T] & f_i[(N-2)T] & \cdots & f_i(T) \end{bmatrix}^{-1} \cdot \begin{Bmatrix} f_j(2T) \\ f_j(3T) \\ \vdots \\ f_j[(N+1)T] \end{Bmatrix}. \quad (11)$$

Once the sampled unit impulse response is obtained, it is possible to determine the response caused by any input by resorting back to either Eq. (8) or Eq. (10). It is also possible to determine the input function required to produce a certain response. This can be done by rewriting Eq. (10) in the equivalent form

$$\begin{Bmatrix} f_j(2T) \\ f_j(3T) \\ \vdots \\ f_j[(N+1)T] \end{Bmatrix} = T \begin{bmatrix} h_{ij}(T) & 0 & 0 & \cdots & 0 \\ h_{ij}(2T) & h_{ij}(T) & 0 & \cdots & 0 \\ \vdots & & & & \\ h_{ij}(NT) & h_{ij}[(N-1)T] & h_{ij}[(N-2)T] & \cdots & h_{ij}(T) \end{bmatrix} \cdot \begin{Bmatrix} f_i(T) \\ f_i(2T) \\ \vdots \\ f_i(NT) \end{Bmatrix}. \quad (12)$$

If $h_{ij}(T) \neq 0$, this equation can be transposed to solve for the sampled $f_i(t)$.

The following points should be considered when using the numerical techniques described in this section:

1. The sampling rate must be consistent and constant, that is, all functions must be

sampled at the same times KT and T must remain constant.

2. The accuracy to which Eqs. (8) through (12) approximate the exact solutions depends on the sampling time increment, T. The smaller T, the more accurate is the approximation. Decreasing T, however, results in larger matrices (assuming that the time duration over which transient responses are to be examined remains fixed). This, in turn, increases computer time and cost. A tradeoff must therefore be determined.

VELOCITY AND DISPLACEMENT TRANSFER EQUATIONS

If a lumped linear mechanical system is initially at rest in its equilibrium position and a force is applied to a mass point, $P_i(x_i, y_i, z_i)$, in the system giving it a velocity as a function of time, then the velocity of another mass point, $P_j(x_j, y_j, z_j)$, in the system is related to the velocity of P_i by the equations

$$\dot{x}_j(t) = \dot{x}_i(t) * h^x_{ij}(t) \qquad (13a)$$

$$\dot{y}_j(t) = \dot{y}_i(t) * h^y_{ij}(t) \qquad (13b)$$

and

$$\dot{z}_j(t) = \dot{z}_i(t) * h^z_{ij}(t) \qquad (13c)$$

where the dot over a letter indicates the velocity of the corresponding coordinate. The displacements are related similarly.

$$\delta x_j(t) = \delta x_i(t) * h^x_{ij}(t) \qquad (14a)$$

$$\delta y_j(t) = \delta y_i(t) * h^y_{ij}(t) \qquad (14b)$$

and

$$\delta z_j(t) = \delta z_i(t) * h^z_{ij}(t) \qquad (14c)$$

where δ indicates the displacement of the point from its equilibrium position.

The interesting fact to remember here is that the inverse transfer functions used in the velocity and displacement equations are identical to the ones used in the acceleration equations. That is, the impulse response is a characteristic of two points in the system that remains invariant with regard to acceleration, velocity, and displacement.

Equations (13) and (14) can be solved by the matrix methods previously discussed. In practice, the matrices would be generated from data obtained from velocity sensors or strain gages.

FORCE TRANSFER EQUATIONS

If a lumped linear system is initially at rest in its equilibrium position and a force, $\phi_i(t)$, is applied to a mass point, $P_i(x_i, y_i, z_i)$, then the acceleration of a mass point, $P_j(x_j, y_j, z_j)$, is related to $\phi_i(t)$ by the equations

$$\ddot{x}_j(t) = \phi^x_i(t) * g^x_{ij}(t) \qquad (15a)$$

$$\ddot{y}_j(t) = \phi^y_i(t) * g^y_{ij}(t) \qquad (15b)$$

and

$$\ddot{z}_j(t) = \phi^z_i(t) * g^z_{ij}(t) \qquad (15c)$$

where $\phi^x_i(t)$, $\phi^y_i(t)$, and $\phi^z_i(t)$ are the components of $\phi_i(t)$ in the x, y, and z directions, respectively, and $g^x_{ij}(t)$, $g^y_{ij}(t)$, and $g^z_{ij}(t)$ are the accelerations of P_j caused by unit impulses of force applied to P_i in the corresponding directions. Here again the superscripts indicate direction and are not exponents. Note that in general, $g_{ij}(t) \neq h_{ij}(t)$.

If the accelerations are multiplied by their corresponding masses, Eqs. (15a), (15b), and (15c) can then be used to relate excitation forces to response forces. The function $g_{ij}(t)$ can be determined experimentally using the same techniques that were used to determine $h_{ij}(t)$.

PRECAUTIONS

Care must be taken when applying Eqs. (3), (13), (14), and (15) to a problem. The following points must be given close attention:

1. The system under study must be initially at rest in its equilibrium position.

2. Equations (3), (13), and (14) relate the vibrations of a response point to the vibrations of the point where the external force is applied. They could be used to relate the vibrations of two points that are caused to vibrate by an external force applied to a different third point, but the inverse transfer function in such a case would not be unique. It would depend upon the point where the external force is applied.

3. Equations (15a), (15b), and (15c) implicitly relate the resultant force at a response

point to the externally applied force at an input point. It does not imply any relationship between the resultant force at a response point and the resultant force at an input point, nor does it imply any relationship between the resultant forces at two response points. Such relationships do exist, however, and can be expressed with convolution integrals; but their inverse transfer functions are not equal to $g_{ij}(t)$, and the inverse transfer functions between response points would not be unique. They would depend upon the point where the external force is applied.

4. The superposition theorem can be applied when using Eqs. (15a), (15b), and (15c). That is, if a number of forces are applied to different mass points in the system, then the response of any mass point in the system is the sum of the responses caused by each force acting independently. Superposition cannot be applied, however, to the relationships expressed in Eqs. (3), (13), and (14).

CONTINUOUS SYSTEMS

The preceding techniques can be applied to a continuous linear system or structure as well as to a lumped linear system. This is because a continuous linear structure, such as one constructed of metal plates, beams, etc., can, in theory, be approximated to any desired degree of accuracy by a lumped linear system composed of masses, springs, and dashpots. The impulse responses of such a structure would then depend upon its material and geometric properties, for example, elasticity, density, and configuration.

Instead of thinking of a continuous linear structure as approximated by a conglomeration of masses, springs, and dashpots, it may be helpful to think of it as a locus of points in space that have definite relationships between them, regarding displacement, velocity, and acceleration. The relationships are expressed in convolution integrals and are characterized by unit impulse responses.

To clarify the point representation concept, consider a structure approximated by a lumped mass-spring system (assuming no damping for simplicity) as shown in Figs. 4(a) and 4(b). (Figure 4(c) shows a more elaborate model.) If more accuracy is desired, the number of masses must be increased, thereby

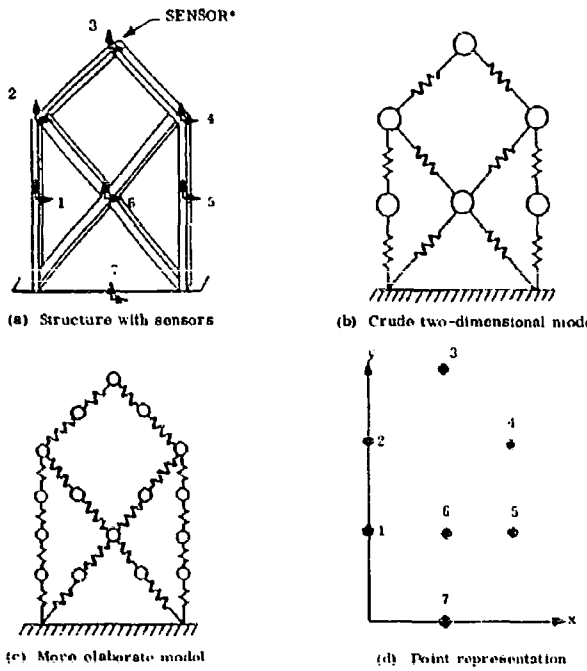

(a) Structure with sensors

(b) Crude two-dimensional model

(c) More elaborate model

(d) Point representation

*Accelerometer, velocity sensor, or strain gage

Fig. 4. Point representation of a continuous linear structure

decreasing the value of each mass. To describe the structure precisely we must go to the limit, that is, let the number of masses approach infinity and the value of each mass approach zero. This limit is represented by the locus of all points in the structure. Figure 4(d) shows the points of interest: accelerometer, velocity sensor, or strain gage locations.

PROCEDURE

The techniques described in this paper can be used with the results of almost any shock or vibration test. Accelerometer, velocity sensor, or strain gage responses are recorded on magnetic tape during the test. The data on this tape are then sampled by use of the proper analog-to-digital conversion equipment. This process results in a tape that contains the sampled responses in a format acceptable by a digital computer. This tape, along with the desired excitation data, is used as input to an appropriate program. Figure 5 is a flow chart illustrating the procedure to be followed utilizing accelerometer data. Similar procedures can be followed to process velocity sensor or strain gage data.

EXAMPLE PROBLEM

Assume that the base of the undamped simple oscillator shown in Fig. 6 is given the step of acceleration

$$\ddot{y}_i(t) = 0 \quad \text{for} \quad t \leq 0 ,$$

$$\ddot{y}_i(t) = 1\,g \quad \text{for} \quad t \geq 0 .$$

A simple analysis will show that the response of mass m_j assuming a value of 4000π for the natural frequency ω_n of the oscillator, is

$$\ddot{y}_j(t) = (1 - \cos 4000\pi t)\,g .$$

The first part of the problem is to obtain the unit impulse response over a period of 0.5 ms. This will be done by the matrix method previously discussed using both 40 kHz and 100 kHz sampling rates. For 40 kHz sampling, $T = 2.5 \times 10^{-5}$ sec, and the samples of $\ddot{y}_i(t)$ are

$$\ddot{y}_i(0) = 1 ,$$
$$\ddot{y}_i(T) = 1 ,$$
$$\vdots$$
$$\ddot{y}_i(NT) = 1 .$$

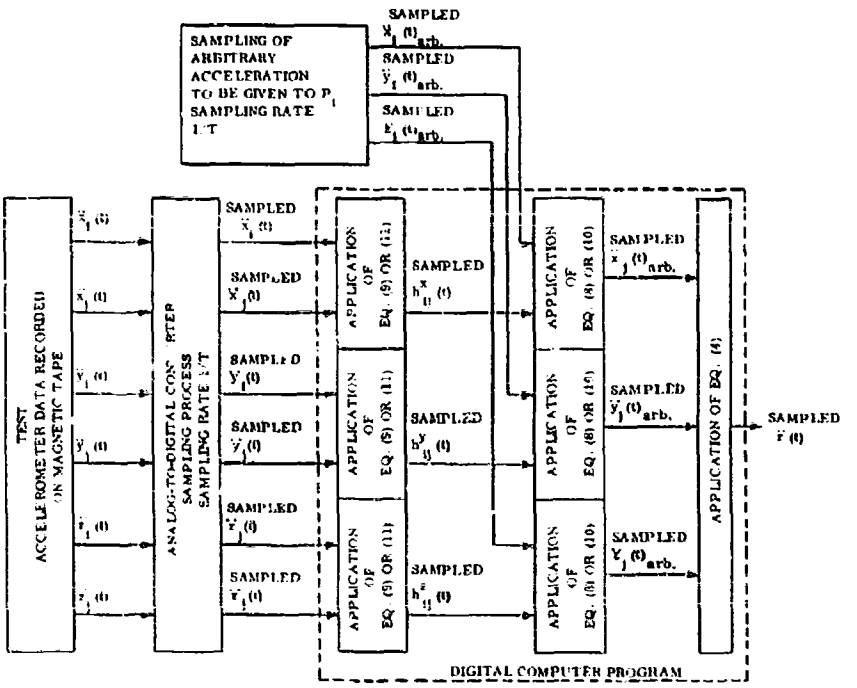

Fig. 5. Procedure for processing accelerometer data

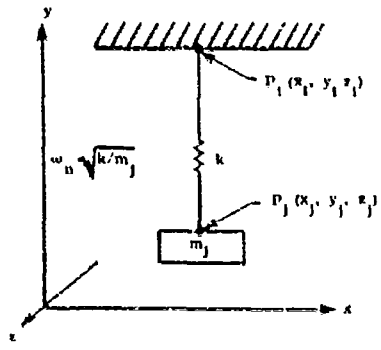

Fig. 6. Simple oscillator of example problem

The samples of $\ddot{y}_j(t)$ are

$$\ddot{y}_j(0) = 1 - \cos 0 ,$$

$$\ddot{y}_j(T) = 1 - \cos (4000\pi \times 1 \times 2.5 \times 10^{-5}) ,$$

$$\vdots$$

$$\ddot{y}_j(NT) = 1 - \cos (4000\pi \times 20 \times 2.5 \times 10^{-5})$$

The samples for the 100 kHz case are similar except that $T = 10^{-5}$ and $N = 50$. Equation (9) was applied to the samples in both cases. The results of the calculations are shown in Fig. 7 with the sample points connected to form a continuous function. Figure 7 also includes the exact impulse response which can be shown to be

$$h_{ij}(t) = (4000\pi \sin 4000\pi t)\, g$$

The next part of the problem is to find the response over a period of 0.5 ms of mass m_j caused by giving the base the acceleration

$$\ddot{y}_i(t) = (\sin 4000\pi t)\, g .$$

This was done by applying Eq. (8) using the 40 kHz sampled unit impulse response calculated in the previous part with the following 40 kHz samples of $\ddot{y}_i(t)$:

$$\ddot{y}_i(0) = \sin (4000\pi \times 0) ,$$

$$\ddot{y}_i(T) = \sin (4000\pi \times 1 \times 2.5 \times 10^{-5}) ,$$

$$\vdots$$

$$\ddot{y}_i(NT) = \sin (4000\pi \times 20 \times 2.5 \times 10^{-5}) .$$

Similar calculations were made for the 100 kHz case. The results of the calculations are shown in Fig. 8. Figure 8 also includes the exact response which can be shown to be

$$\ddot{y}_j(t) = \frac{1}{2} (\sin 4000\pi t - 4000\pi t \cos 4000\pi t)\, g .$$

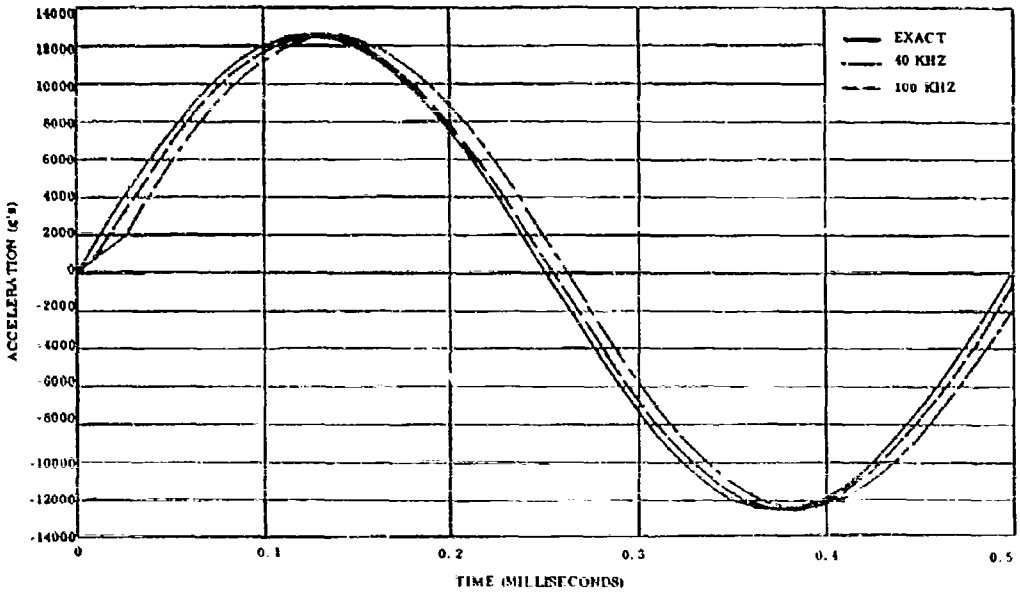

Fig. 7. Comparison of exact and matrix calculated unit impulse responses

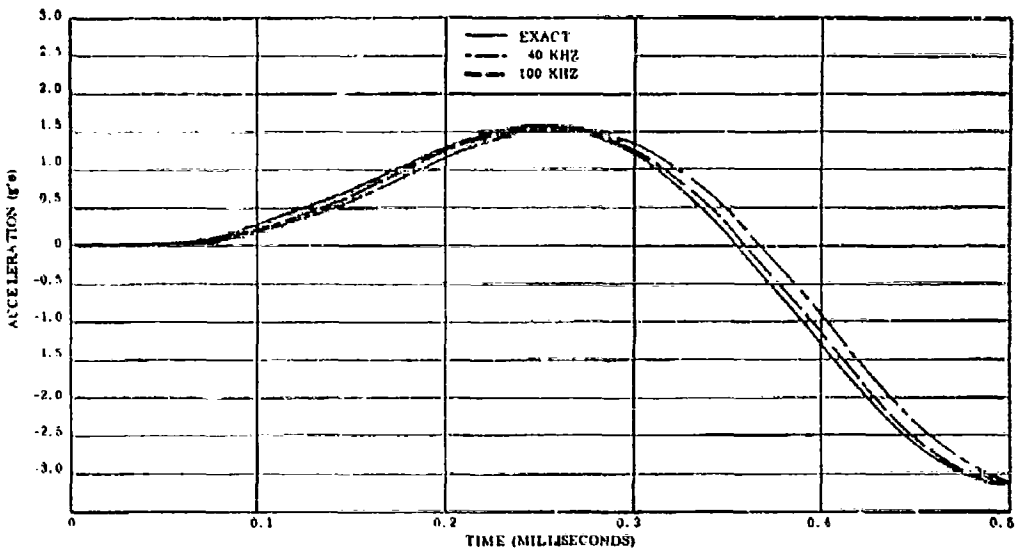

Fig. 8. Comparison of exact and matrix-calculated sin 4000 t responses

An inspection of Figs. 7 and 8 reveals the following interesting facts:

1. The 100 kHz solutions agree more closely with the exact solutions than do the 40 kHz solutions. This was to be expected because of the smaller sampling time increment associated with 100 kHz sampling.

2. The peak values of both the 40 kHz and 100 kHz solutions agree very closely with the peak values of the exact solution.

Also observe in Fig. 7 the noncontinuous nature of the matrix-calculated impulse responses between $t = 0$ and the first sample time. This kink occurs because the solution is exact at $t = 0$ but approximate elsewhere.

ACKNOWLEDGMENTS

The author is indebted to L. E. Chaump and B. F. Price for their helpful suggestions and kind encouragement.

BIBLIOGRAPHY

Thomson, W. T., Vibration Theory and Applications (Prentice Hall, Inc., Englewood Cliffs, N.J.), 1965

Van Valkenburg, M. E., Network Analysis (2nd ed.) (Prentice Hall, Inc., Englewood Cliffs, N.J.), 1965

Wylie, C. R., Advanced Engineering Mathematics (2nd ed.) (McGraw Hill, New York), 1960

Appendix

DEVELOPMENT OF EQUATIONS (3), (13), (14), AND (15)

A three-dimensional mechanical system situated in a rectangular coordinate system can be represented by three independent unidirectional systems, one in the direction of each axis. This is because a spring or dashpot that is oriented at an angle to the axes of the system

can be equivalently represented by three springs or dashpots, each parallel to one of the axes of the coordinate system. This can be shown for a spring by resolving the force exerted by a stretched spring into its components along each axis. The component force along any axis will be equal to that exerted by an identical spring (same spring constant as original) stretched a distance along that axis equal to the component of the elongation of the original spring along that axis. A similar argument applies for dashpots. The developments of Eqs. (3), (13), (14), and (15) will be presented for the component system parallel to the x axis only. Identical arguments apply for the component systems parallel to the other two axes.

The equations of motion for the x component of a lumped linear system can be written in general as

$$
\begin{aligned}
&a_{11}\ddot{\bar{x}}_1 + a_{12}\ddot{\bar{x}}_2 + \cdots + a_{1L}\ddot{\bar{x}}_L + \beta_{11}\dot{x}_1 + \beta_{12}\dot{x}_2 + \cdots \\
&\quad + \beta_{1L}\dot{x}_L + \gamma_{11}\Delta x_1 + \gamma_{12}\Delta x_2 + \cdots + \gamma_{1L}\Delta x_L = \Phi_1^x(t), \\
&a_{21}\ddot{\bar{x}}_1 + a_{22}\ddot{\bar{x}}_2 + \cdots + a_{2L}\ddot{\bar{x}}_L + \beta_{21}\dot{x}_1 + \beta_{22}\dot{x}_2 + \\
&\quad + \beta_{2L}\dot{x}_L + \gamma_{21}\Delta x_1 + \gamma_{22}\Delta x_2 + \cdots + \gamma_{2L}\Delta x_L = \Phi_2^x(t), \\
&\qquad \cdots \qquad \cdots \qquad \cdots \\
&a_{L1}\ddot{\bar{x}}_1 + a_{L2}\ddot{\bar{x}}_2 + \cdots + a_{LL}\ddot{\bar{x}}_L + \beta_{L1}\dot{x}_1 + \beta_{L2}\dot{x}_2 + \cdots \\
&\quad + \beta_{LL}\dot{x}_L + \gamma_{L1}\Delta x_1 + \gamma_{L2}\Delta x_2 + \cdots + \gamma_{LL}\Delta x_L = \Phi_L^x(t)
\end{aligned}
\tag{A-1}
$$

where the a_{pq}'s are constants depending on the masses of the system, the β_{pq}'s are constants depending on the damping coefficients of the system, the γ_{pq}'s are constants depending on the spring constants of the system, and L is the total number of masses in the system. The function $\Phi_p^x(t)$ is the x component of the force applied to mass number p; and $\ddot{\bar{x}}_q(t)$, $\dot{x}_q(t)$, and $\Delta x_q(t)$ are the acceleration, velocity, and displacement from equilibrium respectively of mass number q.

Taking the Laplace transform with respect to $\ddot{\bar{x}}_q(t)$ of both sides of Eq. (A-1), and assuming that the system is initially at rest in its equilibrium position, we get

$$
\begin{aligned}
&(a_{11} + \beta_{11}s + \gamma_{11}s^2)\bar{X}_1(s) + (a_{12} + \beta_{12}s + \gamma_{12}s^2)\bar{X}_2(s) \\
&\quad + \cdots + (a_{1L} + \beta_{1L}s + \gamma_{1L}s^2)\bar{X}_L(s) = \Phi_1^x(s), \\
&(a_{21} + \beta_{21}s + \gamma_{21}s^2)\bar{X}_1(s) + (a_{22} + \beta_{22}s + \gamma_{22}s^2)\bar{X}_2(s) \\
&\quad + \cdots + (a_{2L} + \beta_{2L}s + \gamma_{2L}s^2)\bar{X}_L(s) = \Phi_2^x(s), \\
&\qquad \cdots \qquad \cdots \qquad \cdots
\end{aligned}
\tag{A-2 (Cont.)}
$$

$$
\begin{aligned}
&(a_{L1} + \beta_{L1}s + \gamma_{L1}s^2)\bar{X}_1(s) + (a_{L2} + \beta_{L2}s + \gamma_{L2}s^2)\bar{X}_2(s) \\
&\quad + \cdots + (a_{LL} + \beta_{LL}s + \gamma_{LL}s^2)\bar{X}_L(s) = \Phi_L^x(s)
\end{aligned}
\tag{A-2}
$$

where $\bar{X}_q(s)$ is the Laplace transform of $\ddot{\bar{x}}_q(t)$ and $\Phi_p^x(s)$ is the Laplace transform of $\Phi_p^x(t)$. These equations can be written in matrix notation as

$$
\begin{bmatrix}
a_{11}(s) & a_{12}(s) & \cdots & a_{1L}(s) \\
a_{21}(s) & a_{22}(s) & \cdots & a_{2L}(s) \\
\vdots & \vdots & & \vdots \\
a_{L1}(s) & a_{L2}(s) & \cdots & a_{LL}(s)
\end{bmatrix}
\begin{Bmatrix}
\bar{X}_1(s) \\ \bar{X}_2(s) \\ \vdots \\ \bar{X}_L(s)
\end{Bmatrix}
=
\begin{Bmatrix}
\Phi_1^x(s) \\ \Phi_2^x(s) \\ \vdots \\ \Phi_L^x(s)
\end{Bmatrix}
\tag{A-3}
$$

where

$$
a_{pq}(s) = a_{pq} + \beta_{pq}s + \gamma_{pq}s^2 .
$$

Solving by Cramer's rule for the acceleration transform of mass number j $(q = j)$, we get

$$
\bar{X}_j(s) = D_j(s)/D(s) \tag{A-4}
$$

where $D_j(s)$ is the determinant of the matrix formed by replacing the jth column of the $a_{pq}(s)$ matrix by the column of $\Phi_p^x(s)$, and $D(s)$ is the determinant of the $a_{pq}(s)$ matrix. The numerator of Eq. (A-4) can be expanded by cofactors. Equation (A-4) can then be written

$$
\begin{aligned}
\bar{X}_j(s) = {} & [d_{1j}(s)/D(s)]\Phi_1^x(s) + [d_{2j}(s)/D(s)]\Phi_2^x(s) \\
& + \cdots + [d_{Lj}(s)/D(s)]\Phi_L^x(s)
\end{aligned}
\tag{A-5}
$$

where $d_{pj}(s)$, a cofactor of $D_j(s)$, is the determinant formed by crossing out the pth row and jth column of $D_j(s)$ and multiplying by $(-1)^{p+j}$. Similarly, for the acceleration transform of mass number i, we can write

$$
\begin{aligned}
\bar{X}_i(s) = {} & [d_{1i}(s)/D(s)]\Phi_1^x(s) + [d_{2i}(s)/D(s)]\Phi_2^x(s) \\
& + \cdots + [d_{Li}(s)/D(s)]\Phi_L^x(s)
\end{aligned}
\tag{A-6}
$$

If all forces except $\Phi_j(t)$ are zero, then Eqs. (A-5) and (A-6) reduce to

$$
\bar{X}_j(s) = [d_{1j}(s)/D(s)]\Phi_j^x(s) \tag{A-7}
$$

and

$$
\bar{X}_i(s) = [d_{1i}(s)/D(s)]\Phi_j^x(s) \tag{A-8}
$$

Dividing Eq. (A-7) by Eq. (A-8) and rearranging, we get

$$\ddot{X}_j(s) = d_{jj}(s) d_{ii}(s) \ddot{X}_i(s) - H^{x}_{ij}(s) \ddot{X}_i(s) \qquad \text{(A-9)}$$

where $H^{x}_{ij}(s)$ is the transfer function of the x component of the system. Note that $H^{x}_{ij}(s)$ is dependent only on the physical parameters of the system, but the particular $H^{x}_{ij}(s)$ used is dependent upon the mass numbers i and j.

If $\ddot{X}_i(s)$ is the transform of a unit impulse it is equal to unity. The function $H^{x}_{ij}(s)$ is then the transform of the response acceleration, and its inverse is the unit impulse response $h^{x}_{ij}(t)$.

From the Laplace transform theory, the inverse transform of the product of two transforms is the inverse of one convolved with the inverse of the other. Therefore, the inverse transform of Eq. (A-9) is

$$\ddot{x}_j(t) = \ddot{x}_i(t) * h^{x}_{ij}(t) \qquad \text{(A-10)}$$

which is Eq. (3a).

Velocities can be related by dividing both sides of Eq. (A-9) by s which is equivalent to an integration in the time domain if the system is initially at rest in its equilibrium position. This results in

$$\dot{X}_j(s) = H^{x}_{ij}(s) \dot{X}_i(s) \qquad \text{(A-11)}$$

and

$$\dot{x}_j(t) = \dot{x}_i(t) * h^{x}_{ij}(t) \qquad \text{(A-12)}$$

which is Eq. (13a). Similarly, dividing Eq. (A-9) by s^2 and convolving, we get

$$x_j(t) = x_i(t) * h^{x}_{ij}(t) \qquad \text{(A-13)}$$

which is Eq. (14a).

Equation (A-7) can also be written in the time domain. If we let the inverse transform of $d_{ij}(s)\, D(s)$ be $g^{x}_{ij}(t)$, we can then write

$$\ddot{x}_j(t) = \ddot{g}^{x}_{i}(t) * g^{x}_{ij}(t) \qquad \text{(A-14)}$$

which is Eq. (15a). The superposition property associated with Eq. (A-14) can be seen by inspection of Eq. (A-5).

* * *

A MOMENT TECHNIQUE FOR SYSTEM PARAMETER IDENTIFICATION*

F. Kozin and C. H. Kozin
Midwest Applied Science Corporation
West Lafayette, Indiana

The objective of this study was the development of a practical computational technique for the identification of linear constant coefficient systems, based upon the system output when subjected to random or sinusoidal excitation.

INTRODUCTION

The purpose of this study was the analytical development and digital simulation experiences of a parameter estimation technique that appears to be of superior practical significance for the identification of real systems.

The technique is simply based upon the properties of statistical expectations and time averages and can be applied to nonlinear as well as linear systems. The physical situation that one often encounters is that a dynamical model of the system, through differential equations, is given, but the various physical parameters, in particular, the mass, spring, and damping factors are unknown. To obtain a complete useful model of the system it is necessary that these parameters be known. The technique presented in this report requires knowledge of the dynamics of the system, that is, the displacements, velocities, and accelerations, as well as the input data. From these data all unknown parameters can be determined by forming various moments, or time averages, of the input and the dynamical output variables of the system. The resulting linear equations in the unknown parameters are then solved to yield the desired estimates. A theoretical study of the technique was accomplished for linear systems in both the random and deterministic input case. These results appear in "Theoretical Development," which follows. This theoretical study greatly clarifies the role of such parameters as the length of time over which the system is to be observed and the nature of the spectrum of the excitation, as well as the role of the steady-state dynamics of the system in effecting a usable identification scheme.

When the mass is known, only the displacements and velocities are required to determine the estimates of the spring and damping constants.

The technique is applied to study digitally simulated models of one-dimensional linear systems with 5 degrees of freedom. The parameters for simulation are taken as those of the NASA (Goddard Space Flight Center) five-mass system. The simulated model is subjected to various random as well as sinusoidal excitations. The estimated parameters are found to agree with the actual parameters up to four- and five-place accuracy. An even more significant feature is that the actual system-simulated parameters have a spread of five or six orders of magnitude between the mass and the spring constant. A major problem in parameter search techniques is to determine the range of parameter values. For the present technique this presents no problem as can be seen by the extremely accurate estimated parameter values.

A completely detailed program for simulation and estimation of parameters has been

*This work was supported by Contract No. NAS5-[illegible], National Aeronautics and Space Administration, Goddard Space Flight Center.

developed for linear, chain-like mass-spring-dashpot systems with arbitrary degrees of freedom and an arbitrary number of force inputs to the system. This appears in "Theoretical Development."

The technique was also applied to a simulated two-dimensional system of masses, springs, and dashpots supplied to us by J. Young and F. Ono of NASA. Again, parameter estimation was truly outstanding.

It can safely be stated at this point that when displacement, velocity, and acceleration data are available, system identification can be accomplished quite satisfactorily by our method.

It was hoped that actual data taken from vibration tests on the NASA five-mass system could have been analyzed to estimate the real system parameters. However, the tests yielded only acceleration data. Integration of this data was attempted to yield an estimate of the velocities and displacements of the five masses. A least-squares trend was removed to account for the initial conditions of the velocities and displacements being unknown at the point at which the acceleration record commences. Because of the numerical inaccuracies present when integrating and removing trends twice, satisfactory estimates were not obtainable from the real system data during the contract period. (This is, in part, because of the time required to put the vibration data on tape and then digitize it in a form suitable for computation. This was all accomplished by NASA.) However, we do not hesitate to add that this is merely a numerical problem of simulation that can be resolved with relatively simple investigations and we present a first step in this direction in the present report, by integrating the acceleration once and identifying two parameters of a damped oscillator. Thus, we can say in summary that:

1. A method has been proposed for identification of linear and nonlinear constant coefficient systems, by random or sinusoidal excitations, as discussed in "Parameter Estimation" (not included in this paper).

2. The method is studied here for linear systems, subjected to random or sinusoidal excitations.

3. The theoretical studies have generated a rather broad understanding of the method, as presented in "Theoretical Development."

4. The method yields extremely accurate parameter identification for rather complex systems, as presented in "Identification of Simulated Linear Dynamical Systems" (not included in this paper).

5. A complete discussion of the simulation techniques as well as the program details are presented in "Computer Simulation and Identification" (not included in this paper).

6. Suggestions for future investigations are presented in "Summary and Conclusions" (not included in this paper).

PARAMETER IDENTIFICATION

The problem of identification of a system or of a process is now recognized as a basic part of modern engineering techniques. It is clear that to design and control, in any optimal fashion, we must identify. Thus, the subject of identification has been actively studied in the past decade, and will continue to develop both theoretically and practically as engineers continue to expand technology.

Primarily motivated by the desire for adaptive and optimal control of systems and processes, identification problems in engineering have been most actively pursued by electrical engineers in the past 10 to 15 years. Thus, the ideas of cross correlations and cross-spectral densities for estimating the impulse response function or the frequency response function have been generated by them. Furthermore, electrical engineers and optimal control engineers have been forward in their efforts to apply parameter estimation schemes for identification purposes.

Vibrations engineers have, to a large extent, remained with the classical technique of driving a structural system by sinusoidal excitations at various frequencies to determine the frequency response characteristics of structural systems. Parameter estimation ideas have not as yet permeated the bag of tricks that structural vibrations engineers can use freely in determining models of structural systems, although new techniques based upon second-order statistics, mean-square approximations, or energy techniques are beginning to change that picture somewhat.

The purpose of this report is to present a parameter identification technique. As indicated above, there is certainly no lack of parameter identification techniques in the literature. However, the technique that is presented in the present report possesses a few noteworthy features.

First, the technique is simple to comprehend and apply. Second, the same theoretical concept applies to both random or sinusoidal -- indeed, even sweep sinusoidal -- excitations. Third, it appears that the technique can be extended to the nonlinear systems with unknown parameters as the basic theory would remain unchanged. Fourth, the technique does not appear to be affected by wide ranges of the parameter values that often plague optimum parameter search techniques. Finally, in simulation studies the technique has produced highly accurate parameter estimates for reasonably complex systems.

Thus, it appears that the identification technique proposed in this report holds promise of being of practical significance for identification of arbitrary systems with unknown constant parameters.

This report, the result of a 1-year investigation that was limited to the study of linear systems, presents a theoretical development of the idea, estimates of parameters of simulated five-mass chain-like systems, a two-mass two-dimensional system, and other systems. These systems as well as the actual parameters were supplied by J. Young and F. Ohi of NASA. In each case, the mass, spring, and damping constants are estimated from the digitally simulated system subjected to random and sinusoidal inputs. It should be noted that the mass and spring constants are six orders of magnitude apart in their values, and yet each is estimated with very high accuracy. In addition, a single sinusoidal excitation at what appears to be any arbitrary frequency will yield the entire identification of the system parameters. Thus, one does not have to excite the system at a multitude of frequencies, or in some frequency band-width as has been employed by previous investigations.

The description of the digital simulation techniques and the program for simulation and identification are also presented.

One point must be made concerning the identification of systems by parameter estimation techniques: The methods that have been developed and the method we describe in this report will identify the analytical or simulated model of the actual physical system. Therefore, if the analytical model is not a satisfactory equivalent or approximation to the system, then clearly, one is not identifying the real system. Any analytical model identification scheme (such as parameter estimation) is only as good as the model that will be used to describe the physical system. (We note that identification schemes can sometimes be used to help provide a better system model. However, we will not dwell on that point here.)

With this understanding of the proper role of identification by parameter estimation, we can now proceed to describe our approach.

THEORETICAL DEVELOPMENT

General

The basic assumptions in this discussion are that a linear time invariant system is being driven by some excitation, either random or deterministic. Although the system may be quite general, it serves our purposes to think of the system as being composed of a number of masses connected to one another by linear springs and linear dashpots. We further assume that each mass may be driven by a separate excitation and that the accelerations, velocities, and displacements of each mass, as well as the various excitations, may be noiselessly observed, or at least, obtainable by suitable means. We point out that this rules out white noise as an input for reasons discussed below.

We assume that the various displacements, velocities, and accelerations of the masses are related to the excitations by a system of linear differential equations of known form and order but with unknown mass, spring, and damping parameters.

In general, our systems have the character of those given in Fig. 1. Figure 1(a) shows a one-dimensional, chain-like system; Fig. 1 (b) shows a two-dimensional system.

In either case the form of the linear differential equation that governs the dynamics of these systems is

$$\dot{y}(t) = Ay(t) + F(t) \qquad (1)$$

where the y vector is the vector of all the states of system. That is, its components are the displacements and velocities of the masses, the A matrix is a constant matrix made up of the various spring and damping constants, and the F vector is the excitation vector.

We have assumed all mass and inertia constants to be unity in the general equation of Eq. (1). These constants will enter explicitly in the specific classes of systems we study below.

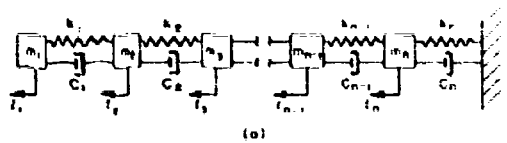

a. Chain-like, one-dimensional system

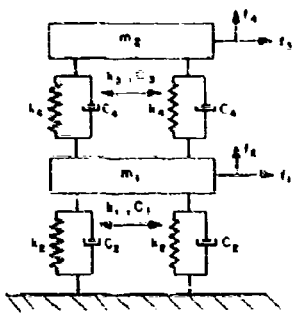

b. Two-dimensional system

Fig. 1. Linear time invariant systems

Thus,

$$y(t) = \begin{pmatrix} y_1(t) \\ \vdots \\ y_n(t) \end{pmatrix} \quad F = \begin{pmatrix} f_1(t) \\ \vdots \\ f_n(t) \end{pmatrix} \quad A = \begin{pmatrix} a_{11} & \cdots & a_{1n} \\ \vdots & & \vdots \\ a_{n1} & & a_{nn} \end{pmatrix} \tag{2}$$

for the vectors and matrix defining the system.

In our development below we shall be concerned with both steady state oscillations and transient oscillations. Naturally, we assume the system to be stable so that the steady state oscillation exists.

Random Excitations

Let us assume that the components $f_i(t)$, $i = 1, \ldots, n$ of the $f(t)$ excitation vector are stationary random processes possessing as many moments as may be required by our analysis. (In general, for linear systems only second moment properties will be required.) We will further assume that the excitation processes are smooth enough to guarantee that all the derivatives $\dot{y}_i(t)$ exist. (The reader may recall that this is not the case if the excitation is a Gaussian White noise with Dirac "Delta" function for its covariance.)

We can immediately write a general solution to the A matrix for the linear system of Eq. (1) as follows. Equation (1) is multiplied by the transpose vector $y'(t)$ and expectations of the resulting equation are taken to yield

$$E\{\dot{y}(t)\, y'(t)\} = A\,E\{y(t)\, y'(t)\} + E\{f(t)\, y'(t)\}. \tag{3}$$

Equation (3) can be solved for the matrix A as,

$$\left[E\{\dot{y}(t)\, y'(t)\} - E\{f(t)\, y'(t)\}\right]\left[E\{y(t)\, y'(t)\}\right]^{-1} = A \tag{3a}$$

assuming that the inverse matrix

$$E\{y(t)\, y'(t)\}^{-1} \tag{4}$$

exists.

The relation of Eq. (3a) presents a general solution of the identification of A for linear systems of the form of Eq. (1), if Eq. (4) exists. The existence of this inverse is guaranteed if there is no linear relationship among the components of the $y(t)$ vector, because the covariance matrix $E\{y(t)\, y'(t)\}$ is symmetric and nonnegative definite. The nonnegative definitives follow from the fact that

$$E\left\{\left[\sum_{i=1}^{n} a_i\, y_i(t)\right]^2\right\} \geq 0 \tag{5}$$

for any constants $(a_1, \ldots, a_n)$. Furthermore, the equality sign in Eq. (5) can hold only if there exists a linear relationship among the components of $y(t)$. Thus, Eq. (4) exists and the constant matrix A is solvable as given in Eq. (3a) on the basis of observations of the y, f vectors.

This is somewhat more general than we wish to consider, as the estimation of the various moments in Eq. (3a), as well as the inverse matrix, especially in the transient situation where the moments are functions of t, are difficult to estimate. Therefore, to proceed with our development let us assume that the transients have, for all practical purposes, died out and the system is operating in the steady state. It is known that the y-process is a statistically stationary process in that case and all the moments present in Eq. (3a) are constant.

Moreover, they can be estimated simply by taking time averages over discrete or continuous values of the time parameter.

It follows, then, in the stationary case, that

$$E\{y_i^r(t)\} = E\{y_i^r(t)\, y_j^s(t)\} \qquad r, s = 0, 1, 2, \ldots \tag{6}$$

exist and are constant in time. Hence,

$$\frac{d}{dt} E\{y_i^r(t)\} = 0$$
$$\frac{d}{dt} E\{y_i^r(t)\, y_j^s(t)\} = 0 \tag{7}$$

for $r = j$ and $r = s$, as above.

We now specify that the y-process is a stationary, mean-square differentiable process. Such processes are generated, for example, by passing a stationary mean-square continuous process (that is, a process with continuous covariance function) through a time invariant linear filter. Accordingly, if the excitation process f is mean-square continuous, we are assured that the stationary y-process is mean-square continuous. It is because of the desired differentiability properties of the y-process that we are ruling out the white-noise type excitations in the random case.

Now as a result of the mean-square differentiability of the y-process the derivative operator in (7) can be taken into the expectation operator to give

$$E\{y_i^{r-1}(t)\, \dot{y}_i(t)\} = 0 \tag{8}$$

$$rE\{y_i^{r-1}(t)\, \dot{y}_i(t)\, y_j^s(t)\} + sE\{y_i^r(t)\, y_j^{s-1}(t)\, \dot{y}_j(t)\} = 0 \tag{9}$$

In particular, it follows that for $r = 2$ in Eq. (8) and $r = s = 1$ in Eq. (9) we obtain

$$E\{y_i(t)\, \dot{y}_i(t)\} = 0 \tag{10}$$

$$E\{y_i(t)\, \dot{y}_j(t)\} + E\{\dot{y}_i(t)\, y_j(t)\} = 0 \tag{11}$$

The first inequality in Eqs. (10) and (11) states the well-known fact that a stationary process and its derivative are uncorrelated at any given time. We repeat that Eqs. (10) and (11) do not hold if the excitation process is a white noise.

On the basis of Eqs. (8) through (11) the identification of the parameter matrix A as given by Eq. (3) reduces greatly in the stationary case. We illustrate these ideas by a few very simple analytical examples.

Example 1 – Consider the system

$$\dot{y}(t) + a y(t) = f(t) \tag{12}$$

Upon multiplying Eq. (12) by $y(t)$ and taking expectations, we find

$$E\{y(t)\, \dot{y}(t)\} + a E\{y^2(t)\} = E\{f(t)\, y(t)\} \tag{13}$$

However, from Eq. (10) it follows that

$$a = \frac{E\{f(t)\, y(t)\}}{E\{y^2(t)\}} \tag{14}$$

For our estimate of a, therefore, one merely estimates the moments that appear in Eq. (14).

Example 2 – We consider here the somewhat more complex system of coupled oscillators as shown in Fig. 2.

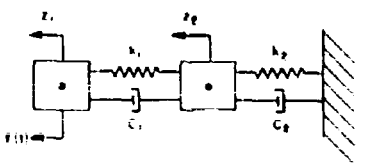

Fig. 2. Complex system of coupled oscillators

Assuming the masses to be unity, we may write the equations of the system as

$$\ddot{z}_1(t) + C_1[\dot{z}_1(t) - \dot{z}_2(t)] + k_1[z_1(t) - z_2(t)] = f(t)$$

$$\ddot{z}_2(t) + C_2 \dot{z}_2(t) + k_2 z_2(t) - C_1[\dot{z}_1(t) - \dot{z}_2(t)] - k_1[z_1(t) - z_2(t)] = 0 \tag{15}$$

Upon setting

$$\begin{pmatrix} z_1 \\ \dot{z}_1 \\ z_2 \\ \dot{z}_2 \end{pmatrix} = \begin{pmatrix} y_1 \\ y_2 \\ y_3 \\ y_4 \end{pmatrix} \tag{16}$$

we may rewrite Eq. (15) as the system

$$\dot{y}_1(t) = y_2(t)$$

$$\dot{y}_2(t) = -C_1[y_2(t) - y_4(t)] - k_1[y_1(t) - y_3(t)] + f(t) \tag{17}$$

(Cont.)

$$\dot{y}_3(t) = y_4(t)$$

$$\dot{y}_4(t) = -C_2 y_4(t) - k_2 y_3(t) + C_1 [y_2(t) - y_4(t)] \quad (17)$$
$$+ k_1 [y_1(t) - y_3(t)]$$

The second equation in Eq. (17) is multiplied by y_1, y_2, and then averaged. The fourth equation in Eq. (17) is multiplied by y_3, y_4, and averaged. On the basis of Eqs. (10) and (11) it will follow that

$$\begin{aligned}
E\{y_2^2\} + E\{fy_1\} &= -C_1 E\{y_1 y_4\} \\
&\quad + k_1 \left(E\{y_1^2\} - E\{y_2 y_3\}\right) \\
E\{fy_2\} &= C_1\left(E\{y_2^2\} - E\{y_4 y_4\}\right) - k_1 E\{y_2 y_3\} \\
-E\{y_4^2\} &= -k_2 E\{y_3^2\} + C_1 E\{y_2 y_3\} \qquad (18) \\
&\quad + k_1 \left(E\{y_1 y_3\} - E\{y_3^2\}\right) \\
0 &= -C_2 E\{y_4^2\} + C_1 \left(E\{y_3 y_4\}\right. \\
&\quad \left. - E\{y_4^2\}\right) + k_1 E\{y_1 y_4\}
\end{aligned}$$

The set of four linear algebraic equations in Eq. (18), in the four unknowns is easily solved to determine the parameters C_1, k_1, C_2, and k_2. For example,

$$C_1 = \frac{\begin{vmatrix} E\{y_2^2\} + E\{fy_1\} & E\{y_1^2\} - E\{y_1 y_3\} \\ E\{fy_2\} & -E\{y_2 y_3\} \end{vmatrix}}{B}$$

$$k_1 = \frac{\begin{vmatrix} -E\{y_2 y_4\} & E\{y_2^2\} + E\{fy_1\} \\ E\{y_2^2\} - E\{y_2 y_4\} & E\{fy_2\} \end{vmatrix}}{B} \qquad (19)$$

where

$$B = \begin{vmatrix} -E\{y_1 y_4\} & E\{y_1^2\} - E\{y_1 y_3\} \\ E\{y_2^2\} - E\{y_2 y_4\} & -E\{y_2 y_3\} \end{vmatrix}.$$

Similar equations yield C_2, k_2 as well.

For the case of unknown mass, spring, and damping constants one must obtain one more set of moment equations to obtain a solvable set of linear simultaneous equations. We illustrate the problems that may occur in the proper choice of the third moment equation by the following simple oscillator.

Let us consider the case of the system given by

$$m\ddot{y}(t) + C\dot{y}(t) + ky(t) = f(t) \qquad (20)$$

where m, C, k are all unknown.

Upon multiplying Eq. (20) by $y, \dot{y}$ and taking expectations we obtain equations analogous to those in our previous examples, as,

$$\begin{aligned}
m E(y\ddot{y}) + C E(y\dot{y}) + k E(y^2) &= E(fy) \\
m E(\dot{y}\ddot{y}) + C E(\dot{y}^2) + k E(y\dot{y}) &= E(f\dot{y})
\end{aligned} \qquad (21)$$

By Eq. (10) we can reduce these equations to yield

$$-m E(\dot{y}^2) + k E(y^2) = E(fy) \qquad (22a)$$

$$C E(\dot{y}^2) = E(f\dot{y}). \qquad (22b)$$

However, we require one more equation. One might consider multiplying Eq. (20) by y^2, for example, and then take expectations to yield

$$m E(y^2\ddot{y}) + C E(y^2\dot{y}) + k E(y^3) = E(fy^2) \qquad (23)$$

where, by Eq. (10) it follows that $E(y^2\dot{y})$ is identically zero.

But, generally, in practice the excitation function will be a zero mean Gaussian random process. Hence, $y, \dot{y}, \ddot{y}$ are all Gaussian processes; each is a linear operator of the input process f.

Then, specifically, one has

$$y(t) = \int_{-\infty}^{t} H(t-\tau)\, f(\tau)\, d\tau$$

$$\dot{y}(t) = \int_{-\infty}^{t} \dot{H}(t-\tau)\, f(\tau)\, d\tau \qquad (24)$$

$$\ddot{y}(t) = -\frac{1}{m}\int_{-\infty}^{t} [CH(t-\tau) + kH(t-\tau)]\, f(\tau)\, d\tau + \frac{1}{m} f(t)$$

and any third-order moment in $y, \dot{y}, \ddot{y}$ will involve moments of the form

$$E\{f(t_1)\, f(t_2)\, f(t_3)\} \qquad (25)$$

However, it is a well-known fact that all third-order moments of a Gaussian process

are identically zero. Indeed, all odd-order moments of a Gaussian process are zero so that Eq. (23) cannot yield any new information as all its terms are zero.

Hence, if we cannot apply odd-order moments to yield our third equations, the next question is: What about even moments? Here, we get into trouble of a different nature, as we now demonstrate. For example, let us choose

$$m E(y^3\ddot{y}) + C E(y^3\dot{y}) + E(y^4) = E(fy^3) \qquad (26)$$

as our third equation. Again the term $E(y^3\ddot{y})$ is zero. It is well known that the even product moments of zero-mean, jointly distributed Gaussian random variables can be evaluated in terms of the second moments. In particular for X_1, X_2, X_3, X_4, jointly Gaussian, one has

$$E(X_1X_2X_3X_4) = E(X_1X_2)\,E(X_3X_4) + E(X_1X_3)\,E(X_2X_4) + E(X_1X_4)\,E(X_2X_3) \qquad (27)$$

If we apply the identity of Eq. (27) to the terms of Eq. (26) we obtain

$$E(y^3\ddot{y}) = 3E(y^2)\,E(y\ddot{y})$$
$$E(y^4) = 3\left(E(y^2)\right)^2 \qquad (28)$$
$$E(fy^3) = 3E(y^2)\,E(yf).$$

Therefore, Eq. (26) may be written as

$$3m\,E(y^2)\,E(y\ddot{y}) + 3k\left(E(y^2)\right)^2 = 3\,E(y^2)\,E(yf). \qquad (29)$$

We immediately recognize that Eq. (29) is Eq. (22a) multiplied by the factor $3E(y^2)$. So, Eq. (26) yields no new information. Again, if one chooses any even moment equation, it will always reduce to a linear combination of Eqs. (22a) and (22b) for the zero-mean Gaussian case.

Because, in practice, noise generators yield Gaussian or near Gaussian processes, it will not be possible to identify the three unknowns on the basis of moments obtained from Eq. (20) by multiplying by powers of $y, \dot{y}$ and averaging. We hasten to add that if the noise process used for excitation is definitely non-Gaussian then one can establish moments of the nature of those we have described. How then are we to obtain a third condition for evaluating the unknown parameters? The most obvious choice is to use the acceleration variable. This is quite practical because, in general, it is the acceleration data that are actually obtained from experimental tests.

Therefore, we can multiply Eq. (20) by $\ddot{y}$ and take expectations giving us our third, and independent, equation.

$$m E(\ddot{y}^2) + C E(y\ddot{y}) + k E(y\ddot{y}) = E(x\ddot{y}) \qquad (30)$$

Finally, then, the system of linear equations available for parameter identification is given as

$$\begin{aligned} -m E(\dot{y}^2) + k E(y^2) &= E(xy) \\ C E(\dot{y}^2) - E(x\dot{y}) &= \\ m E(\ddot{y}^2) - k E(\dot{y}^2) &= E(x\ddot{y}) \end{aligned} \qquad (31)$$

To identify linear systems by random excitations, we shall construct moment equations by multiplying the coupled equations by the displacement, the velocity, and then the acceleration. We illustrate this for the general one-dimensional chain-like system as shown in Fig. 1(a).

Denoting the displacement, velocity, and acceleration of the ith mass by $x_i, \dot{x}_i, \ddot{x}_i$, the equations of motion for N masses in the chain are

$$\begin{aligned} m_1\ddot{x}_1 &= f_1 - C_1(\dot{x}_1 - \dot{x}_2) - k_1(x_1 - x_2) \\ m_2\ddot{x}_2 &= f_2 - C_2(\dot{x}_2 - \dot{x}_3) - k_2(x_2 - x_3) \\ &\quad + C_1(\dot{x}_1 - \dot{x}_2) + k_1(x_1 - x_2) \\ &\vdots \\ m_N\ddot{x}_N &= f_N - C_N\dot{x}_N - k_Nx_N + C_{N-1}(\dot{x}_{N-1} - \dot{x}_N) \\ &\quad + k_{N-1}(x_{N-1} - x_N) \end{aligned} \qquad (32)$$

Upon multiplying the ith equation in Eq. (32) by $x_i, \dot{x}_i, \ddot{x}_i$, respectively, we obtain the following system of parameter identification equations:

$$\left.\begin{aligned} m_1E(x_1\ddot{x}_1) &= E(x_1f_1) - C_1E(x_1(\dot{x}_1 - \dot{x}_2)) \\ &\quad - k_1E(x_1(x_1 - x_2)) \\ m_1E(\dot{x}_1\ddot{x}_1) &= E(\dot{x}_1f_1) - C_1E(\dot{x}_1(\dot{x}_1 - \dot{x}_2)) \\ &\quad - k_1E(\dot{x}_1(x_1 - x_2)) \\ m_1E(\ddot{x}_1^2) &= E(\ddot{x}_1f_1) - C_1E(\ddot{x}_1(\dot{x}_1 - \dot{x}_2)) \\ &\quad - k_1E(\ddot{x}_1(x_1 - x_2)) \end{aligned}\right\} \qquad (33)\ (\text{Cont.})$$

$$
\begin{aligned}
m_2E(\ddot{x}_2\ddot{x}_2) &= E(\ddot{x}_2f_2) - C_2E(\dot{x}_2(\dot{x}_2-\dot{x}_3)) \\
&\quad - k_2E(x_2(\dot{x}_2-\dot{x}_3)) + C_1E(\dot{x}_2(\dot{x}_1-\dot{x}_2)) \\
&\quad + k_1E(x_2(x_1-x_2)) \\
m_2E(\dot{x}_2\ddot{x}_2) &= E(\dot{x}_2f_2) - C_2E(\dot{x}_2(\dot{x}_2-\dot{x}_3)) \\
&\quad - k_2E(x_2(\dot{x}_2-\dot{x}_3)) + C_1E(\dot{x}_2(\dot{x}_1-\dot{x}_2)) \\
&\quad + k_1E(x_2(x_1-x_2)) \\
m_2E(\dot{x}_2^2) &= E(\dot{x}_2f_2) - C_2E(\dot{x}_2(\dot{x}_2-\dot{x}_3)) \\
&\quad - k_2E(x_2(\dot{x}_2-\dot{x}_3)) + C_1E(\dot{x}_2(\dot{x}_1-\dot{x}_2)) \\
&\quad + k_1E(x_2(x_1-x_2))
\end{aligned}
$$

. . . , etc.

Naturally, in the steady-state case we can apply the identities of Eqs. (10) and (11) to further simplify the system of Eqs. (33). It is worth noting that the chain-like nature of the system of Eq. (32) yields a set of parameter estimation equations that can be solved sequentially. In Eq. (33) we can solve for m_1, C_1, and k_1 from the first three equations, then substitute these estimates in the next set of three equations to yield estimates of m_2, C_2, and k_2. This procedure may be continued along the chain.

An obvious question that must be considered concerns the errors that are made when the system is not yet in the stationary state. This is likely to occur when the damping factor, C, is small, relative to the spring constant, k. We can easily illustrate the effects of an error that is made in the estimated value, $E(y\dot{y})$, say, for the simple oscillator.

Let us assume the mass, m, is unity in Eq. (20) for the simple 1-degree-of-freedom oscillator. We assume C, k are unknown.

Then Eqs. (21) yield for estimates

$$
\begin{aligned}
\hat{C} &= \frac{E(\widehat{f\dot{y}}) - kE(\widehat{y\dot{y}}) - E(\widehat{\ddot{y}\dot{y}})}{E(\widehat{\dot{y}^2})} \\
\hat{k} &= \frac{E(\widehat{fy}) - CE(\widehat{y\dot{y}}) - E(\widehat{\dot{y}\dot{y}})}{E(\widehat{y^2})}
\end{aligned}
\qquad (34)
$$

where " $\hat{}$ " denotes estimate.

If k is very large relative to C, then a small error in the estimate of $E(y\dot{y})$ will create a large error in $\hat{C}$. Thus, placing $E(y\dot{y})$ equal to zero when it is not quite zero can yield large errors in $\hat{C}$. Indeed, the $kE(y\dot{y})$ greatly dominates the $E(\dot{y}\dot{y})$ term, so a small error in $E(y\dot{y})$ will not affect the $\hat{C}$ as much.

The story is quite different for the estimate of k (that is, $\hat{k}$). By setting $E(y\dot{y})$ equal to zero, the error has very little effect on $\hat{k}$ if $\hat{C} \ll k$. One would conclude that $\hat{k}$ could still be estimated reasonably well by setting various second moments equal to zero, even when this is in error because the system has not yet reached steady state. One would also conclude that the damping coefficient estimate would suffer greatly. This is exactly what was observed in our simulation experiments.

When the system is in the steady state, the estimates obtained from simulations were quite acceptable.

Deterministic Excitations

We shall now concentrate upon the problem of identification of linear systems by means of deterministic excitations of the type that are readily available in laboratory test situations. The most common types of excitations that can be generated in the laboratory are the pure-sinusoidal and the sweep-sinusoidal oscillations.

To illustrate the approach one takes for such a deterministic input, let us consider the simple oscillator with a sinusoidal excitation. Consider

$$
m\ddot{y} + C\dot{y} + ky = \sin \omega t \qquad (35)
$$

We assume the system to be asymptotically stable so that the transients will die out. In this case, it is equivalent to specify that bounded inputs yield bounded outputs.

For zero initial conditions the solution may be written as

$$
y_t = \int_{-\infty}^{t} d\tau\, H(t-\tau) \sin \omega\tau \qquad (36)
$$

where

$$
H(t) = \frac{1}{m\sqrt{\frac{k}{m} - \frac{C^2}{4m^2}}}\, e^{-\frac{C}{2m}t} \sin \sqrt{\frac{k}{m} - \frac{C^2}{4m^2}}\, t \qquad (37)
$$

We define an average operator of the form

$$
\langle u(t) \rangle = \lim_{T \to \infty} \frac{1}{T} \int_{0}^{T} u(t)\, dt \qquad (38)
$$

for functions [illegible] for which this operator exists.

Now on the basis of this operator, let us attempt to identify the constants m, C, k. Equation (35) is multiplied by [illegible], and $\ddot{y}$, respectively, and averages are taken as defined by Eq. (38) to yield

$$\begin{aligned} m\langle y\ddot{y}\rangle + C\langle y\dot{y}\rangle + k\langle y^2\rangle &= \langle fy\rangle \\ m\langle \dot{y}\ddot{y}\rangle + C\langle \dot{y}^2\rangle + k\langle y\dot{y}\rangle &= \langle f\dot{y}\rangle \\ m\langle \ddot{y}^2\rangle + C\langle \dot{y}\ddot{y}\rangle + k\langle y\ddot{y}\rangle &= \langle f\ddot{y}\rangle \end{aligned} \tag{39}$$

We now wish to investigate these terms in somewhat more detail.

One simply obtains

$$\langle y\dot{y}\rangle = \lim_{T\to\infty}\frac{1}{T}\int_0^T y(t)\,\dot{y}(t)\,dt$$

$$= \lim_{T\to\infty}\frac{1}{2T}\left[y^2(t)\right] = 0 \tag{40}$$

where the initial conditions are zero and $y(t)$ is bounded on the interval $(0, t)$ because the excitation is bounded.

Therefore, we can determine in the same fashion that

$$\begin{aligned} \langle y\dot{y}\rangle &= 0 \\ \langle y\ddot{y}\rangle &= -\langle \dot{y}^2\rangle \end{aligned} \tag{41}$$

It will follow that Eq. (39) can be written as

$$\begin{aligned} -m\langle \dot{y}^2\rangle + k\langle y^2\rangle &= \langle fy\rangle \\ C\langle \dot{y}^2\rangle &= \langle f\dot{y}\rangle \\ m\langle \ddot{y}^2\rangle - k\langle \dot{y}^2\rangle &= \langle f\ddot{y}\rangle \end{aligned} \tag{42}$$

The reader will recognize Eq. (42) to be identical to the parameter identification of Eq. (31), except that the expectation operator in Eq. (31) is replaced by the time average operator as defined in Eq. (38).

There is a very significant distinction to be made in the derivation of Eq. (42) as opposed to the derivation of Eq. (31). In the derivation of Eq. (31) it was assumed that the processes over which the expectations are applied are stationary processes (at least up to the second moments).

This is guaranteed by our assumptions of a stationary process input, into the system, where the constant matrix A is a stability matrix. In that case, the steady state solution is a stationary random process and Eqs. (31) apply.

On the other hand, Eqs. (42) did not make use of the assumption of stationarity, or steady state, for its derivation. This is a very significant point. In fact, for the sinusoidal input case, if $y_s(t)$ is the steady state solution, we cannot identify all three constants m, C, k.

This can be illustrated very simply in the following fashion. The steady state solution is given

$$\begin{aligned} y_s(t) &= \int_{-\infty}^{t} H(t-\tau)\sin\omega\tau\,d\tau \\ &= \int_0^{\infty} H(\tau)\sin\omega(t-\tau)\,d\tau \\ &= k\sin(\omega t+\phi) \end{aligned} \tag{43}$$

where k, ϕ are easily determined in terms of the integrals

$$\int_0^{\infty} d\tau\, H(\tau)\sin\omega\tau, \quad \int_0^{\infty} d\tau\, H(\tau)\cos\omega\tau$$

Therefore, we find,

$$\begin{aligned} \dot{y}_s(t) &= \omega k\cos(\omega t+\phi) \\ \ddot{y}_s(t) &= -\omega^2 k\sin(\omega t+\phi) \end{aligned} \tag{44}$$

Upon applying Eqs. (44) to Eqs. (42) we find the equations

$$\begin{aligned} -m\omega^2\langle y_s^2\rangle + k\langle y_s^2\rangle &= \langle fy_s\rangle \\ C\omega^2\langle y_s^2\rangle &= \langle f\dot{y}_s\rangle \\ m\omega^2\langle y_s^2\rangle + k\langle y_s^2\rangle &= \langle f\ddot{y}_s\rangle \end{aligned} \tag{45}$$

We easily evaluate

$$\langle y_s^2\rangle = \lim_{T\to\infty}\frac{1}{T}\int_0^T k^2\sin^2(\omega t+\phi)\,dt = \frac{k^2}{2}$$

$$\langle \dot{y}_s^2\rangle = \lim_{T\to\infty}\frac{1}{T}\int_0^T \omega^2 k^2\cos^2(\omega t+\phi)\,dt = \frac{\omega^2 k^2}{2}$$

(46)
(Cont.)

$$\langle y_k^2 \rangle = \lim_{T \to \infty} \frac{1}{T} \int_0^T [illegible] \quad (46)$$

The determinant of the linear system of Eqs. (45) in the unknowns [illegible] is

$$\begin{vmatrix} -\frac{\omega^2 k^2}{2} & 0 & \frac{k^2}{2} \\ 0 & -\frac{\omega^2 k^2}{2} & 0 \\ \frac{\omega^4 k^2}{2} & 0 & -\frac{\omega^2 k^2}{2} \end{vmatrix} = 0 \quad (47)$$

because the third row is $-\omega^2$ times the first row.

Consequently, we cannot identify all three unknowns by these equations in the steady-state case with sinusoidal excitations. The reason is quite clear: y_s and its two derivatives are not linearly independent of one another. However, any two unknown parameters can be identified. Of course, this problem does not enter into the random excitation case simply because the sample functions and their derivatives are not linearly dependent, so one would not expect to obtain linearly dependent moments from the stationary solution processes.

Equations (42) were obtained for a simple oscillator. We can easily establish that similar equations are possible in higher-degree-of-freedom systems as well. Let us consider the general solution to the system

$$\frac{dy(t)}{dt} = Ay(t) + f(t) \quad (48)$$

where A, y, f are defined earlier in this paper. (See "Theoretical Development.")

For zero initial conditions, the solution process can be written as

$$y(t) = \int_0^t e^{-A(t-\tau)} f(\tau)\, d\tau \quad (49)$$

Any component $y_i(t)$ of the state vector y can be given by the integral

$$y_i(t) = \sum_{j=1}^{n} \int_0^t H_{ij}(t-\tau)\, f_j(\tau)\, d\tau \quad (50)$$

where $f_j(\tau)$ is the excitation at the jth driving point and $H_{ij}(t-\tau)$ is the influence function or impulse response between the jth driving point and the ith state. From our assumed stability we have

$$\int_0^\infty H_{ij} [illegible] \quad (51)$$

We are assuming the $f_j(t)$ to be of the form

$$f_j(t) = k_j \sin \omega_j t \quad (52)$$

It follows, then, that y_i and its derivatives are bounded.

To achieve equations of the form analogous to Eqs. (42) we must establish

$$\left\langle y_i^n(t) \frac{dy_i(t)}{dt} \right\rangle = 0 \quad (53a)$$

$$\left\langle \frac{dy_i(t)}{dt} y_j(t) \right\rangle = -\left\langle y_i(t) \frac{dy_j(t)}{dt} \right\rangle \quad (53b)$$

But this is immediate for by definition

$$\lim_{T \to \infty} \frac{1}{T} \int_0^T dt\, y_i^n(t) \frac{dy_i(t)}{dt} = \lim_{T \to \infty} \frac{1}{T} \frac{1}{n+1} y_i^{n+1}(T)$$

$$= 0 \quad (54a)$$

$$\lim_{T \to \infty} \frac{1}{T} \int_0^T dt\, \frac{dy_i(t)}{dt} y_j(t) = \lim_{T \to \infty} \frac{1}{T} y_i(T)\, y_j(T)$$

$$(54b)$$

$$- \lim_{T \to \infty} \frac{1}{T} \int_0^T dt\, y_i(t) \frac{dy_j(t)}{dt}$$

$$= - \lim_{T \to \infty} \frac{1}{T} \int_0^T dt\, y_i(t) \frac{dy_j(t)}{dt} \quad (54c)$$

In the derivation of Eq. (54b) we have used only the fact that the components $y_i(t)$ are bounded on $(0, \infty)$ and that the initial conditions are zero. (This last condition is clearly not a requirement for establishing Eq. (54b).)

It was pointed out above that the steady-state solution is not required for identification. We should now notice another remarkable fact. That is, the requirement of sinusoidal excitations is not basic in the derivations above. All that is basic is that the system is stable in the sense of bounded inputs yielding bounded outputs. Therefore, all that we require is that a bounded function, any function for that matter, be used for excitation purposes. For example, a sweep-sinusoidal or even a damped-sinusoidal function

can lead, theoretically, to the identification of the parameters of the system. Even more interesting, a sample excitation from a random process such as those discussed in "Random Excitations" will yield identification on this basis. We must stop a moment and reflect upon this last point.

Our whole approach to the identification of the unknown parameters has been motivated by the statistical reasoning put forth in "Random Excitations"; yet we now see that there is perhaps a more fundamental point that underlies the proposed procedure. We are led to think this simply because we can establish the same technique for identification with any test excitation. Furthermore, it appears that steady-state properties are not required.

There is, in fact, a more basic mechanism here that subsumes all of the previous analyses in "Random Excitations" and in this section as special cases.

We illustrate this mechanism, again, with the simple linear damped oscillator. We consider the oscillator driven by a bounded excitation $f(t)$,

$$m\ddot{y}(t) + C\dot{y}(t) + ky(t) = f(t) \tag{55}$$

Suppose we are able to observe the excitation, the displacement, velocity, and acceleration exactly at three different instants t_1, t_2, t_3. It would then follow that we would have three equations,

$$\begin{aligned} m\ddot{y}_1 + C\dot{y}_1 + ky_1 &= f_1 \\ m\ddot{y}_2 + C\dot{y}_2 + ky_2 &= f_2 \\ m\ddot{y}_3 + C\dot{y}_3 + ky_3 &= f_3 \end{aligned} \tag{56}$$

at the observation times.

With only three observations, these equations, if not singular, would lead to identification of the parameters. But, even if we can obtain simultaneous records of the excitation, displacement, and so forth, we cannot expect to achieve exact observations of the four quantities at any given time.

Indeed, the observations would yield some error of an independent random type with zero mean. That is, the observations would be of the form

$$\begin{aligned} m(\ddot{y}_1 + n_{11}) + C(\dot{y}_1 + n_{12}) + k(y_1 + n_{13}) &= f_1 + n_{14} \\ m(\ddot{y}_2 + n_{21}) + C(\dot{y}_2 + n_{22}) + k(y_2 + n_{23}) &= f_2 + n_{24} \\ m(\ddot{y}_3 + n_{31}) + C(\dot{y}_3 + n_{32}) + k(y_3 + n_{33}) &= f_3 + n_{34} \end{aligned} \tag{57}$$

where the n's are independent, identically distributed, and $E(n_{ij}) = 0$.

But because the noise in the observations has mean zero, it follows that

[illegible]

If we write the observed excitation and dynamical variables as

[illegible]

then it will follow that

[illegible] (58)

That is, the errors in observation will, so to speak, average out to zero.

If $f(t)$ is identically zero, then all terms in Eq. (58) will be zero. Directly taking a time average of Eq. (55) would not yield a usable equation for identification purposes. For this reason we will use, as before, time averages of second powers for identification of linear systems.

The actual identification equations that we apply in the case of the linear system of Eq. (55) are given as

$$\begin{aligned} m\frac{1}{T}\int_0^T \ddot{y}(t)\,y(t)\,dt + C\frac{1}{T}\int_0^T \dot{y}(t)\,y(t)\,dt \\ + k\frac{1}{T}\int_0^T y^2(t)\,dt = \frac{1}{T}\int_0^T f(t)\,y(t)\,dt \\ m\frac{1}{T}\int_0^T \ddot{y}(t)\,\dot{y}(t)\,dt + C\frac{1}{T}\int_0^T \dot{y}^2(t)\,dt \\ + k\frac{1}{T}\int_0^T y(t)\,\dot{y}(t)\,dt = \frac{1}{T}\int_0^T f(t)\,\dot{y}(t)\,dt \\ m\frac{1}{T}\int_0^T \ddot{y}^2(t)\,dt + C\frac{1}{T}\int_0^T \dot{y}(t)\,\ddot{y}(t)\,dt \\ + k\frac{1}{T}\int_0^T y(t)\,\ddot{y}(t)\,dt = \frac{1}{T}\int_0^T f(t)\,\ddot{y}(t)\,dt \end{aligned} \tag{59}$$

where all of the variables are considered to be the observed variables.

We wish to make it quite clear that Eq. (59) holds in all cases, random or deterministic. If $f(t)$ is a sample of a random process and T is large enough, then the averages can be replaced

by expectation operators, allowing a number of the terms to go to zero as we have discussed before, and the analysis discussed in "Random Excitations" can be followed. But, whether T is large or not, these equations will always hold. As we shall see, they yield extremely accurate parameter estimates.

The equations analogous to Eq. (33) for an N mass chain are

$$m_1 \frac{1}{T}\int_0^T y_1(t)\,\ddot{y}_1(t)\,dt = \frac{1}{T}\int_0^T y_1(t)\,f_1(t)\,dt$$
$$- C_1 \frac{1}{T}\int_0^T y_1(t)\left[\dot{y}_1(t) - \dot{y}_2(t)\right]$$
$$- k_1 \frac{1}{T}\int_0^T y_1(t)\left[y_1(t) - y_2(t)\right]$$
$$m_1 \frac{1}{T}\int_0^T \dot{y}_1(t)\,\ddot{y}_1(t)\,dt = \frac{1}{T}\int_0^T \dot{y}_1(t)\,f_1(t)\,dt$$
$$- C_1 \frac{1}{T}\int_0^T \dot{y}_1(t)\left[\dot{y}_1(t) - \dot{y}_2(t)\right]dt$$
$$- k_1 \frac{1}{T}\int_0^T \dot{y}_2(t)\left[y_1(t) - y_2(t)\right]dt$$
$$m_1 \frac{1}{T}\int_0^T \ddot{y}_1^2(t)\,dt = \frac{1}{T}\int_0^T \ddot{y}_1(t)\,f_1(t)\,dt$$
$$- C_1 \frac{1}{T}\int_0^T \ddot{y}_1(t)\left[\dot{y}_1(t) - \dot{y}_2(t)\right]dt$$
$$- k_1 \frac{1}{T}\int_0^T \ddot{y}_1(t)\left[y_1(t) - y_2(t)\right]dt$$
$$m_2 \frac{1}{T}\int_0^T y_2(t)\,\ddot{y}_2(t)\,dt = \frac{1}{T}\int_0^T y_2(t)\,f_2(t)\,dt$$
$$- C_2 \frac{1}{T}\int_0^T y_2(t)\left[\dot{y}_2(t) - \dot{y}_3(t)\right]$$
$$- k_2 \frac{1}{T}\int_0^T y_2(t)\left[y_2(t) - y_3(t)\right]dt$$
$$+ C_1 \frac{1}{T}\int_0^T y_2(t)\left[\dot{y}_1(t) - \dot{y}_2(t)\right]dt$$
$$+ k_1 \frac{1}{T}\int_0^T y_2(t)\left[y_1(t) - y_2(t)\right]dt \,. \qquad (60)$$

(60) (Cont.)

etc. We repeat that these equations hold for any T. In some cases many of the terms will be close to zero relative to the other terms. This is especially so when the excitation is a sample from a stationary process and the system is operating in steady state. In that case, the analysis in "Random Excitations" will apply.

We also wish to repeat that Eqs. (60) hold for any excitation function as long as there is an appreciable magnitude of the output vector. This is quite distinct from the analysis in "Random Excitations" where the stationary properties were significant.

DISCUSSION

R. H. Dudley (Aerospace Corp.): With any simulation study one wants to be able to estimate the precision and confidence as a function of the number of random variables sampled. Have you done this?

Mr. Kozin: A rather comprehensive report will come out of NASA's Goddard Space Flight Center, or you can write to our organization and we will send you a copy. In a sense it is not exactly a statistical approach. We made a number of studies as to the relative errors in the estimates on the basis of the time interval over which you estimate the number of samples that one obtains per second, and so on. In the report you will find that in some cases we were able to estimate on the basis of just two cycles of the lowest natural frequency and we are rather encouraged.

G. C. Smith (Bell Aerosystems): Your abstract indicated applicability to nonlinear systems. Could you say a little bit more about that, please?

Mr. Kozin: I can say a lot more on an analytical basis, but we have not made any study of the general nonlinear system at this time.

Mr. Smith: How does your work extend to continuous systems where one would have accelerations and velocities at particular points?

Mr. Kozin: I have not looked at the case where one has a continuous number of modes. I would say that if one looked at the problem that Dr. Paney did, where you are interested in looking at equations of the modes, he could use the same type of idea as here. In the continuous case, I do not know. I think it is a very interesting problem that one could very well look at.

* * *

REINFORCED CONCRETE BEAM RESONANCES

Fred G. Krach
Barry Controls
Division of Barry Wright Corporation
Watertown, Massachusetts

The principal objective of this paper is to present design techniques that have been found to be effective when designing reinforced concrete test piers for metrology labs.

The experience of the author indicates, and this paper illustrates, that steel reinforcement has a negligible effect on the dynamic response characteristics of a concrete beam and, in fact, the error caused by neglecting the existence of the re-bars is usually compensated for by concrete strength in excess of the contractually specified value.

Finally, this paper presents test results that indicate that when the ratio of beam stiffness to the stiffness of the isolation system is sufficiently large (approximately 100), the beam responds as a free-free beam (as opposed to the usual) simply supported beam). The test results further demonstrate that the theory applies to vibrations with the "micro-g" accelerations (seismic disturbances).

INTRODUCTION

As our scientific society advances its technological capabilities, many test facilities are being built that are capable of making extremely accurate measurements. This is especially true in the field of optics and related metrological sciences. The ability to make measurements with increasing accuracy must be matched by a capability to control the dynamic responses of test facilities to a correspondingly precise degree.

In particular, optical experiments require that angular deviations between the light source and the light sensor must be minimized. The principal source of measurement error is usually the bending response of the beam (optical bench) that supports the components of the experiment. Figure 1 illustrates the effect of this bending on the accuracy of a typical experiment.

Barry Controls has designed, fabricated, and tested many dynamically stable test piers for the optical industry, as well as for other

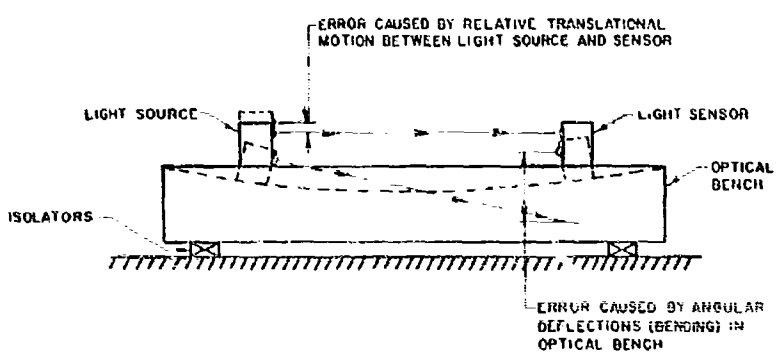

Fig. 1. Optical measurement errors

industries with similar requirements. Frequently, our design has employed reinforced concrete beams on servo-controlled pneumatic isolation systems.

Reinforced concrete is usually employed because it has the desirable characteristic of being highly damped, internally, and it is readily available and economical.

We have found by experience that precision test facilities will have desirable frequency response characteristics if the lowest resonant frequency in the concrete structure is at least 10 times the highest natural frequency of the isolation system;

$$\frac{f_n \text{ (beam)}}{f_n \text{ (isolation sys.)}} \geq 10 \qquad (1)$$

where f_n is natural frequency (Hz).

When the above inequality is satisfied, then the following three conditions exist:

1. The environmental vibration will excite the isolation system primarily at its resonant frequency. This frequency is far enough below the structural resonances so that the beam responds essentially as a rigid body; that is, no relative motion between the test components.

2. Environmental vibrations that exist at, or near, the structural resonant frequencies of the beam are attenuated 95 percent, or more, by the isolation system, thus reducing the resonant response of the beam to acceptable levels.

3. The lowest resonant frequency of the beam will approach the fundamental frequency of a free-free beam, which is approximately 2.3 times higher ($2.3^2 = 5.3$ times stiffer) than the fundamental frequency of a simply supported beam. The beam responds freely (as if it were floating) because it is 100 times stiffer than the isolation system that supports it.

To realize the design goal represented by Eq. (1), the designer must have available reliable techniques for predicting the dynamic characteristics of reinforced concrete under conditions that are not normally encountered by structural designers. For example, typical allowable deflections for concrete beams, floors, and roofs in normal structural applications are rarely limited to less than 0.1 percent of the span. Deflections of this magnitude in an optical bench would render it useless; they are commonly limited to values on the order of 0.003 percent of the length. Stiffnesses of this order are required to maintain dynamic responses (and the corresponding angular errors) within allowable limits.

Barry Controls has been concerned with the following aspects of concrete design for precision laboratory applications:

1. Experimental verification of the mathematically predicted dynamic responses of vibration isolated reinforced concrete beams to seismic disturbances.

2. Optimization of the dynamic characteristics of the system composed of the reinforced concrete beam and low-frequency vibration isolators.

This paper presents a brief summary of typical design calculations and the substantiating test results. The example chosen is a 50-ft-long optical test bench mounted on four standard, 6-in.-tall Barry Controls Serva-Level® pneumatic isolators. The vertical natural frequency of the isolator-bench system is approximately 2 Hz, requiring a minimum structural resonant frequency of 20 Hz, in accordance with Eq. (1), above.

CALCULATING REINFORCED CONCRETE BEAM RESONANCES

The primary bending natural frequency of a free-free beam [1] is

$$\omega_n = 22.4 \sqrt{\frac{EI}{\mu L^4}} \qquad (2)$$

where

E = modulus of elasticity (psi),

I = area moment of inertia of beam cross section (in.^{4}),

μ = mass/unit length of beam (lb-sec^2/in.^{2}),

L = length of beam (in.), and

ω_n = natural frequency (rad/sec).

Because concrete is a composite structure, the effect of the reinforcing steel on the natural frequencies is considered by calculating an equivalent area moment of inertia (I_{equiv}) as follows:

$$I_{equiv} = I_{X\text{-}X \text{ (of Fig. 2)}} - \frac{bd^3}{12} + \sum (n-1) A_s D^2 \qquad (3)$$

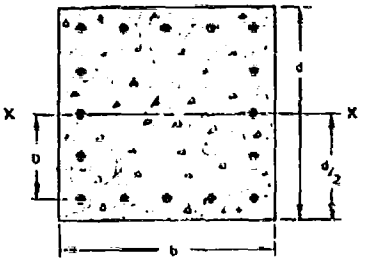

Fig. 2. Typical cross section of a reinforced concrete beam

where b, d, and D are all linear dimensions, as shown in Fig. 2 (in.),

A_s = area of the reinforcing steel (sq in.),

I_{X-X} = area moment of inertia about the neutral axis, shown as the X-X axis of Fig. 2 ($in.^4$), and

n = modulus of elasticity of steel (E_s) (psi)/modulus of elasticity of concrete (E_c) (psi).

This approach generates a fictitious concrete beam, which is equivalent to the reinforced beam being analyzed, and therefore, the modulus of elasticity of concrete (E_c) would be used, along with the above moment of inertia (Eq. (3)), in Eq. (2) to calculate the natural frequency of the reinforced concrete beam. We find the modulus of elasticity of concrete [2] from:

$$E_c = w^{1.5}\, 33\sqrt{F'_c} \qquad (4)$$

where

F'_c = compressive strength of concrete (psi), and

w = weight of cubic foot of concrete (lb).

GENERAL DESIGN PHILOSOPHY

Our experience has emphasized that a good seismic mass design will limit the length of the seismic mass to approximately 10 times the depth of the cross section of the mass, or

$$L \leq 10\,h \qquad (5)$$

where L and h are linear dimensions, as shown in Fig. 3 (in.).

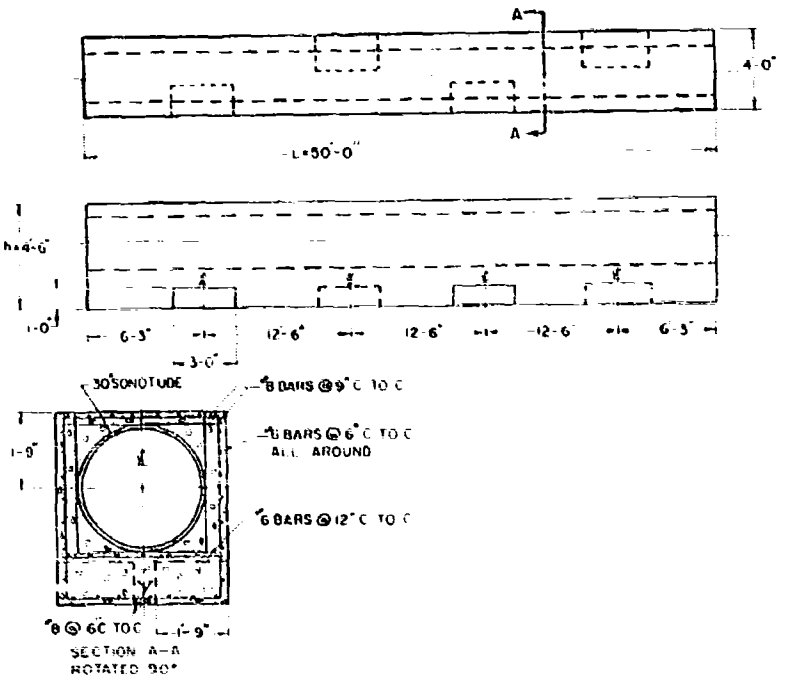

Fig. 3. Construction details of a 50 ft optical bench (typical beam design that optimizes dynamic response characteristics of a reinforced concrete beam)

We also use pipes (paper and/or steel) to remove concrete from the center of the seismic block, as shown in Fig. 3. Removing concrete from near the center of the beam can result in large weight reductions without decreasing the beam's stiffness appreciably; that is, beam weight is reduced more than "I". Thus, the efficient use of voids (pipes) can generate a much higher primary bending mode in the beam. Beam resonances have been doubled by the aforementioned design technique.

Generally, employment of Eq. (5), and the judicious use of voids in the cross section of a beam, will result in first bending modes in the beam of more than 20 Hz. In the Introduction, we explained why it is desirable to have a beam's primary bending resonance at least 10 times higher than the supporting isolation system's natural frequency; and if a 20-Hz beam is generated, Eq. (1) will be satisfied by using a 2-Hz isolation system to support the mass. A 2-Hz isolation system is not difficult to design, Serva-levl ® systems, manufactured by Barry Controls, have been designed that have natural frequencies of less than 0.5 Hz, and 2.0-Hz systems are standard.

SAMPLE CALCULATIONS

The following example of a typical seismic mass design is presented to illustrate the design techniques discussed in this paper. This example is an actual system that was later tested, and this paper contains test results that verified the theory.

The natural frequency of the reinforced concrete seismic mass, shown in Fig. 3, is found by incorporating Eqs. (3) and (4) into Eq. (2) to generate Eq. (6), as follows:

$$\omega_n = 22.4\sqrt{\frac{E_c\, I_{equiv}}{\mu L^4}} \qquad (6)$$

From Fig. 3, the components of the above equation are found to be

$$L = 50\times12 = 6.00\times10^{2}\ \text{in.},$$

$$L^4 = 1.29\times10^{11}\ \text{in.}^4,$$

$$\mu = \frac{[(48\times54)-(\pi15^2)-(21\times12\times12/50)]150}{1{,}728\times386},$$

$$\mu = 4.1\times10^{-1}\ \text{lb-sec}^2/\text{in.}^2,$$

$$E_c = 144^{1.5}\times33\sqrt{3{,}000}\ \text{psi},$$

$$E_c = 3.27\times10^{6}\ \text{psi}.$$

Using $E_c = 2.8\times10^{7}$, and knowing the neutral axis of the beam shown in Fig. 3 to be 24.6 in. above the base of the beam, from Eq. (3) we get

$$I_{equiv} = [48\times54\times2.1^2 + \dots + 48\times54\times1.2^2) - (\pi15^2\times8.4^2) - (15.4\times4) + \{5.55A_p D^2\}$$

$$(5.63\times10^{5}) - 4.43\times10^{4}]$$

$$= 6.07\times10^{5}\ \text{in.}^4$$

When the above values are inserted into Eq. (6) we obtain

$$\omega_n = 22.4\sqrt{\frac{3.27\times10^{6}\times6.07\times10^{5}}{4.1\times10^{-1}\times1.29\times10^{11}}}$$

$$= 22.4\sqrt{\frac{1.985\times10^{12}}{5.3}} = 22.4\sqrt{37.5}$$

$$= 137\ \text{rad/sec}$$

$$f_n = 137/2\pi = 21.8\ \text{Hz}.$$

TEST RESULTS

Figure 4 shows oscilloscope traces of a voltage signal generated by a sensitive velocity pickup (seismometer) that was set on top of the beam which we analyzed earlier in this paper.

Figure 4(a) shows the block responding to a step-function input pulse. The input pulse was generated by quickly removing a small steel mass (approximately 10 lb) from the top surface of the seismic mass. The predominant 2.1-Hz oscillation (in Fig. 4(a)) is a standard, 6-in.-high, Serva-Levl Vibration Isolation System's response. The 21-Hz oscillation which is superimposed on the system response curve is the mass resonating caused by frictional energies being released because contact between the steel weight and the seismic mass was not broken quickly enough — that is, the weight was not taken off "cleanly."

The response shown in Fig. 4(b) was generated by removing the same weight from the system. This time the 2.1-Hz isolation system's response is "clean" because the weight was set on a thin piece of leather that was on the top surface of the mass. Then, when the weight was pulled off the mass, no contact friction energy was released.

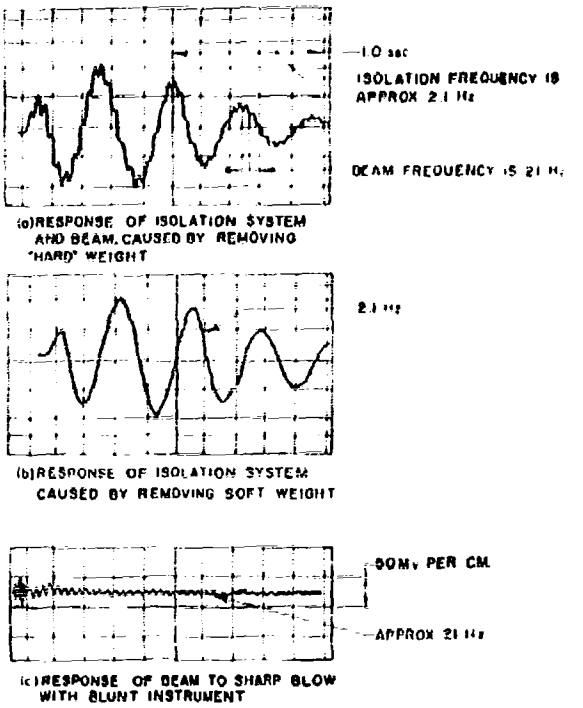

Fig. 4. Seismometer traces, as seen on an oscilloscope, showing the frequency response of a reinforced concrete beam on vibration isolators

The response of the seismic mass to a sharp blow with a blunt instrument and the 21-Hz primary bending frequency of the mass are shown in Fig. 4(c).

CONCLUSIONS

The calculations presented in this paper are a result of engineering efforts expended prior to the generation of construction drawings by the designer. These construction drawings are then used by the contractor as the specification for the work to be done. Thus, it is necessary to calculate the modulus of elasticity of concrete (E_c) by using the compression strength (f'_c) specified on the drawing. However, the compression tests on the concrete cores taken from the pour for the beam discussed under Sample Calculations indicated that the strength achieved was actually 3820 psi instead of 3000 psi used in the design. If we recalculate the natural frequency of the beam, using this actual compressive strength of the concrete we will get

$$f_n = 21.8 \sqrt{\left(\frac{3820}{3000}\right)^{(?)}}$$

$$= 23.1 \text{ Hz}$$

The above correction changes the theoretical response by less than 7 percent and, therefore, can be considered negligible.

Similarly, we observe that if the effect of the reinforcing steel on the theoretical value of the moment of inertia (of the cross section of the beam) is not taken into account, the calculated natural frequency of the beam decreases from 21.8 Hz to

$$f_n = 21.8 \sqrt{\frac{5.63}{6.07}} = 21.0 \text{ Hz}.$$

The above change in natural frequency is calculated for a beam (shown in Fig. 3) that employs much more reinforcing steel than is normally used. Nevertheless, the above calculation shows a negligible change in the natural

frequency prediction. Because a relatively small change in frequency, like the one above, has been encountered during many design calculations, the change in stiffness caused by reinforcing steel can be ignored.

The reinforcing steel shown in Fig. 3 was not incorporated in the design to enhance the strength or the stiffness of the beam. That reinforcement was used only to optimize the shrinkage resistance characteristics of the beam. In other words, we did not want the beam to warp excessively as the concrete cured.

The length-to-depth ratio of the beam shown in Fig. 3 is L/h = 600/54 = 11.1. This ratio is larger than recommended by Eq. (5); however, the increase in beam resonances, which were gained by the addition of the 30-in.-diameter void in the beam's cross section, offset the high length-to-depth ratio, and the frequency ratio that was recommended in Eq. (1), was achieved.

The principal investigation disclosed by this paper is the verification that the theoretical dynamic responses of beams to microinch environments are compatible with calculated response characteristics using standard structural engineering techniques.

In Fig. 4(a) we see that the beam resonance response was driven by the release of contact friction caused by removing a weight that is less than 0.01 percent of the beam's weight. This very small energy input was, therefore, compatible with energy inputs caused by seismic disturbances.

In Figs. 4(a) and 4(c), the amplitude of the oscilloscope trace is approximately 20 mv as the seismometer used to generate these signals has a sensitivity of about 20 v/in./sec, the peak velocity of the beam's response is

$$\frac{0.020}{20} = 0.001 \text{ in./sec} \qquad \text{double amplitude.}$$

This velocity, at 21 Hz, is equivalent to 34 μin., single amplitude. Thus, the beam responses in Fig. 4 are in the microinch range, and the theory contained herein seems accurate at these very small amplitudes of response.

Barry Controls has used the principles expressed in Eqs. (1) and (5) to design many vibration isolated precision test piers. When these piers are tested to verify beam resonances, the test results demonstrate that the calculated natural bending frequencies are within 10 percent of actual measured responses. Also, the users of these test piers are able to make measurements that are advancing the state-of-the-art of the metrological sciences.

Therefore, the design goals outlined in this paper achieve, and often exceed, the objectives that imposed their invention.

REFERENCES

1. C. M. Harris and C. E. Crede, Eds., Shock and Vibration Handbook (1) (McGraw-Hill, New York), Ch. 1, pp. 1-14

2. "Building Code Requirements for Reinforced Concrete" (ACI 318-63) ACI, Detroit, Mich., Ch. 10, pp. 318-349, June 1963

* * *

STRUCTURAL DYNAMIC ANALYSIS OF THE MARINER MARS 1969 SPACECRAFT*

H. J. Helbeck
Jet Propulsion Laboratory
California Institute of Technology
Pasadena, California

and

T. D. Arthurs and W. J. Gaugh
Northrop Systems Laboratory
Northrop Corporation
Hawthorne, California

The structural dynamic analysis approach for the MARINER MARS 1969 spacecraft is presented in this paper. In the analysis technique used, based on the component mode synthesis method, the modal characteristics of the composite structure are synthesized from those of the component modes. The equations of motion of the composite, formulated in terms of generalized coordinates which are a truncated set of the synthesized modes, are solved to give the dynamic response of the structure to sinusoidal base accelerations. Integrated with a correlative test program, which included static, modal, and forced vibration tests, this analysis provided a sound basis for confidence in the integrity of the structure. Correlation between test results and analytic predictions is discussed and some results are given. In general, reasonably good agreement was obtained, indicating the basic soundness of the analysis approach.

INTRODUCTION

The primary objectives of a spacecraft structural analysis program are to support design decisions, provide pretest confidence, and form the basis for responding to later problems and changes. A planetary spacecraft program imposes special requirements because of schedule inflexibility and the late availability of representative test hardware. The structural analysis approach of the MARINER spacecraft programs is best illustrated by that of the MARINER MARS 1969 program (MM'69) that has also utilized some recently developed techniques.

The MARINER MARS 1969 (M69) spacecraft required maximum usage of MARINER IV technology and design. However, the mission required extensive changes. The instruments on the planetary science platform increased in weight from 35 to about 170 lb, while the total spacecraft weight increased from 570 to about 900 lb. The use of the Atlas/Centaur launch vehicle in place of the Atlas/Agena led to a redefinition of the level and location of steady and vibration loads. The spacecraft configuration, with greatly increased adapter length, was far more susceptible to "beam" motion than was MARINER IV. Additionally, the four solar panels were latched together at their tips rather than separately supported.

These factors required that the spacecraft be considered as a new design from the structural analysis standpoint. The recent development of the Structural Analysis Matrix Interpretive System (SAMIS) [1,2], and the modal combination program [3] provided powerful tools for more effective implementation of the

*This paper presents the results of one phase of research carried out at the Jet Propulsion Laboratory, California Institute of Technology, under Contract No. NAS 7-100, sponsored by the National Aeronautics and Space Administration.

basic MARINER analysis approach. In the following sections descriptions are given of this approach and the analytical techniques used in its implementation. The purpose here is not to report on the techniques themselves, but rather on their usage in a spacecraft structural analysis program. Analyses of the M69 spacecraft are not yet fully complete, but preliminary results have been obtained together with some test correlation.

MARINER STRUCTURAL ANALYSIS APPROACH

The MM'69 structural design criteria [4], has two basic requirements. Structural elements must be capable of withstanding design limit loads without yielding and without causing deflections in excess of specified limits. They must also be capable of withstanding design ultimate loads, defined as 25 percent greater than design limit loads, without failure and without causing deflections that result in unintentional contact. Design limit loads are the maximum expected flight loads and environments defined in project environmental specifications.

Design limit loads are considered for various conditions and configurations, but this discussion will be limited to the specifications that represent the loads and vibration environments resulting from launch and exit. These include the steady accelerations owing to thrust and angle of attack and the vibrations caused by the dynamic response of the space vehicle to the transient excitations of liftoff, atmospheric disturbances, staging, and other events. Lack of definitive information regarding these transient responses above the frequency range of primary launch vehicle modes has resulted in the traditional representation of these responses by enveloped, sinusoidal, input excitations in project test requirements.

There is considerable discussion in the structural dynamics field regarding the rationality of this traditional approach, but this is not the subject of this paper. It can be noted, however, that alternative approaches typically rely on loads analyses of the composite space vehicle requiring the same types of spacecraft structural dynamic analyses as those described herein. MARINER specifications use the most severe combinations of specified static and vibration load envelopes as design limit load conditions. Additionally, it has been required that qualification vibration test levels, 50 percent greater than design levels, be considered as design limit load conditions, without combining other loads. These vibration test conditions become the critical design conditions for most lightly damped structural elements.

Structural design for such vibration loading conditions poses a dilemma for the structural designer and analyst. The load distribution depends not only on the load input and the structural stiffness, but on the dynamic response characteristics of the supporting and the supported structure as well. In addition, the load distribution differs for each mode. Therefore, an iterative approach to structural design and analysis is required, as the design itself affects not only the load paths, but the response characteristics, and hence the inertial loading, as well.

Initial subsystem designs for dynamic loading conditions are, of necessity, based on estimated equivalent static loads. Dynamic, modal analyses of the subsystems show the fundamental mode shapes and frequencies for qualitative consideration of potential coupling interactions. These analyses are repeated as the design evolves. When the design is relatively stable, a composite spacecraft analysis indicates modal coupling directly. Forced-response analyses, using assumed damping characteristics check the preliminary assumed equivalent static loads. The number of iterations of this cycle depends on design changes, analytical difficulties, schedule, and economic tradeoffs.

Early, simple tests may be conducted to check doubtful analytical assumptions, but representative structural models are unavailable until late in the program, when the design is frozen. Then, static and modal survey tests of a Developmental Test Model (DTM) and its subsystems provide correlation of analytical results by checking stiffness and inertial characteristics. Modal surveys utilize multiple exciters to investigate the characteristics of particular modes. The location, excitation level and phasing (0 or 180 degrees) of the individual exciters can be adjusted to most "cleanly" excite a desired mode. Lissajous plots, waveform, and orthogonality checks indicate test accuracy. Static and modal survey test results provide bases for rational analytical modifications, but random changes are not made solely to improve correlation because such changes give misleading results and are generally futile. Indications of modal damping are obtained from logarithmic decrements, response levels, and bandwidth. However, experience has shown that structural damping is amplitude dependent and that the low-level excitations of modal surveys give unrealistically

low damping indications. Forced vibration testing has the multiple purposes of analytical correlation, prequalification, and development of qualification test procedures. The DTM has the basic structural characteristics of a flight spacecraft, but inertial mockups represent many components. Response characteristics of the flight spacecraft are simulated only for frequencies below 200 Hz. Therefore, the prequalification function of the DTM is limited, particularly in the higher, "nonstructural" frequency range.

This analysis approach, integrated with a correlative test program, provides earlier and sounder bases for structural confidence than does a demonstration testing approach. If problems occur during testing, correlated analytical results can be used to evaluate failures and changes with a confidence not possible with intuition and testing alone. Analyses also provide the bases for pretest evaluation of proposed design modifications and for parametric investigations impossible to implement in a test program.

BACKGROUND OF APPROACH AND TECHNIQUES

The basic structural analysis approach just described has been used, to some extent, in all MARINER spacecraft programs. In earlier stages, the basic analytical tool was the Stiff-Eig [5] computer program that uses the stiffness matrix approach to solve static and normal mode problems with a maximum of 130 degrees of freedom, each point requiring 3 or 6 degrees of freedom. A major limitation of this program is the requirement that the entire structural model must take the form of a truss, grid, or beam-frame. A coarse, truss representation was necessary for the composite spacecraft model, which was also limited to 130 degrees of freedom. Some increase in capability was achieved by utilizing spacecraft symmetry, but the size and type limitations were still severe.

The modal combination technique was under development during the MARINER IV program, and there were tentative plans for using it to combine subassemblies in a composite spacecraft analysis. This would have allowed the various subsystem models to be of different Stiff-Eig structural types and would have alleviated the severe size constraint. The program also provides response information, including the effects of coupling through linear damping, by solution of the complex eigenvalue problem. The modal combination technique was not available for full utilization on MARINER IV. However, portions of the program were used to obtain the forced response of solar panels supported on viscous spring/dampers.

The modal combination program and portions of the newly developed SAMIS were available for use on the MARINER V program. However, because most design changes involved reduced weight, and because the project was under severe budget, manpower, and schedule constraints, a composite spacecraft structural analysis was not undertaken and only selected analyses utilized the increased capability. Geometric constraints required the redesign of high gain antenna and its support structure, and SAMIS allowed the antenna dish to be modeled as a shell structure using the finite element approach. A related constraint required a modified support system for the solar panels, and a tip-latched, panel-to-panel support system was used. The modal combination technique was used to obtain modal and response analyses of the four panels, eight spring/dampers, composite system.

The M69 structural analysis program has made full use of SAMIS and the modal combination program for subsystem and composite spacecraft analyses. Because of the developmental nature of the techniques, an early test model of a partial spacecraft was constructed from leftover MARINER IV hardware and crude mockups. Some analytical discrepancies were noted, but sufficient confidence in the approach was obtained to proceed with more complex analytical models. Delays resulted from computer programing development problems, but a preliminary analytical modal and response analysis of the composite spacecraft was obtained prior to assembly of the DTM. Reasonably good correlation with the DTM test results has been achieved, and significant discrepancies have been reconciled. Details of the analyses and correlation are discussed in the following sections. An improved analysis, now in process, incorporates analytical improvements based on DTM test results, and includes recent spacecraft design changes. Modification of the analytical techniques has also resulted in simpler, more efficient procedures.

ANALYSIS TECHNIQUE

A concept for analyzing the dynamic response of a complex structural system is described by Hurty [6]. A digital computer program [3], developed by Bamford at the Jet Propulsion Laboratory and based generally on Hurty's component mode synthesis method, was used in the analysis of the M69 spacecraft. In this technique, called "modal combination," the structure is divided into components, and a

representative structural model of each is constructed using the finite element technique. Mass and inertia properties are lumped at structural gridpoints (element joints). SAMIS is used to assemble the component stiffness matrix and compute the normal modes of vibration and frequencies. The modal combination program formulates the Lagrange equations of motion for the component in terms of generalized coordinates. These coordinates consist of selected displacement vectors including rigid body modes, a truncated set of normal modes, and modes caused by unit constraint displacements or concentrated loads at attachment interfaces. The requirement for compatibility of displacement at connections between components gives rise to a set of equations of constraint. Combination of the component equations of motion and constraint leads to a set of composite system equations of motion in terms of system generalized coordinates. The program formulates and solves these equations for system response to sinusoidal force inputs either in the form of base accelerations, analogous to the vibration test condition, or in the form of force inputs at unconstrained points on the assembly.

At critical response frequencies, the component generalized coordinate accelerations are computed. Returning to SAMIS, the inertial forces caused by these accelerations, together with concentrated forces at the attachment points of other components, are applied through the component stiffness matrix to obtain joint displacements. SAMIS is then used to calculate the internal load distribution in the finite element model. The final step in the analysis is the examination of the dynamic stress distribution in the component, a step which thus far has not been automated.

Structural Analysis and Matrix Interpretive System (SAMIS)

SAMIS is a system of digital computer programs, primarily oriented toward the solution of problems in structural analysis by the stiffness method. It does however, possess a general capability in manipulating matrices and solving problems in linear algebra.

The stiffness method of analysis is widely used and extensively documented. (For example, see Ref. [7].) Its central concept is the division of the structure into finite elements by a series of cuts. Intersections of cutting lines are called gridpoints or nodes. For each element considered individually, the loads and deflections at its nodal points are related through an elemental stiffness matrix. From these matrices the assembly of the structural stiffness matrix, $[k]$, which relates loads and displacements at all nodes on the structure, is a relatively straightforward procedure.

In the present system, structure types are limited to those that can be represented as assemblages of flat triangular facets, joined along their edges, and line elements, joined to the rest of the structure at their ends. All elements are capable of resisting stretching, shearing, bending, and twisting stresses. It is assumed that deflections are small and materials are monotropic with linear stress-strain relationships.

From geometric and material properties, system routines generate the elemental stiffness matrices and assemble $[k]$. For dynamics problems, involving the derivation of normal modes, masses are lumped at gridpoints, each of which may have as many as 6 degrees of freedom. Limitations on the eigenvalue routine require that the total number of lumped mass degrees of freedom in the structure not exceed 130. The requirement is mitigated by the ability to assign mass only to those degrees of freedom considered significant, a considerable reduction from the total number of possible lumped-mass displacements.

The equation of dynamic equilibrium for the structure vibrating in its ith undamped normal mode is written

$$-\omega_i^2[m]\{u\} - [k]\{u\} = 0 \qquad (1)$$

where ω_i is the modal frequency in rad/sec and $[m]$ is the mass matrix. Multiplying across by $[k]^{-1}$ and dividing by $-\omega_i^2$, Eq. (1) becomes

$$[k]^{-1}[m]\{u\} - \frac{1}{\omega_i^2}\left[1\right]\{u\} = 0 \qquad (2)$$

where $[1]$ is a unit matrix. Because the mass matrix, $[m]$, is positive definite there exists a lower triangular matrix $[L]$ such that

$$[L][L^T] = [m]$$

where superscript T denotes the transpose of the matrix.

Multiplying across Eq. (2) by $[L]$ and letting $[L^T]\{u\} = \{v\}$ leads to

$$[L^T][k]^{-1}[L]\{v\} - \frac{1}{\omega_i^2}\left[1\right]\{v\} = 0 \qquad (3)$$

Writing $[D] = [L^T][k]^{-1}[L]$ and $\lambda_i = 1/\omega_i^2$, Eq. (3) takes the form of the classical eigenvalue problem

$$\left[[D] - \lambda_i \left[I_N\right]\right]\{v\}_i = \{0\} \qquad (4)$$

$[D]$, referred to as the dynamic matrix, is positive definite, that is, all its roots are real. Equation (4) is solved for λ_i and the natural frequencies of the structure are given by

$$\omega_i = \frac{1}{\sqrt{\lambda_i}} \qquad (5)$$

The associated eigenvectors, $\{v\}_i$, lead to the normal mode vectors

$$\{u\}_i = \left[L^T\right]^{-1}\{v\}_i \qquad (6)$$

Solution of the above problem is typical of the capabilities of SAMIS. Routines are available to perform all the matrix operations required by the foregoing equations, which include inversion, decomposition, and eigenvalue solution. The user "programs" the problem through "pseudo instructions" [1,2], that call the appropriate system routines and control storage and manipulation of data in the computer.

Component Modes

The modal combination program uses rigid body, constraint, attachment, and normal modes in formulating the component equations of motion. Rigid body modes arise from unit displacement (translation or rotation) of the unconstrained structure, without deformation, with respect to the component coordinate system. If the structure is stable as a free body, there are six such modes that are computed from component geometry. The remaining modal types are generated by SAMIS and constitute part of the punched card input data to the modal combination program.

For modal analysis, the component may be constrained in a statically indeterminant manner, in which case constraint modes are used. These arise from unit displacement of each redundant constraint in turn, with all other constraints fixed. The rigid body modes together with the constraint modes are equal in number to the number of constraints. For small displacements, linear combinations of these modes permit any arbitrary combination of constraint displacements.

Attachment modes result from concentrated loads. They are used when another component is attached at an unrestrained point, and it is felt that the loads imposed will significantly affect mode shapes or stresses. Although there is a basic similarity between constraint and attachment modes, use of the latter obviates the need for unnecessary constraints in the component analysis. From a practical standpoint, this is especially important if the normal modes from analysis are to be compared to test results, in which case, extensive fixturing of the test specimen is avoided.

The number of normal modes is equal to the number of unrestrained mass degrees of freedom in the component. Because these may number up to 130, it is necessary to select a truncated set of modes to keep the problem size within reasonable bounds. Typically, a frequency cutoff is used to limit the number of selected modes. This upper frequency limit is primarily determined by the desired frequency range of applicability of the forced-response solution for the composite structure.

Composite System Analysis

The equation of motion (or dynamic equilibrium) for the ith component in terms of its lumped mass degrees of freedom may be written in matrix form as

$$[m]_i\{\ddot{u}\}_i + [c]_i\{\dot{u}\}_i + [k]_i\{u\}_i = \{f\}_i \qquad (7)$$

where $[c]_i$ is a matrix of undefined damping coefficients and $\{f\}_i$ is a column matrix of time-dependent forces in the lumped mass degrees of freedom. One set of equations in Eq. (7) may be written for each component, each set containing up to 130 equations. Because the solution of equations in this form presents unmanageable computational difficulties, a series of coordinate transformations is used, with the object of uncoupling and reducing the number of coordinates.

The component equations are first transformed to generalized coordinates, namely the previously described rigid body, constraint, attachment, and normal modes. We require that the displacement vector $\{u\}_i$ be a linear combination of the modes retained. If $[\phi]_i$ is the matrix of modal vectors, this coordinate transformation is of the form

$$\{u\}_i = [\phi]_i\{q\}_i \qquad (8)$$

Applying this to Eq. (7) and premultiplying across by $[\phi^T]_i$, the component equations of motion become

$$[M]_i\{\ddot{q}\}_i + [C]_i\{\dot{q}\}_i + [K]_i\{q\}_i = \{F\}_i \quad (9)$$

where $[M]_i$, $[C]_i$, and $[K]_i$ are the generalized mass, generalized damping, and generalized stiffness matrices, respectively, and $\{F\}_i$ is the vector of generalized forces in the modes. In formulating Eq. (9), the modal combination program takes advantage of some well-known properties of normal modes. The submatrices associated with mass and stiffness coupling between normal modes are diagonal in form. Other submatrices associated with stiffness coupling between rigid body and elastic modes, between constraint and attachment modes, and between constraint and normal modes, are null [3,6].

The generalized damping matrix $[C]$ is assumed to be the diagonal, $[C]_i = [c_i]$. Modal damping coefficients constitute part of the program input and may be obtained either directly from modal tests or based on past experience with similar structures. A basic, and as-yet-unresolved, difficulty exists in estimating damping in the constraint and attachment modes. An attempt was made in the M69 analysis to account for this and is discussed in a later section of the paper.

For a composite structural system, consisting of j components, the equations of motion for the unconnected components are written as a single group of uncoupled sets of equations in terms of generalized coordinates, $\{q\}$, of the form

$$\{q\} = \begin{Bmatrix} \{q\}_1 \\ \cdots \\ \{q\}_2 \\ \cdots \\ \vdots \\ \cdots \\ \{q\}_j \end{Bmatrix}$$

and the equations of motion become

$$[M]\{\ddot{q}\} + [C]\{\dot{q}\} + [K]\{q\} = \{F\} . \quad (10)$$

As the components are assembled, the requirement for compatibility of displacements at points of attachment gives rise to equations of constraint, one for each degree of freedom of attachment. For example, if the equations of constraint of any two components are formulated in terms of m and n generalized coordinates respectively, and one component is attached to the other in k degrees of freedom, then k equations of constraint exist between the $n + m$ coordinates. Any k coordinates, designated as dependent, can be solved for in terms of the remaining $m + n - k$. The procedure is repeated for each component added and a linear transformation, $[R]$, is constructed which transforms the uncoupled component generalized coordinates into a set of independent composite system coordinates,

$$\{q\} = [R]\{p\} . \quad (11)$$

Provision is made in the program for the analyst to specify which modes are to be retained as independent. However, care must be taken to insure that those chosen are in fact independent, because a dependency or "near" dependency can lead to numerical difficulties in subsequent eigenvalue calculations. Also, the six rigid body modes of the first component, referred to as the base system, must be retained as independent, while all other rigid body modes in the composite must be designated as dependent. The sinusoidal force inputs to the composite structure take the form of rigid body accelerations of the base system.

By substituting for $\{q\}$ from Eq. (11) and premultiplying across Eq. (10) by $[R^T]$, the equations of motion for the structural assembly in terms of the independent generalized coordinates of the components take the form

$$[\bar{M}]\{\ddot{p}\} + [\bar{C}]\{\dot{p}\} + [\bar{K}]\{p\} = \{\bar{F}\} \quad (12)$$

where $[\bar{M}]$, $[\bar{C}]$, and $[\bar{K}]$ are the generalized mass, damping, and stiffness matrices, respectively, and $\{\bar{F}\}$ is the vector of generalized forces in the independent modes. Because the rigid body accelerations of the base system are specified, these may be eliminated as unknowns and the number of Eqs. (12) is reduced by six. At present, program storage limitations require that the total number of independent component generalized coordinates shall not exceed 100.

Formulation of the damped composite system equations of motion in terms of fully uncoupled coordinates requires the solution of the damped eigenvalue problem. However, because the damped eigenvalue computer routine used is restricted to coefficient matrices of order 50×50 or less, the number of coordinates in the equation of motion must be reduced to 50 or less.

This is accomplished by first solving the undamped eigenvalue problem,

$$[\bar{M}]\{\ddot{p}\} + [\bar{K}]\{p\} = \{0\} . \quad (13)$$

Transformation of Eq. (13) into the form of the classical eigenvalue problem follows the algorithm previously outlined. The resulting modes

are the undamped normal modes of the composite structure, which are normalized so that the generalized mass in each is unity. A selected number (≤ 50) of the lower frequency modal vectors, in matrix form, $[\Phi_u]$, are used to transform the coordinates in a manner similar to the use of $[\gamma]$, of Eq. (8). The transformation

$$\{p\} = [\Phi_u]\{p_u\} \tag{14}$$

is applied to Eq. (12) which take the form

$$[I]\{\ddot{p}_u\} + [C]\{\dot{p}_u\} + [\omega_u^2]\{p_u\} = \{Q_u\} \tag{15}$$

where the diagonal form of the coefficient matrices of $\{\ddot{p}_u\}$ and $\{p_u\}$ follows from the properties of normal modes. $[\omega_u]$ is the diagonal matrix of undamped modal frequencies of the composite structure in radians per second.

The damped eigenvalue problem

$$[I]\{\ddot{p}_u\} + [C_u]\{\dot{p}_u\} + [\omega_u^2]\{p_u\} = \{0\} \tag{16}$$

is solved for the complex eigenvectors, $[V_D]$.

Writing

$$\{p_u\} = [V_D]\{p_D\}$$

the complex equations for damped motion of the composite system, in uncoupled form, are

$$[R]\{\dot{p}_D\} - [R][\lambda]\{p_D\} = \{Q_D\} \tag{17}$$

where

$$[R] = 2[\lambda][V_D^T][V_D] + [V_D^T][C_u][V_D]$$

and

$$\{Q_D\} = [V_D^T]\{Q_u\} .$$

$[\lambda]$ is a diagonal matrix of complex eigenvalues associated with the eigenvectors, $[V_D]$. Derivation of this final transformation to uncouple the coordinates is described in Ref. [8].

With the equations of motion in uncoupled form, solution for the response of the composite structure to steady state sinusoidal accelerations of the base system is a straightforward procedure. For steady state sinusoidal response at frequency ω,

$$\{\dot{p}_D\} = i\omega\{p_D\} . \tag{18}$$

Substituting for $\{\dot{p}_D\}$ from Eq. (18) into Eq. (17),

$$[D]\{p_D\} = \{Q_D\} \tag{19}$$

where

$$[D] = [i\omega[I] - [R][\lambda]]$$

is a complex diagonal matrix.

The generalized forces in the damped modes are given by

$$\{Q_D\} = -[V_D^T][\Phi_u^T][M_{ER}]\{\ddot{p}_R\} \tag{20}$$

where $\{\ddot{p}_R\}$ are the specified input accelerations of the base system and $[M_{ER}]$ is the mass coupling submatrix between the rigid body modes of the base system and the independent elastic component modes.

Equation (19) is solved for $\{p_D\}$ at discrete frequencies in the range over which the dynamic response of the structure is to be investigated. Frequencies are increased in equal increments, specified in the program input data, from the minimum to the maximum value. The uncoupled composite system coordinates, $\{p_D\}$, are related to the component lumped mass degrees of freedom by

$$\{u\} = [T]\{p_D\} \tag{21}$$

where

$$[T] = [\gamma][\lambda][\Phi_u][V_D] .$$

By applying the appropriate inverse transformation, the frequency responses of selected lumped mass degrees of freedom are obtained. The program generates data required for automatic plotting of these responses. A typical frequency response plot is shown in Fig. 1. At peak resonant frequencies, the participation factors (complex) for the component normal modes are computed. At those frequencies judged critical for a particular component from the loads standpoint, attachment forces are calculated.

Returning to the SAMIS program, the inertia forces in the modes at critical response frequencies, together with concentrated attachment forces, are applied through the component stiffness matrix to obtain joint displacements. The corresponding internal load distribution in the finite element model of the component is then computed.

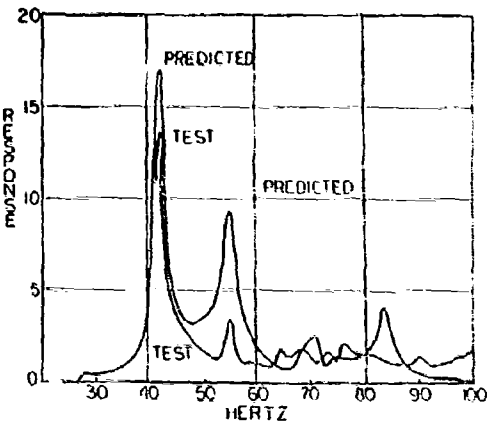

Fig. 1. Frequency response of infrared spectrometer mounted on the PSP

M69 ANALYSIS

The structure analyzed consisted of the M69 spacecraft mounted on two cylindrical adapters that constitute the structural interface between the spacecraft and launch vehicle. The primary structure or bus forms the structural core of the spacecraft, providing support for the other subsystems (Fig. 2). It consists of two octagonal rings approximately 66 in. in diameter joined at the eight corners by longerons each about 16 in. long. Chassis, which house electronic component modules, occupy seven bays of the octagonal framework and, acting as shear plates, form an integral part of the load carrying structure. The eighth bay contains the propulsion subsystem.

A truss-type structure inside the bus supports the planetary scan platform, which is latched to the lower octagon ring during launch. Four solar panels, hinged at the upper octagon ring, are coupled together through spring/dampers at their tips during launch, forming a box-like structure (Fig. 3). The parabolic reflector of the high gain antenna is mounted on a truss-type superstructure which is also attached to the upper ring of the bus. The low gain antenna, a 4-in. diameter mast about 7 ft long is mounted on one of the spokes of the upper octagon ring and is supported in a vertical position by two spring/damper struts at a point approximately 24 in. above the spoke. Other items of less structural importance include the attitude control gas bottles, various instruments and sensors, and cabling support structures. The total spacecraft weight is 830 lb, while the combined weight of the two adapter assemblies is 85 lb.

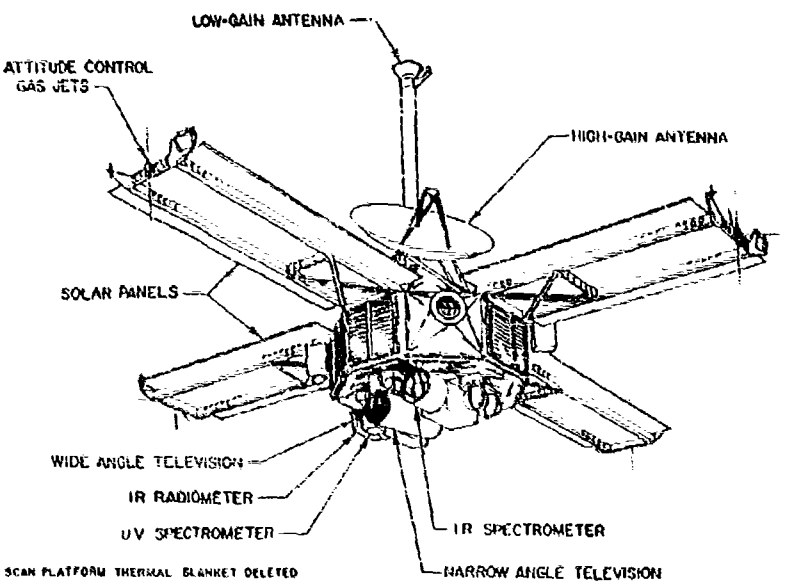

Fig. 2. MARINER MARS 1969 spacecraft

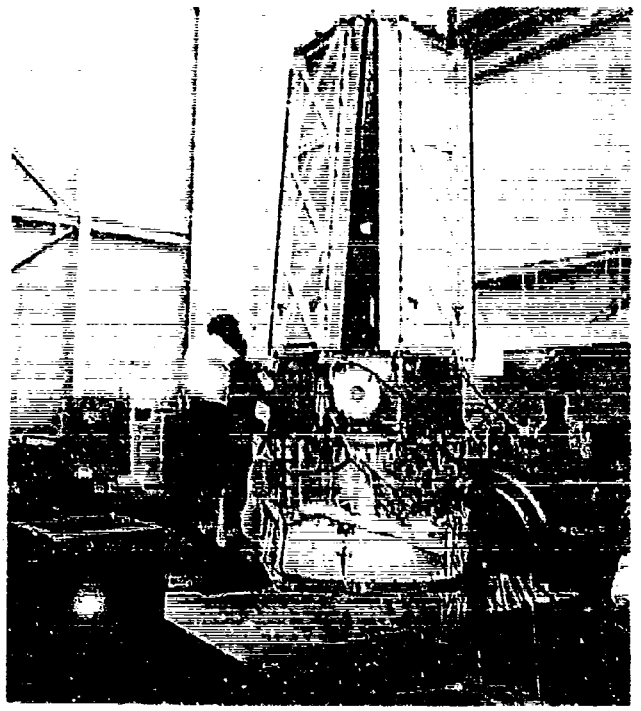

Fig. 3. DTM forced vibration test setup

Component Analyses

Finite element analyses were performed on six structural components: bus/two adapter assembly, planetary scan platform (PSP), propulsion subsystem (PROPS), solar panel, high gain antenna and superstructure, and low gain antenna mast.

The boundary conditions for the isolated components approximated the actual support while minimizing the number of constraints. A finite element model of each of the above structures was built and the component modes, required for modal combination analysis of the composite, were generated using SAMIS. A brief outline of the solar panel analysis is given as a typical example of a component analysis.

Each panel (Fig. 4) has a rectangular platform with an 84-in. span and a 35-in. chord. The panels are of lightweight construction with a structural weight of 0.6 lb per sq ft. The main load carrying structure consists of two hat-section spars, cross-braced and joined by intercostals. The 0.005-in. face sheet, which supports solar cells, is bonded to a corrugated backing sheet (Fig. 5). This assembly, referred to as the substrate, is bonded to the spars which are hinged to the bus through fittings at their inboard ends.

A finite element model of the panel consisting of an assemblage of beam (line) elements was constructed (Fig. 6). The locations and stiffness assigned to the elements were chosen so as to realistically represent the panel shear, bending, and torsional stiffnesses. Spar and intercostal elements were located at the neutral axes of these members. Typically, each had stiffness in all 6 degrees of freedom, while cross-bracing elements were assigned axial stiffness only. The panel was divided into sections by a series of spanwise and chordwise cuts. The effective shear, bending, and torsional stiffness of the 12-in. wide strips of substrate were assigned to chordwise elements located at the neutral axis of the substrate. Spanwise and nonintersecting criss-cross elements in the plane of the face sheet, with axial stiffness only, were also used. The stiffnesses were such as to approximate the effective contribution of the face sheet to in-plane shear and axial stiffness. Along the spars, spanwise

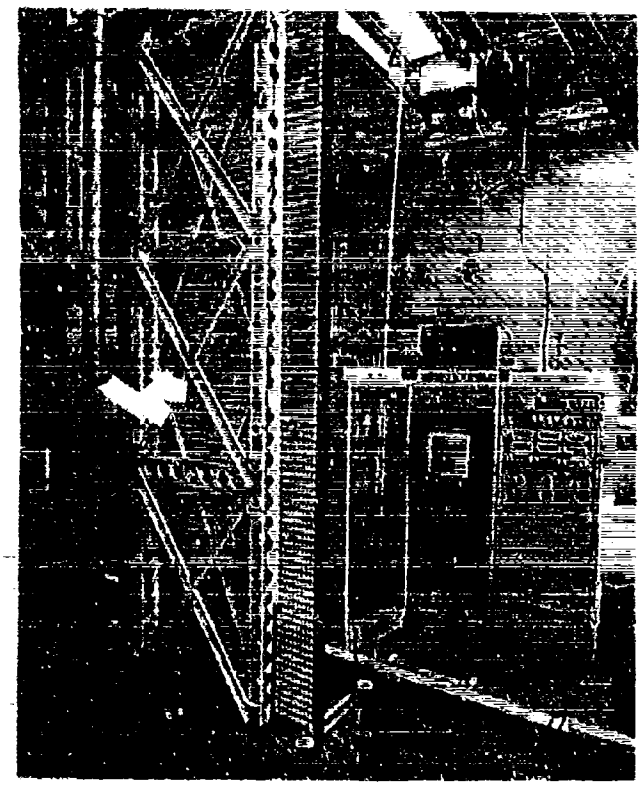

Fig. 4. Solar panel static test setup

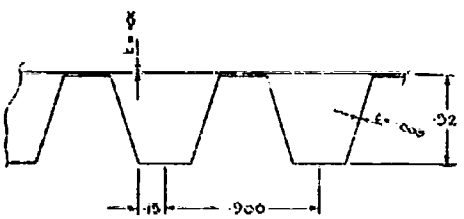

Fig. 5. Cross section of solar panel substrate

displacement discontinuities, between the substrate and the spars, were introduced by allowing for the effective spring between the substrate and the spars, thereby permitting in-plane motion of the substrate relative to the spars.

The panel weight was lumped at 56 node points. However, because of the restriction on the number of lumped mass degrees of freedom (≤ 130) imposed by the eigenvalue routine, a different mass lumping pattern was used in each of three mutually perpendicular directions. A relatively refined distribution was used in the out-of-plane direction of primary panel motion, while coarser distributions were used in the in-plane directions. In the boost configuration each solar panel is hinged at the bus and coupled through the tip latch spring/dampers to the two adjacent panels with boundary conditions somewhere between hinged-free and hinged-pinned. Either assumption could have been used to generate modes, because the modal combination analysis can combine either kind of attachment if proper allowance is made for the spring/dampers. The hinged-free condition was chosen as this was closer to the composite condition and as the single panel modal test was easier to implement with this type of support. Some results of this analysis are listed in Table 1, and a typical mode shape is shown in Fig. 7

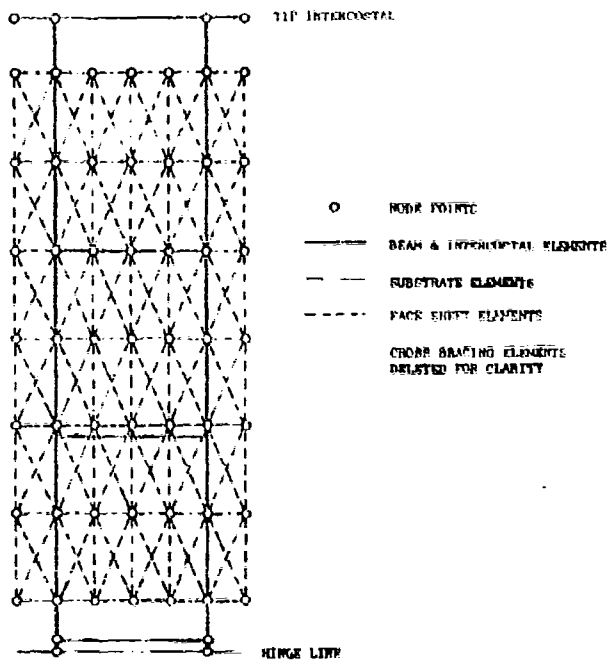

Fig. 6. Finite element model of solar panel

TABLE 1
Solar Panel Modal Characteristics

Mode No.	Predicted , Hz	Test , Hz	Type of Mode Shape
1	18	23	First Torsion
2	27	29	First Spar Bending
3	37	34	First In-Plane Bending
4	57	63	Second Torsion
5	76	78	Second Spar Bending
6	96	94	Third Torsion

System Analyses

The solar panel and low gain antenna analyses were complicated by the presence in each of nonlinear spring/dampers, whose stiffness and damping coefficients are functions of frequency and amplitude. Spring/damper characteristics were based on extensive tests. The modal combination program, however, in its present form, is limited to linear damping inputs. This problem was circumvented by the use of an iterative technique wherein the damper coefficients corresponding to a single peak response frequency were estimated. A response analysis was conducted over a relatively narrow frequency band for each resonance. Amplitudes were examined, adjusted coefficients were computed, and the response analysis was then repeated until a satisfactory match between input and calculated coefficients was obtained. This procedure was used with reasonable success to predict amplitudes and frequencies of low frequency resonances of the solar panels and low gain antenna.

Analog computer studies of the nonlinear response of the solar panel system have also been conducted and are being refined. A number of lower frequency undamped modes of the assembly were generated for use in these studies, which give real time variation of spring/damper coefficients with frequency and amplitude. Differences between individual spring/dampers, as obtained from tests, are also accounted for.

Composite Spacecraft Analyses

After assembly of the components, the number of independent component modes must

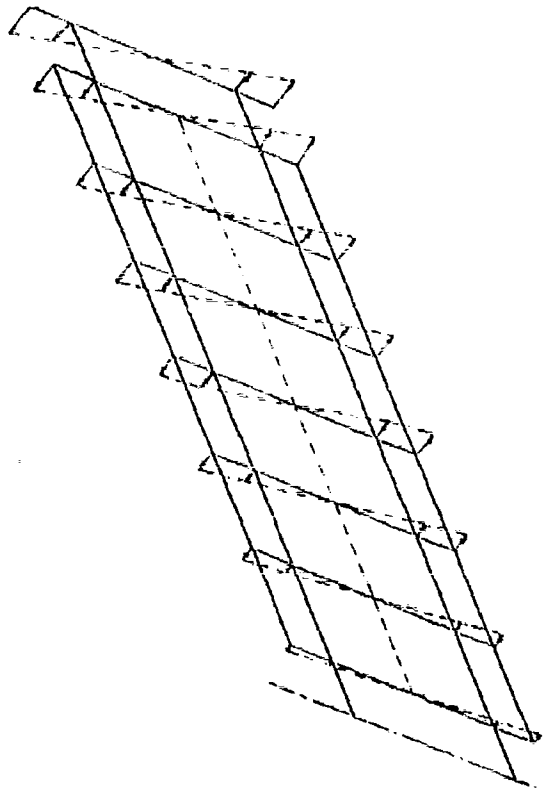

Fig. 7. First torsional mode of solar panel

be less than or equal to 100. The uncoupled generalized coordinates of Eq. (17), the damped modes of the composite structure, are linear combinations of a truncated set of undamped modes. These may not exceed 50 in number. On the MM'00 project, it was judged that for all major structural components, high gain antenna reflector excepted, most critical resonances would occur in the low frequency range up to 100 Hz. This established an upper frequency of about 100 Hz as one truncation criterion, as higher frequency modes would not significantly affect the response below 100 Hz.

The number of modes and the frequency range of normal modes for major components of the M69 composite spacecraft analysis are shown in Table 2. In addition to the components listed in Table 2, the ten spring/dampers were included as separate basic systems with simple axial displacement modes. This brought the total number of independent modes to 96, four less than the maximum allowed by the program. The lowest 50 composite system modes, ranging in frequency from 0 to 114 Hz, were retained.

Structural damping information is input to the modal combination program in the form of single generalized damping coefficients associated with each component mode. For normal modes, these were either estimated from modal test results or assumed to be one percent of critical damping. The damping coefficient C_i for the ith mode is given by

$$C_i = 2\left(\frac{C_i}{C_c}\right) M_i \omega_i \tag{22}$$

where M_i is the generalized mass in the ith mode, and ω_i is the ith modal frequency (rad/sec). It follows from the properties of normal modes that

$$\omega_i = \sqrt{\frac{K_i}{M_i}} \tag{23}$$

TABLE 3
List of Component Modes Included in Composite Analysis

Basic System No.	Component	Number of Modes				Frequency Range (Hz)	No. of Independent Modes
		Rigid Body	Constraint	Attachment	Normal		
1	Bus Adapters	6	0	7	11	45-157	24
2	Planetary Scan Platform (PSP)	6	3	0	6	81-158	6
3	Propulsion Subsystem (PROPS)	6	3	6	6	110-228	6
4	Solar Panel (Each Panel)	6	1	0	10	19-124	10
5	High Gain Antenna	6	3	0	6	113-230	6
6	Low Gain Antenna	6	2	0	9	15-177	0

Therefore,

$$C = 2\left(\frac{C}{C_c}\right)\sqrt{M_i K_i} \quad (24)$$

Although no relationship similar to Eq. (24) exists for constraint and attachment modes, an attempt was made to treat them in a manner similar to normal modes with an equivalent damping ratio of 0.01. Justification for this rationalized approach exists only where the generalized mass and stiffness submatrices associated with the constraint and attachment modes are dominantly diagonal. The treatment of structural damping has been the least satisfactory aspect of the M69 analysis and is being studied further using modal survey and forced vibration test data. Iteration of solar panel and low gain antenna damped characteristics in the composite spacecraft analysis would have required a prohibitive amount of computer time. The problem was avoided by assigning representative linear characteristics to the spring dampers in the 25 to 100 Hz range, an approach justifiable on the basis that amplitudes for frequencies greater than 25 Hz are relatively smaller and hence nonlinear effects are less significant. The composite spacecraft analysis was therefore considered applicable to all components in the 25 to 100 Hz range.

The frequency response of acceleration at selected points on the structure to various lateral and axial sinusoidal accelerations of the base system was computed. Of special interest were points on the scan platform, solar panels, and low gain antenna. Some of the more significant results are discussed and correlated with test data in a later section.

TEST PROGRAM

The primary objective of the M69 structural test program has been to obtain data for correlation with analytic results. Three types of structural tests have been conducted: static, modal, and forced response. The first series of tests took place early in the program using a crude Structural Analysis Model (SAM) to investigate the structural characteristics of the primary structure. The model consisted of a MARINER '64 octagon with simulated chassis boxes and motor, together with the Centaur adapter, an early version of the spacecraft adapter and a crude simulation of the PSP. Testing has just been completed on the Developmental Test Model (DTM), a structurally complete spacecraft. This model was composed of MARINER '69 flight type structural hardware. Noncritical structures that had resonances below 200 Hz could be simulated but correct elastic and mass distribution were required. Noncritical structures with primary resonances above 200 Hz were generally only mass simulated.

Static tests were conducted on several structural assemblies by recording load/deflection data to obtain flexibility influence coefficients. For example, a solar panel static test was conducted with the panel hung from its octagon-mounting-hinges as shown in Fig. 4. One damper attach point was constrained while incremental loads were applied at the other. This test provided data for direct comparison with the analytic constraint mode shape. Flexibility values were obtained on the isolated spacecraft adapter and on the spacecraft together with the Centaur adapter for radial, tangential, and axial loading conditions. Similar tests were conducted with the spacecraft structure attached by introducing lateral, torsional, and axial loads separately into the top of the bus structure. An axial load test was also conducted on the PSP support structure.

Modal survey tests were conducted on the high gain antenna dish, on individual solar panels, on the PROPS (Fig. 6) and on the primary structure mounted on two adapters, both with

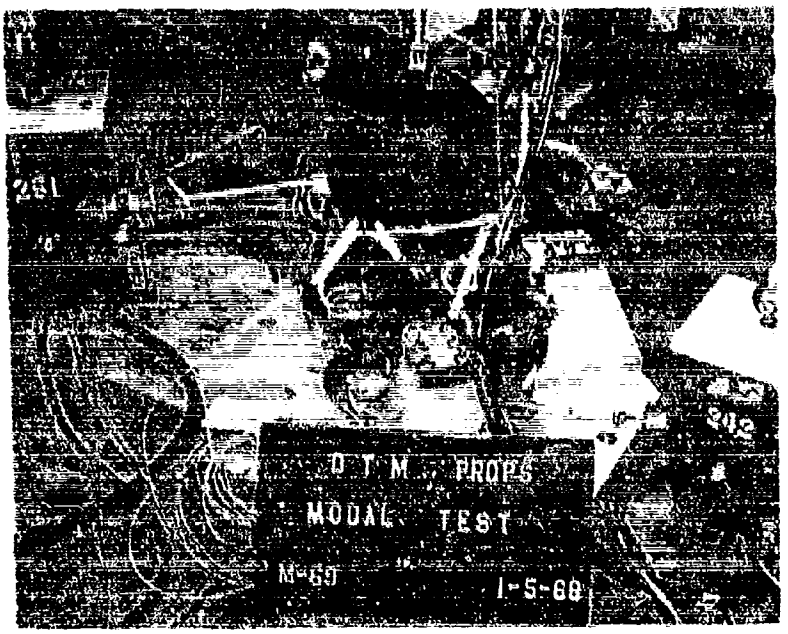

Fig. 8. Preps modal test setup

and without the PSP (Fig. 9). The solar panels and antennas were omitted because better analytic correlation could be obtained without the damped solar panel system and because the primary modal frequencies of the high gain antenna were considerably greater than those of the primary structure. In addition, accessibility through the top of the primary octagon structure facilitated driving and probing the PSP.

Each point in a lightly damped structure, vibrating in one of its normal modes, moves sinusoidally either in-phase with or 180 degrees out-of-phase with all other points. In the modal survey tests, electro-mechanical shakers were used to excite this condition. Up to eight small shakers, with variable force output directly proportional to the shaker current applied, were connected to the horizontal, abscissa sweep of an oscilloscope, and the instantaneous shaker current was connected to the vertical, ordinate sweep. This produced an elliptical Lissajous figure on the oscilloscope that closed into a sloping straight line at the modal frequency if shaker placement and excitation were exactly correct. An accelerometer response survey was then conducted. The accelerometers outputs were projected on an oscilloscope to establish the phase relationship and their amplitudes were recorded from voltmeter measurements. One accelerometer was fixed at a reference point that had relatively high displacement. The other, "rover" response accelerometer was moved to some 50 predetermined points on the structure recording amplitude and phase relationship. With the "rover" fixed at a high response point, a decay trace was obtained when the shaker current was abruptly terminated. This trace was subsequently analyzed using a logarithmic decrement expression to obtain an estimate of the amount of equivalent viscous damping. This estimate was sometimes verified by the half-power point technique to obtain response variation with shaker frequency for a constant shaker force input. By repeating this procedure, a plot of response vs frequency was constructed, and the "half-power point" frequencies were then used to calculate a value for the critical damping ratio present in that mode.

The experimentally determined mode shapes were investigated for orthogonality by computing the normalized form of the symmetric, generalized mass matrix. The amount by which the off-diagonal term values differ from zero is indicative of the degree of orthogonality that exists between the modes and

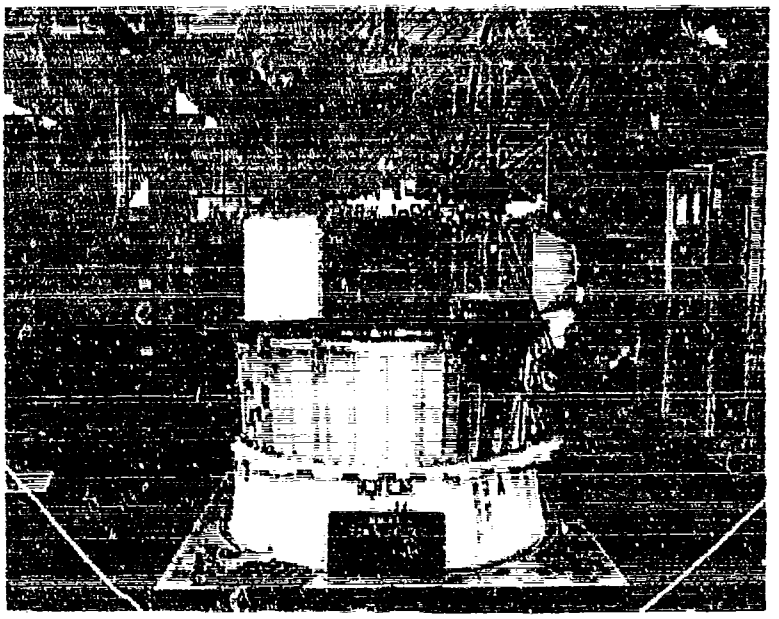

Fig. 9 Modal test setup for DTM modal configuration

provides confidence that a satisfactory mass matrix has been used.

A series of forced vibration tests was conducted on the assembled spacecraft and adapters mounted on an electromechanical shaker. For the structural development portion of these tests, logarithmic sine sweeps were conducted from 10 to 200 Hz at three levels of input excitation. The recorded response of some 10 critical accelerometers, out of a total of 80, were reviewed prior to going to the next input excitation level. Input excitation was applied along three lateral axes and in the thrust direction. After the test, the recorded outputs from some 10 strain gages and 80 accelerometers were narrow-band filtered and plotted for correlation with the predicted results.

ANALYSIS-TEST CORRELATION

In constructing finite element models of the various components it was necessary to make certain simplifying assumptions, with respect to weight distribution and geometry, to comply with program limitations. When the components were assembled analytically, further assumptions were made about modal content, attachment effectiveness, and damping in the modes. The test program provided a means of assessing the validity of these assumptions and assuring the development of a representative structural model of the composite spacecraft.

Structural Analysis Model (SAM)

Despite the relative crudeness of the hardware used, the SAM tests led to improvements both in modeling techniques and in actual structural hardware. Static and modal tests indicated an overestimation of the lateral and axial stiffnesses of the adapters. These discrepancies, traced to incorrect assumptions made in modeling the skin and the upper ring, were later resolved.

Unacceptably large excursions of the PSP, during forced vibration tests, were suppressed by the addition of more support structure. The forced vibration tests also provided data on vibration control techniques. All of the foregoing information was subsequently incorporated in the design, modeling, and testing of the DTM.

Developmental Test Model (DTM)

No structural failures were encountered in the DTM test program conducted during the period of January through April of this year. Comparison of test and analytic modal characteristics for the solar panel, PROPS, and DTM modal configuration are given in Tables 1, 3, and 4, respectively. In general, component and subsystem modal predictions show acceptable agreement with the test, the most notable exception being the higher modes of the DTM modal configuration (Fig. 9). For example the fourth predicted mode, the first torsional mode with a frequency of 70 Hz, was detected in test as the sixth mode at 92 Hz. This was considered surprising in view of the good agreement on static torsional stiffness. The discrepancy is attributed to the unanticipated stiffness contribution of the individual electronic component modules. Unavailable for the static tests, the modules were replaced by simple shear plates, resulting in a configuration that happened to coincide with modeling assumptions.

Orthogonality checks on the test modes indicate that the energy associated with the rotary inertias of instruments on the PSP is significant. For simplicity, this effect had been neglected in the SAMIS analysis. The analysis is currently being revised to include the PSP rotary inertias and improved modeling of the electronic modules.

Because much of the forced response test data had not been reduced at the time of writing, no general observations on test/analysis correlation can be made. However, Fig. 1 presents a fairly typical comparison of predicted and test frequency responses of an instrument on the PSP. While agreement on frequency is good, the predicted amplitude becomes increasingly conservative at higher resonances. It is anticipated that with the above noted analytical refinements and better estimates of modal damping, particularly in the higher modes, closer agreement between test and analysis over the full frequency range (25 to 100 Hz) will result.

TABLE 3
Propulsion Subsystem
Modal Characteristics

Mode No.	Predicted ω, Hz	Test ω, Hz	Type of Mode Shape
1	110	117	Tank Moving Vertically
2	137	142	Tank Moving Sidewise
3	152	168	Nozzle Canted Left
4	156	203	Nozzle Canted Right
5	222	220	Thrust Plate Oil Canning

TABLE 4
Modal Characteristics of
DTM Modal Configuration

Mode No.	Predicted ω, Hz	Test ω, Hz	Type of Mode Shape
1	35	35	Adapter Lateral Shear Bending
2	37	37	Adapter Lateral Shear Bending
3	51	43	PSP Rocking
4	70	55	PSP Rotating
5	74	57	PSP Bending
6	77	92	Adapter Twisting
7	85	104	PSP Rocking
8	100	112	Octagon Bus Breathing

REFERENCES

1. R. J. Melosh and H. N. Christiansen, "Structural Analysis and Matrix Interpretive System (SAMIS): Tech. Rept.," JPL TM 33-11, Nov. 1966

2. R. J. Melosh et al., "Structural Analysis and Matrix Interpretive System (SAMIS): Prog. Rept., JPL TM 33-307, Dec. 1966

3. R. M. Bamford, "A Modal Combination Program for Dynamic Analysis of Structures," JPL TM 33-290, Aug. 1966

4. Functional Requirement Mariner Mars 1969 Flight Equipment Structural Design Criteria," JPL M69-3-100A, June 1967

5. B. Wada, "Stiffness Matrix Structural Analysis," JPL TR 32-774, Oct. 1965

6. W. C. Hurty, "Dynamic Analysis of Structural Systems by Component Mode Synthesis," JPL TR 32-530, Jan. 1964

7. M. J. Turner et al., "Stiffness and Deflection Analysis of Complex Structures," J. Aero. Sci., 23(9):805-823 (Sept. 1956)

8. K. A. Foss, "Coordinates Which Uncouple the Equations of Motion of Damped Linear Solutions," J. Appl. Mech., 25 (1958)

DISCUSSION

F. Collopy (Itek Corp.): Was your mass matrix a consistent mass matrix?

Mr. Gaugh: Just on the diagonals.

Mr. Collopy: It was not necessarily a consistent mass matrix as defined by Archer?

Mr. Gaugh: No.

Mr. Collopy: Did you look into what effects it might have had?

Mr. Gaugh: No. We did consider the number of modal points to carry. For example, a propulsion motor has 43 mass points and we only monitor three. We were carrying some 50 points on our modal tests in three directions, so there are 150 readings to deal with. It took about a day for each mode.

P. Raney (NASA Langley Research Ctr.): I am interested in carrying a structural dynamics analysis along with the development of spacecraft. I think that is very laudable. To what extent did the people who are responsible for specifying environmental tests use your work and how much use would you see them making of it in the future?

Mr. Gaugh: They are aware of what we are doing. The biggest use they made was the use of our model once we got it all together. They are aware of our problems and we help them out too. As for using our program, yes, we could give them numbers, but what does it mean at the higher frequencies?

D. Stewart (McDonnell Douglas Corp.): Am I correct that the only load condition that you considered was a 2-g vibration test? Under what actual flight load conditions did you use your model?

Mr. Gaugh: The environment people specify the flight acceptance level and the type approval (TA) level. Then, in our structural requirements specification, we specify just how high we are going to take our development test model. We took it up to design ultimate.

Mr. Stewart: But what is that design ultimate based on? What kind of load condition?

Mr. Gaugh: The flight acceptance is the maximum expected load in flight. The TA is a 50 percent increase or 1.5 times the flight acceptance. The design ultimate is 1.25 times the TA loads. That was 1 g rms from 10 to 12 Hz to 150 Hz.

Mr. Stewart: Is this associated with a launch and ascent transient condition? Is there a relationship between your specification and design ultimate and a real launch condition, or is it just an arbitrary sine test that someone has found develops a good spacecraft?

Mr. Gaugh: I think the later statement is the true one. It is an envelope specified by the environments group. They leave it up to us as to how far above this condition we want to go. For instance, this summer the PTM will be taken to TA levels; then the two spacecraft will be taken to flight acceptance levels or what they really expect to encounter, not only during launch but also during exit.

W. Forlifer (NASA Goddard Space Flight Ctr.): The situation at Goddard is that the environmental test specification is not a requirement for designing the strength of the structure. The structure is designed based on the flight load. When the flight loads are exceeded by the vibration test, the test is notched down to the expected flight loads so that it partially compensates for that particular problem.

* * *

LINE SOLUTION TECHNOLOGY AS A GENERAL ENGINEERING APPROACH TO THE STATIC, STABILITY, AND DYNAMIC RESPONSE OF STRUCTURAL MEMBERS AND MECHANICAL ELEMENTS

Walter D. Pilkey
IIT Research Institute
Chicago, Illinois

and

Richard Nielsen, Jr.
Department of Transportation
Washington, D.C.

A structural analysis manual is described in this paper that can be used in a systematic fashion to find the static, stability, or dynamic response of a wide range of classical structural members and mechanical elements with arbitrary geometry and loading. The relatively unknown but efficacious line solution method is used throughout the manual to provide analytical solutions that are suitable for computational implementation. The computer-oriented version of line solution methodology which does not require the analytical solutions presented in the manual is also discussed.

INTRODUCTION

Line solution methodology provides a general approach to the response of structural members and mechanical elements. Through either analytical or computational means a static, stability, or dynamic response can be obtained for bars, spring mass systems, beams, thin-walled beams, strings, arches, membranes, plates, gridworks, thick shells, thin shells, and simple frameworks. These members are represented by classical theories of linear elasticity and strength of materials; the material may be elastic or simple viscoelastic; the geometries are basically those of classical structural members with arbitrary cross section; the loadings may be thermal or mechanical.

Frequently used synonyms for the line solution approach include the "transfer matrix method" or the "method of initial parameters." The approach differs inherently from the structural analysis technologies of "force" and "displacement" methods, although the line solutions can be coupled with other methods or transformed into them. Line solution methodology provides a highly efficient and general solution for the type of member for which it is suitable, that is, for a member exhibiting a naturally occurring (beam) or artificially derived (Levy rectangular plate) principal direction.

The purpose of this paper is to bring to attention a new manual [1] that uses the line solution methodology to provide analytical solutions for the response of structural members. The paper further provides an introduction to this method.

The manual and accompanying computer code will be available this year to Government agencies. The manual is arranged in chapters according to the type of members, beginning with simple extension and ending with thick and thin shells. The essential ingredients of the manual are tables that can be used in a systematic fashion to achieve response information. This is not a stress analysis handbook in which, for a prescribed loading and geometry, the maximum response variables, for example, stress or displacement, are tabulated; rather, this manual contains the information necessary to develop a complete solution for almost any geometric configuration and loading of structural members and mechanical elements. The pertinent design variables of high stresses and

displacements are readily ascertained from these solutions. The manual is intended to expedite the solutions of both simple and complex analysis problems and is suitable for use by graduates of engineering curricula.

The Basic Euler-Bernoulli beam is chosen here as a vehicle for explaining the mechanics of line solution methodology and the format and use of the manual. The other beam theories (shear, Rayleigh, Timoshenko) as well as the models for the previously mentioned structural members are treated in the manual in precisely the same fashion as the simple Euler-Bernoulli beam.

STATIC RESPONSE

The response of a beam to static loading takes the form

$$
\begin{aligned}
w(x) &= w_o L_{ww}(x,a_o) + \theta_o L_{w\theta}(x,a_o) + M_o L_{wM}(x,a_o) \\
&\quad + V_o L_{wV}(x,a_o) + L_{wF}(x,a_o) \\
\theta(x) &= w_o L_{\theta w}(x,a_o) + \theta_o L_{\theta\theta}(x,a_o) + M_o L_{\theta M}(x,a_o) \\
&\quad + V_o L_{\theta V}(x,a_o) + L_{\theta F}(x,a_o) \\
M(x) &= w_o L_{Mw}(x,a_o) + \theta_o L_{M\theta}(x,a_o) + M_o L_{MM}(x,a_o) \\
&\quad + V_o L_{MV}(x,a_o) + L_{MF}(x,a_o) \\
V(x) &= w_o L_{Vw}(x,a_o) + \theta_o L_{V\theta}(x,a_o) + M_o L_{VM}(x,a_o) \\
&\quad + V_o L_{VV}(x,a_o) + L_{VF}(x,a_o) .
\end{aligned}
\tag{1}
$$

where

x = coordinate along the beam (Fig. 1),

a_o = location of left end of beam,

w = deflection,

θ = slope,

M = moment,

V = shearing force,

w, θ, M, V = the state variables or the physical variables (deflection, slope, moment, and shearing force) that characterize the condition (state) of the beam,

$L_{kj}(x,a_o)$ ($k = w, \theta, M, V$ and $j = w, \theta, M, V$) = solution components, which as a whole comprise the field matrix, that are listed in tables for various beam types (Euler-Bernoulli, shear), geometries (constant or varying cross section) or material properties.

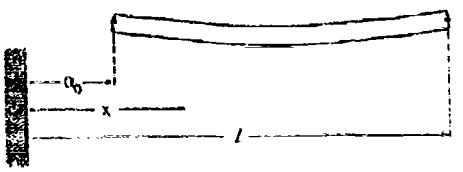

Fig. 1. Notation for beam

Much of the manual is composed of these tables which appear in the format of Table 1. The notation (x,a_o) indicates that the component L_{kj} is a function of x and is valid for a beam section beginning at $x = a_o$.

$$
\left.
\begin{aligned}
L_{wF} &= \sum_i L_{wF_i} \\
L_{\theta F} &= \sum_i L_{\theta F_i} \\
L_{MF} &= \sum_i L_{MF_i} \\
L_{VF} &= \sum_i L_{VF_i}
\end{aligned}
\right\} =
$$

loading functions that are listed in the form of Table 2 for particular thermal or mechanical loadings. The sum on i is taken over each loading that appears on the beam.

w_o, θ_o, M_o, V_o = the initial parameters or the initial ($x = a_o$) values of the state variables. The initial parameters are listed in tables such as Table 3 according to the conditions on the two ends of the beam. They are functions of the field matrix components $L_{kj}(x,a_o)$ and the loading functions $L_{kF}(x,a_o)$.

Equation (1) is the complete solution of the fundamental equations of motion in line solution or initial parameter form. These expressions describe the deflection, slope, moment, and shearing force for any value of the coordinates, and are fully determined by the contents of tables regardless of the complexity of the beam. The maximum values of the stresses and displacements along the beam are also determined from Eq. (1)

TABLE 1
Field Matrix

L_{jk} (k / j)	w	θ	M	V
w	L_{ww}	$L_{w\theta}$	L_{wM}	L_{wV}
θ	$L_{\theta w}$	$L_{\theta\theta}$	$L_{\theta M}$	$L_{\theta V}$
M	L_{Mw}	$L_{M\theta}$	L_{MM}	L_{MV}
V	L_{Vw}	$L_{V\theta}$	L_{VM}	L_{VV}

TABLE 2
Loading Functions

L_{jk} (k / j)	P F_1	M_1 F_2	q F_3	q F_4	q F_5	Thermal F_6	A Sudden Change in Any State Variable F_7
w	L_{wF_1}	L_{wF_2}	L_{wF_3}	L_{wF_4}	L_{wF_5}	L_{wF_6}	L_{wF_7}
θ	$L_{\theta F_1}$	$L_{\theta F_2}$	$L_{\theta F_3}$	$L_{\theta F_4}$	$L_{\theta F_5}$	$L_{\theta F_6}$	$L_{\theta F_7}$
M	L_{MF_1}	L_{MF_2}	L_{MF_3}	L_{MF_4}	L_{MF_5}	L_{MF_6}	L_{MF_7}
V	L_{VF_1}	L_{VF_2}	L_{VF_3}	L_{VF_4}	L_{VF_5}	L_{VF_6}	L_{VF_7}

TABLE 3
Initial Parameters for Static Solution

Pinned $\|\leftarrow a_o \rightarrow\|$ $w(a_o) = M(a_o) = 0$	Fixed $\|\leftarrow a_o \rightarrow\|$ $w(a_o) = \theta(a_o) = 0$	All $L_{kj} = L_{kj}(\ell, a_o)$
$w_o = 0$ $\theta_o = (L_{MF}L_{wV} - L_{wF}L_{MV})\,V$ $M_o = 0$ $V_o = (L_{wF}L_{M\theta} - L_{MF}L_{w\theta})\,V$ $V = L_{w\theta}L_{MV} - L_{M\theta}L_{wV}$	$w_o = 0$ $\theta_o = 0$ $M_o = (L_{MF}L_{wV} - L_{wF}L_{MV})\,V$ $V_o = (L_{MM}L_{wF} - L_{wM}L_{MF})\,V$ $V = L_{wM}L_{MV} - L_{MM}L_{wV}$	Pinned ℓ $w(\ell) = M(\ell) = 0$
$w_o = 0$ $\theta_o = (L_{\theta F}L_{wV} - L_{wF}L_{\theta V})\,V$ $M_o = 0$ $V_o = (L_{wF}L_{\theta\theta} - L_{\theta F}L_{w\theta})\,V$ $V = L_{w\theta}L_{\theta V} - L_{\theta\theta}L_{wV}$	$w_o = 0$ $\theta_o = 0$ $M_o = (L_{\theta F}L_{wV} - L_{wF}L_{\theta V})\,V$ $V_o = (L_{\theta M}L_{wF} - L_{wM}L_{\theta F})\,V$ $V = L_{wM}L_{\theta V} - L_{\theta M}L_{wV}$	Fixed ℓ $w(\ell) = \theta(\ell) = 0$

Tables 1 and 2 are listed in the manual for beams of constant and variable cross section, lying on Winkler or second-order foundations, with or without axial load, and of rigid material. Although no solution derivations are required for use of the manual, it may be of interest to study the origin of this type of solution.

A solution of the form of Eq. (1) is simply the conventional solution in which the arbitrary constants are written in terms of the initial parameters. Consider the derivation of this solution. The fundamental equations of motion for an Euler-Bernoulli beam are

$$EI\frac{d^4w}{dx^4} = q(x)$$

$$V(x) = -EI\frac{d^3w}{dx^3}$$

$$M(x) = -EI\frac{d^2w}{dx^2} \qquad (2)$$

$$\theta(x) = -\frac{dw}{dx}$$

where q, E, I are the loading intensity, Young's modulus, and moment of inertia, respectively. Direct integration gives

$$V(x) = C_1 - \int^x q(u)\,du$$

$$M(x) = C_2 + C_1x - \iint^x q(u)\,du$$

$$\theta(x) = C_3 + \frac{C_2x}{EI} + \frac{C_1}{2EI}x^2 - \iiint^x \frac{q(u)\,du}{EI} \qquad (3)$$

$$w(x) = C_4 - C_3x - \frac{C_2x^2}{2EI} - \frac{C_1x^3}{3!EI} + \iiiint^x \frac{q(u)\,du}{EI}$$

where C_1, C_2, C_3, and C_4 are arbitrary constants of integration that, when evaluated, provide the desired solution as the state variables w, θ, M, V are then fully determined functions of the known loading q, EI and the coordinate x. These integration constants are selected so that conditions on the ends of the beam are satisfied.

Although the integration constants are readily found for prescribed end (boundary) conditions, the task is eased, especially for complex members, if the integration constants C_1, C_2, C_3, and C_4 are rewritten in terms of physically significant variables at some point along the beam. There are four boundary conditions for a beam, two of which will be known at each end. If the four integration constants are written as functions of the four physical variables, deflection w, slope θ, moment M, and shear V, at one end of the beam then two of the constants will always be known by inspection. The state variables at the left hand end of the beam are chosen for this purpose. Because these are located at what is usually referred to as the origin, they are given the name initial parameters and are designated by w_o, θ_o, M_o, V_o.

It is clear from Eq. (3) that

$$w_o = w(0) = C_4$$

$$\theta_o = \theta(0) = C_3$$

$$M_o = M(0) = C_2$$

$$V_o = V(0) = C_1.$$

Then, Eq. (3) becomes

$$w(x) = w_o - \theta_o x - M_o\frac{x^2}{2EI} - V_o\frac{x^3}{3!EI} + \iiiint^x \frac{q(u)\,du}{EI}$$

$$\theta(x) = \theta_o + M_o\frac{x}{EI} + V_o\frac{x^2}{2EI} - \iiint^x \frac{q(u)\,du}{EI} \qquad (4)$$

$$M(x) = M_o + V_ox - \iint^x q(u)\,du$$

$$V(x) = V_o - \int^x q(u)\,du.$$

In terms of solution, Eq. (1) or Tables 1 and 2

$$L_{ww}(x,0) = 1, \quad L_{w\theta}(x,0) = -x, \quad L_{wM}(x,0) = -\frac{x^2}{2EI},$$

$$L_{wV}(x,0) = -\frac{x^3}{3!EI},$$

$$L_{wF}(x,0) = \iiiint^x \frac{q(u)\,du}{EI}$$

$$L_{\theta w}(x,0) = 0, \quad L_{\theta\theta}(x,0) = 1, \quad L_{\theta M}(x,0) = \frac{x}{EI},$$

$$L_{\theta V}(x,0) = \frac{x^2}{2EI},$$

$$L_{\theta F}(x,0) = -\iiint^x \frac{q(u)\,du}{EI} \qquad (5)$$

(Cont.)

$$L_{Ms}(x,0) = 0 \qquad L_{M\theta}(x,0) = 0,$$

$$L_{MN}(x,0) = 1, \qquad L_{MV}(x,0) = x, \qquad L_{MF}(x,0) = -\iint q(u)du$$

$$L_{Vw}(x,0) = 0, \qquad L_{V\theta}(x,0) = 0,$$

$$L_{VN}(x,0) = 0 \qquad L_{VV}(x,0) = 1,$$

$$L_{VF}(x,0) = \int q(u)du \qquad (5)$$

Tables 1 and 2 are developed in a similar fashion for members with axial loads, lying on foundations, with variable cross section, with various specific loadings q (for example, concentrated force or moment), etc. The loading functions for a uniformly distributed loading q_o spread along a uniform Euler-Bernoulli beam are given by (the F_3 column of Table 2)

$$L_{wF}(x,0) = \frac{q_o x^4}{4!EI}, \qquad L_{MF}(x,0) = -\frac{q_o x^2}{2} \qquad (6)$$

$$L_{\theta F}(x,0) = -\frac{q_o x^3}{3!EI}, \qquad L_{VF}(x,0) = q_o x.$$

These expressions are derived by setting $q(x) = q_o$ in the integrals of Eq. (4).

The initial parameters (that is, constants of integration) of Eq. (4) remain to be determined to complete the solution. Consider the simply supported beam of Fig. 2. The end conditions are

$$w(0) = 0, \quad M(0) = 0, \quad w(\ell) = 0, \quad M(\ell) = 0. \qquad (7)$$

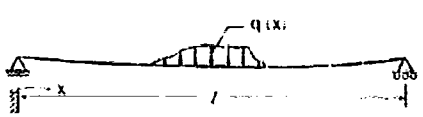

Fig. 2. Loaded beam

It is noted by inspection that

$$w(0) = 0 = w_o, \qquad M(0) = 0 = M_o. \qquad (8)$$

The remaining two initial parameters are evaluated by applying the final two conditions of Eq. (7) to Eq. (4). Thus,

$$w(\ell) = 0 = \theta_o \ell + V_o \frac{\ell^3}{3!EI} + \iiiint \frac{q(u)du}{EI}$$

$$M(\ell) = 0 \qquad V_o \ell = \iint q(u)du \qquad (9)$$

or

$$V_o = \frac{\iint q(u)du}{\ell}$$

$$\theta_o = -V_o \frac{\ell^2}{3!EI} + \frac{1}{\ell} \iiiint \frac{q(u)du}{EI}$$

$$= -\frac{\ell}{3!} \iint \frac{q(u)du}{EI} + \frac{1}{\ell} \iiiint \frac{q(u)du}{EI}. \qquad (10)$$

The solution is complete. These same results for the initial parameters are found by using Table 3, which is simply a tabulation of a more general version of Eqs. (8) and (10). Thus, referring to Table 3 for a pinned-pinned bar,

$$w_o = 0$$

$$\theta_o = \left[L_{MF}(\ell,0)\, L_{wV}(\ell,0) - L_{wF}(\ell,0)\, L_{MV}(\ell,0) \right] / \nabla$$

$$M_o = 0 \qquad (11)$$

$$V_o = \left[L_{wF}(\ell,0)\, L_{M\theta}(\ell,0) - L_{w\theta}(\ell,0)\, L_{MF}(\ell,0) \right] / \nabla$$

$$\nabla = L_{w\theta}(\ell,0)\, L_{MV}(\ell,0) - L_{M\theta}(\ell,0)\, L_{wV}(\ell,0).$$

Insertion of the components of Eq. (5) in relations of Eq. (11) gives

$$\nabla = (-\ell)(\ell) - (0)\left(\frac{-\ell^3}{3!EI}\right) = -\ell^2$$

$$w_o = 0$$

$$\theta_o = \left[\left(-\iint q(u)du \right) \left(-\frac{\ell^3}{3!EI} \right) - \left(\iiiint \frac{q(u)du}{EI} \right) \ell \right] / \nabla$$

$$= -\frac{\ell}{3!} \iint \frac{q(u)du}{EI} + \frac{1}{\ell} \iiiint \frac{q(u)du}{EI}$$

$$M_o = 0$$

$$V_o = \left[\iiiint \frac{q(u)du}{EI} (0) - \left(-\iint q(u)du \right) (-\ell) \right] / \nabla$$

$$= \iint \frac{q(u)du}{\ell} \qquad (12)$$

which coincide with the previous results (Eqs. (8) and (10)).

The initial parameters for a beam with uniformly distributed load q_o are given by Eq. (11) in which loading functions of Eq. (6) replace those of Eq. (5). In this case

$$w_o = 0$$

$$\theta_o = \left[\left(-\frac{q_o \ell^2}{2}\right)\left(-\frac{\ell^3}{3!EI}\right) - \left(\frac{q_o \ell^4}{4!EI}\right)\ell\right]\Big/ V = -\frac{q_o \ell^3}{24EI}$$

$$M_o = 0$$

$$V_o = \left[\left(\frac{q_o \ell^4}{4!EI}\right)(0) - (-\ell)\left(-\frac{q_o \ell^2}{2}\right)\right]\Big/ V = \frac{q_o \ell}{2}.$$

As Tables 1, 2, and 3 are provided in the manual for most beams, loadings, and all end conditions of interest, many of the above manipulations need not be conducted. The solution to a given problem is found by

1. Selecting the components L_{jk} ($j = w, \theta, M, V$ and $k = w, \theta, M, V$) for the appropriate beams from Table 1.

2. Taking L_{jF} ($j = w, \theta, M, V$) from Table 2 for the given loading.

3. Using Table 3 to calculate w_o, θ_o, M_o, V_o.

4. Inserting these results in Eq. (1) to give the full solution.

Because stresses are proportional to $M(x)$ and $V(x)$ they can be considered as known.

Often field matrices for structural members that possess abrupt in-span changes in cross section or material or in-span supports (for example, continuous beams) are not explicitly tabulated in the manual. In this case components L_{kj} ($k, j = w, \theta, M, V$) that take these intermediate changes into account must be developed for the whole span. Fortunately, this requires only a perfunctory effort. Changes that are not explicitly covered in the tables are accounted for by piecing together, with the aid of matrix multiplication, the field matrices from both sides of the change. No new unknowns are introduced by this manipulation. It is convenient to write the line solution of Eq. (1) in the extended matrix form

$$\begin{bmatrix} w \\ \theta \\ M \\ V \\ 1 \end{bmatrix}_x = \begin{bmatrix} L_{ww} & L_{w\theta} & L_{wM} & L_{wV} & L_{wF} \\ L_{\theta w} & L_{\theta\theta} & L_{\theta M} & L_{\theta V} & L_{\theta F} \\ L_{Mw} & L_{M\theta} & L_{MM} & L_{MV} & L_{MF} \\ L_{Vw} & L_{V\theta} & L_{VM} & L_{VV} & L_{VF} \\ 0 & 0 & 0 & 0 & 1 \end{bmatrix}_{(x, a_o)} \begin{bmatrix} w \\ \theta \\ M \\ V \\ 1 \end{bmatrix}_{a_o} \tag{13}$$

or

$$\bar{s}_x = \bar{L}(x, a_o)\bar{s}_{a_o} \tag{14}$$

where

$$\bar{s}_o = \bar{s}_{a_o}$$

$$\bar{s} = \begin{bmatrix} w \\ \theta \\ M \\ V \\ 1 \end{bmatrix}, \tag{15}$$

$$\bar{L}(x, a_o) = \begin{bmatrix} L_{ww} & L_{w\theta} & L_{wM} & L_{wV} & L_{wF} \\ L_{\theta w} & L_{\theta\theta} & L_{\theta M} & L_{\theta V} & L_{\theta F} \\ L_{Mw} & L_{M\theta} & L_{MM} & L_{MV} & L_{MF} \\ L_{Vw} & L_{V\theta} & L_{VM} & L_{VV} & L_{VF} \\ 0 & 0 & 0 & 0 & 1 \end{bmatrix}_{(x, a_o)} \tag{16}$$

If the field matrix appropriate for a particular section of a beam is designated by a superscript, then the solution for a beam with several changes in section (for example, Fig. 3) takes the form

$$\bar{s}_x = \bar{L}^0(x, a_o)\bar{s}_o, \qquad a_o \le x \le a_1$$

$$\bar{s}_x = \bar{L}^1(x, a_1)\bar{L}^0(a_1, a_o)\bar{s}_o, \qquad a_1 \le x \le a_2$$

$$\bar{s}_x = \bar{L}^2(x, a_2)\bar{L}^1(a_2, a_1)\bar{L}^0(a_1, a_o)\bar{s}_o, \qquad a_2 \le x \le a_3$$

$$\cdots\cdots\cdots\cdots\cdots\cdots\cdots\cdots\cdots\cdots$$

$$\bar{s}_x = \bar{L}^{n-1}(x, a_{n-1})\bar{L}^{n-2}(a_{n-1}, a_{n-2}) \cdots \bar{L}^2(a_3, a_2) \times \bar{L}^1(a_2, a_1)\bar{L}^0(a_1, a_o)\bar{s}_o, \qquad a_{n-1} \le x \le \ell$$

$$\bar{s}_\ell = \bar{L}^{n-1}(\ell, a_{n-1})\bar{L}^{n-2}(a_{n-1}, a_{n-2}) \cdots \bar{L}^2(a_3, a_2) \times \bar{L}^1(a_2, a_1)\bar{L}^0(a_1, a_o)\bar{s}_o = \bar{L}(\ell, a_o)\bar{s}_o \tag{17}$$

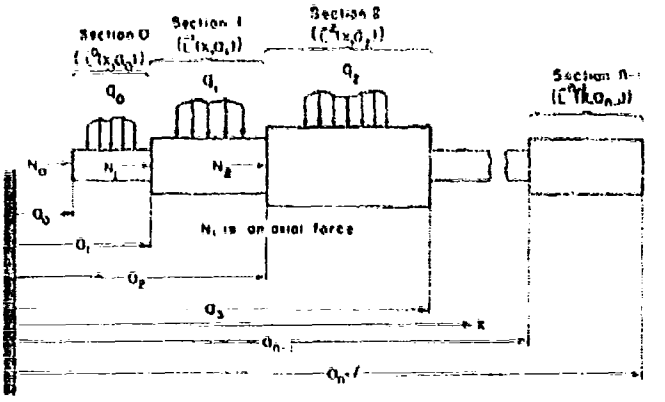

Fig. 3 Composite beam

This is a fully determined solution because the only apparent unknowns in Eq. (17) are the initial parameters $\bar{s}_{x_i}$ that are still evaluated by the expressions of Table 3 using the components of $L(x_n)$.

The reasoning behind Eq. (17) is worth considering. The first equation, that is,

$$\bar{s}_x = L^0(x, a_0)\bar{s}_{a_0} \qquad a_0 \le x \le a_1 \qquad (18)$$

is just a rewritten version of Eq. (1). For the second section isolated from the rest of the members

$$\bar{s}_x = L^1(x, a_1)\bar{s}_{a_1} \qquad a_1 \le x \le a_2 \qquad (19)$$

where the origin is now $x = a_1$. But, from Eq. (18),

$$\bar{s}_{a_1} = L^0(a_1, a_0)\bar{s}_{a_0} \qquad (20)$$

so that Eq. (19) becomes

$$\bar{s}_x = L^1(x, a_1)L^0(a_1, a_0)\bar{s}_{a_0} \qquad (21)$$

which corresponds to the second equation of Eq. (17). The remaining equations of Eq. (17) follow in suit.

The process of achieving a static solution can be briefly summarized as follows:

1. The solution is given by Eq. (1).

2. Find the appropriate components $L_{ij}(k = x, M, V)$ for the member at hand from the field matrix tables (for example, Table 1). If there are in-span changes in material or geometry, or supports, look up the components for each section of the member.

3. Find the loading components $L_{i,F}(k = x, M, V)$ for each section from the loading table (Table 2).

4. Use Eq. (17) to develop an overall field matrix that is valid for the whole member.

5. Use the components of the overall field matrix (step 4) to evaluate the initial parameters selected from Table 3 for the appropriate end conditions.

An array of beams that can be systematically solved using the manual is shown in Fig. 4. The field matrices (Table 1) essential for every occurrence shown are given in the manual and in no instance does the solution procedure differ from that just outlined.

STABILITY

The critical (buckling or unstable) load for a member is determined by following the first four steps of a static solution and then finding the lowest value of the axial load for which V of Table 3 is zero. This value is the critical load for the beam. The logic of this manipulation comes from classical buckling being a state for which, roughly speaking, the response variables increase inordinately. This state is reached if the denominator of the response, Eq. (1), approaches zero, that is, V as found in the initial parameter expressions (Table 3).

(a) Simple Beam

(b) Beam on Elastic Foundation

(c) Beam Column on Elastic Foundation

(d) Beam Column on Variable Elastic Foundation

(e) Stepped Beam Column on Variable Elastic Foundation

(f) Continuous Stepped Beam Column on Variable Elastic Foundation

(g) Continuous Stepped Beam with Variable Axial Load and Elastic Foundation

(h) Continuous Stepped Beam with Variable Axial Load and Both Continuous and Discrete Generalized Elastic Foundations

Fig. 4. Typical beams

DYNAMIC RESPONSE

Several time dependent motions, including free, steady state, quasi-static viscoelastic, viscous damped, and transient, can be treated using the manual. Only transient and free motions (frequencies and mode shapes) will be considered here because steady state and quasi-state responses reduce to static problems.

Normal mode transient solutions are employed in the manual. They take the form

$$w(x,t) = \sum_{i=1}^{\infty} A_i(t)\, w_i^*(x) \qquad (22)$$
(Cont.)

$$v(x,t) = \sum_{i=1}^{\infty} A_i(t)\, v_i^*(x)$$

$$M(x,t) = \sum_{i=1}^{\infty} A_i(t)\, M_i^*(x) \qquad (22)$$

$$V(x,t) = \sum_{i=1}^{\infty} A_i(t)\, V_i^*(x)$$

where

$$A_i(t) = \frac{e^{-\zeta_i \omega_i t}}{\omega_{di}} \left(\cos \omega_{di} t + \frac{\zeta_i}{\sqrt{1-\zeta_i^2}} \sin \omega_{di} t \right) \int_0^t m w(x,0)\, w_i^*(x)\, dx \qquad (23)$$
(Cont.)

$$+ \frac{e^{-\zeta_i \omega_i t}}{\omega_i \sqrt{1-\zeta_i^2}} \sin \omega_i t \int_{x_0}^{f} m w_i^*(x) \frac{\partial w(x,0)}{\partial t} dx$$

$$+ \int_0^t \left[\int_{x_0}^{f} q(x,\tau) w_i^*(x) dx + f_i(a_i, \tau) \right]$$

$$\cdot \frac{e^{-\zeta_i \omega_i (t-\tau)}}{\omega_i \sqrt{1-\zeta_i^2}} \sin \omega_i (t-\tau) d\tau \qquad (23)$$

and

t = time,

m = mass per unit length,

$q(x,t)$ = loading intensity,

ω_i = natural frequencies,

$w_i^*(x), \theta_i^*(x), M_i^*(x), V_i^*(x)$ = mode shapes,

$\omega_i = \omega_i (1-\zeta_i^2)^{1/2}, \zeta_i < 1$,

ζ_i = damping factor (= 0 for no damping),

$\gamma_i = \int_{x_0}^{f} m w_i^*(x) w_i^*(x) dx$, and

$f_i(a_i, \tau)$ = a function that takes into account prescribed time dependent in-span or end conditions (for example, displacements) at $x = a_i$.

For the Euler-Bernoulli beam the equations in Eq. (22) are the solutions of the equations of motion

$$\frac{\partial^2}{\partial x^2} EI \frac{\partial^2 w}{\partial x^2} = -m \frac{\partial^2 w}{\partial t^2} + q(x,t)$$

$$V(x) = -\frac{\partial}{\partial x} EI \frac{\partial^2 w}{\partial x^2}$$

$$M(x) = -EI \frac{\partial^2 w}{\partial x^2}$$

$$\theta(x) = -\frac{\partial w}{\partial x}$$

The mode shapes are constructed from the equations

$$w^*(x) = w_0 L_{ww}(x, a_0) + \theta_0 L_{w\theta}(x, a_0)$$

$$+ M_0 L_{wM}(x, a_0) + V_0 L_{wV}(x, a_0) \qquad (24)$$

(Cont.)

$$\theta^*(x) = w_0 L_{\theta w}(x, a_0) + \theta_0 L_{\theta\theta}(x, a_0)$$

$$+ M_0 L_{\theta M}(x, a_0) + V_0 L_{\theta V}(x, a_0)$$

$$M^*(x) = w_0 L_{Mw}(x, a_0) + \theta_0 L_{M\theta}(x, a_0)$$

$$+ M_0 L_{MM}(x, a_0) + V_0 L_{MV}(x, a_0) \qquad (24)$$

$$V^*(x) = w_0 L_{Vw}(x, a_0) + \theta_0 L_{V\theta}(x, a_0)$$

$$+ M_0 L_{VM}(x, a_0) + V_0 L_{VV}(x, a_0)$$

which are solutions of the free motion relations

$$\frac{d^2}{dx^2} EI \frac{d^2 w^*}{dx^2} = m \omega^2 w^*$$

$$V^*(x) = -\frac{d}{dx} EI \frac{d^2 w^*}{dx^2}$$

$$M^*(x) = -EI \frac{d^2 w^*}{dx^2}$$

$$\theta^*(x) = -\frac{dw^*}{dx}$$

The components L_{kj} $(k, j = w, \theta, M, V)$ are listed in the form of Table 1. Loadings are accounted for in Eq. (22) and are not considered in Eq. (24). The overall field matrix that embraces in-span changes is developed for Eq. (24) in the same manner as for the static response of Eq. (1). The initial parameters, w_0, θ_0, M_0, V_0, of Eq. (24) are taken from tables that appear as Table 4. The components L_{kj} $(k, j = w, \theta, M, V)$ contain a frequency parameter ω. The natural frequencies ω_i $(i = 1, 2, 3, 4, \ldots)$ are those values of ω for which V of Table 4 vanishes. These ω_i are substituted in solutions $w^*(x)$, $\theta^*(x)$, $M^*(x)$, $V^*(x)$ to give the mode shapes $w_i^*(x)$, $\theta_i^*(x)$, $M_i^*(x)$, $V_i^*(x)$ in Eq. (22). That is

$$w_i^*(x) = w^*(x)_{\omega=\omega_i}$$

$$\theta_i^*(x) = \theta^*(x)_{\omega=\omega_i}$$

$$M_i^*(x) = M^*(x)_{\omega=\omega_i} \qquad (25)$$

$$V_i^*(x) = V^*(x)_{\omega=\omega_i}.$$

This completes the dynamic solution. It is essentially classical normal mode theory in which tabularized line solution technology is used to develop the mode shapes. The array of

TABLE 4
Initial Parameters for Mode Shapes

Pinned	Fixed	
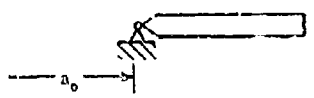	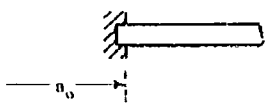	All $L_{kj} = L_{kj}(\ell, a_o)$
$w^*(a_o) = M^*(a_o) = 0$	$w^*(a_o) = \theta^*(a_o) = 0$	
$w_o = 0$ $\theta_o = \theta_o$ $M_o = 0$ $V_o = -\theta_o \frac{L_{M\theta}}{L_{MV}}$ $\nabla = L_{w\theta} L_{MV} - L_{M\theta} L_{wV}$	$w_o = 0$ $\theta_o = 0$ $M_o = M_o$ $V_o = -M_o \frac{L_{MM}}{L_{MV}}$ $\nabla = L_{wM} L_{MV} - L_{MM} L_{wV}$	Pinned 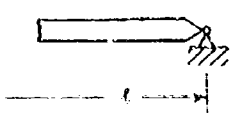 $w^*(\ell) = M^*(\ell) = 0$
$w_o = 0$ $\theta_o = \theta_o$ $M_o = 0$ $V_o = -\theta_o \frac{L_{\theta\theta}}{L_{\theta V}}$ $\nabla = L_{w\theta} L_{\theta V} - L_{\theta\theta} L_{wV}$	$w_o = 0$ $\theta_o =$ $M_o = M_o$ $V_o = -M_o \frac{L_{\theta M}}{L_{\theta V}}$ $\nabla = L_{wM} L_{\theta V} - L_{\theta M} L_{wV}$	Fixed 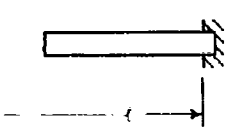 $w^*(\ell) = \theta^*(\ell) = 0$

beams shown in Fig. 4 with time dependent thermal or mechanical loadings can be solved using the manual, as can beams with prescribed time varying displacements (Fig. 5). Beam theories in the manual include Euler-Bernoulli (bending only), shear, Rayleigh (bending and rotary inertia), Timoshenko (bending, shear, and rotary inertia), and gyroscopic effects for rotating shafts. In addition, acceleration method (Mindlin-Goodman, Williams) solutions are contained in the manual because of their more rapid convergence characteristics.

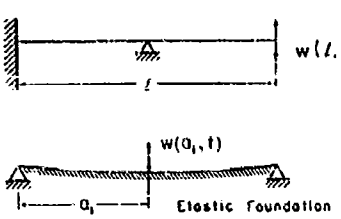

Fig. 5. Beams with prescribed displacements

REDUCTION OF MULTIPLE DIMENSION PROBLEMS TO LINE SOLUTION FORM

The line solution method deals fundamentally with structures possessing a chain-like geometry. Members not naturally exhibiting such a property must be appropriately transformed before line solution technology can be applied. This is accomplished [2] by applying, in all but one direction, a different analysis approach such as separation of variables [3], operational methods [4], finite differences [5], and stiffness or flexibility matrices [6,7].

SOLUTION TO MULTILINE PROBLEMS

Certain classes of problems of which gridworks or villages are prime examples consist of multiline topology with cross coupling between

lines. Cross coupling factors are obtained depending upon the particular problem at hand as in the reduction of multiple dimension problems discussed previously [7]. The solutions to these multiline problems are analogous to single line solutions. The field matrix elements in Table 1 are now square matrices of order equal to the number of lines. The loading function elements as given in Table 2 are now column matrices. Equation (15) then becomes

$$\bar{s} = \begin{bmatrix} w_i \\ \theta_i \\ M_i \\ V_i \\ I_i \end{bmatrix} \tag{26}$$

where i (=1, . . . , N) designates a line, w_i, θ_i, M_i, V_i are column matrices, and I_i is the unit column matrix. Equation (16) is changed in the same manner. Thus

$$\bar{L}(x, a_o) = \begin{bmatrix} L_{w,w} & L_{w,\theta} & L_{w,M} & L_{w,V} & L_{w,F} \\ L_{\theta,w} & L_{\theta,\theta} & L_{\theta,M} & L_{\theta,V} & L_{\theta,F} \\ L_{M,w} & L_{M,\theta} & L_{M,M} & L_{M,V} & L_{M,F} \\ L_{V,w} & L_{V,\theta} & L_{V,M} & L_{V,V} & L_{V,F} \\ [0] & [0] & [0] & [0] & [I] \end{bmatrix}_{(x, a_o)} \tag{27}$$

where [I] and [0] are the identity and null matrices, respectively, of order N. The solution proceeds now in all respects as before.

COMPUTER CODE

A FORTRAN IV computer code has been written to execute the solutions of the manual. The code is designed for use in conjunction with the manual in that it contains no reference to particular members or loadings although it automatically performs the manipulations essential to construct overall field matrices, to find critical loads, and to develop static and dynamic responses.

NUMERICAL DIFFICULTIES

Because the effect of loading on one end of a very long structural member is frequently not great on the other end, numerical difficulties during computations can occur. Moreover, the search for frequencies in $\nabla = 0$ often entails the differences of almost equal large quantities and again leads to an unfavorable computational situation. The determination of higher order frequencies for members with stiff in-span spring conditions or flexible in-span joints is particularly troublesome. A variety of schemes has been developed for overcoming these difficulties [8,9], the most effective being one that segments the member into computationally tractable sections.

COMPUTATIONAL VERSION OF THE LINE SOLUTION METHOD

Tables 1 and 2, the most essential ingredients of line solutions and hence of the manual, can be developed numerically [3,10-12]. Not only can all analytical solutions be duplicated numerically, but many problems for which analytical solutions are not available (for example, certain thin shell theories) can be solved by computational line solution methodology. The field matrices (Table 1) are usually constructed numerically by the integration of the first-order form of the differential equations of motion. In the case of the Euler-Bernoulli beam the equivalent first-order form of Eq. (2) is

$$\begin{aligned} \frac{dw}{dx} &= -\theta \\ \frac{d\theta}{dx} &= \frac{M}{EI} \\ \frac{dM}{dx} &= V \\ \frac{dV}{dx} &= -q \end{aligned} \tag{28}$$

Apart from the computational derivation of the basic field matrices, the analytical and numerical forms of line solutions are identical. That is, the manipulations essential to account for in-span and boundary conditions remain unaltered.

CONCLUSIONS

Line solution methodology has its origin [2] in the German elasticity school of more than a hundred years ago [13]. Its center of development moved to Russia [14] and then back to Germany [15]. Several thousand technical documents that employ this methodology have been written. Proponents of this approach to structural analysis laud the simplicity and

generality acquired while retaining a desirable degree of physical insight into the problem.

This approach, and hence the manual discussed here, involves no new structural models, theories of strength, constitutive or geometric representations, or enlightening results for specific members. Rather the manual has been developed for use in solving problems that historically belong to strength of materials. Structural member responses are achieved in the manual in a readily comprehensible systematic fashion.

ACKNOWLEDGMENTS

The development of this manual is supported by the U.S. Office of Naval Research; Naval Ship Systems Command; Naval Facilities Engineering Command; Office of Chief of Engineers, U.S. Army; Interdepartmental Ship Structure Committee; U.S. Air Force, Headquarters, Directorate of Civil Engineering. Contributions of R. Nielsen are supported by the Department of Transportation.

REFERENCES

1. W. D. Pilkey, R. Nielsen, and J. Tylke, "Manual for the Response of Structural Members," ONR Rept., 1968

2. W. D. Pilkey, "The Method of Initial Parameters," Proc., 4th Intl. Congress of Eng. Math., 1967

3. W. Wunderlich, "Calculation of Transfer Matrices Applied to the Bending Theory of Shells of Revolution," Proc. Intl. Symp., The Use of Electronic Digital Computers in Structural Engineering, Univ. of Newcastle Upon Tyne, 1966

4. J. Sulocki, "Application of Differential Operators to Problems of the Theory of Elasticity," Rozp. Inz., 1964, 12:339-396

5. S. M. A. Kazimi and C. A. Coull, "The Application of Line Solution Techniques for the Solution of Plane Stress Problems," Intl. J. Mech. Sci., 6:391-399, 1964

6. R. Kersten, Das Reduktionsverfahren der Baustatik (Springer, Berlin), 1962

7. R. Nielsen and F. C. Michelsen, "Grillage Structure Analysis Through Application of Laplace Integral Transform," Trans. Soc. Naval Arch. Marine Engrs., 1965, 73:216-240

8. C. A. Mercer, "On the Application of Transfer Matrices," Revue Francaise de Mecanique, 1965, 13:15-20

9. R. Uhrig, "The Transfer Matrix Method Seen as One Method of Structural Analysis Among Others," J. Sound and Vibration, 1966, 4:136-148

10. J. E. Goldberg, J. L. Bogdanoff, and W. D. Glauz, "General Computer Analysis of Beams," ASCE Proc., J. Engr. Mech. Div., 1964, 90:135-146

11. J. E. Goldberg, J. L. Bogdanoff, and L. Marcus, "On the Calculations of the Axisymmetric Modes and Frequencies of Conical Shells," Am. Acoust. Soc., 1960, 32:738-742

12. A. Kalnins, "Free Vibration of Rotationally Symmetric Shells," Amer. Acoust. Soc., 1964, 26:1355-1365

13. A. Clebsch, Theory of Elasticity of Solids (Teubner, Leipzig) 1862

14. I. M. Rabinovich, Structural Mechanics in the USSR 1917-1957 (Pergamon Press, New York), 1960

15. E. C. Pestel and F. A. Leckie, Matrix Methods in Elastomechanics (McGraw-Hill, New York), 1963

* * *

UPPER AND LOWER BOUNDS TO BENDING FREQUENCIES OF NONUNIFORM SHAFTS, AND APPLICATIONS TO MISSILES

Nathan Rubinatein, Vincent G. Sigillito, and James T. Stadter
Applied Physics Laboratory, The Johns Hopkins University
Silver Spring, Maryland

In this paper we compute upper and lower bounds to bending frequencies of nonuniform shafts. The mass and bending rigidity distributions are approximated by piecewise constant functions. Nonuniform free shafts often serve as good models for the study of missile bending vibrations. The upper bounds are obtained from the Rayleigh-Ritz method, the lower bounds result from an application of recently developed techniques of Bazley and Fox. A brief theoretical description of the lower-bound methods is included along with several illustrative examples.

INTRODUCTION

In missile development it is important to know precisely the frequencies of free vibration of elastic structures and structural elements. For a missile as a whole the frequencies and mode shapes in bending and torsion have a strong influence on performance of the control system. The frequencies and mode shapes of such other structural components as wings, fins, and panels are crucial in their aeroelastic (flutter) behavior in flight.

The nonuniform free shaft often serves as a good model for the study of missile bending vibrations; in this paper we assume the shaft to have piecewise constant stiffness and mass, both of which are distributed rather than lumped.

Although in principle this problem can be solved exactly, it is generally impractical to do so. To obtain the exact frequencies of a shaft with only a few nonuniformities it is necessary to find the roots of a large-order determinant with nonlinear entries. Methods are available for finding these roots; however, their use leads to many computational problems, as they are quite sensitive to roundoff error and usually require much computation time. Other existing methods, such as those that concentrate the mass and stiffness at points or apply difference techniques, give approximations of the frequencies but do not provide error estimates. Consequently, one cannot be certain of how accurate these approximations are. The methods presented here, however, give upper and lower bounds that bracket the true frequencies of the missile model, are computationally fast and accurate, can handle a large number of nonuniformities, and can be extended easily to handle shafts with more complicated variations of stiffness and mass.

The well-known Rayleigh-Ritz procedure is used to obtain the upper bounds. The problem of obtaining lower bounds is much more difficult, but recent work of Bazley and Fox has provided useful lower-bound procedures that are applicable to a wide variety of vibration problems [1,2]. More recently the authors were able to apply these theoretical results to obtain lower bounds to frequencies of various beams and shafts [3-6].

THEORETICAL BACKGROUND

The differential equation of the free bending vibrations of a free shaft is given by

$$\frac{d^2}{dx^2}\left[EI(x)\frac{d^2u}{dx^2}\right] - \omega^2 \rho(x) u = 0, \quad 0 \le x \le L,$$

$$u''(0) = u''(L) = u'''(0) = u'''(L) = 0,$$

where

$EI(x)$ is the bending rigidity,

$\rho(x)$ is the mass per unit length,

L is the length of the shaft, and

f is the circular frequency of bending vibration.

We assume $EI(x)$ and $\mu(x)$ are piecewise constant. Physical considerations dictate that the solution u be continuous, and $EI(x)u'$ continuously differentiable over the length of the shaft.

Because the theoretical methods are naturally expressed in terms of operators in Hilbert space, we treat the missile as a free shaft of unit length whose bending vibrations can then be described in the real Hilbert space $\mathcal{L}^2(-1/2,1/2)$* with inner product

$$(u,v) = \int_{-1/2}^{1/2} uv\,dx .$$

Let

$$h(x) = EI(x)$$

and

$$B(x) = \mu(x) .$$

Then the above eigenvalue problem becomes

$$\frac{d^2}{dx^2}\left[h(x)\frac{d^2u}{dx^2}\right] - \lambda B(x)u = 0 , \tag{1}$$

$$u'(-1/2) = u'(1/2) = u'''(-1/2) = u'''(1/2) = 0 ,$$

where the eigenvalue λ is related to the frequency f by†

$$\lambda = 4\pi^2 f^2 .$$

The stiffness and mass functions are chosen to be piecewise constant and to satisfy

$$0 < h^0 < h(x) \le H$$

$$0 \le m \le B(x) \le M ,$$

where h^0, H, m, and M are constants.

We now describe the methods used to compute upper and lower bounds to the eigenvalues of Eq. (1).

*We denote by $\mathcal{L}^2(-1/2,1/2)$ the space of all square integrable functions on the interval $(-1/2,1/2)$.

†The frequency for a beam of length L can be obtained from the equation $\lambda = 4\pi^2 f^2 L^4$.

Lower Bounds

The lower bounds are obtained using the method of intermediate problems [7-9] with special choice developed by Bazley and Fox [1].

The quadratic forms associated with the elastic (or strain) energy and the kinetic energy are given by

$$J_A(u) = \int_{-1/2}^{1/2} h(x)\,[u''(x)]^2\,dx$$

$$J_B(u) = \int_{-1/2}^{1/2} B(x)\,[u(x)]^2\,dx ,$$

respectively.

As required by the method, J_A can be decomposed as

$$J_A(u) = J_{A^0}(u) + (T_1u, T_1u)$$

$$= \int_{-1/2}^{1/2} h^0[u''(x)]^2dx + \int_{-1/2}^{1/2} [h(x)-h^0]\,[u''(x)]^2dx . \tag{2}$$

Therefore the operator T_1 is given by

$$T_1u(x) = [h(x)-h^0]^{1/2}u''(x)$$

and its adjoint T_1^* is given by

$$T_1^*v(x) = \frac{d^2}{dx^2}\left\{[h(x)-h^0]^{1/2}\,v(x)\right\}$$

with domain of definition $\mathcal{D}_{T_1^*}$ given by

$$\mathcal{D}_{T_1^*} = \Big\{ v \mid [h(x)-h^0]\,v \in \mathcal{L}^2(-1/2,1/2) ,$$

$$v(-1/2) = v(1/2)$$

$$= v'(-1/2) = v'(1/2) = 0 ,$$

$$\{(h(x)-h^0)^{1/2}v'(x)\}_{\xi_i} = 0,\ i = 2,3,\ldots,k \Big\} .$$

Here $\{\cdot\}_\xi$ denotes the jump in the function at the point ξ.

Also as required by the method, the quadratic form J_B can be decomposed as

$$J_B(u) = J_{B^0}(u) - (T_2u, T_2u)$$

$$= \int_{-1/2}^{1/2} M[u(x)]^2dx - \int_{-1/2}^{1/2} [M-B(x)]\,[u(x)]^2\,dx . \tag{3}$$

It therefore follows that the operator T_1 is given by

$$T_1 u(x) = [M - B(x)]^{1/2} u(x)$$

and its adjoint T_1^*

$$T_1^* v(x) = [M - B(x)]^{1/2} v(x)$$

with domain of definition

$$\mathfrak{D}_{T_1^*} = \mathfrak{D}^2(-1/2, 1/2)$$

The variational problem

$$\delta\left[\frac{J_{A^0}(u)}{J_{B^0}(u)}\right] = 0$$

for variations taken in $\mathfrak{D}_{J_{A^0}}$ gives rise to the eigenvalue problem

$$A^0 u - \lambda B^0 u = 0$$

which in our case is given by

$$u^{IV}(x) - \lambda \frac{M}{h^0} u(x) = 0,$$

$$u''(-1/2) = u''(1/2) = u'''(-1/2) = u'''(1/2) = 0.$$

This eigenvalue problem, referred to as a base problem, is resolvable as it corresponds to the problem of bending vibrations of a uniform beam with constant stiffness h^0 and constant mass M. Its eigenvalues λ_ν^0 and corresponding normalized eigenvectors u_ν^0, are given by

$$\lambda_\nu^0 = \begin{cases} 0, & \nu = 1 \\ 0, & \nu = 2 \\ \dfrac{h^0}{M}\alpha_{\nu-2}^4, & \nu = 3,4,\ldots \end{cases}$$

$$u_\nu^0 = \begin{cases} 2\sqrt{\dfrac{3}{M}}\,x, & \nu = 1, \\ \sqrt{\dfrac{1}{M}}, & \nu = 2, \\ \sqrt{\dfrac{2}{M(\cosh^2\alpha_{\nu-2} + \cos^2\alpha_{\nu-2})}}\,[\cosh\alpha_{\nu-2}\cos 2\alpha_{\nu-2}x \\ \quad + \cos\alpha_{\nu-2}\cosh 2\alpha_{\nu-2}x], & \nu = 3,5,7,\ldots \\ \sqrt{\dfrac{2}{M(\sinh^2\alpha_{\nu-2} - \sin^2\alpha_{\nu-2})}}\,[\sinh\alpha_{\nu-2}\sin 2\alpha_{\nu-2}x \\ \quad + \sin\alpha_{\nu-2}\sinh 2\alpha_{\nu-2}x], & \nu = 4,6,8,\ldots \end{cases}$$

where $\theta_\nu = (\alpha_{\nu-2}/2)$ and $\alpha_{\nu-2}$ is the $(\nu-2)$th positive root of the transcendental equation

$$1 + \cos\alpha\cosh\alpha = 0 \qquad (4)$$

or, equivalently, the α's with odd subscript can be obtained as the roots of the equation

$$\tan\frac{\alpha}{2} + \tanh\frac{\alpha}{2} = 0$$

and the α's with even subscript can be obtained as the roots of the equation

$$\tan\frac{\alpha}{2} - \tanh\frac{\alpha}{2} = 0.$$

The eigenvalues λ_ν^0 satisfy

$$0 = \lambda_1^0 \le \lambda_2^0 \le \cdots.$$

Because the quadratic form J_{A^0} is obtained from J_A by dropping the positive term $(T_1 u, T_1 u)$, and the quadratic form J_{B^0} is obtained from J_B by subtracting the positive term $(T_2 u, T_2 u)$, the eigenvalues λ_ν^0 give crude lower bounds to the eigenvalues of Eq. (1); that is, the eigenvalues satisfy

$$\lambda_\nu^0 \le \lambda_\nu, \qquad \nu = 1,2,\ldots. \qquad (5)$$

The lower bound procedure which is described in detail in Ref. [1], pp. 8-12, uses the first k_i elements of a given sequence $\{p_1^i, p_2^i, \ldots\}$ of linearly independent vectors belonging to $\mathfrak{D}_{T_i^*}$, $i = 1,2$, to construct intermediate quadratic forms that satisfy

$$\begin{aligned} J_{A^0} &\le J_{A^{k_1}} \le J_{A^{k_1+1}} \le J_A \\ J_{B^0} &\ge J_{B^{k_2}} \ge J_{B^{k_2+1}} \ge J_B \end{aligned} \qquad (6)$$

Consequently, the operator eigenvalue problem

$$A^{k_1} u - \lambda B^{k_2} u = 0 \qquad (7)$$

obtained from the variational equation

$$\delta\left[\frac{J_{A^{k_1}}}{J_{B^{k_2}}}\right] = 0$$

has ordered eigenvalues $\lambda_\nu^{k_1,k_2}$ that satisfy

$$\lambda_\nu^0 \le \lambda_\nu^{k_1,k_2} \le \left\{\begin{matrix} \lambda_\nu^{k_1+1,k_2} \\ \lambda_\nu^{k_1,k_2+1} \end{matrix}\right\} \le \lambda_\nu, \quad \nu = 1,2,\ldots. \qquad (8)$$

The operator eigenvalue equation (Eq. (7)) is given explicitly by

$$A^0 u + \sum_{i,j=1}^{k_1} (u, T_1^* p_i^1)\, b_{ij}^1\, T_1^* p_j^1 - \lambda \left\{ B^0 u - \sum_{i,j=1}^{k_2} (u, T_2^* p_i^2)\, b_{ij}^2 T_2^* p_j^2 \right\} = 0 \quad (9)$$

where the constants b_{ij}^1 and b_{ij}^2 are elements of the matrix inverse to that with elements (p_i^1, p_j^1) and (p_i^2, p_j^2) respectively.

The method of special choice requires us to find vectors $p_i^1 \in \mathfrak{D}_{T_1^*}$ and $p_i^2 \in \mathfrak{D}_{T_2^*}$ satisfying

$$T_1^* p_i^1 = \sum_{\sigma=1}^{n} \beta_{i\sigma}^1 B^0 u_\sigma^0, \qquad i = 1, 2, \ldots, k_1$$

and (10)

$$T_2^* p_i^2 = \sum_{\sigma=1}^{n} \beta_{i\sigma}^2 B^0 u_\sigma^0, \qquad i = 1, 2, \ldots, k_2.$$

Such a set of vectors satisfying Eq. (10) is given by

$$p_i^1 = \begin{cases} 0, & i = 1, \\ 0, & i = 2, \\ \sqrt{\dfrac{2M}{[h(x) - h^0](\cosh^2\theta_i + \cos^2\theta_i)}} \left(\dfrac{1}{2\theta_i}\right)^2 \\ \quad \times [\cos\theta_i \cosh 2\theta_i x - \cosh\theta_i \cos 2\theta_i x], & i = 3, 5, 7, \ldots, \\ \sqrt{\dfrac{2M}{[h(x) - h^0](\sinh^2\theta_i - \sin^2\theta_i)}} \left(\dfrac{1}{2\theta_i}\right)^2 \\ \quad \times [\sin\theta_i \sinh 2\theta_i x - \sinh\theta_i \sin 2\theta_i x], & i = 6, 8, \ldots, \end{cases}$$

$$p_i^2 = \begin{cases} \sqrt{\dfrac{12M}{M - B(x)}}\, x, & i = 1, \\ \sqrt{\dfrac{M}{M - B(x)}}, & i = 2, \end{cases}$$

(Cont.)

$$p_i^2 = \begin{cases} \sqrt{\dfrac{2M}{(M - B(x))(\cosh^2\theta_i + \cos^2\theta_i)}} \\ \quad \times [\cosh\theta_i \cos 2\theta_i x + \cos\theta_i \cosh 2\theta_i x], & i = 3, 5, 7, \ldots, \\ \sqrt{\dfrac{2M}{(M - B(x))(\sinh^2\theta_i - \sin^2\theta_i)}} \\ \quad \times [\sinh\theta_i \sin 2\theta_i x + \sin\theta_i \sinh 2\theta_i x], & i = 4, 6, 8, \ldots. \end{cases}$$

Upper Bounds

The upper bounds are obtained using the well-known Rayleigh-Ritz procedure in which we diagonalize a symmetric matrix with elements $R_{\mu\nu} = J_A(\Phi_\mu, \Phi_\nu)$ relative to the matrix $Q_{\mu\nu} = J_B(\Phi_\mu, \Phi_\nu)$ where the trial vectors Φ_μ are in $\mathfrak{D}_{J_A}$ and satisfy $(B\Phi_\mu, \Phi_\nu) = \delta_{\mu\nu}$.

Here we chose modified eigenvectors of the base problem, $u_i^{0\prime}$s, as the trial vectors Φ_ν. These are given by

$$\Phi_\nu = \begin{cases} 2\sqrt{3}\, x, & \nu = 1, \\ 1, & \nu = 2, \\ \sqrt{\dfrac{2}{\cosh^2\theta_\nu + \cos^2\theta_\nu}} \left(\dfrac{1}{2\theta_\nu}\right)^2 \\ \quad \times [\cosh\theta_\nu \cos 2\theta_\nu x + \cos\theta_\nu \cosh 2\theta_\nu x], & \nu = 3, 5, 7, \ldots, \\ \sqrt{\dfrac{2}{\sinh^2\theta_\nu - \sin^2\theta_\nu}} \left(\dfrac{1}{2\theta_\nu}\right)^2 \\ \quad \times [\sinh\theta_\nu \sin 2\theta_\nu x + \sin\theta_\nu \sinh 2\theta_\nu x], & \nu = 4, 6, 8, \ldots, \end{cases}$$

where $\theta_\nu = (\nu - 2)\pi/2$ and $\tau_{\nu-2}$ is the $(\nu-2)$th positive root of Eq. (4), above.

This leads to a symmetric matrix eigenvalue problem of order n given by

$$\sum_{\nu=1}^{n} \left[J_A(\Phi_\mu, \Phi_\nu) - \tilde{\lambda}^0 J_B(\Phi_\mu, \Phi_\nu) \right] c_\nu = 0, \qquad \mu = 1, 2, \ldots, n. \quad (13)$$

We choose k_1 of the vectors p_i^1 and k_2 of the vectors p_i^2, where p_i ($i=2$) and a_{i-2} is the $(i-2)$th positive root of Eq. (4) above. Here $\beta_{ij}^1 = \delta_{i+2,j}$, $\beta_{ij}^2 = \delta_{i,j}$ and $n = k_1 + 2 - k_2$. The integer n will correspond to the order of the matrix problem. Increasing the integer k_1 increases the quadratic form $J_{A^{k_1}}$ toward J_A and increasing the integer k_2 decreases the quadratic form $J_{B^{k_2}}$ toward J_B (see Eq. (6)), thus improving the lower bounds. Equation (9) now becomes a linear algebraic eigenproblem,

$$\sum_{j=1}^{n} \gamma_j \left\{ \lambda_0^0 \delta_{ij} + \sum_{r,s=1}^{k_1} \beta_{ir}^1 b_{rs}^1 \beta_{js}^1 - \lambda \left[\delta_{ij} - \sum_{r,s=1}^{k_2} \beta_{ir}^2 b_{rs}^2 \beta_{js}^2 \right] \right\} = 0 , \tag{11}$$

or equivalently in matrix notation

$$\gamma \left\{ A^0 + \beta_1^T B^1 \beta_1 - \lambda \left[I - \beta_2^T B^2 \beta_2 \right] \right\} = 0 , \tag{12}$$

where we have written β^T for the transpose of β. The eigenvalues $\lambda_{n+1}^0, \lambda_{n+2}^0, \ldots$, together with those determined from Eq. (12) are, when ordered according to magnitude, the eigenvalues $\lambda_i^{k_1,k_2}$ that provide lower bounds according to Eq. (8).

The eigenvalue λ_{n+1}^0 is the lowest persistent eigenvalue (P.E.) of the base problem, and the eigenvalues $\lambda_i^{k_1,k_2}$ that provide lower bounds are, for simplicity, written as $\bar{\lambda}_i^n$. We observe that only the eigenvalues less than λ_{n+1}^0 (the P.E.) give improved lower bounds. The eigenvalues of Eq. (13) satisfy

$$\lambda_i \leq \bar{\lambda}_i^n , \qquad i = 1, 2, \ldots, n ,$$

that is, they are upper bounds.

ILLUSTRATIVE EXAMPLES AND RESULTS

Digital programs that solve Eq. (12) for lower bounds and Eq. (13) for upper bounds have been written. The programs require only stiffness and mass data in standard engineering units. All necessary conversions, matrix constructions, arithmetic operations and inversions are done automatically by the programs. A detailed description of the programs and their use is given in our report [6].

We now give the results of two sample problems. In both examples we have used, as a model for the missile, a shaft with piecewise constant bending rigidity and mass per unit length.

The first example treats a simple case that illustrates the type of results obtainable from the procedure. Figures 1 and 2 give the bending rigidity and mass per unit length. The bounds to eigenvalues obtained from 15th-order

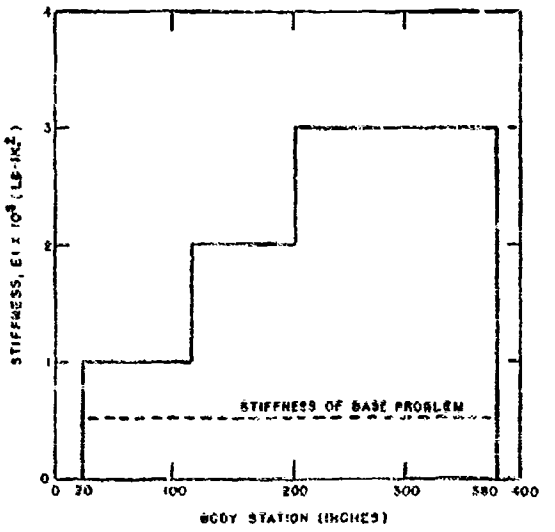

Fig. 1. Bending rigidity of a missile

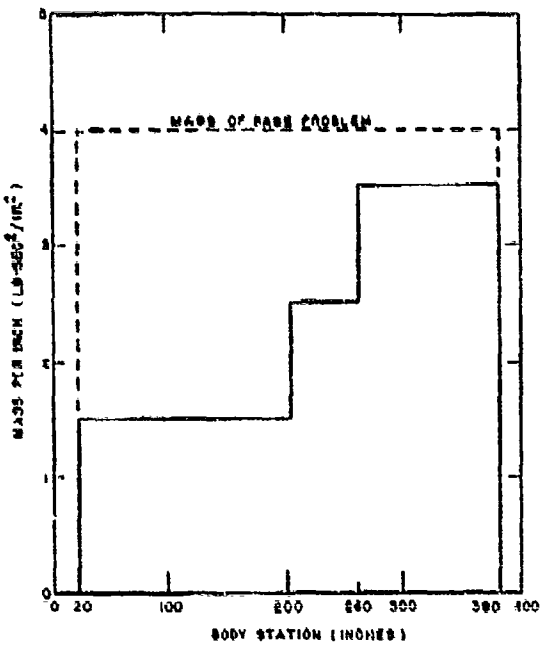

Fig. 2. Mass per unit length

calculations are given in the last two columns of Table 1; the corresponding bounds to the first 10 frequencies are given in Table 2. Both calculations required 0.03 hr running time on the 7094 digital computer at the Applied Physics Laboratory.

TABLE 1
Bending Vibrations of a Missile with Piecewise Constant Stiffness and Mass
(Bounds to Eigenvalues)

ν	15th Order Lower Bounds $\check{\lambda}_\nu^{15}$	15th Order Upper Bounds $\hat{\lambda}_\nu^{15}$
1	0	0
2	0	0
3	533.36904	541.40554
4	3072.6719	3733.3126
5	13127.906	13301.866
6	38142.218	38351.832
7	83437.986	84905.867
8	162550.79	164945.92
9	283705.27	289462.44
10	478565.63	482810.00
11	742855.86	761370.07
12	1096716.2	1130130.1
13	1572879.4	1611112.0
14	2295110.9	2384883.2
15	2458319.5	3276915.0

TABLE 2
Bending Vibrations of a Missile with Piecewise Constant Stiffness and Mass
(Bounds to Frequencies (Hz))

ν	15th Order Lower Bounds $\check{f}_\nu^{15}$	15th Order Upper Bounds $\hat{f}_\nu^{15}$
1	0	0
2	0	0
3	0.28361489	0.28574357
4	0.74422833	0.75034726
5	1.4070608	1.4163526
6	2.3983806	2.4049617
7	3.5472927	3.5783595
8	4.9511909	4.9875345
9	6.5410705	6.6071054
10	8.4954400	8.5330296

Our second example treats a more realistic missile structure. We have used a model with 16 discontinuities in bending rigidity and 45 in mass per unit length (see Figs. 3 and 4). The bounds to frequencies resulting from 10th- and 15th-order calculations are given in Table 3. (Notice that the higher-order problems give improved bounds.) The combined running time for the two cases for both upper and lower bounds was 0.17 hr.

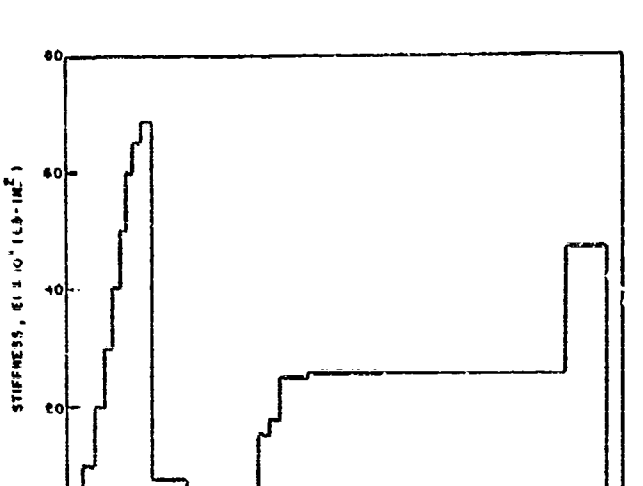

Fig. 3. Bending rigidity of a missile

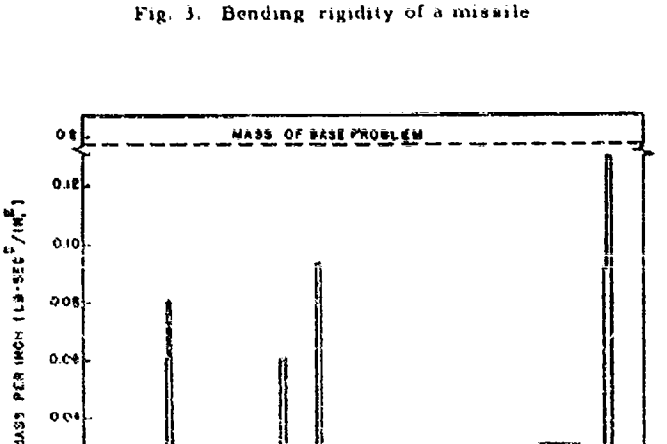

Fig. 4. Mass per unit length

TABLE 3
Bending Vibrations of a Missile with Piecewise Constant Stiffness and Mass
(Bounds to Frequencies (Hz))

r	10th Order Lower Bounds $\bar{f}_r^{10}$	10th Order Upper Bounds $\bar{f}_r^{10}$	15th Order Lower Bounds $\bar{f}_r^{15}$	15th Order Upper Bounds $\bar{f}_r^{15}$
1	0	0	0	0
2	0	0	0	0
3	35.443966	39.346530	35.553020	38.909800
4	82.901103	92.241955	83.072340	90.358313
5	—	—	169.25000	182.73066

REFERENCES

1. N. W. Bazley and D. W. Fox, "Methods for Lower Bounds to Frequencies of Continuous Elastic Systems," Zeits. angew. Math. u. Phys., 17:1-37 (1966)

2. N. W. Bazley and D. W. Fox, "Lower Bounds to Eigenvalues Using Operator Decompositions of the Form B*B," Archive for Rat. Mech. and Anal., 10:362-380 (1962)

3. N. Rubinstein, "Frequencies of Beams on Partial Elastic Foundations," Appl. Phys. Lab. Tech. Rept. TG-804, Mar. 1966

4. N. Rubinstein, V. G. Sigillito, and J. T. Stadter, "Torsional Frequencies of Uniform Shafts with Elastic Restraints and Elastically Attached Masses," Appl. Phys. Lab. Tech. Rept. TG-833, June 1966

5. N. Rubinstein, V. G. Sigillito, and J. T. Stadter, "Bounds to Torsional Frequencies of Non-uniform Shafts, and Applications to Missiles," Appl. Phys. Lab. Tech. Rept. TG-858, Oct. 1967

6. N. Rubinstein, V. G. Sigillito, and J. T. Stadter, "Bounds to Bending Frequencies of Non-uniform Shafts, and Applications to Missiles," Appl. Phys. Lab. Tech. Rept. TG-866, Feb. 1968

7. N. Aronszajn, "Approximation Methods for Eigenvalues of Completely Continuous Symmetric Operators," Proc. Symp. Spectral Theory and Differential Problems, Okla. A&M College, Stillwater, Okla., 1951, pp 179-202

8. S. H. Gould, Variational Methods for Eigenvalue Problems (Univ. of Toronto Press, Toronto), 1957

9. A. Weinstein, "Etudes des Spectres des Equations aux Dérivées Partielles de la Théorie des Plaques Elastiques," Memorial des Sciences Mathématiques, fasicule No. 88, Gauthier-Villars, Paris, 1937

* * *

DAMAGE PREDICTION FOR OPEN-FRAME STRUCTURES SUBJECT TO LIQUID PROPELLANT EXPLOSIONS

George C. Kao and Vince M. Conticelli
Wyle Laboratories
Huntsville, Alabama

and

Myer J. Rosenfield
U.S. Army Corps of Engineers
Ohio River Division Laboratories
Cincinnati, Ohio

The objective of this paper is to develop a method to predict damage to an aluminum open-frame structure subject to liquid propellant explosions.

Test structures were built and tested in actual explosive environments; this was conducted under Project PYRO, which is jointly sponsored by NASA and USAF. This project includes an extensive series of explosion tests using different kinds of cryogenic and hypergolic rocket propellants. The test structures were located along lines passing through ground zero and oriented 120 degrees with respect to each other and at distances of 23, 38, 67, and 117 feet, respectively, from the center of explosion. After each test, damaged structures were photographed, and strain responses were recorded by magnetic tape. Laboratory testing was also conducted to determine dynamic characteristics of the open frame structure.

Based on these data, analytical models for the test structures were formulated. Dynamic responses (stresses and displacements) of structural members subject to equivalent triangular impulsive loadings were evaluated. The failure criterion for each individual member was defined as the maximum stress which exceeds the yield stress of the structural material.

The comparison between the analytical and the experimental results is considered to be satisfactory.

INTRODUCTION

The sudden release of liquid propellant energy could create impulsive force sufficient to cause substantial damage (or destruction) to surrounding structures. Consequently, precautions must be taken to minimize such destructive effects on structures by providing adequate loading criteria for propellant explosions and practical design techniques for selecting structural members. The purpose of this paper is to report the development of a method to predict damage to open frame structures subject to liquid propellant explosions.

The typical structure to be investigated in this report consists of an open-frame, aluminum tubular structure, as shown in Fig. 1, designed and fabricated by the U.S. Army Corps of Engineers, Ohio River Division Laboratories, and tested at the Air Force Rocket Propulsion Laboratory, Edwards, Calif., under Project PYRO, which is jointly sponsored by NASA and USAF.

Test structures were placed in the test area along the three gage lines passing through ground zero and oriented 120 degrees with each other, and were spaced at distances of 23, 38, 67, and 117 ft, respectively, as shown in Fig. 2. After each explosive test, visual examination was made of damage occurring to structural members, and photographs of test structures were taken. Examination of damaged structures has revealed that the structural damage severities are directly related to the propellant yields and the distances from ground zero. The results of current explosive tests were compiled

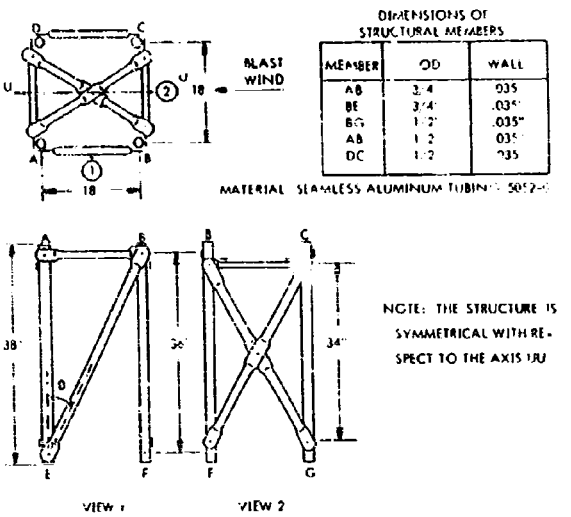

DIMENSIONS OF STRUCTURAL MEMBERS

MEMBER	OD	WALL
AB	3/4"	.035"
BE	3/4"	.035"
BG	1 1/2"	.035"
AB	1 1/2"	.035"
DC	1 1/2"	.035"

MATERIAL SEAMLESS ALUMINUM TUBING 5052-T6

Fig. 1. Aluminum open-frame structure used during Project PYRO tests

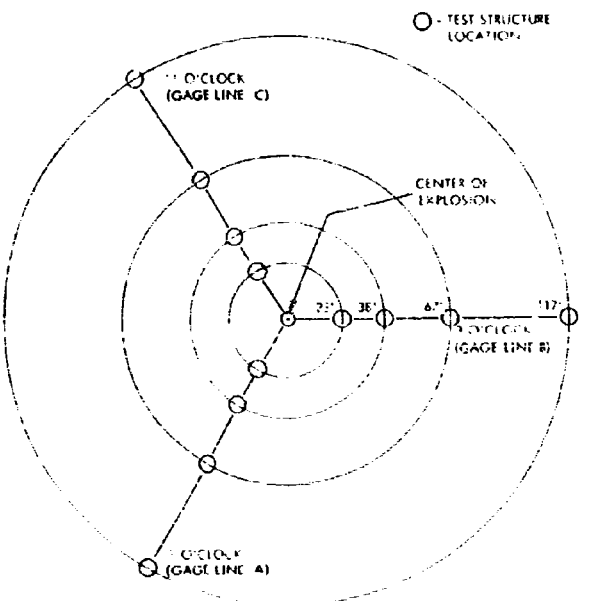

Fig. 2. Layout of test structure locations

and listed in Table 1. The structural damage severities can also be classified, according to the deformations of individual structural members, into the following four basic categories:

1. No damage (Fig. 3).
2. Deformation of bracings (Fig. 4).
3. Deformation of diagonals (Fig. 5).
4. Deformation of columns (Fig. 6).

Analytical procedures to predict critical loadings for which structural members will fail, are therefore, of practical interest to design engineers.

TABLE 1
Listing of Tests with Available Photographic Evidence of Structure Damage and Measured Equivalent TNT Yield

Test No.	Charge (lb	Propellant Type	Distance (ft)	Measured Equivalent TNT Yield (%) [1]	TNT Equivalent Charge (lb)	Symbol Used in Fig. 12
192-A	1000	LO_2/RP-1	23	10	100	□ 1
192-B	1000	LO_2/RP-1	38	6	60	△ 2
192-C	1000	LO_2/RP-1	67	9	90	☆ 3
193-A	1000	LO_2/RP-1	23	15	150	□ 4
193-B	1000	LO_2/RP-1	38	15	150	□ 5
193-C	1000	LO_2/RP-1	67	12	120	☆ 6
195-A	200	LO_2/LH_2	23	60	120	□ 7
195-C	200	LO_2/LH_2	67	40	80	☆ 8
209	1000	LO_2/RP-1	23	10	100	□ 9
209-A	1000	LO_2/RP-1	38	7	70	△ 10
209-B	1000	LO_2/RP-1	67	10	100	○ 11
209-C	1000	LO_2/RP-1	117	11	110	☆ 12
211-A	1000	LO_2/LH_2	23	7	70	□ 13
211-B	1000	LO_2/LH_2	38	4	40	○ 14
211-C	1000	LO_2/LH_2	67	6	60	☆ 15
213-A	1000	LO_2/LH_2	23	15	150	□ 16
213-B	1000	LO_2/LH_2	38	15	150	□ 17
213-C	1000	LO_2/LH_2	67	15	150	☆ 18
262-A	1000	LO_2/LH_2	38	28	280	□ 19
262-B	1000	LO_2/LH_2	67	30	300	☆ 20
266-A	1000	LO_2/LH_2	23	7	70	□ 21
266-B	1000	LO_2/LH_2	38	8	80	□ 22
275-A	25,000	LO_2/RP-1	67	1	250	□ 23
275-B	25,000	LO_2/RP-1	117	1	250	☆ 24

In the following analysis, the determination of impulsive loads generated by liquid propellant explosions will be investigated. The analytical models will be formulated to predict dynamic responses subject to propellant explosions.

DETERMINATION OF LOADS ACTING ON OPEN-FRAME STRUCTURES CAUSED BY PROPELLANT EXPLOSIONS

Once a propellant explosion occurs, a shock wave is generated. It moves outward at supersonic speed and is followed by a high velocity hot wind. On the shock front the pressure of the air rises almost instantaneously to a peak value, p_{so}, to decay rapidly afterward.

For open structures composed only of beams, columns, trusses, or other members with only small areas opposing the blast, each member receives an impulsive loading caused by the overpressure, and then is exposed to drag from the wind accompanying the blast. Unless the open-frame structure fails as a whole or in part without plastic deformation, it is reasonably accurate to consider the structure as being subjected only to drag, neglecting the impulsive loading caused by the overpressure. To simplify the loading function, its shape will be assumed to be triangular, as shown in Fig. 7, with the same positive impulse as that of the original. For this reason, the duration will be called equivalent duration, t_{qe}, and the negative phase will not be considered. Another important subject concerns the TNT yield of propellants that provides a way of relating the propellant explosions to TNT explosions, as far as the pressure-time history is concerned.

The TNT yield is defined [1] as the amount of TNT that, if put at the position of the propellant explosion, would produce the same value of a particular shock wave parameter at the same distance as that of the propellant explosion. Now, if it were possible to determine the TNT equivalent yield for each type of propellant, the loading function caused by a propellant explosion could be predicted. Unfortunately, this could only be done in the far-field region, that

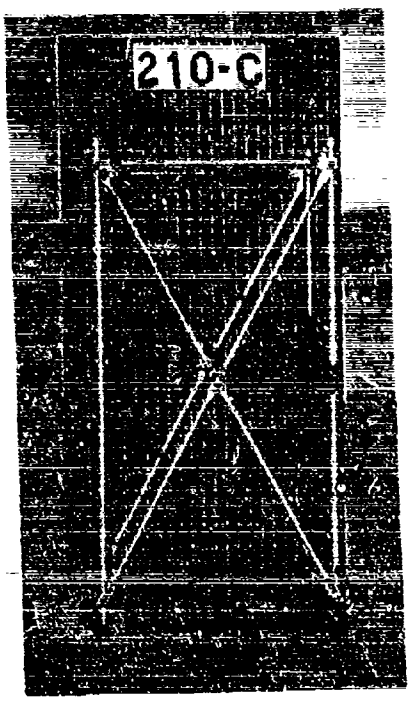

Fig. 3. Test structure with no visible damage

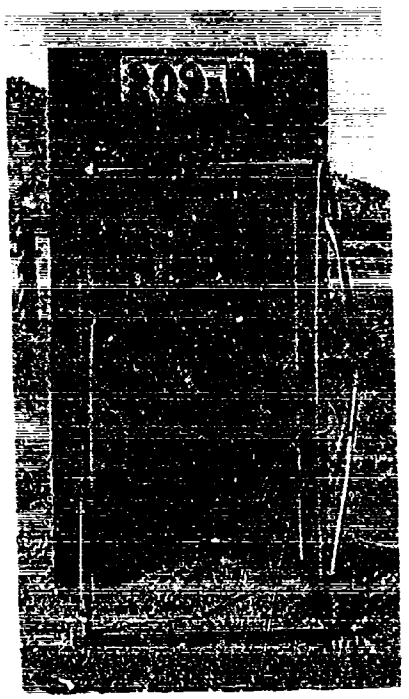

Fig. 4. Test structure with damage to bracings

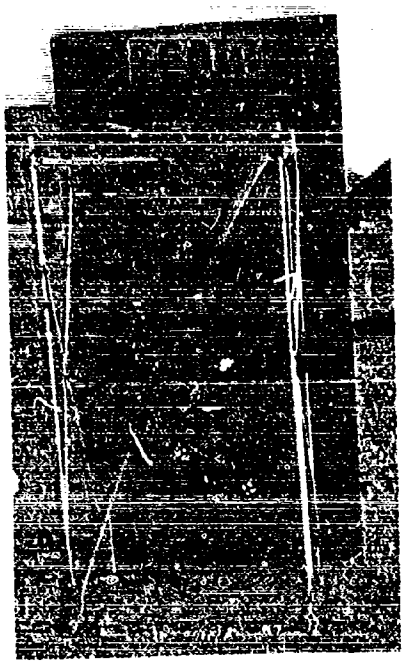

Fig. 5. Test structure with damage to diagonals

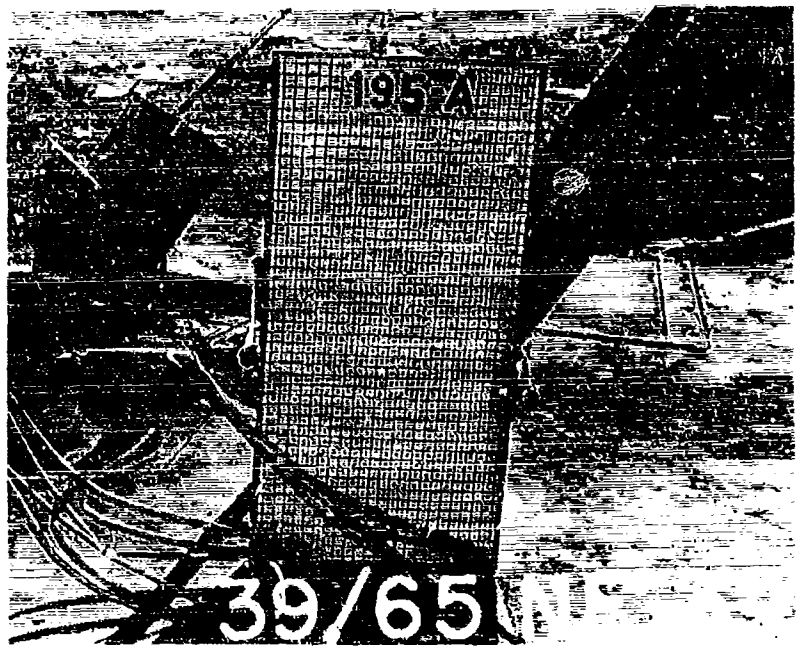

Fig. 6. Test structure with damage to columns

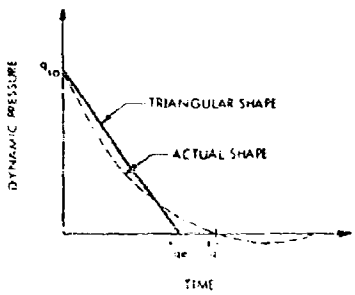

Fig. 7. Simplification of the dynamic pressure-time history

is at large distances from the point of explosion where the air blast parameters are functions only of the total energy released. In the close-field region, the air blast parameters depend on many other factors, such as explosive-mass-to-energy ratio, rate of energy release, initial air shock velocity, chemical properties of the explosive, and others, in addition to the total energy released [2]. For these reasons, the TNT equivalent yield cannot be found for the close field, and the only approach is to find its probability distribution by means of a long series of tests. The air shock parameters caused by liquid propellant explosions have been investigated in Refs. [2] and [3], and a design chart was developed in terms of liquid propellant explosions parameters, namely, the peak dynamic pressure, q_{so}, the equivalent phase duration, t_{qe}, the distance from ground zero, R, and the equivalent TNT yield, W_T. This chart, shown in Fig. 8, provides a very convenient loading criterion for evaluating dynamic responses of open-frame structural members.

ANALYTICAL MODELS

In the current analysis, attempts have been made to formulate analytical models for individual structural members, rather than treating the open-frame structure as a continuous system, and also the dynamic instability problems were not considered in the analysis. The assumptions made on the structural systems are:

1. The members AB, DC, DB, and AC are not subjected to wind load.

2. All the other members are loaded by a uniformly distributed dynamic load.

3. The structure is symmetrical with respect to the center. For this reason the analysis

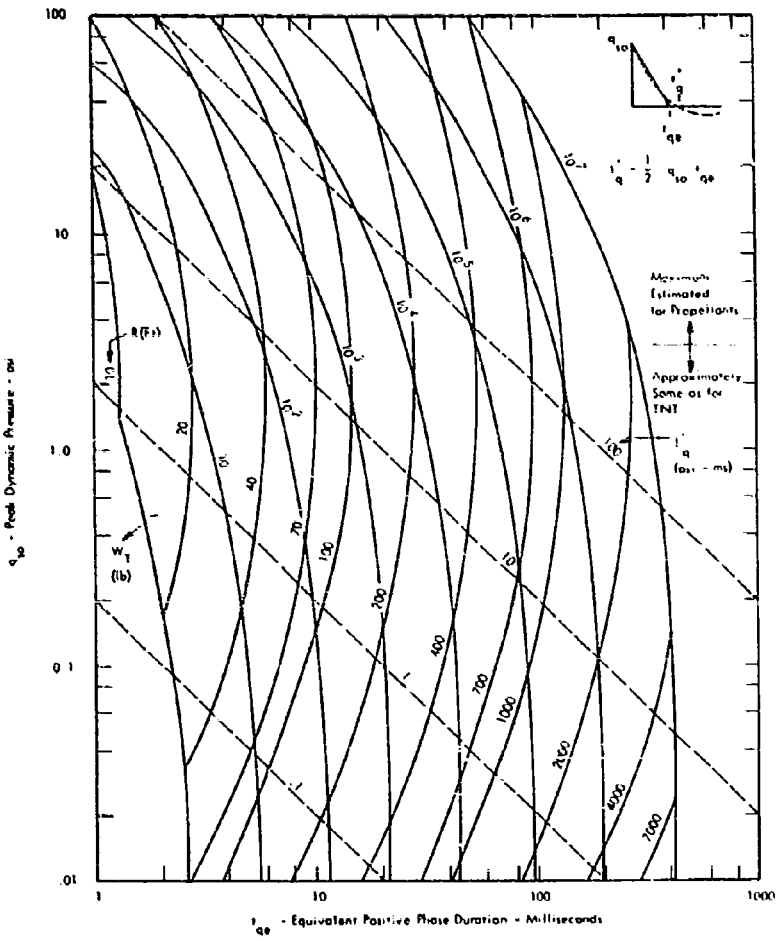

Fig. 8. Estimated peak dynamic pressure (q_{so}) and equivalent duration (t_{qe}) for propellant explosions related to distance (R) and equivalent TNT weight (W_T) (Ref. [4])

can be concerned with half structures, and only two-dimensional problems will be involved.

4. The struts, AB, DC, and the upper cross-bracings, AC, DB, are assumed to be infinitely rigid.

The mathematical model for diagonals is shown in Fig. 9, which is essentially a simply supported uniform beam subject to end loads, $R_{ax}(t)$. The mathematical model for struts and bracings is shown in Fig. 10, which represents a simply supported uniform beam. Column members of the open-frame structure are presented by a uniform cantilever beam model, as shown in Fig. 11, subject to a concentrated normal load $W(t)$ and to an axial load $R_j(t)$. The

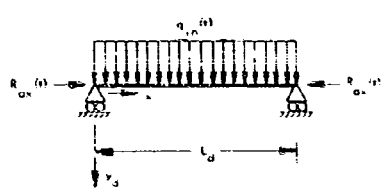

Fig. 9. Analytical model for diagonals

stiffnesses of these beam members are equivalent to those of the structural members.

The forcing functions for the aforementioned structural members are defined as follows:

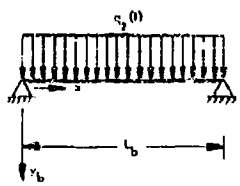

Fig. 10. Analytical model for struts and bracings

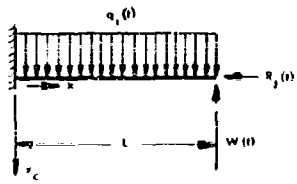

Fig. 11. Analytical model for columns

Diagonals:

$$q_{1n}(t) = D_1 q_0 \left(1 - \frac{t}{t_{qe}}\right) \cos \theta . \qquad (1a)$$

$$R_{ax}(t) = \gamma_1 q_0 \left(1 - \frac{t}{t_{qe}}\right) . \qquad (1b)$$

Bracings and Struts:

$$q_2(t) = D_2 q_0 \left(1 - \frac{t}{t_{qe}}\right) . \qquad (2)$$

Columns:

$$q_1(t) = D_1 q_0 \left(1 - \frac{t}{t_{qe}}\right) \qquad (3a)$$

$$R_2(t) = \gamma_2 q_0 \left(1 - \frac{t}{t_{qe}}\right) . \qquad (3b)$$

$$W(t) = \gamma_3 q_0 \left(1 - \frac{t}{t_{qe}}\right) . \qquad (3c)$$

where

D_1 = width of the diagonal and the column,

D_2 = width of the bracing and the strut,

q = loading pressure given by the dynamic pressure times the proper drag coefficient, and

$\gamma_1, \gamma_2, \gamma_3$ = constants determined by static analysis.

Equations (1), (2), and (3) are valid only if

$$0 < t < t_{qe} \qquad (4)$$

and all the forcing functions will vanish when

$$t > t_{qe} . \qquad (5)$$

DAMAGE PREDICTION

The failure criterion for each individual structural member is defined by the loading condition for which the maximum dynamic stress exceeds the yield stress of the structural material. To determine dynamic stress of the open frame structure subject to liquid propellant explosions, the following equations of motion are used to evaluate responses.

The equation of motion of the diagonal member is given as

$$EI \frac{\partial^4 y_d}{\partial x^4} + m_1 \frac{\partial^2 y_d}{\partial t^2} + R_{ax}(t) \frac{\partial^2 y_d}{\partial x^2} = q_{1n}(t) \qquad (6)$$

where

E = Young's modulus,

I_1 = moment of inertia of the diagonal, and

m_1 = mass per unit length.

Similarly, the equation of motion for bracings and struts is given by

$$EI_2 \frac{\partial^4 y_b}{\partial x^4} + m_2 \frac{\partial^2 y_b}{\partial t^2} = q_2(t) \qquad (7)$$

where

I_2 = moment of inertia of bracings and struts, and

m_2 = mass per unit length.

The equation of motion for columns can be found by using the normal mode method and is given by

$$y_c(x,t) = y_c(x)\, \eta(t) \qquad (8)$$

where

$y_c(x)$ = shape of the first normal mode = $\cos Kx - \cosh Kx - 0.734 (\sin Kx - \sinh Kx)$,

$$K = \frac{1.875}{L} \qquad (9)$$

$\rho(t)$ = normalized coordinate which is obtained from

$$\ddot{\rho} + \omega_c^2 \rho = \frac{Q}{M} \qquad (10)$$

$$\omega_c = K^2 \sqrt{\frac{EI_1}{m_1}}$$

Q = generalized force

$$= \int_0^L q_1(t)\, y_c(x)\, dx + W(t)\, y_c(L) \qquad (11)$$

M = generalized mass

$$= \int_0^L y_c^2(x)\, m_1 dx + y_c^2(L)\, M_a \qquad (12)$$

where

m_1 = mass per unit length,

M_a = concentrated mass at the free end, and

I_1 = moment of inertia of the column.

The maximum stresses for the diagonal, bracing (or strut), and column could be obtained by Eqs. (13), (14), and (15), respectively,

$$\sigma_d(x,t) = \left| \frac{EI_1}{s_d} \frac{\partial^2 y_d}{\partial x^2} \right| + \frac{R_{ax}(t)}{A_d} \qquad (13)$$

$$\sigma_b(x,t) = -\frac{EI_2}{s_b} \frac{\partial^2 y_b}{\partial x^2} \qquad (14)$$

$$\sigma_c(x,t) = \left| \frac{EI_1}{s_c} \frac{\partial^2 y_c}{\partial x^2} \right| + \frac{R_1(t)}{A_c} \qquad (15)$$

where σ, s, and A represent, respectively, the stress, section modulus, and cross-sectional area of structural members.

The procedures for obtaining solutions for Eqs. (6), (7), and (8) are quite straightforward and have been documented in Ref. [3]. The assumptions made in the derivation are:

1. In Eq. (6), the axial load, $R_{ax}(t)$, acting at the diagonal is treated as constant and equal to one-half the initial peak dynamic pressure.

2. In Eq. (11), the reaction, $R_1(t)$, has been neglected to increase compressive stress caused by bending.

The damage criterion for the test structure is defined as the maximum dynamic stress that exceeds the yield stress of the structural material; the yield stress for the test structure is assumed to be 13,000 psi.

The minimum impulse loading with peak dynamic pressure, q_{so}, and its equivalent duration, t_{qe}, which causes dynamic stress starting to exceed 13,000 psi is defined as the critical loading. For the case of the diagonal which is compressed by an axial force, $R_{ax}(t)$, the critical loading is also given by the critical pressure causing the diagonal to buckle. This critical pressure, q_{cr}, can be found by means of Euler's instability formula and is given by

$$q_{cr} = \frac{\pi^2 EI_1}{\gamma_1 L_d^2} \qquad (16)$$

To check the validity of the analytical models developed in this paper, the critical loadings for columns, struts, diagonals, and bracings have been computed and plotted in Fig. 12, and are designated by curves C, S, D, and B, respectively. These curves also could be used as damage prediction curves for individual members. A group of selected test results, as listed in Table 1, has been plotted as test points in Fig. 12. These test points are designated by four types of symbols and are evaluated according to actual equivalent TNT yield and corresponding test ranges. The comparison between the analytical and experimental results appears to be satisfactory.

CONCLUSIONS

The following conclusions can be drawn from the present analysis:

1. The analytical models for structural members developed in this paper are considered to be satisfactory to predict structural damage of the aluminum test structure.

2. The extension of the present method to predict structural damage for general open-frame structures is very promising.

ACKNOWLEDGMENT

This paper presents the partial result of the work on structural damage prediction

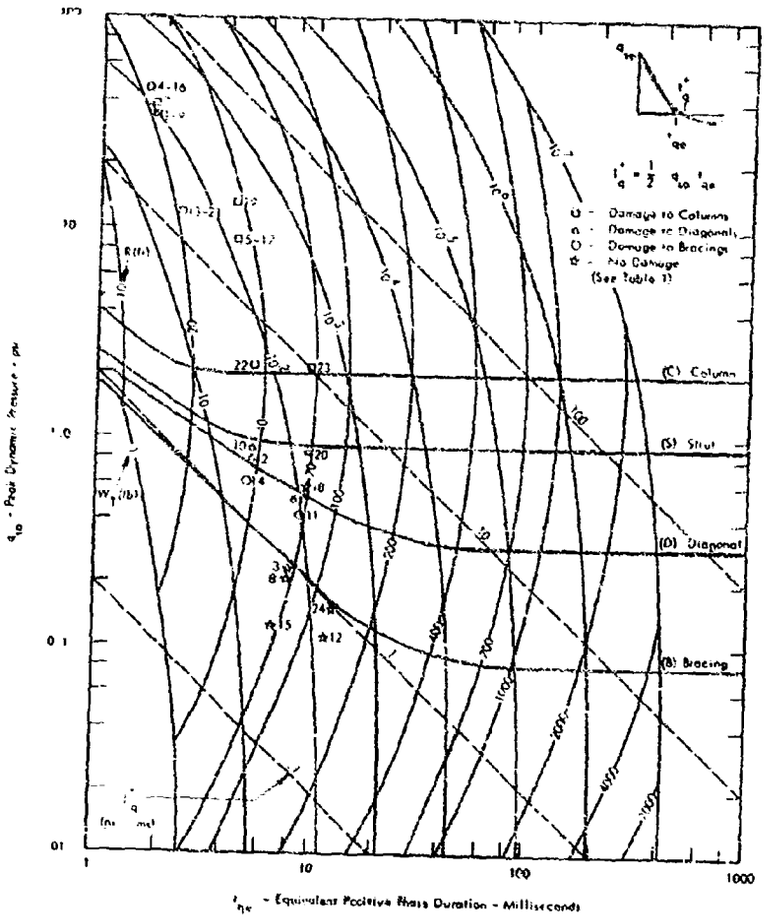

Fig. 12. Zones of damage for various members of an aluminum open-frame structure and comparison between theoretical and experimental data based on measured equivalent TNT yield data (Ref. [4])

techniques sponsored by Facilities Technology Branch, John F. Kennedy Space Center. The authors are indebted to Mr. J. H. Deese for his encouragement and constant support of this program.

REFERENCES

1. A. B. Willoughby, et al., "Study of Liquid Propellant Blast Hazards," Project PYRO Prog. Rept. for period ending 30 June 1965 through 30 Sept. 1967

2. F. V. Bracco, "Air Shock Parameters and Design Criteria for Rocket Explosions," Wyle Laboratories, Res. Staff Rept. WR 65-21, Sept. 1965

3. V. M. Conticelli and G. C. Kao, "Development of Damage Indexes for Open Frame Structures Subject to Liquid Propellant Explosions," Wyle Laboratories, Rept. WR 67-13, Oct. 1967

4. L. C. Sutherland, Ed. and principal author, "Sonic and Vibration Environments for Ground Facilities," Wyle Laboratories Rept. WR 68-2, Mar. 1968

P. Schrantz (Appl. Phys. Lab.): Did you have any thermal problem? It looked as if things were burning.

Mr. Rosenfield: The things which you saw burning were bits of urethane insulation from around the cryogenic portion of the tank. There were no thermal problems whatsoever in the field, even though occasionally the structures were engulfed by the fireball. The duration of the temperature was so short — a matter of milliseconds — that the temperature did not affect these at all.

G. Dyer (Naval Weapons Station): What type of provision did you take to assure mixing the propellant to give a high-order detonation before ignition?

Mr. Rosenfield: This program was not mine. That is a project jointly sponsored by NASA Kennedy Space Center, Marshall Space Flight Center, and the USAF. It was called Project PYRO. The part of it I had was strictly related to these little structures. I had nothing to do with setting up the test explosion program. I just used their data. I know what the fuels were, if you are interested. They used hypergolics which were N_2O_4, 50-50, and cryogenics which were LOX RP-1 and LOX hydrogen. They had a glass diaphragm within the tank separating the two portions. A plunger was driven into the diaphragm by means of a small charge of composition C which was exploded on top of it. It shattered the tempered glass causing the oxygen in the upper tank to fall into the hydrogen or kerosene in the lower tank. There was mixing and, with luck, an explosion. Sometimes it froze.

Mr. Dyer: Approximately what quantities of propellant did you operate with?

Mr. Rosenfield: The smallest size charge was 200 lb; the next was 1000 and they went to 25,000 lb. They exploded one Saturn S IV with 92,000 lb and two Titan I's with 113,000 lb.

* * *

SIMPLIFIED DYNAMICS OF HARDENED BURIED BUILDINGS

J. V. Poppitz*
Bell Telephone Laboratories, Inc.
Whippany, New Jersey

A technique is presented here for determining the airblast- and ground-shock-induced vertical structural response of a shallowly buried hardened building. The response is calculated by first selecting a module to represent most of the building, resolving that module into a lumped-mass mathematical model that is excited by forces analogous to airblast and ground shock, and then solving the second-order differential equations that describe the motion of the model. Response motions are predicted for all slabs in the building, from the roof down to the base slab. The motions at a column/slab junction and at the center of the unsupported area on a slab within a four-column array should be the most diverse of the motions occurring on each level and are predicted for each slab. This technique considers the flexibility and damping of the building subsoil and the damping effects of the building materials.

INTRODUCTION

Large underground buildings, "hardened" to withstand overpressures from a nuclear burst, are proliferating today. As more and more of these buildings appear, it becomes increasingly desirable to have a convenient method for analyzing them to determine dynamic response – a method that will approach the ideal of an "exact" solution as closely as possible while maintaining enough simplicity and ease of operation to allow its use when time, funds, and computer facilities are limited. This paper presents a method of analysis that, despite the complexity inherent to real structures, predicts dynamic response with reasonable accuracy and still maintains the requirement of relative simplicity.

NOMENCLATURE

- a Center-to-center distance between adjacent columns
- A Cross-sectional area
- B Parameter of infinite series: $(16\pi^4 z^4 + m^4 + 2m^2 n^2 + n^4)$, where m and n are indices
- C_C Coefficient of critical viscous damping
- C_{CE} Critical damping coefficient, equivalent system
- C_E Coefficient of viscous damping, equivalent system
- C_{soil} Coefficient of viscous damping for soil
- $C_1, C_2, \ldots$ Damping coefficient associated with locations 1, 2, ...
- d Width of column capital or column base
- D Slab parameter: $Et^3/12(1-\nu^2)$
- E Young's modulus of elasticity
- F_A Force, actual system
- F_E Force, equivalent system
- F_c Force applied by column on base slab
- F_1, F_2 Force applied at locations 1 and 2
- F_2' Reactive force of roof on top of column (location 2)
- G Shear modulus of elasticity for soil

*Member of Staff, Bell Telephone Laboratories, Inc., Whippany, N.J.

G_{seis} Seismic shear modulus of elasticity for soil

h Height of a point on a column, measured from fixed base

H Height of column

I Moment of inertia

k Spring or stiffness coefficient

k_A Stiffness coefficient, actual system

k_E Stiffness coefficient, equivalent system

$k_1, k_2, \ldots$ Stiffness coefficients associated with locations 1, 2, ...

k_f' Foundation modulus (psi/in.)

K_L Load- or spring-transformation factor

K_M Mass-transformation factor

K_{ME} Dynamic mass-transformation factor

$K_{M\,col}$ Dynamic mass-transformation factor for column

$K_{M\,slab}$ Dynamic mass-transformation factor for slab

KE_A Kinetic energy, actual system

KE_E Kinetic energy, equivalent system

m Mass per unit length (beam), per unit height (column), or per unit area (slab)

M Total mass

M_A Total mass, actual system

M_E Total mass, equivalent system

$M_1, M_2, \ldots$ Total equivalent masses of components associated with locations 1, 2, ...

n Number

N A constant

N_c A constant representing the ratio of base slab deflection at a column, z_c, to the average slab deflection, z_{ave}

N_m A constant representing the ratio of base slab deflection at midspan, z_m, to the average slab deflection, z_{ave}

Q Fraction of critical damping

r Radius

R Reaction

R_E Reaction, equivalent system

$R_1, R_2, \ldots$ Reactions associated with locations 1, 2, ...

t Time, or slab thickness, depending upon context

t_{r1}, t_{r2} Rise time for F_1 and F_2, respectively

U Blast-wave velocity

V Velocity

V_A Velocity, actual system

V_E Velocity, equivalent system

V_{seis} Seismic velocity in soil

V_i, V_j Velocities at locations i and j, respectively

W_A Total strain energy, actual system

W_E Total strain energy, equivalent system

x Horizontal coordinate of orthogonal $x\,y\,z$ system

y Horizontal coordinate of orthogonal $x\,y\,z$ system

z Vertical coordinate of orthogonal $x\,y\,z$ system; also, vertical deflection

z_A Vertical deflection, actual system

z_E Vertical deflection, equivalent system

z_b Vertical deflection at base of column

z_t Vertical deflection at top of column

z_s Vertical deflection of base slab at column

z_m Vertical deflection of base slab at mid-span

z_{avg} Average vertical deflection of base slab

z_g Vertical deflection of ground caused by ground shock

$\dot{z}_g$ Vertical velocity of ground caused by ground shock

$\ddot{z}_g$ Vertical acceleration of ground caused by ground shock

$z_1, z_2, \ldots, z_i$ Vertical deflections associated with locations 1, 2, . . . , i

$\dot{z}_1, \dot{z}_2, \ldots, \dot{z}_i$ Vertical velocities associated with locations 1, 2, . . . , i

$\ddot{z}_1, \ddot{z}_2, \ldots, \ddot{z}_i$ Vertical accelerations associated with locations 1, 2, . . . , i

a_m $m = 2$, where m is an index

b_m $m = a$, where m is an index

c_{mn} A constant whose value depends upon indices m and n

$z_{r1}, z_{r2}, \ldots, z_{ri}$ Vertical deflections, relative to ground, associated with locations 1, 2, . . . , i

$\dot{z}_{r1}, \dot{z}_{r2}, \ldots, \dot{z}_{ri}$ Vertical velocities, relative to ground, associated with locations 1, 2, . . . , i

$\ddot{z}_{r1}, \ddot{z}_{r2}, \ldots, \ddot{z}_{ri}$ Vertical accelerations, relative to ground, associated with locations 1, 2, . . . , i

ν Poisson's ratio

ρ_{slab} Mass density of slab

ρ_{soil} Mass density of soil

ω Angular frequency

TYPICAL BUILDING

A common type of hardened buried building is a multifloor reinforced-concrete structure composed of floor slabs, supporting columns, and outside walls. Columns typically are spaced evenly in the two directions parallel to the building walls and extend through floor slabs from the roof down to a base slab that acts as a mat foundation. The entire structure is monolithic — it contains continuous and rigid connections between floor slabs and columns.

Many hardened buildings follow this general description, and one of this type has been chosen to illustrate the application of the method presented here.

REPRESENTATIVE MODULE

With the exception of a small portion along the peripheral walls, the building described here can be thought of as being composed of identical modules — vertical cores, extending from roof to base — each made up of square sections of slab supported by a single column at the center of the core. The soil below the base-slab component is included as part of the module. Figure 1 is a cutaway view of the type of building being considered, with a representative module shown removed from its position in the building.

Because the sections of roof and floor slab included in a representative module are only those portions supported by a single column, and if each slab is subject to a uniformly distributed load, the edges of the slabs in a module are lines of zero shear. Consequently, the response of a module to an applied uniform overpressure may not appreciably affect the response of adjacent modules, and every module should respond dynamically much like every other module. (See Fig. 2.) If one allows the validity of this simplification, then only one module need be analyzed to find results that apply to most of the typical building.

ANALYSIS OF THE MODULE

A two-story building will be used as an example. The components of a module for this building include (a) a roof slab, (b) an intermediate slab, (c) a base slab, and (d) and (e) the two column components — that between the roof and intermediate slab and that between the intermediate slab and base.

These five components will be considered individually. A dynamic model will be determined for each component, and the five component models will then be synthesized into a model for the entire module. The response of this mathematical model to inputs analogous to airblast and ground shock will represent the response of the actual module that, in turn, will be representative of the response of the whole building.

An elastic building response has been assumed to apply in this analysis. Elastic building response as used here implies no appreciable

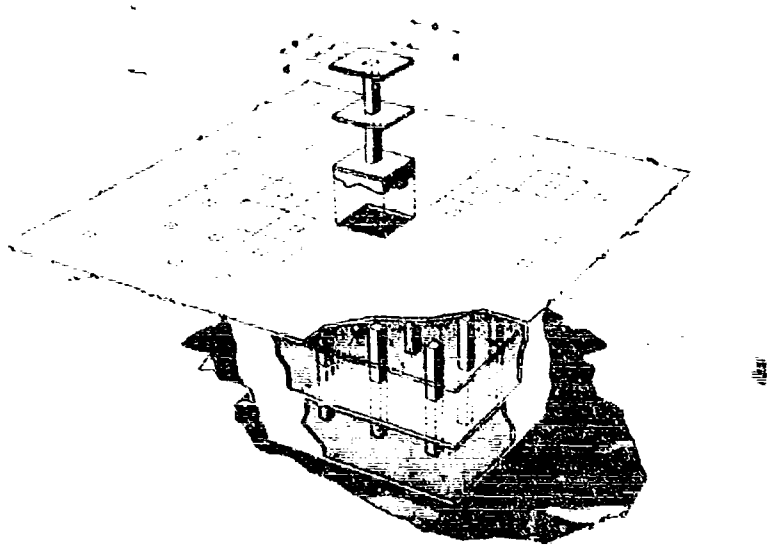

Fig. 1. Typical buried building with module removed

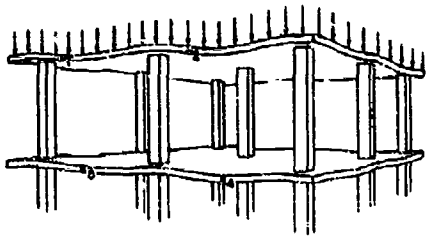

Fig. 2. Dynamic response of monolithic slabs and columns subjected to overpressure. The response at any location in a module should equal the response at the corresponding location in any other module ($z_1 = z_2$, $z_3 = z_4$).

permanent set, no development of plastic hinges, nor any other plastic failure in the structure. This assumption will apply throughout the discussion.

Equivalent System

Norris et al. [1] show that a simple mass-spring model can be used to represent the response of a real building component. With the use of appropriate load-transformation and mass-transformation factors, the response of the mass-spring model can be made identical to the actual response of some point on a building component. Here, we will create such models of the various components of the module, then couple them together to form a synthesized mass-spring model, and determine the response of this combination.

The aim will thus be to represent each component of a module by a lumped mass and linear spring and to develop the transformation factors that must be applied to the actual loads, stiffnesses, and masses to make the responses of the simple mass-spring models equal to the responses of the actual components. In the analysis to follow, the module and each of its components will be referred to as the actual system, and the idealized models will be referred to as the equivalent system.

The load-transformation factor, K_L, relates the load applied to the equivalent system, F_E, to that applied to the actual system, F_A. Its determination, and hence the determination of the load applied to the equivalent system, is based on the criterion that, in addition to the deflections of the two systems being equal ($z_A = z_E$), the strain energies of the two systems are also to be equal ($W_A = W_E$). Strain energy is a function of both the applied load and deflection of a system; hence $W(F_A, z_A) = W(F_E, z_E)$, and as the deflections of the two systems are equal, $W(F_A) = W(F_E)$. From this it follows that the ratio of F_E to F_A is a constant, which is defined here to be the load-transformation factor, K_L:

$$K_L = \frac{F_E}{F_A}$$

It should be mentioned that, because the stiffness, k, of a system is equal to the load divided by the deflection, the load-transformation factor here is equal also to the ratio of k_E to k_A. Therefore, K_L will also serve to evaluate the stiffness of the equivalent system.

The mass-transformation factor, K_M, relates the mass of the equivalent system, M_E, to that of the actual system, M_A. Its determination is based on the criterion that, in addition to the velocities of the two systems being equal ($V_A = V_E$), the kinetic energies of the two systems are also to be equal ($KE_A = KE_E$). Because kinetic energy is a function of the mass and velocity of a system, $KE(M_A, V_A) = KE(M_E, V_E)$, and because the velocities are equal, $KE(M_A) = KE(M_E)$. Thus the ratio of M_E to M_A is a constant, which is defined here to be the mass-transformation factor, K_M:

$$K_M = \frac{M_E}{M_A} .$$

If the mass-spring models defined by these transformation factors are to be reasonably accurate representations of the actual components, some modification must be introduced to account for the dissipative nature of building materials. It is often assumed that viscoelastic damping adequately describes this dissipation. The equations of motion are then modified by introducing a damping coefficient, C, that represents some portion of critical damping. This procedure will be followed here, and will be explained more fully in the following sections.

Module Components

Roof Slab — Imagine the roof slab to be infinite in area. It is supported by an array of equidistant columns, as described earlier. The dynamic response of such a slab to a sudden increase in overpressure should be primarily in the first mode. In that case, the most severe vibratory motion would occur on the slab at the midspan locations — the centers of the unsupported areas within each four-column array. On the representative module, these points would be at the corners of the roof-slab component. The mass-spring model to be devised for the roof-slab component should represent the motion at such a location.

The stiffnesses and load- and mass-transformation factors that apply to a slab supported by columns have been derived by Biggs [2] and are presented in tabular form in Fig. 3. On the representative module, the transformation factors apply to the area of the roof-slab component outside the column capital, as the column capital is considered to be inflexible. The overpressure load on the roof over the capital is carried directly by the column.

The transformation factors are general and apply to any uniformly loaded concrete slab supported by an array of columns. They need not be derived, therefore, every time such a slab is analyzed. This is fortunate, because the derivation is long and complex. Biggs' derivation of K_M involved integrating the expression for kinetic energy across the slab in two directions and equating the result to the expression for kinetic energy of the equivalent system, $(1/2)M_E V^2$. Biggs' derivation of K_L involved a similar integrating of the expression for strain energy across the slab and setting the result equal to the expression for strain energy of the equivalent system, $(1/2)F_E z$.

From the table of Fig. 3, the equivalent stiffness of the roof slab can be determined directly for various values of d/a — the ratio of the width of the column capital to the center-to-center distance between adjacent columns. In general, the actual stiffness of the roof slab approximates the relation

$$k_A = \frac{EI}{a^2}\left[185 + 465\left(\frac{d}{a}\right)\right] .$$

Because $k_E = K_L k_A$, and, from Fig. 3, $K_L = 8/15$,

$$k_E = \frac{8}{15}\frac{EI}{a^2}\left[185 + 465\left(\frac{d}{a}\right)\right] .$$

The derived factors of Fig. 3 make it possible to represent the roof slab mathematically as a simple mass-spring system. To complete this model, it is necessary to include the effect of a viscoelastic damper — a "dashpot" — that will account for energy dissipation in the actual system. A damping coefficient that defines the dashpot is usually expressed as some fraction of critical damping, where the coefficient of critical damping is given by

$$C_C = 2\sqrt{kM} .$$

Because the roof-slab component has been represented in the mass-spring model by an equivalent stiffness coefficient, k_E, and an equivalent mass, M_E, it is possible to express the equivalent value for the critical damping coefficient as

$$C_{CE} = 2\sqrt{k_E M_E} .$$

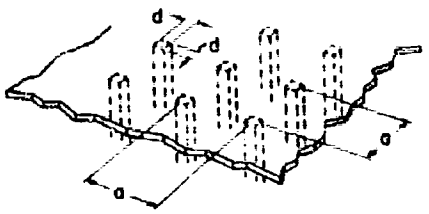

a = center-to-center distance between adjacent columns; equal in magnitude to width of module (in.)
d = width of column capital (in.)
E = Young's modulus of elasticity for slab (psi)
I = average of gross and transformed moments of inertia per unit width, equal in both directions ($in.^4/in.$)
F = total uniform load on slab panel of one module, excluding column capital (lb)
R = total reaction of one slab panel, excluding capital (lb)

Strain Range	d/a	Stiffness Coefficient, k_A ($lb/in.$)*	Load-Transformation Factor, K_L	Mass-Transformation Factor, K_M	Dynamic Column Load (lb)
Elastic Only	0.05	$208\ EI/a^2$	8/15	0.34	$0.16F + 0.84R$ (F load on capital)
	0.10	$230\ EI/a^2$	8/15	0.34	
	0.15	$252\ EI/a^2$	8/15	0.34	
	0.20	$276\ EI/a^2$	8/15	0.34	
	0.25	$302\ EI/a^2$	8/15	0.34	

*The constants in these expressions, which are functions of (d/a), may be approximated by the expression $[185 + 465(d/a)]$.

Fig. 3. Load- and mass-transformation factors for uniformly loaded flat slabs supported by a square column array (from a table by Biggs)

If the fraction of critical damping to be assigned is represented by Q, the dashpot is defined by the coefficient

$$C_E = 2Q\sqrt{k_E M_E}$$

and is inserted parallel to the linear spring in the equivalent model. Values for Q from 0.01 to 0.03 are recommended for deflections of concrete slabs within the elastic limit.

The dynamic reaction of the roof-slab component of the module is, in turn, a load carried by the supporting column. The total dynamic column load would be expected to equal this reaction of the slab on the column plus the overpressure load applied directly to the column through the column capital. Biggs [2] has found, however, that the dynamic column load equals the sum of three load components – the overpressure load applied directly to the column, 84 percent of the dynamic slab reaction on the column, plus 16 percent of the overpressure load applied directly to the roof slab. This is the expression noted in Fig. 3. (Norris et al. and Biggs present the development of dynamic column load in detail.)

Intermediate Slab – Because a two-story building is being analyzed here, only one intermediate slab exists. A three-story building would have two, with three column components, and so on.

Unlike the roof slab, the intermediate slab has no external load applied to it. The dynamic load on the columns is therefore equal to the slab reaction, R, where R in this case is the reaction of the intermediate slab. The slab thus can be represented by a mass-spring oscillator with a base excitation equal to the motion that would occur at the slab/column junctions in the actual structure. As with the roof slab, a dashpot must be incorporated in the model to account for structural damping.

The weight of the equipment carried by the intermediate slab is here assumed to act as a

uniformly distributed mass attached to the slab, which makes it possible to use the load- and mass-transformation factors and stiffnesses of Fig. 3. It must be assumed that such equipment is uniformly distributed across the slab and rigidly attached to it; any other assumption would invalidate the transformation factors of Fig. 3. If over half the total equipment mass is spring-mounted rather than rigidly attached, it is recommended that a portion of the mass of that equipment — approximately 2/3 — be used to represent that equipment. This would compensate somewhat for the added flexibility caused by the spring mounts.

Upper and Lower Columns — The upper column is analyzed in the same manner as the lower column; hence, consider the column on either level. The load- and mass-transformation factors for a column component are developed by the procedure outlined under Equivalent System.

First, to determine the load-transformation factor, K_L, consider the strain energy of the system. An elastic column in compression has deflection characteristics like those of an ideal spring. Consequently, the total strain energy stored is simply obtained by a strain integration, and is

$$W_A = \frac{F_A z_A}{2}$$

This is to be set equal to the strain energy of the mass-spring model of the equivalent system,

$$W_E = \frac{F_E z_E}{2}$$

With W_A equal to W_E, and z_A equal to z_E,

$$\frac{F_E}{F_A} = 1 = K_L$$

Next, consider the determination of the equivalent stiffness, k_E, of the model. The deflection of the column at its top, with the base fixed, is given by the familiar formula for a column in compression,

$$z_A = \frac{F_A H}{AE}$$

where F_A is the load applied to the column, H is the column height, A is the cross-sectional area of the column, and E is Young's modulus for the column material. The stiffness is simply the load divided by the deflection:

$$k_A = \frac{F_A}{z_A} = \frac{AE}{H}$$

Because, as discussed under Equivalent System, the load-transformation factor is also equal to the ratio between the stiffnesses of the two systems, the equivalent stiffness for the column component is given by

$$k_E = K_L^2 k_A = K_L^2 \frac{AE}{H}$$

and, because $K_L = 1$,

$$k_E = \frac{AE}{H}$$

To determine the mass-transformation factor, K_M, consider the kinetic energy of the system. It is assumed that the base of the column is fixed and that the velocity at any point on the column is proportional to its distance from the base:

$$V = \frac{V_A h}{H} \sin \omega t$$

where V_A is the velocity at the column top, h is the distance from the column's fixed base, and H is the column height. The $\sin \omega t$ term implies harmonic motion. The kinetic energy of the actual system is therefore

$$KE_A = \int_0^H \frac{1}{2} m V^2 dh$$

where m is the mass per unit height of the column. As the two systems are to undergo identical motions, their kinetic energies may be equated at any time. When the velocity is a maximum, $\sin \omega t$ equals unity, and the above becomes

$$KE_A = \int_0^H \frac{1}{2} m \left(V_A \frac{h}{H}\right)^2 dh$$

$$= \frac{1}{2} Hm \frac{V_A^2}{3}$$

$$= \frac{1}{2} M_A \frac{V_A^2}{3}$$

where M_A is the total mass of the column. This expression is now set equal to that for the maximum kinetic energy of the equivalent system:

$$\frac{1}{2} M_E V_E^2 = \frac{1}{2} M_A \frac{V_A^2}{3}$$

and, with V_A equal to V_E,

$$\frac{M_E}{M_A} = \frac{1}{3} K_M$$

To complete the mass-spring models for the columns, a dashpot must be included with each to account for structural damping, as with the models for the roof and intermediate slabs.

As before, the equivalent damping coefficient is given by

$$C_E = 2Q\sqrt{k_E M_E}$$

where values of Q from 0.01 to 0.02 are recommended for columns in the elastic range.

The dynamic reaction, R, of the column, which is the load applied to the supporting component, is equal to $k_A(x_t - x_b)$, where x_t and x_b are the deflections at the top and the base of the column, and k_A is the stiffness of the column.

Base Slab — The remaining module component to be idealized is the base slab, which rests on the soil subbase. In developing a mass-spring model for the base slab, it is important to recognize that the soil subbase is to be included as a part of the base-slab component, and that energy dissipation into the soil is significant and must be taken into account.

Load- and mass-transformation factors will not be developed for the base slab; an equivalent mass and stiffness will be arrived at by other means. Norris et al. and Biggs present a technique for developing transformation factors by assuming some deflected shape; they give factors for column-supported slabs, but their factors do not apply to a slab resting on a soil subbase. Further, their models do not include the effect of damping. Weissmann [3] and many others,* however, present a model of a foundation on soil that can be described with sufficient accuracy by an equivalent mass, a viscous dashpot, and a linear spring. Although the Weissmann model is admittedly a compromise between accuracy and convenience, its validity has been justified by empirical evidence; model-predicted responses fall well within the range of empirical responses measured from any particular foundation/soil system.

Weissmann's model has the advantage of including the effect of energy dissipation by the soil, the actual nonlinear damping being represented in the equivalent system by the linear damping of a viscous dashpot.†

The stiffness of Weissmann's model is described by a foundation modulus, k_f', expressed in psi per inch of deflection.‡ This modulus can be converted to an equivalent stiffness, k_E, if its value is multiplied by the area of the foundation being analyzed. Because a representative module is being studied, the product of k_f' and the area of the base-slab component of the module will be the equivalent stiffness that applies to that component.

Weissmann's model is developed as follows. By solving the theoretical problem of a rigid round foundation on an elastic half space, the foundation modulus is found to be

$$k_f' = \frac{4G}{\pi(1-\nu)r}$$

where G is the shear modulus of the soil, ν is Poisson's ratio for the soil, and r is the radius of the foundation area. This modulus can be converted for use with a square or rectangular mat foundation by means of the relationship

$$A = \pi r^2$$

where A is the total foundation area of the building. The foundation modulus then becomes

$$k_f' = \frac{2.26G}{(1-\nu)A^{1/2}}.$$

For a large building, however, where the foundation area is quite large, experimental data from Barken [4] indicate that the area of the foundation is related to the foundation modulus by some power smaller than the 1/2 power. Weissman, in another publication [5], recommends the area relationship

$$k_f' = N\left(\frac{1}{A}\right)^{(1/2)-n}$$

where N is some constant and n varies from zero for small areas to almost 1/2 for very large areas. It is sometimes desirable to

*Sochter, Novak, Pauw, Barkan, Lysmer, and Richart, etc. Much of their work is reviewed in Weissmann's report [3].

†It is interesting that most of the damping in a large foundation/soil system, of a size that would apply to actual buried buildings, does not result from internal friction of the soil, but rather from energy being radiated into the soil. For small foundation/soil systems, however, the energy lost in friction becomes significant.

‡This modulus is also called "modulus of subgrade soil reaction" or "coefficient of subgrade reaction."

determine k_i for both large and small values of ν; these would be limiting values within which any real value of k_i would fall. Accordingly, values of zero and 3/8 for ν are suggested for the determination of these limiting situations. For a best single value, 1/6 is recommended for ν, which makes the value of the exponent equal to 1/3. The single value, $\nu = 1/6$, will be used in the remainder of this discussion.

k_i may thus be expressed as

$$k_i = \frac{2.26G}{(1-\nu)A^{1/3}}$$

It should be pointed out again that A represents the area of the entire base slab, not just the base area of the module. If k_i is now multiplied by the base area of the module, a^2, the equivalent stiffness of the base-slab component of the module results:

$$k_g = k_i a^2 = \frac{2.26Ga^2}{(1-\nu)A^{1/3}}$$

It is important to determine a reasonable value for G, the shear modulus of the soil. The shear modulus increases with an increase in strain rate; values calculated from seismic measurements, in fact, are in many instances an order of magnitude higher than those obtained from static bearing tests. Therefore, it is desirable to use a modulus corresponding to some expected strain rate. For conditions such as those anticipated for this example – vibrations amounting to a fraction of an inch occurring at around 10 or 20 cps – the value of shear modulus should be between the values obtained for static conditions and seismic conditions. Table 1, which gives recommended values for G, has been prepared using data from Barkan [6] and with assistance from Weissmann. Weissmann notes that it is sometimes desirable to determine k_i for upper and lower limiting values of G, as was done with ν in the previous equation. Table 1 indicates acceptable ranges of for various soil categories

Weissmann gives an expression for the equivalent mass that accounts for some of the soil vibrating in phase with the base slab. This expression, for a round foundation, is

$$M_E = M\left(1 + 0.28\frac{k_g t^2}{MV_{seis}}\right)$$

where M is the mass of the round foundation in Weissmann's model, and V_{seis} is the seismic shear-wave velocity in the soil. This may be converted to a rectangular building foundation by again using the relation $A = \pi r^2$ and

TABLE 1
Recommended Soil Parameters – G, G_{seis}, and ν

Category	Soil Group	Dynamic Load Shear Modulus, G (psf), to Calculate k_i	Seismic Shear Modulus, G_{seis} (psf), to Calculate G_{soil}
I	Weak soils (clays and silty clays with sand, in a plastic state; clayey and silty sands; also soils of categories II and III with layers of organic silt and of peat)	Up to 4×10^5	Up to 8×10^5
II	Soils of medium strength (clays and silty clays with sand, close to the plastic limit, sand)	3.5 to 6.0×10^5	7 to 12×10^5
III	Strong soils (clays and silty clays with sand, of hard consistency; gravels and gravelly sands; loess and loessial soils)	6.0 to 15×10^5	12 to 30×10^5
IV	Rocks	$> 15 \times 10^5$	$> 30 \times 10^5$

Recommended values for Poisson's ratio, ν:

Clay	0.5
Clay-sand mixture	0.42
Sand	0.35
Loess, gravels, and rock	0.33

substituting the expression for k_z already determined. Then, because

$$V_{seis} = \sqrt{\frac{G_{seis}}{\rho_{soil}}}$$

where G_{seis} is the seismic shear modulus of the soil and ρ_{soil} is the soil density, the expression for the equivalent mass of the base-slab/soil component becomes

$$M_E = M_A \left[1 + \frac{0.2\pi^2 \rho_{soil} G}{(1-\nu) t A^{1/2} \rho_{slab} G_{seis}} \right]$$

Here, M_A is the mass, t the thickness, and ρ_{slab} the density of the base-slab component of the module; other variables are as defined before. The quantity within brackets has an upper limit of 1.5, which must not be exceeded. Table 1 includes recommended values for G_{seis}.

Along with the equivalent stiffness and equivalent mass, an equivalent coefficient of viscous damping must be determined. For the round foundation of Weissmann's example,

$$C_E = 0.8 \frac{1}{V_{seis}} k_E$$

Again using $A = \pi r^2$ and the expressions for V_{seis} and k_E, this coefficient can be converted for use with a rectangular building foundation.

$$C_E = \frac{A^{1/2} \rho_{soil} G^{1/2}}{(1-\nu) G_{seis}^{1/2}}$$

The dispersion of energy below the base slab occurs at seismic velocities, consequently the seismic modulus is applicable.

The Weissmann model, as presented in his publication, applies to a rigid foundation on flexible subgrade material. For the building under consideration here, however, it is desirable to consider the base slab to be flexible as well. Personal correspondence with Weissmann indicates that the modeling technique and parameter values formulated above are equally applicable to the case of average deflection of a flexible foundation. This is substantiated by Barkan [7], who reports the theoretical difference between the deflections of completely rigid and the average deflections of completely flexible base slabs to be less than 3 percent. The applicability of Weissmann's model to the case of average deflection of a flexible foundation is substantiated further by the limited deflection and flexure expected — an average deflection of an inch or less to compare with a module span of about 20 ft.

If, now, there is some way to predict the average base-slab deflection, it is possible to predict the response anywhere on the base slab by simply assuming some deflection shape. This is similar to Biggs' technique, except that in his technique a deflection shape, for static deflection, is assumed to develop the transformation factors, and here a deflection shape will be assumed to relate deflection at any point on the slab to the average slab deflection.

Therefore, the deflection at a point on the slab, as a function of time, will be assumed to be directly proportional to the average deflection, z_{avg}. The deflections of the slab at the column and at midspan — the center of the area within a four-column array — are

$$z_c(t) = N_c z_{avg}(t)$$

and

$$z_m(t) = N_m z_{avg}(t)$$

where z_c is the deflection of the base slab at a column, z_m is the deflection of the base slab at the midspan location, and N_c and N_m are constants to be calculated from the assumed deflection shape.

The static deflection shape of a mat-foundation slab that supports rows of equidistant columns is given in Timoshenko [8], the same source used by Biggs for deflection shapes in calculating the factors for column-supported slabs. This deflection shape is represented by

$$z(x,y) = \frac{4F_c}{a^2 d^2} \sum_{m=0}^{\infty} \sum_{n=0}^{\infty} \varepsilon_{mn} \sin\frac{m\pi d}{a} \sin\frac{n\pi d}{a} \cos\frac{2m\pi x}{a} \cos\frac{2n\pi y}{a}$$

where

F_c = force applied by column on base slab,

d = width of column base,

a = center-to-center distance between adjacent columns,

ε_{mn} = 1/4 (for $m = n = 0$),

= 1/2 (for either m or $n = 0$),

= 1 (for neither m nor $n = 0$),

$B = \frac{16\pi^4}{a^4}(m^4 + 2m^2n^2 + n^4)$

$D = Et^3/12(1 - \nu^2)$

t = slab thickness,

E = modulus of elasticity for slab material,

ν = Poisson's ratio for slab material,

k_f = foundation modulus.

The development of this deflection shape and its use in vibration analysis is dependent on two important assumptions. The first is that the deflection at any location does not affect the stiffness of the soil at another location. For the small deflections (compared with foundation size) expected here this is a reasonable assumption. The second assumption is that the base slab is in perfect contact with the soil at all times. This too is reasonable, as the dead weight of the structure and the applied overpressure should preclude any tendency of the slab and soil to separate.

When the expression for deflection shape is expanded, it becomes

$$z(x,y) = \frac{F_c}{a^2k_f}$$

$$+ \frac{4F_c}{\pi d}\sum_{m=1}^{\infty}\frac{1}{2}\,\frac{\sin\frac{m\pi d}{a}\left(\cos\frac{2m\pi x}{a} + \cos\frac{2m\pi y}{a}\right)}{m\left(D\frac{16\pi^4}{a^4}m^4 + k_f\right)}$$

$$+ \frac{4F_c\left(\sin\frac{\pi d}{a}\right)^2\cos\frac{2\pi x}{a}\cos\frac{2\pi y}{a}}{\pi^2d^2\left(D\frac{64\pi^4}{a^4} + k_f\right)}$$

$$+ \frac{4F_c\sin\frac{\pi d}{a}}{\pi^2d^2}\sum_{m=2}^{\infty}$$

$$\frac{\sin\frac{m\pi d}{a}\left(\cos\frac{2\pi x}{a}\cos\frac{2m\pi y}{a} + \cos\frac{2m\pi x}{a}\cos\frac{2\pi y}{a}\right)}{m\left[D\frac{16\pi^4}{a^4}(m^4 + 2m^2 + 1) + k_f\right]}$$

$$+ \frac{4F_c}{\pi^2d^2}\sum_{m=2}^{\infty}\sum_{n=2}^{\infty}\frac{\sin\frac{m\pi d}{a}\sin\frac{n\pi d}{a}\cos\frac{2m\pi x}{a}\cos\frac{2n\pi y}{a}}{mn(DB + k_f)}$$

The first term of this expanded expression, F_c/a^2k_f, which results from both original indices being zero, is the average deflection of the base slab. This is the z_{avg} required to evaluate the constants k_c and k_m. The fact that the first term represents average deflection can be verified readily. Average deflection is determined by double integration of the series with respect to x and y between the limits of $-a/2$ and $a/2$, and dividing by a^2. By examining the expanded form above, it can be seen that each term except the first has a $\cos(2m\pi x/a)$ factor, and the integral of that factor, evaluated between the limits of $-a/2$ and $a/2$, is zero. Hence, upon integration, only the first term does not go to zero, and hence it alone represents the average deflection.

Substituting appropriate values for x and y in the expanded expression above results in expressions for base-slab deflection at a column ($x = y = 0$) and at midspan -- the center of the area within a four-column array ($x = y = a/2$).

Deflection of the base slab at a column is

$$z_c(0,0) = \frac{F_c}{a^2k_f} + \frac{4F_c}{\pi d}\sum_{m=1}^{\infty}\frac{1}{2}\,\frac{\left(\sin\frac{m\pi d}{a}\right)(2)}{m\left(D\frac{16\pi^4}{a^4}m^4 + k_f\right)}$$

$$+ \frac{4F_c\left(\sin\frac{\pi d}{a}\right)^2}{\pi^2d^2\left(D\frac{64\pi^4}{a^4} + k_f\right)}$$

$$+ \frac{4F_c\sin\frac{\pi d}{a}}{\pi^2d^2}\sum_{m=2}^{\infty}\frac{\sin\frac{m\pi d}{a}(2)}{m\left[D\frac{16\pi^4}{a^4}(m^4 + 2m^2 + 1) + k_f\right]}$$

$$+ \frac{4F_c}{\pi^2d^2}\sum_{m=2}^{\infty}\sum_{n=2}^{\infty}\frac{\sin\frac{m\pi d}{a}\sin\frac{n\pi d}{a}}{mn\left[D\frac{16\pi^4}{a^4}(m^4 + 2m^2n^2 + n^4) + k_f\right]}$$

Deflection at midspan is

$$z_m\left(\frac{a}{2},\frac{a}{2}\right) = \frac{F_c}{a^2k_f} + \frac{4F_c}{\pi d}\sum_{m=1}^{\infty}\frac{1}{2}\,\frac{\sin\frac{m\pi d}{a}(2)(-1)^m}{m\left(D\frac{16\pi^4}{a^4}m^4 + k_f\right)}$$

$$+ \frac{4F_c\left(\sin\frac{\pi d}{a}\right)^2}{\pi^2d^2\left(D\frac{64\pi^4}{a^4} + k_f\right)}$$

(Cont.)

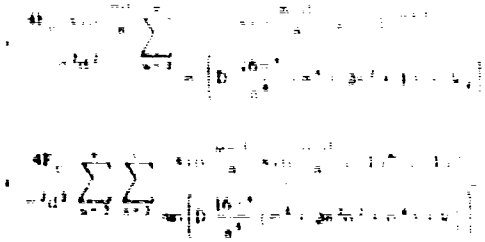

It would expedite their use if the above formulas could be plotted to allow immediate evaluation, but there are too many variables (a, d, t, k'_1, E, and ν) to justify the effort. The quantitative effect of the factor F_c, column load, could be eliminated by normalizing (dividing by F_c) but that would simplify very little, and it is felt that some additional insight might be obtained with the use of realistic values of deflection.

It is therefore necessary to evaluate the above expressions for deflection for each case considered. This is not a lengthy task, however, because the series converges rapidly. In the several cases evaluated – considering only the first two terms in the first series, the first three terms in the second series, and the two constant terms, and then neglecting the double-summed series entirely – the largest term truncated was less than 1 percent of the largest sine term.

Note that all of the terms in the deflection-at-column formula are equal in magnitude to the corresponding terms in the deflection-at-midspan formula; only the sign is different for every other term. As such, very little additional effort is required to evaluate the second formula.

With the terms evaluated, the equations can be put in the form $x(t) = N x_{avg}(t)$. From this, N_c and N_m can easily be evaluated, and when x_{avg} is determined the deflections at the column and at midspan immediately follow.

SYNTHESIS OF COMPONENTS

The models of the individual building components must now be synthesized into a mathematical model that is analogous to the entire representative module. Figure 4 shows the equivalent component models assembled into a configuration corresponding to the orientation of the actual components in the module.

This synthesis is necessary to formulate the differential equations of motion, the solutions of which constitute the ultimate goal of the analysis. Before these equations are presented, several pertinent considerations must be discussed.

Coupling of Roof Slab and Upper Column

When the mass-spring model of the roof slab was determined, the equivalent overpressure load on the roof was found to be 8/15 of the actual overpressure load – 8/15 being the load-transformation factor, from Fig. 3, that applied to the roof slab. Hence, any reaction of the roof-slab model will likewise be 8/15 of the actual reaction. When the roof-slab model is coupled to the model of the upper column (as a first step in building up the synthesized model of the entire representative module), the magnitude of the roof-slab reaction in the equivalent system must be brought back to its full value in the actual system by multiplying by 15/8. This is required because the upper column has a load-transformation factor of 1, and, therefore, actual values must be used for any inputs to the upper-column model.

Accordingly, the roof-slab reaction in the equivalent system, as noted in Fig. 3, is

$$R_1(t) = 0.16 F_1(t) + 0.84 R_2(t)$$

where F_1 is the force applied to the roof in the equivalent system, and R_2 is the spring reaction in the equivalent system and equal to $k_2(x_2 - x_3)$. Now, because this is reduced by a factor of 8/15, the load-transformation factor of the roof slab, it must be increased by a factor of 15/8 before it can be used as an input to the upper column. Therefore,

$$F'_2(t) = \frac{15}{8}\left[0.16 F_1(t) + 0.84 k_2(x_2 - x_3)\right]$$

An additional load to the upper column is the force of the overpressure applied directly to the column through the column capital. This force, F_3, will be explained in detail in a later section.

Coupling of Columns and Floor Slab

Because the load-transformation factors for the columns and base slab are equal to 1, the magnitudes of equivalent loads are equal to the magnitudes of actual loads for these components. The reaction of a component is the input to the subsequent component. Consequently, all the idealized models, except that which represents the roof slab, can be coupled directly into the synthesized model shown in Fig. 4.

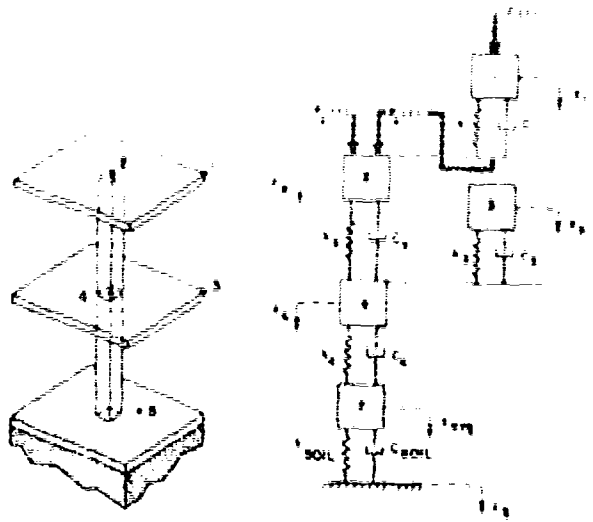

Fig. 4 Module of buried building converted to equivalent coupled mass-spring system

Note on this model that the vertical deflection of the base slab, x_{avg}, is the average response of the base. The response at a column location or a diagonally midspan location on the base slab can be determined if the x_{avg} response is multiplied by N_c or N_m, respectively (discussed under Base Slab).

Dynamic Mass-Transformation Factors

The previous determination of mass-transformation factors, K_M, involved the equating of the kinetic energies of the actual and equivalent systems. The kinetic energy of the actual system was determined by assuming some velocity distribution with the base of each component fixed. However, because the components supported by others move with their supports, the assumption of a fixed-base component is unrealistic. Some adjustment must be made to account for the base motions of most components of the representative module.

The adjustment will be to consider velocities that represent total motion — relative motion plus the base motion — and subsequently to develop new factors, called dynamic mass-transformation factors, K_M, that take the total motions of the components into account.

To do this, the entire module must be considered at once. The procedure of equating the kinetic energies of the actual and equivalent systems is followed, as before. In this case, however, the total kinetic energy of the actual system is determined by assuming deflection shapes for the whole module — the same shapes that were used before — but then integrating over the entire module. The resulting energy expression is a function of the velocities at the various specified locations in the module (see Fig. 4).

The energy of the equivalent system is, of course, the sum of the energies, $\frac{1}{2} M_i v_i^2$, of each of the lumped masses. This energy is also a function of the velocities at the various

specified locations in the module. When the energy of the equivalent system is set equal to the energy of the actual system, many of the terms in the two expressions correspond. The simplified relation yields an expression for dynamic mass-transformation factor, K_M. As with the static mass-transformation factor, K_M is defined as the ratio of the mass of the equivalent system to the mass of the actual system.

It can be shown that, when the above procedure is followed, the same K_M results every time a column-supported slab is analyzed, and the same K_M results every time a column is analyzed. The general expressions for K_M to be applied to any slab or any column are given below.

For slabs,

$$\bar{K}_{M\,slab} = \frac{1 + 0.66\frac{V_i}{V_j} + 1.34\left(\frac{V_i}{V_j}\right)^2}{3}.$$

For columns,

$$\bar{K}_{M\,col} = \frac{1 + \frac{V_i}{V_j} + \left(\frac{V_i}{V_j}\right)^2}{3}.$$

In these formulas, V_i represents the absolute velocity of the supporting component at the support points, and V_j represents the absolute velocity of the component in question (at the diagonally midspan location on a slab or the top of a column, depending on which kind of component is being considered). The factors are plotted for various ratios of V_i/V_j in Fig. 5.

It is necessary to assume that the various components of the building move in phase with one another. This assumption allows the calculation of kinetic energy for the entire system at an instant when all the vibratory energy is in kinetic form. Of the several actual buildings analyzed by this technique, all have exhibited in-phase response.

Because the expressions for $\bar{K}_M$ include the ratio of velocities, V_i/V_j, for specific locations on the module, it is first necessary to estimate these values and iterate, if required, until reasonable values are obtained. A recommended ratio to start with is the ratio of static deflections that result at the corresponding locations when the coupled model is subjected to equal-magnitude roof and upper-column forces. An alternative is to start with K_M, the static (fixed-base) mass-transformation factor,

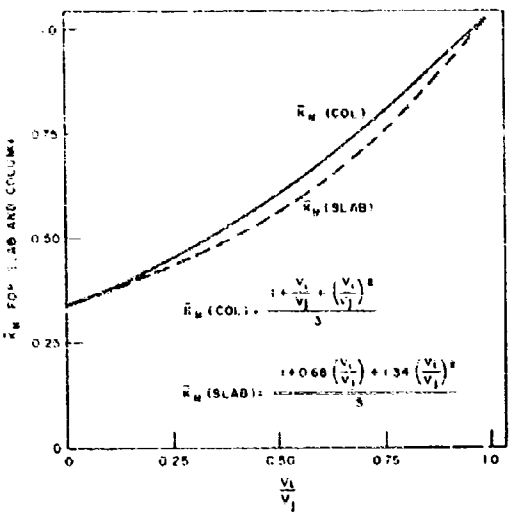

Fig. 5. Dynamic mass-transformation factors

and iterate from that point to acceptable response values. Generally, only one rerun is necessary.

The dynamic mass-transformation factors are used to calculate the M_E's, the equivalent masses for the various module components. The static-base mass transformation factors that were discussed earlier, those available from Biggs, are used only to evaluate the equivalent viscous damping coefficients, C_E, as discussed earlier and presented in Fig. 5.

In the remainder of the discussion, the "E" subscript has been dropped from the equations that refer to the equivalent system. Numerical subscripts to denote locations in the module are used instead, according to the following system:

1 — diagonally midspan on roof slab (corner point of roof-slab component on module)

2 — top of upper column

3 — diagonally midspan on intermediate slab (corner point of roof-slab component on module)

4 — top of lower column

5 — base slab.

Figure 4 shows the locations on the module to which these subscripts refer and the

corresponding equivalent models coupled together into the synthesized model which represents the entire module. z_g refers to a vertical motion of the ground far below the structure; it may be zero, or it may be a time-varying motion which represents ground shock.

MODEL EXCITATION

The hardened building will be subjected to airblast or ground shock or both. Excitation of the mathematical model requires the application of forces to the roof of the model to simulate airblast, and of motion at the model base to simulate ground shock. The model provides for vertical response only; therefore, the inputs should be the vertical components of the applicable forces or motion.

Airblast Overpressure

The airblast overpressure is converted to force by multiplying the overpressure, as a function of time, by the applicable area and the load-transformation factor, K_L. The applicable area for the force $F_1(t)$, which is applied to mass 1 of Fig. 4, is the roof area of the module minus the cross-sectional area of the column capital (a^2-d^2; see Fig. 1). The load-transformation factor for $F_1(t)$ is 8/15, from Fig. 3. For $F_2(t)$, the force applied to mass 2, which represents the column top, the applicable area is d^2 and the load-transformation factor is 1.

Figure 4 shows that mass 2 is excited by the reaction of mass 1. Rather than directly couple the mass and spring of mass 1 atop mass 2, the reactive force is applied separately and called $F_2'(t)$. The reason for this is that the reactive force is not simply $k_1(z_1 - z_2)$, but is $15.8\{0.16F_1(t) + 0.84k_1(z_1 - z_2)\}$, as was explained under Coupling of Roof Slab and Upper Column.

The time characteristics of $F_1(t)$ and $F_2(t)$, in general, are directly related to the overpressure as a function of time. An exception occurs when a radially expanding airblast shock front approaches a buried structure as a vertically fronted Mach stem. In this case the shock front sweeps over the module, first applying a force to only one side of the module roof area, and then progressively advancing and applying pressure to additional area until the entire module is engulfed. It is recommended that this time-dependent phenomenon be accounted for by giving the $F_1(t)$ force a linear rise time equal to the time required for the blast wave to pass over the module. This time is equal to the span of the module roof divided by the blast-wave velocity ($t_{r,1} = a/U$). Similarly, $F_2(t)$ should be given a rise time equal to the column capital width divided by the blast-front velocity $t_{r,2} = d/U$. After peaking, both forces would then decay in time, in the same manner as the overpressure. The time characteristics of $F_2'(t)$ are dictated by $F_1(t)$, z_1, and z_2.

Ground Shock

The model is formulated so that the ground shock at the base is expressed in terms of deflection and velocity, $z_g(t)$ and $\dot{z}_g(t)$, respectively, or acceleration, $\ddot{z}_g(t)$. Later in this paper the alternatives will be explained.

The prime intent here is to subject the model to the motion caused by outrunning ground shock -- the motion that occurs at a specific location prior to the arrival of the airblast at that location. (Ground shock is commonly divided into two parts, outrunning and superseismic. Outrunning ground shock is characterized by relatively low-frequency oscillations, similar to earthquake tremors, which precede the airblast. The building response to outrunning ground shock is accounted for by the motion input at the base. Superseismic ground shock is that caused by transients of the arriving airblast front and by the subsequent overpressure. The building response owing to the airblast and overpressure is accounted for by the forces applied to the top of the model.)

A typical excitation of the model would thus include some motion at the base, as a function of time, which represents outrunning ground shock, followed in time by forces $F_1(t)$ and $F_2(t)$ at the top of the building, which represent the arrival of airblast.

EQUATIONS AND SOLUTIONS

With the synthesized model assembled as illustrated in Fig. 4, the second-order differential equations that define the coupled system may now be written. They are

$$M_1\ddot{z}_1 + C_1(\dot{z}_1 - \dot{z}_2) + k_1(z_1 - z_2) = F_1(t)$$

$$M_2\ddot{z}_2 + 0.84\left(\frac{15}{8}\right)C_1(\dot{z}_2 - \dot{z}_1) + C_2(\dot{z}_2 - \dot{z}_4) + 0.84\left(\frac{15}{8}\right)k_1(z_2 - z_1) + k_2(z_2 - z_4) = F_2(t) + 0.16\left(\frac{15}{8}\right)F_1(t)$$

$$M_3\ddot{z}_3 + C_3(\dot{z}_3 - \dot{z}_4) + k_3(z_3 - z_4) = 0$$

$$M_4\ddot{z}_4 + C_2(\dot{z}_4 - \dot{z}_2) + C_3(\dot{z}_4 - \dot{z}_3) + C_4(\dot{z}_4 - \dot{z}_5) + k_2(z_4 - z_2) + k_3(z_4 - z_3) + k_4(z_4 - z_5) = 0$$

$$M_5\ddot{z}_5 + C_4(\dot{z}_5 - \dot{z}_4) + C_5\dot{z}_5 + k_4(z_5 - z_4) + k_5z_5 = C_5\dot{z}_g(t) + k_5z_g(t) .$$

In these equations the M's, k's, C's, and F(t)'s are the equivalent parameters as illustrated and evaluated in Fig. 4 and Table 2. Solution of the above equations for the z's, as functions of time, will yield the vertical displacements at the various locations of the model, each of which represents the displacement at some location in the building module. With these responses determined, the analysis is completed.

The one or two dots above the z's represent first and second time derivatives — velocity and acceleration — of the corresponding displacement. Note that in the above formulation the coordinates describe the absolute motion of the structure.

In the above form, the ground shock input must be expressed in velocity and displacement, whereas ground shock is commonly expressed as acceleration. The equations can be converted into terms of acceleration by means of a change in the coordinate system, with the following result. The coordinate change is

$$\zeta_i = z_i - z_g , \qquad \dot{\zeta}_i = \dot{z}_i - \dot{z}_g$$

and

$$\ddot{\zeta}_i = \ddot{z}_i - \ddot{z}_g .$$

Converting to the ζ-coordinate system, the original equations become

Table 2
System Parameters for Equivalent Coupled Mass-Spring System of Fig. 4

Component	k_i	M_i	C_i
Roof $[z_1(t)]$	$\frac{8}{15}\frac{EI}{a^2}\left[185 + 465\left(\frac{d}{a}\right)\right]$	$\bar{K}_{M\,slab} \times M_A$	$2Q\sqrt{\frac{k_i M_A}{3}}$
Upper column $[z_2(t)]$	$\frac{AE}{H}$	$\bar{K}_{M\,col} \times M_A$	$2Q\sqrt{\frac{k_i M_A}{3}}$
Intermed. slab $[z_3(t)]$	$\frac{EI}{a^2}\left[185 + 465\left(\frac{d}{a}\right)\right]$	$\bar{K}_{M\,slab} \times M_A$	$2Q\sqrt{\frac{k_i M_A}{3}}$
Lower column $[z_4(t)]$	$\frac{AE}{H}$	$\bar{K}_{M\,col} \times M_A$	$2Q\sqrt{\frac{k_i M_A}{3}}$
Base slab $[z_{avg}(t)]$	$\frac{2.26Ga^2}{(1-\nu)A_f^{1.3}}$	$M_A\left[1 + \frac{0.2a^2\rho_{soil}G}{(1-\nu)tA_f^{1.3}\rho_s G_{seis}}\right]$	$\frac{A_f^{1.6}\rho_{soil}^{1.2}G_{seis}^2}{(1-\nu)G_{seis}^{1.2}}$

a = center-to-center distance between adjacent columns
A = cross-sectional area of column
A_f = plan area of building mat foundation
d = width of column capital
E = Young's modulus of elasticity
G = shear modulus of elasticity for soil
G_{seis} = seismic shear modulus of elasticity for soil
H = height of column
I = slab moment of inertia (see Fig. 3)
k_o = stiffness coefficient of actual system
K_L = load-transformation factor
K_M = mass-transformation factor
$\bar{K}_M$ = dynamic mass-transformation factor
M_A = total mass of component, actual system
Q = fraction of critical damping
t = slab thickness
ρ_s = slab density
ρ_{soil} = soil density
ν = Poisson's ratio

*Additional levels might exist. In that case each additional intermediate floor and length of column constitute a pair of intermediate components, with parameters equal to those bracketed here.

$$M_1\ddot{z}_1 + C_1(\dot{z}_1 - \dot{z}_2) + k_1(z_1 - z_2) = F_1(t) - M_1\ddot{z}_g$$

$$M_2\ddot{z}_2 + 0.84\left(\frac{15}{8}\right)C_1(\dot{z}_2 - \dot{z}_1) + C_2(\dot{z}_2 - \dot{z}_4) + 0.84\left(\frac{15}{8}\right)k_1(z_2 - z_1) + k_2(z_2 - z_4) = F_2(t) + 0.15\left(\frac{15}{8}\right)F_1(t) - M_2\ddot{z}_g$$

$$M_3\ddot{z}_3 + C_3(\dot{z}_3 - \dot{z}_4) + k_3(z_3 - z_4) = -M_3\ddot{z}_g$$

$$M_4\ddot{z}_4 + C_2(\dot{z}_4 - \dot{z}_2) + C_3(\dot{z}_4 - \dot{z}_3) + C_4(\dot{z}_4 - \dot{z}_5) + k_2(z_4 - z_2) + k_3(z_4 - z_3) + k_4(z_4 - z_5) = -M_4\ddot{z}_g$$

$$M_5\ddot{z}_5 + C_4(\dot{z}_5 - \dot{z}_4) + C_5\dot{z}_5 + k_4(z_5 - z_4) + k_5z_5 = -M_5\ddot{z}_g.$$

The ground shock input is now in terms of acceleration. Note that in this form the z's represent motion of the structure relative to the unaffected soil deep below the base.

In either form, the coupled equations would probably be too complex to solve without a computer. Most computers, however, either analog or digital, would be adequate and would solve the coupled equations with ease; the equations would simply have to be programmed in a form compatible with the computer to be used.

Computer output, in the form of motion-vs-time plots for various locations within the building, are very illustrative. Such plots readily portray frequency characteristics, peak response (both positive and negative) characteristics of decay, phase relation of the various motions, and so forth. It is also desirable to have the deflection of some specific location relative to another determined with the computer and plotted. For example, it would be desirable to determine $z_1 - z_2$, which represents the maximum deflection of the midspan location on the roof relative to the column supports, or $z_2 - z_4$, which represents the deflection of the top of the upper column relative to its base. Such deflections would represent the flexure of a single component of the building.

The many possible manipulations and forms of computer input and output are dependent to a large degree on the specific computer facilities available. Consequently, the method of programing and solving the above equations is largely up to the user, and will not be further discussed here.

SPECIAL CHARACTERISTICS

Various assumptions were made during the development of the technique presented here. The computer outputs should be checked, therefore, to verify that the assumptions made were valid.

First, it is desirable to check whether the various masses of the coupled model responded primarily in phase. In-phase response is necessary to justify the use of the dynamic mass-transformation factors described under Dynamic Mass-Transformation Factors. An out-of-phase response indicates appreciable error in the calculated response, in which case it would be more desirable to return to the rigid-base mass-transformation factors, recalculate, and accept the new calculated response as a crude estimate. The response error with an out-of-phase response is probably quite large, because such response implies that applicable mass-transformation factors are changing in time in relation to the response. Such a situation almost precludes analyses that produce anything but rough estimates of the response.

Second, it is desirable to compare the assumed ratio of maximum velocities with that which resulted, and to reevaluate the dynamic mass-transformation factors and rerun if necessary.

Third, it is desirable to convert the flexural deflections within the various components to terms of stress, and compare each stress with the maximum elastic stress for the material of which the applicable component is composed. This entire analysis is based on an elastic material response, and, therefore, no deflection should be great enough to induce permanent set in the building.

CONCLUSIONS

A technique is presented here by which a typical hardened building of modular design can be analyzed for response to airblast and ground shock induced by a nuclear weapon. A module that, repeated many times, forms the buried building is isolated for study.

The response of this module is thought to be representative of the response of most of the building. The module is idealized as a mass-spring analytical model that includes the effects of the subsoil and structural damping.

The airblast and ground shock to which the actual building would be subjected by a nuclear

burst are converted to analogous forces that excite the model. The resulting motions that the individual masses of the model undergo are representative of the motion of selected locations within the actual building. Two locations are selected on each slab: One at a column/floor-slab junction and the other on the slab midway between columns. These locations were chosen because they should exhibit extremes in the response of each slab. The response at any other location can thus be interpolated from the response at those selected points.

Finally, the differential equations that define the analytical model are presented. These equations, too complex to be solved by hand, can be solved quite easily by most computers with a capability of handling differential equations. The form of the computer output -- the information that describes the building response -- can be varied somewhat by the user, so that motion-vs-time plots and other useful data can be obtained.

ACKNOWLEDGMENTS

The writer is indebted to many members of the staff at Bell Telephone Laboratories, especially Mr. G. F. Weissmann, who gave counsel and many specific contributions to the sections concerning soils and slabs on subsoil.

REFERENCES

1. Norris et al., Structural Design for Dynamic Loads (McGraw-Hill), 1959, Ch. 7
2. J. M. Biggs, Introduction to Structural Dynamics (McGraw-Hill), 1964, Ch. 5
3. G. F. Weissmann, "A Mathematical Model of a Vibrating Soil-Foundation System," Bell System Tech. J. 45:177-226 (Jan. 1966)
4. D. D. Barkan, Dynamics of Bases and Foundations (McGraw-Hill, New York), 1962, pp. 26-28
5. G. F. Weissmann, "Measuring the Modulus of Subgrade Soil Reaction," Materials Research and Standards, 5, 1965
6. D. D. Barkan, op. cit., p. 30
7. D. D. Barkan, op. cit., pp. 23-25
8. Timoshenko and Woinowsky-Krieger, Theory of Plates and Shells, 2nd ed. (McGraw-Hill, New York), 1959, p. 277

* * *

INFLUENCE COEFFICIENT MATRIX QUICK-CHECK PROCEDURE*

George W. Bishop
Bishop Engineering Company
Princeton, New Jersey

Influence coefficient matrices are often useful for the solution of problems involving vibration frequencies and mode shapes. A quick-check procedure (consisting of three steps) which is applicable to any influence coefficient matrix and which will determine whether the matrix satisfies three necessary conditions is presented here. If these three conditions are not satisfied, then this procedure will pinpoint the offending elements of the matrix. It is, of course, possible for a matrix to meet the three necessary conditions described here and still contain other errors, which may be more difficult to discover.

INTRODUCTION

Influence coefficient matrices are defined on page 32 of Ref. [1] in connection with the computation of normal modes of vibration. Much work is involved in calculating all the elements of such matrices for multimass systems; this is true whether these calculations are performed manually or by computer programs. A great amount of such work is required to obtain the spring constants and lumped masses involved in a mechanical system using design drawings as the primary source of information. In view of this large investment in time and money, it is useful, and in fact imperative, to have a few quick-check methods to locate some of the more usual errors that seem to find their way into influence coefficient matrices. These errors may be misplaced decimal points or other careless mistakes in transposition, in addition to fundamental errors in structural analysis.

A three-step procedure has been evolved that has proved extremely useful in locating some of the possible influence coefficient mistakes. Steps 1 and 2 are well known to engineers familiar with the solution of dynamics problems using influence coefficient matrix manipulations. The third step does not appear to be common knowledge, and for convenience all three steps are presented as a quick double-check on influence coefficient matrices.

STEP 1 — THE LEADING DIAGONALS MUST ALL BE POSITIVE

The leading diagonals in an influence coefficient matrix are those elements that define the deflection at a mass resulting from a force at this same mass. A general expression for such a leading diagonal can be found on page 32 of Ref. [1] as δ_{jj}. For consistency, the deflection in this case would be in the same direction as the force. For example, in the case of vertical direction influence coefficients, if the 1-pound force at a given mass were defined as positive downward, then the deflection at this same mass would also be defined as positive for the downward direction.

In mathematical terms, step 1 could be written as $\delta_{jj} \geq 0$. It is obvious that a downward force on a point cannot produce an upward deflection at this same point in a conservative system. Indeed, if a conservative system could violate this rule it then would be a perpetual motion machine.

In essence then, step 1 consists of examining all leading diagonals such as δ_{11}, δ_{11}, δ_{22}, δ_{33}, δ_{11}, δ_{nn} and so forth, to insure that none of them is negative.

*This paper was not presented at the Symposium.

STEP 2 – OFF-DIAGONAL ELEMENTS MUST SATISFY MAXWELL'S RECIPROCITY THEOREM

Off-diagonal elements may be defined as all of the elements in a matrix except leading diagonal elements. Stated in mathematical terms, step 2 becomes $\delta_{ij} = \delta_{ji}$. Page 32 of Ref. [1] describes this rule that makes the influence coefficients symmetrical about the leading diagonal. Equation (A10) on page 36 of Ref. [1] illustrates this symmetry numerically in a 6 × 6 influence coefficient matrix. Page 132 of Ref. [2] clearly explains the meaning of this theorem. A more general explanation of Maxwell's theorem is given in the footnote on page 176 of Ref. [3] where couples and rotations are also included.

In essence, step 2 can be accomplished by examining each off-diagonal element and comparing it with its reciprocity element to insure that it agrees in both sign and magnitude.

STEP 3 – THE SQUARE OF ANY OFF-DIAGONAL ELEMENT MUST NOT EXCEED THE PRODUCT OF LEADING DIAGONAL ELEMENTS IN THE RESPECTIVE ROW AND COLUMN

Stated in general mathematical terms, $(\delta_{ij})^2 \leq (\delta_{ii})(\delta_{jj})$. Page 47 of Ref. [1] gives a formula for the two frequencies (in radians per second) for both modes of a two-mass system as follows:

$$\omega^2_{1,2} = \frac{M_1\delta_{11} + M_2\delta_{22} \pm \sqrt{(M_1\delta_{11} + M_2\delta_{22})^2 - 4M_1M_2(\delta_{11}\delta_{22} - \delta_{12}^2)}}{2M_1M_2(\delta_{11}\delta_{22} - \delta_{12}^2)} .$$

For the particular case of a two-mass system the influence coefficients could be written in a 2×2 matrix, and it will be noted that the above equation therefore contains only the following influence coefficients: δ_{11}, δ_{22}, and δ_{12}. A careful examination of this equation will indicate that for both of the mode frequencies to be positive, the denominator must be positive. Therefore, the term in parentheses in the denominator, $(\delta_{11}\delta_{22} - \delta_{12}^2)$, must not be negative; or, stated in mathematical terms, $(\delta_{12})^2 \leq (\delta_{11})(\delta_{22})$.

This last expression is of the same form as the first expression written above; namely, $(\delta_{ij})^2 \leq (\delta_{ii})(\delta_{jj})$. It remains now only to prove that the two-mass requirement can be extended to the multimass system. This can be accomplished by assuming that all masses (in a multimass system) except the one row mass and the one column mass under consideration are zero. For example, in a seven-mass system, if we wish to postulate that $(\delta_{1,7})^2$ must not exceed the product of δ_{11} and δ_{77}, we need only assume that masses 3, 4, 5, 6, and 7 are all zero and then the system becomes a two-mass system and the rule must hold. That there are additional influence coefficients in the matrix does not nullify the requirement. Likewise, for example, if we wish to postulate that $(\delta_{56})^2$ must not exceed the product of δ_{55} and δ_{66}, we need only assume that masses 1, 2, 3, 4, and 7 are all zero.

Step 3 applies to negative off-diagonal elements as well as to positive off-diagonal elements. In using step 3, it is necessary only to check each of the off-diagonal elements that lies on one side of the leading diagonals, because step 2 has insured that the off-diagonal elements lying on the other side of the leading diagonals are identical.

ILLUSTRATIVE EXAMPLES

Table 1 illustrates six matrices (A, B, C, D, E, and F) that might apply to a three-mass system.

Four of these matrices contain errors that can be located by using the three-step procedure:

1. Matrix A violates step 3 because $(50)^2 > (10)(100)$.

2. Matrix B does not violate any of the three steps.

3. Matrix C violates step 3 because $(200)^2 > (1)(100)$.

4. Matrix D violates step 1 because -100 must be positive.

5. Matrix E does not violate any of the three steps.

6. Matrix F violates step 2 because $0.001 \neq 0.010$.

Of course, matrices B and E may violate some other rules beyond the scope of this paper.

A 10×10 matrix can be checked with these three steps in less than 15 min. Therefore it would seem to be poor economy to ignore this

TABLE 1
Matrices for a Three-Mass System

A

	①	②	③
①	15	5	20
②	5	10	50
③	20	50	100

D

	①	②	③
①	10	5	20
②	5	-100	50
③	20	50	90

B

	①	②	③
①	0.001	0.001	0.001
②	0.001	5	5
③	0.001	5	1,000

E

	①	②	③
①	10	5	-5
②	5	5	5
③	-5	5	25

C

	①	②	③
①	1	5	200
②	5	100	50
③	200	50	100

F

	①	②	③
①	0.001	0.001	0.001
②	0.001	5	5
③	0.010	5	100

quick-check procedure and put this influence coefficient matrix into a computer for the solution of eigenvalues and eigenvectors, possibly even using the results in further stress analysis, when the original influence coefficient matrix may violate one of these three rules.

ACKNOWLEDGMENT

We wish to give credit to Mr. Kim J Calvin, Marine Engineer, Naval Ship Engineering Center, Washington, D.C., for recognizing the applicability of the formula on page 47 of Ref. [1] as a more restrictive rule in step 3.

REFERENCES

1. R. O. Belsheim and G. J. O'Hara, "Shock Design of Shipboard Equipment – Dynamic Design Analysis Method," NAVSHIPS 250-423-30, BuShips, Dept. of Navy, Washington, D.C., May 1961
2. J. P. Den Hartog, Mechanical Vibrations, 4th ed (McGraw-Hill, New York), 1956
3. S. Timoshenko and G. H. MacCullough, Elements of Strength of Materials, 2nd ed. (D. Van Nostrand Co., Inc., New York), May 1940

* * *

MECHANICAL IMPEDANCE

DETERMINATION OF FIXED-BASE, NATURAL FREQUENCIES OF DUAL-FOUNDATION, SHIPBOARD EQUIPMENTS BY SHAKE TESTS

Lawrence E. Fetah and George J. O'Hara
Naval Research Laboratory
Washington, D.C.

This paper investigates the application of resonance testing to determine the fixed-base, natural frequencies of an in-place shipboard equipment-foundation system that is supported at two base points. The structure can rotate as well as translate when the base points translate. A method was proposed previously that required the simultaneous use of two shakers capable of phase control and a range of force ratios at each driving frequency; this method would be quite difficult and expensive to apply in the field. A new technique is proposed herein that requires only one shaker to be applied at a time, thereby reducing the difficulties and restrictions considerably. An application of the technique to a theoretical model is presented.

INTRODUCTION

The determination of the fixed-base, natural frequencies* of in-place structures has been a recurrent problem to engineers interested in structural dynamics, particularly from the point of view of shock analysis. At present, the most convenient method for obtaining these fixed-base frequencies is that of shake tests. This involves exciting the structure with a sinusoidal force over a range of frequencies and recording the response at significant locations. If the structure were truly attached to a fixed base, peaks resulting from resonance would occur in the response at the fixed-base, natural frequencies of the structure. Unfortunately, however, few structures rest on bases that are infinitely stiff and heavy, and this condition creates a problem in applying field test techniques. This is especially true in shipboard situations where in-place equipment-foundation systems have base supporting structures that are relatively flexible, such as decks and bulkheads.

A paper presented at the 34th Shock and Vibration Symposium [1], and subsequently published as a Naval Research Laboratory report [2], examined this problem, and concluded that it is impossible to determine fixed-base frequencies of in-place structures by the commonly accepted test means, that is, by driving on the in-place equipment and seeking nulls at its base for various frequencies. A dynamic chain-type structure was examined, and those frequencies that can be found by driving at various locations were discussed. That paper also proposed a technique for finding fixed-base frequencies for the dynamic chain-type structure.

The new technique is this: Drive at a point on or below the base of the equipment-foundation system and record the responses of the base and a point on the equipment. Note prominent valleys in the response of the base; these points occur at the fixed-base frequencies of the system above the base and of the system below the driving point. The equipment response will

*A fixed-base, natural frequency is a natural frequency that would exist if the base were infinitely stiff so that its motion would not be affected by the motion of the system mounted upon it.

exhibit prominent valleys at the fixed base frequencies of the system above the equipment response point and of the system below the driving point. After eliminating the frequencies of the system below the driving point (those frequencies at which there are valleys in both the equipment and base responses), the remaining valleys in the base response will indicate the desired frequencies. A convenient experimental technique is to plot the ratio of equipment response to base response. This method eliminates the extraneous frequencies of the system below the driving point, and the fixed-base frequencies of interest are then the points where prominent peaks occur in the ratio plot. These peaks coincide with valleys in the base response plot. Note that for the very special case where a fixed-base frequency of the system above the equipment response point coincides with a fixed-base frequency of the equipment-foundation system, the ratio plot does not have a prominent peak at that frequency.

A section of the previous paper contained a brief discussion of a structure supported at two base points. The structure is capable of rotation as well as translation when the base points translate. A technique using two shakers with variable force and phase control was proposed at that time. The purpose of this paper is to examine the problem in detail to determine a more convenient experimental technique for obtaining those frequencies.

THE PROBLEM

A simplified case will be discussed first to allow the reader to follow the mathematical argument more easily. Consider a structure such as that shown in Fig. 1. This configuration with unequal parameters allows small rotations coupled with translation. The upper massless bar with lumped masses represents the equipment-foundation system shown in Fig. 2; the lower bar, masses, and springs represent the supporting structure. All joints are considered pinned and the structure is assumed stable.

The equipment-foundation system has two natural frequencies and two associated mode shapes. These mode shapes cause displacements across springs K_1 and K_2 and resultant spring forces. If the entire system (Fig. 1) is excited at points C and D with forces having magnitudes proportional to the respective modal spring forces and the driving frequency equaling the modal frequency for the upper system, then it will act as a fixed-base system and the motion of points C and D will tend to vanish as this condition is approached

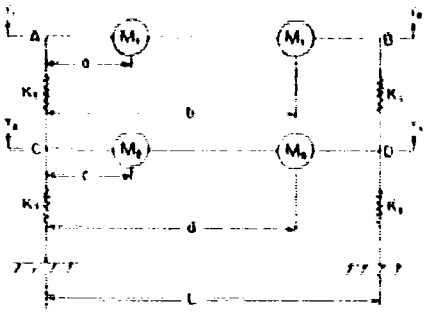

Fig. 1 Simulated shipboard system with equipment-foundation system in place

This method would yield correct results, but difficulties in application are apparent. For the case illustrated, two shakers are required, one at C and one at D. The shakers must not only sweep through the frequency range of interest, but at each frequency they must also sweep through a range of force ratios. They must (for this undamped system) operate in phase to obtain one frequency and out of phase to obtain the other. The system of interest will act as on a fixed base only when the driving frequency, force ratio, and phase are simultaneously coincident with the respective quantities for a fixed-base, natural mode of the system. This of course presents obvious difficulties that would make such field measurements costly and time consuming.

Further attention has been applied to this problem, and as a result, a much more convenient technique has been devised.

THEORY AND ANALYSIS

Consider again the structure shown in Fig. 1. The equations of motion for free vibration may be written as

$$\left[\left(\frac{L-a}{L}\right)^2 + \left(\frac{L-b}{L}\right)^2\right] M_1 \ddot{y}_1 + \left[\frac{a}{L}\left(\frac{L-a}{L}\right) + \frac{b}{L}\left(\frac{L-b}{L}\right)\right] M_2 \ddot{y}_2 + K_1(y_1 - y_3) = 0$$

$$\left[\frac{a}{L}\left(\frac{L-a}{L}\right) + \frac{b}{L}\left(\frac{L-b}{L}\right)\right] M_1 \ddot{y}_1 + \left[\left(\frac{a}{L}\right)^2 + \left(\frac{b}{L}\right)^2\right] M_2 \ddot{y}_2 + K_2(y_2 - y_4) = 0 \quad (1)$$

(Cont.)

$$\left[\left(\frac{L-a}{L}\right)^2+\left(\frac{L-c}{L}\right)^2\right]M_1\ddot{y}_1+\left[\frac{a}{L}\left(\frac{L-a}{L}\right)+\frac{c}{L}\left(\frac{L-c}{L}\right)\right]M_2\ddot{y}_2$$

$$-K_1(y_3-y_1)+K_3y_1=0$$

$$\left[\frac{a}{L}\left(\frac{L-a}{L}\right)+\frac{c}{L}\left(\frac{L-c}{L}\right)\right]M_1\ddot{y}_1+\left[\left(\frac{a}{L}\right)^2+\left(\frac{c}{L}\right)^2\right]M_2\ddot{y}_2$$

$$-K_2(y_4-y_2)+K_4y_2=0 \qquad (1)$$

By making the substitutions

$$\begin{aligned}
&=\left[\left(\frac{a}{L}\right)^2+\left(\frac{b}{L}\right)^2\right]\\
&=\left[\frac{a}{L}\left(\frac{L-a}{L}\right)+\frac{b}{L}\left(\frac{L-b}{L}\right)\right]\\
&=\left[\left(\frac{L-a}{L}\right)^2+\left(\frac{L-b}{L}\right)^2\right]\\
&=\left[\left(\frac{c}{L}\right)^2+\left(\frac{d}{L}\right)^2\right]\\
&\left[\frac{c}{L}\left(\frac{L-c}{L}\right)+\frac{d}{L}\left(\frac{L-d}{L}\right)\right]\\
&\left[\left(\frac{L-c}{L}\right)^2+\left(\frac{L-d}{L}\right)^2\right]
\end{aligned} \qquad (2)$$

and the usual solution assumption

$$y_i = \bar{y}_i \sin(\omega t+\phi) \qquad (3)$$

a set of algebraic equations results, whose characteristic equation is

$$\begin{vmatrix}
-\omega^2M_1+\omega^2M_1+K_1 & 0 & -K_1 & 0\\
+K_3 & & & \\
\omega^2M_1+\omega^2M_1 & 0 & -K_2 & \\
+K_2 & & & \\
-K_1 & 0 & -\omega^2M_2+\omega^2M_2 & \\
 & & K_1+K_3 & \\
0 & -K_2 & -\omega^2M_2+\omega^2M_2 & \\
 & & K_2+K_4 &
\end{vmatrix}=0 \qquad (4)$$

Similarly, the characteristic equation of the upper system, shown in Fig. 2, can be shown to be

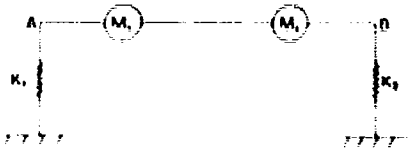

Fig. 2. Equipment-foundation system of interest for which fixed-base, natural frequencies are desired

$$\begin{vmatrix}
-\omega^2M_1+K_1+K_3 & -\omega^2M_1\\
-\omega^2M_1 & -\omega^2M_1+K_2
\end{vmatrix}=0 \qquad (5)$$

Thus, the complete system frequencies are the roots of Eq. (4); the fixed-base, natural frequencies of the system of interest are the roots of Eq. (5).

If sinusoidal forces, $P_C \sin \omega t$ and $P_D \sin \omega t$, are applied at points C and D, respectively, of Fig. 1, the equations of motion become

$$\begin{aligned}
&-M_1\ddot{y}_1-\omega^2M_1\ddot{y}_1+K_1(y_1-y_3)=0\\
&-M_2\ddot{y}_2-\omega^2M_2\ddot{y}_2+K_2(y_2-y_4)=0\\
&-M_3\ddot{y}_3-\omega^2M_3\ddot{y}_3-K_1(y_1-y_3)+K_3y_3=P_C\sin\omega t\\
&-M_4\ddot{y}_4-\omega^2M_4\ddot{y}_4-K_2(y_2-y_4)+K_4y_4=P_D\sin\omega t
\end{aligned} \qquad (6)$$

The solution is of the form

$$y_i = \bar{y}_i \sin \omega t \qquad (7)$$

so that the responses at the base points are

$$\begin{aligned}
\bar{y}_C &= \frac{1}{\omega_4}\left\{(-\omega^2M_2-\omega^2M_4+K_2+K_4)\omega_2-K_2^2(-\omega^2M_1-\omega^2M_3+K_1+K_3)\right\}P_C\\
&+\frac{1}{\omega_4}\left\{(-\omega^2M_2+K_2)K_1K_2(-\omega^2M_1+K_1)\right\}P_D\\
\bar{y}_D &= \frac{1}{\omega_4}\left\{(-\omega^2M_2+K_2)\omega_2+K_1K_2(-\omega^2M_1+K_1)\right\}P_C\\
&+\frac{1}{\omega_4}\left\{(-\omega^2M_2-\omega^2M_4+K_2+K_4)(-\omega^2M_1-\omega^2M_3+K_1+K_3)-K_1^2(-\omega^2M_1-\omega^2M_3+K_1)\right\}P_D
\end{aligned} \qquad (8)$$

Let

$$\begin{aligned}
\omega_{CC} &= \left\{(-\omega^2M_2-\omega^2M_4+K_2+K_4)\omega_2-K_2^2(-\omega^2M_1-\omega^2M_3+K_1+K_3)\right\}\\
\omega_{CD} &= \omega_{DC}=\left\{(-\omega^2M_2+K_2)\omega_2+K_1K_2(-\omega^2M_1+K_1)\right\}\\
\omega_{DD} &= \left\{(-\omega^2M_2-\omega^2M_4+K_2+K_4)(-\omega^2M_1-\omega^2M_3+K_1+K_3)-K_1^2(-\omega^2M_1-\omega^2M_3+K_1)\right\}
\end{aligned} \qquad (9)$$

Then the response equations reduce to

$$\bar{y}_C = \frac{\chi_{CC}}{\psi_4} P_C + \frac{\chi_{CD}}{\psi_4} P_D$$
$$\bar{y}_D = \frac{\chi_{CD}}{\psi_4} P_C + \frac{\chi_{DD}}{\psi_4} P_D . \quad (10)$$

The results of previous work [1] indicate that the condition of interest is that for which the base responses simultaneously become zero. This gives

$$\frac{\chi_{CC}}{\psi_4} P_C + \frac{\chi_{CD}}{\psi_4} P_D = 0$$
$$\frac{\chi_{CD}}{\psi_4} P_C + \frac{\chi_{DD}}{\psi_4} P_D = 0 . \quad (11)$$

To have a solution other than the trivial one, the determinant of the coefficients of the P's must vanish. Therefore

$$\frac{\chi_{CC}\chi_{DD} - \chi_{CD}^2}{(\psi_4)^2} = 0 . \quad (12)$$

Evaluating the numerator gives

$$\chi_{CC}\chi_{DD} - \chi_{CD}^2 = (-\delta M_2\omega^2 + K_2 + K_4)(-\gamma M_2\omega^2 + K_1 + K_3)(\psi_2)^2$$
$$-K_1^2(-\alpha M_1\omega^2 + K_2)(-\delta M_2\omega^2 + K_2 + K_4)\psi_2$$
$$-K_2^2(-\gamma M_1\omega^2 + K_1)(-\gamma M_2\omega^2 + K_1 + K_3)\psi_2$$
$$+K_1^2K_2^2(-\gamma M_2\omega^2 + K_1)(-\alpha M_1\omega^2 + K_2)$$
$$-(\epsilon M_2\omega^2)^2(\psi_2)^2 - 2K_1K_2(\beta M_1\omega^2)(\epsilon M_2\omega^2)\psi_2$$
$$-K_1^2K_2^2(\beta M_1\omega^2)^2 \quad (13)$$

and because in Eq. (5)

$$\psi_2 = (-\gamma M_1\omega^2 + K_1)(-\alpha M_1\omega^2 + K_2) - (\beta M_1\omega^2)^2 .$$

Eq. (13) reduces to

$$\chi_{CC}\chi_{DD} - \chi_{CD}^2 = \{[(-\delta M_2\omega^2 + K_2 + K_4)(-\gamma M_2\omega^2 + K_1 + K_3)$$
$$-(\epsilon M_2\omega^2)^2]\psi_2$$
$$-K_1^2(-\alpha M_1\omega^2 + K_2)(-\delta M_2\omega^2 + K_2 + K_4)$$
$$-K_2^2(-\alpha M_1\omega^2 + K_1)(-\gamma M_2\omega^2 + K_1 + K_3)$$
$$-2K_1K_2(\beta M_1\omega^2)(\epsilon M_2\omega^2) + K_1^2K_2^2\} \ldots \quad (14)$$

The enclosed term is simply ψ_4, by means of Eq. (4). Thus

$$\chi_{CC}\chi_{DD} - \chi_{CD}^2 = (\psi_4)(\psi_2) \quad (15)$$

so Eq. (12) now becomes

$$\frac{(\psi_4)(\psi_2)}{(\psi_4)^2} = 0 \quad (16)$$

or

$$\frac{\psi_2}{\psi_4} = 0 . \quad (17)$$

There are three frequencies at which simultaneous nulls can occur: λ_1 and λ_2, the fixed-base frequencies of the upper system; and infinite frequency, because the order of ψ_4 is greater than that of ψ_2. Associated with each of the finite frequencies is a force ratio that will satisfy Eq. (11). Simultaneous base nulls will occur only when these frequency and force ratio relationships are satisfied by the driving forces. Because this occurrence is unique it could be utilized to obtain the desired frequencies; this is the basis of the previously proposed technique. However, a field test that attempted to obtain simultaneous base nulls would obviously be cumbersome to perform.

If in Eq. (10) the ratio of $\bar{y}_C$ to $\bar{y}_D$ were taken, then

$$\frac{\bar{y}_C}{\bar{y}_D} = \frac{\chi_{CC}P_C + \chi_{CD}P_D}{\chi_{CD}P_C + \chi_{DD}P_D} . \quad (18)$$

This ratio will be independent of the P's when

$$\frac{\chi_{CC}}{\chi_{CD}} = \frac{\chi_{CD}}{\chi_{DD}} . \quad (19)$$

However, this is exactly

$$\chi_{CC}\chi_{DD} - \chi_{CD}^2 = (\psi_4)(\psi_2) = 0 . \quad (20)$$

Therefore, the ratio of $\bar{y}_C$ to $\bar{y}_D$ is independent of the P's at the complete system natural frequencies and at the fixed base natural frequencies of the upper system. Because the ratio is independent of the P's at these frequencies, it makes no difference if one of the P's is zero. This provides a convenient technique for finding the desired fixed-base, natural frequencies.

TECHNIQUE

In the system of Fig. 1, apply the driving force at C and sweep through the frequency

range. Monitor the response at C, at D, and the ratio of the response at C to the response at D. The system natural frequencies will show as resonant peaks in the plots of the responses at C and D. The ratio

$$\left(\frac{\bar{y}_C}{\bar{y}_D}\right)_C = \frac{Y_{CC}}{Y_{DC}} \qquad (21)$$

has been obtained.

Repeat the above procedure with the force applied at D. Again, the system frequencies appear as resonant peaks in the direct response plots. The ratio

$$\left(\frac{\bar{y}_C}{\bar{y}_D}\right)_D = \frac{Y_{CD}}{Y_{DD}} \qquad (22)$$

has also been obtained.

Now, superpose the ratio plots (Eqs. (21) and (22)). The curves will cross at frequencies where the two ratios are equal. These points must be at either the complete system frequencies or the fixed-base frequencies of the upper system, by reason of Eqs. (19) and (20). The complete system frequencies are found by examination of the responses at C and D; crossings at these frequencies can be eliminated from consideration, then the remaining crossings must occur at the desired fixed-base frequencies for this model.

THEORETICAL APPLICATION

To illustrate the technique proposed in the preceding section, the following values were assigned to the parameters of the system in Fig. 1:

$$M_1 = 1 \quad K_1 = 1 \quad K_2 = \frac{11}{25} K_1$$

$$M_2 = 2M_1K_3 = 2K_1K_4 = \frac{33}{25} K_1 .$$

The system natural frequencies for these parameters are

$$\omega_1 = 0.596 \text{ rad/sec}$$

$$\omega_2 = 1.154 \text{ rad/sec}$$

$$\omega_3 = 1.896 \text{ rad/sec}$$

$$\omega_4 = 3.717 \text{ rad/sec}$$

and the fixed-base, natural frequencies of the upper system are

$$\lambda_1 = 0.775 \text{ rad/sec}$$

$$\lambda_2 = 2.569 \text{ rad/sec}.$$

Proceeding with the proposed method, a theoretical shake test was performed upon the structure. The response at C, response at D, and the ratio of the response of C to that at D for a driving force applied at C are shown in Figs. 3, 4, and 5, respectively. These graphs are plotted as absolute amplitude vs driving frequency because this is the most probable way that real data would be presented. Figures 6, 7, and 8 present the respective quantities for a driving force applied at D. The two ratio plots are superposed to give the graph of Fig. 9. Inspection of this graph shows six points where the ratios are

$$\omega = 0.60 \text{ rad/sec}$$

$$\omega = 0.77 \text{ rad/sec}$$

$$\omega = 1.15 \text{ rad/sec}$$

$$\omega = 1.90 \text{ rad/sec}$$

$$\omega = 2.57 \text{ rad/sec}$$

$$\omega = 3.72 \text{ rad/sec}.$$

These six frequencies include the four complete system frequencies and the two upper system fixed-base frequencies. However, the complete system frequencies can be determined by examination of the direct response plots. Resonance peaks in those plots occur at

$$\omega_1 = 0.60 \text{ rad/sec}$$

$$\omega_2 = 1.15 \text{ rad/sec}$$

$$\omega_3 = 1.90 \text{ rad/sec}$$

$$\omega_4 = 3.72 \text{ rad/sec}.$$

Now, eliminating crossings at these frequencies from consideration; two crossing points remain at $\omega = 0.77$ and $\omega = 2.57$. These are the fixed-base, natural frequencies of the upper system, the system of interest.

A MORE GENERAL CASE

A more general situation encountered in the practice of resonance testing on in-place structures is found in Fig. 10. Once again, the upper system (Fig. 11) is the system of interest for which the fixed-base, natural frequencies must be determined. The behavior of this

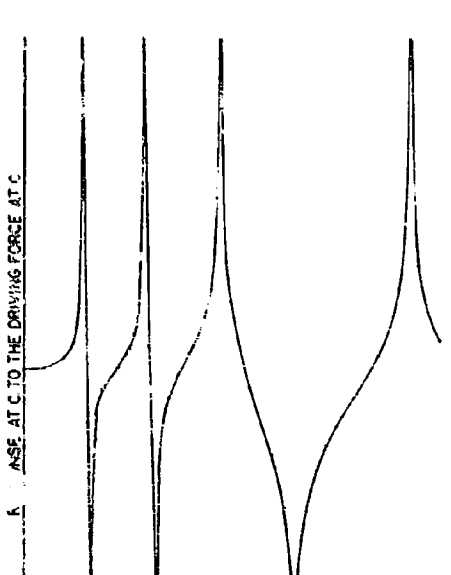

Fig. 3. Response at C to driving force at C in system of Fig. 1

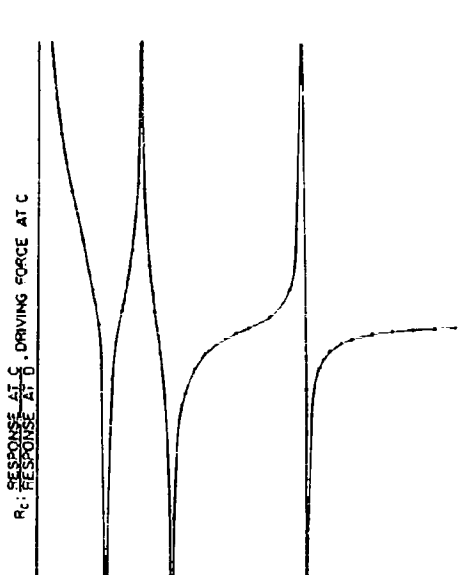

Fig. 5. Ratio of response at C to that at D when driving force is at C

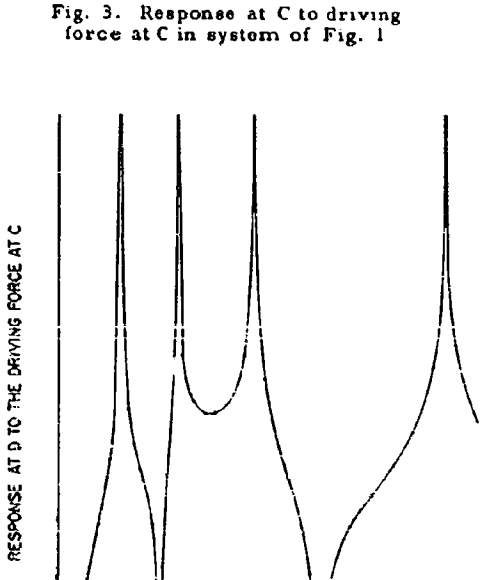

Fig. 4. Response at D to driving force at C

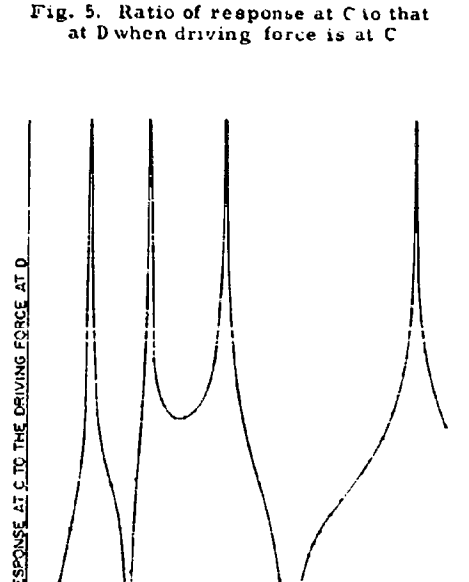

Fig. 6. Response at C to driving force at D in system of Fig. 1

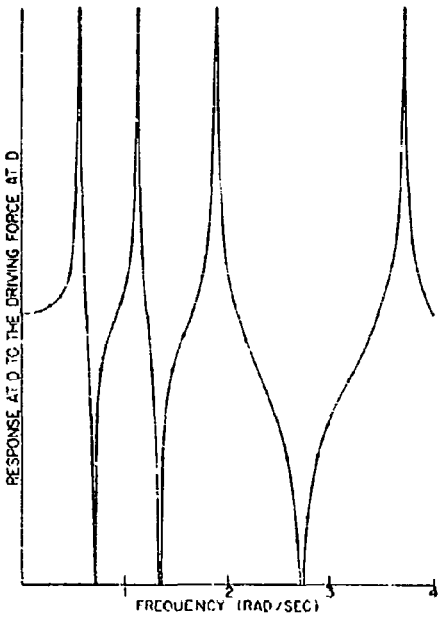

Fig. 7. Response at D to driving force at D

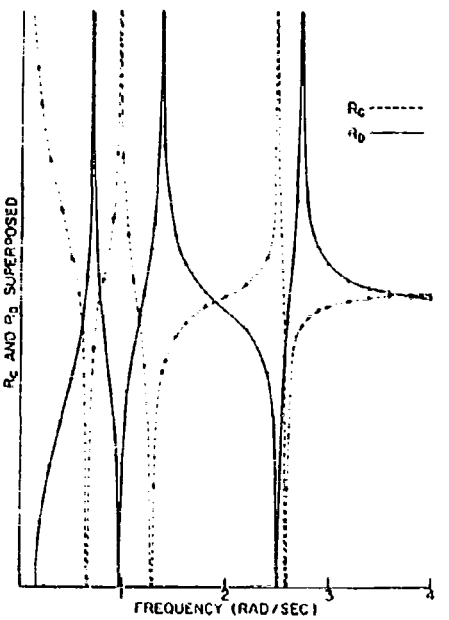

Fig. 9. Ratio plots (Figs. 5 and 8), superposed to determine at which frequencies ratios are of equal value

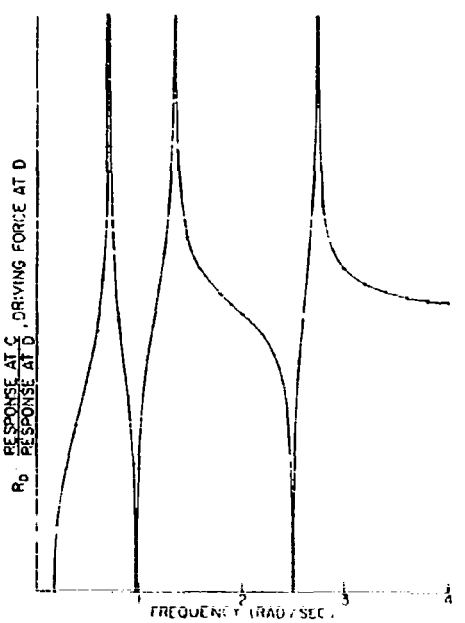

Fig. 8. Ratio of response at C to that at D when driving force is at D

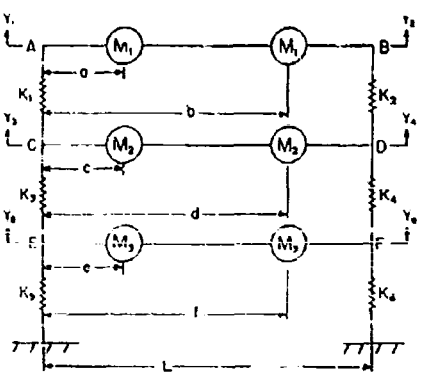

Fig. 10. More general system with system of interest in place

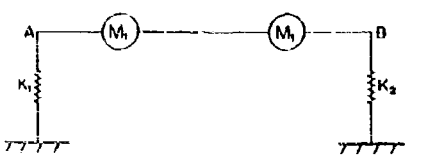

Fig. 11. System of interest for which fixed-base, natural frequencies are desired

system combines the characteristics of the two-base model with those of the chain model. Accordingly, the procedure necessary to find the desired frequencies combines the techniques for each of the two models.

In the dynamic chain, driving forces must be applied at or below the base. When driving forces are applied at points C and D of Fig. 10, the ratio of the response of C to that of D becomes independent of the ratio of the driving forces at the complete system frequencies, at the fixed-base frequencies of the system above points C and D, and at the fixed-base frequencies of the system below points C and D. (The system below points C and D is shown in Fig. 12.) The problem remaining is to separate the desired frequencies from the extraneous frequencies of the complete system and the system below points C and D. As in the chain model, points on the structure of interest must be considered. The ratio of the response of A to that of B becomes independent of the ratio of the driving forces, still at C and D, only at the complete system frequencies and at the fixed base frequencies of the system below points C and D. These frequencies can be eliminated from consideration, and those remaining as crossings on the superposed C-D ratio plot are the fixed-base, natural frequencies of interest. Thus, by using the dynamic chain characteristics to select driving and response points, and the techniques used previously in this paper to determine the frequencies at which the particular response ratios become independent of their excitation ratios, it is possible to find the desired frequencies.

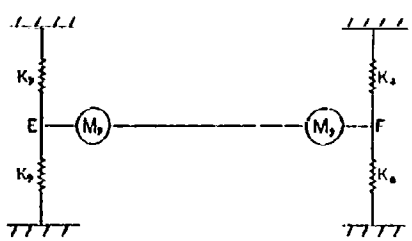

Fig. 12. System located below driving points C and D

A general rule for this type of structural system is that if two points, a and b, on the structure are excited with sinusoidal force P_a and P_b, and the responses of two points, 1 and 2, located above the driving points are recorded, then the ratio of the responses, R_1 R_2, will become independent of the ratio of the driving forces, P_a/P_b, at the fixed-base frequencies of the system above the response points (as if the response points were fixed against translation), at the fixed-base frequencies of the system below the driving points (as if the driving points were fixed against translation), and at the complete system frequencies. (For example, suppose that driving forces were placed at points C and F on the structural system of Fig. 10 and the responses of points A and B were monitored. Then the ratio of the responses, R_A R_B, would become independent of the ratio of the driving forces, P_C/P_F, at the frequencies of the complete system and at the frequencies of the systems shown in Fig. 13.) If the response points are located below the driving points, then the ratio of the responses will become independent of the ratio of the driving forces at the fixed-base frequencies of the system below the response points, at the fixed-base frequencies of the system above the driving points, and at the complete system frequencies.

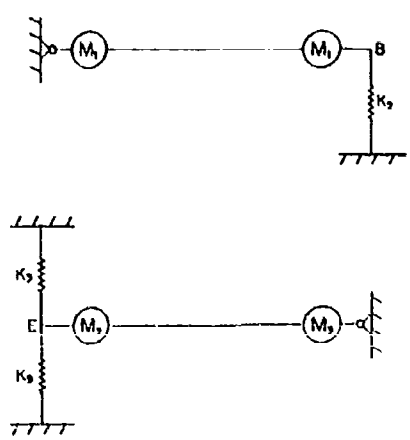

Fig. 13. System located above response points A and B, and system located below driving points C and F

CONCLUSIONS

The determination of the fixed-base, natural frequencies of in-place structures has been a recurrent problem to certain engineers interested in structural dynamics. The most convenient method to date for obtaining these frequencies has been through shake tests. A method proposed in the past for finding the frequencies of a certain type of structure, one

that rests on two base points that are not fixed and is capable of rotation as well as translation, would be cumbersome to apply. This paper presents a new technique that is much more convenient to implement, and describes how it can be applied to analyze a more general class of structures.

The new technique is this: Choose two driving points, (m,n), at or below the base points, (j,k), of the equipment-foundation system for which fixed-base frequencies are desired. Choose two points, (r,s), on the system of interest; the responses of these two points along with those of the base points will be necessary to the analysis. Apply a sinusoidal force to one of the driving points and record the responses of the specified points. Plot the ratio of the motion of one base point to that of the other, $(R_j/R_k)_m$, and also the ratio of the motion of one equipment point to that of the other, $(R_r/R_s)_m$. Apply the exciting force at the other driving point and repeat the procedure; plot the same response ratios as before. Superpose the two base point response ratio plots and note the frequencies where crossings occur. These crossings will be at the complete system frequencies, at the fixed-base, natural frequencies of the system above the base points (the desired frequencies), and at the fixed-base frequencies of the system below the driving points. Next, superpose the two equipment point response ratios and once again note the frequencies where crossings occur. These crossings will be at the complete system frequencies, the fixed-base frequencies of the system above the equipment response points, and at the fixed-base frequencies of the system below the driving points. When the frequencies of the complete system, and of the system below the driving points are known, they may be eliminated from consideration in the set of frequencies noted previously. The frequencies remaining in that set will be the desired fixed-base natural frequencies.

REFERENCES

1. R. E. Kaplan and L. P. Petak "Determination of System Fixed Base Natural Frequencies by Shake Tests," Shock and Vibration Bull. No. 34, Part 3, Dec. 1964, pp. 95

2. L. P. Petak and R. E. Kaplan, "Resonance Testing in the Determination of Fixed Base Natural Frequencies of Shipboard Equipment," NRL Rept. 6176, Dec. 1964

* * *

VIBRATION ANALYSIS OF A STRUCTURAL FRAME USING THE METHOD OF MOBILITY

John Verga
Hazeltine Corporation
Little Neck, New York

A typical structural frame comprises two or more structural elements, usually beams, for each of which we can find individual dynamic solutions using classical methods. However, because of the interaction among the various elements, the classic solution of the overall frame becomes too involved with simultaneous differential equations that are too difficult to handle. A useful method for solving such complex dynamic problems is the mobility method, in which the differential equations are converted to algebraic expressions. This paper applies this method, also identified as "mechanical impedance" and "receptance," to determine the various natural frequencies and corresponding deflection shapes of a diagonally braced portal frame, with vibration limited to the plane of the frame.

The mobility functions of the individual elements of the frames are derived in several textbooks. These functions are mostly combinations of trigonometric and transcendental terms acting on a parameter that includes the frequency of vibration. Numerical values of these functions are also found in textbooks; therefore, we need only select the proper functions, establish their relationship in the frequency equation of the total frame, and then plot the mobility or impedance curves with respect to frequency. Finally, from this plot, the fundamental and all other higher order natural frequencies and modes can be determined, almost by inspection.

Tests were conducted using a frame model of cold rolled steel, 0.020 in. thick, 1 in. wide in cross section, 7.5 in. high, and 12.5 in. long. The fundamental frequencies for both the symmetrical and antisymmetrical modes were found to be within 2 percent of their calculated values. Higher resonances were detected, but unfortunately, their deflection shape was not very clear owing to the imperfections in the model and the superposition of other modes.

INTRODUCTION

The portal frame (the subject of the analysis in this paper) is a common design in structures either by itself or as a basic component of more complex structures. With diagonal braces (Fig. 1), the frame includes seven beam segments with three interaction points (0,2,3). By any standard this constitutes a rather difficult condition to analyze by the basic method involving differential equations. The mobility method, however, eliminates all the complex mathematics. Nevertheless, for practicality, the following assumptions, which would be desirable and justifiable for any method of analysis, are made to further simplify the task:

1. At the frame joints, the angles formed by the frame members remain unchanged with deflections.

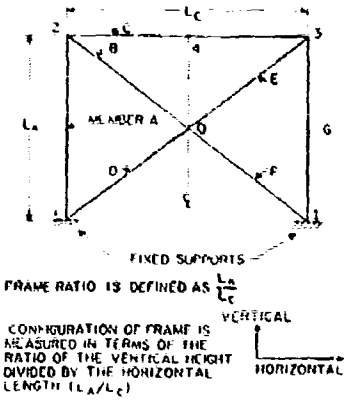

Fig. 1 Portal frame with diagonal braces

2. The shear deflections are negligible.

3. The energy resulting from rotary inertia is negligible.

4. The section properties are uniform throughout the frame.

5. Longitudinal deflection is negligible.

When examining motion within its own plane (Fig. 2), it is noticed that the frame can deflect in only two basic ways; namely, the "symmetrical" and "antisymmetrical" modes. Sketches of the fundamental symmetrical and antisymmetrical modes are also shown in Fig. 2. The antisymmetrical modes are those in which there is no vertical displacement and no bending moment at the center of the top member. The deflection shapes on both sides of the centerline are obviously not symmetrical. The symmetrical modes will be those in which the center of the top member deflects but remains horizontal. As such, the deflection shapes on both sides of the vertical centerline bisecting the frame are always symmetrical. The analysis and discussion of the two modes is carried out separately.

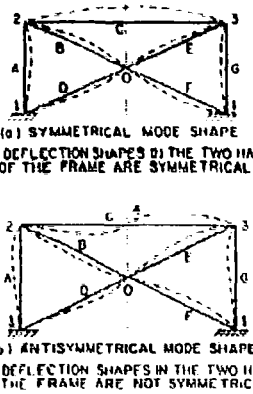

(a) SYMMETRICAL MODE SHAPE
(THE DEFLECTION SHAPES IN THE TWO HALVES OF THE FRAME ARE SYMMETRICAL)

(b) ANTISYMMETRICAL MODE SHAPE
(THE DEFLECTION SHAPES IN THE TWO HALVES OF THE FRAME ARE NOT SYMMETRICAL)

Fig. 2. Fundamental deflection shapes in portal frame

NOMENCLATURE

A_n Coefficient of natural frequency

DM Displacement mobility or receptance (will be referred to as "mobility")

DM_a Mobility in member "a"

$DM_{a1,1}$ Mobility in member "a" involving linear displacement at point "1" owing to a reaction at point "2"

$DM_{a1,2}$ Mobility in member "a" involving angular displacement at point "1" owing to a moment at point "2"

E Young's modulus

F_1, F_2, F_3 Mathematical functions of the beam

g Gravity acceleration, 386 in./sec^2

L Length of the member of the full frame

M Twisting moment

ω_n Angular natural frequency – rad per sec

Z Impedance (mechanical)

λ Beam frequency factor $= \omega^2 \mu / EI)^{1/4}$

μ Mass per unit length

A, B, C, Labels of member of the full frame

a, b, c, ... Labels of members of the half frame

θ Angle of twist

r Frame configuration ratio – $r = L_A/L_C$

Subscripts

a, b, c, ... Pertaining to frame member a, b, c, ...

1, 2, 3, ... Pertaining to point 1, 2, 3, ...

n Pertaining to natural frequencies

ANTISYMMETRICAL MODES

The antisymmetrical modes, which predominate when vibrating in the horizontal direction, are greatly reinforced by the diagonal members. These members prevent translation of the top points 2 and 3 (see Fig. 2(b)). This translation could only come about with longitudinal deflection in the frame members but it has been assumed to neglect longitudinal deflections. This same argument also establishes that the intersection joint at "0" and the top

midpoint at "4," as well, cannot translate. However, rotation at these points does take place to distribute the strain energy through all the frame members in the compliant mode of bending. With rotation thus occurring and translation not occurring, all of these points can then be assumed to act as simple supports.

Because each half of the frame has the same modal form, the system can be represented by one-half of the frame with the constraints from the other half applied to it. The half-frame model is shown in Fig. 3(a). The constraints derived from the other half of the frame consist of the simple support at the midpoint of the top member and at the midpoint of the diagonals. The members of the half frame are identified by the small letters which correspond to the same letters used in capitals for the full frame. (Note: "A" is equal to "a," "B" is equal to "b," "D" is equal to "d"; however, "C" is twice the length of "c.")

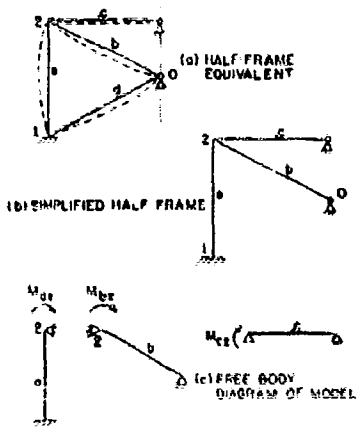

Fig. 3. Vibration model for antisymmetrical mode

The member "d" in the half-frame model is joined to the frame at points "1" and "0." Both of these points are grounded, point "1" as a clamped support and point "0" as a simple support. Therefore, as long as these supports are maintained, for the purpose of simplification it will be assumed that with member "d" removed, the dynamic property of the rest of the frame is not disrupted. This is based on the assumption that the kinetic energy and the strain energy of member "d" are both reasonably small and approximately equal so that their overall effect upon the frame would tend to balance out. (The tests that have been performed seem to bear this out.) This assumption greatly simplifies the half frame to the model shown in Fig. 3(b) with the remaining three members, "a," "b," and "c," commonly joined at point "2." As for member "d," it can be treated separately as a clamped-pinned end beam with its slope at point "0" equal to that in member "b."

A free body diagram of the simplified half-frame model is shown in Fig. 3(c). Because point "2" can rotate but can not translate, its condition is equivalent to a pinned support loaded with a twisting moment, M_2.

For equilibrium to be maintained at the common point, "2," it is necessary that the sum of the moments be zero. The angle of twist must be equal for all three elements to comply with the assumption that the angles formed by the frame members at the joints remain unchanged with deflection. Therefore, the following equations apply:

$$M_{a2} + M_{b2} + M_{c2} = 0 \qquad (1)$$

$$\theta_{a2} = \theta_{b2} = \theta_{c2} = \theta_2 \qquad (2)$$

Dividing Eq. (1) by Eq. (2)

$$\frac{M_{a2}}{\theta_2} + \frac{M_{b2}}{\theta_2} + \frac{M_{c2}}{\theta_2} = 0. \qquad (3a)$$

Each of the fractional terms in Eq. (3a) is by definition the reciprocal of the mobility (or the impedance) of the corresponding frame members. Therefore, the same equation can be written as follows:

$$\frac{1}{[M_{a2,2}]} + \frac{1}{[M_{b2,2}]} + \frac{1}{[M_{c2,2}]} = 0 \qquad (3b)$$

where $[M_{a2,2}]$ represents the displacement mobility of member "a" in terms of angular displacement at point 2 owing to a bending moment at point 2. The same equation may also be written as follows:

$$Z_{a2,2} + Z_{b2,2} + Z_{c2,2} = 0 \qquad (3c)$$

where $Z_{a2,2}$ stands for impedance of member "a" in terms of a bending moment at point 2 owing to an angular displacement at point 2.

Equations (3a), (3b), and (3c) constitute the natural frequency equation for the three elements a, b, and c when connected in parallel [1]. The system is at its natural frequency when the overall impedance of the system is zero.

The mobility of beams with different end conditions is tabulated in Table 1. The suffix with an accent designates the angular sense as against translation when no accent is shown. For example, for the member "a," which is a clamped-pinned beam, the mobility at point 2 in rotation owing to the moment at point 2 is

$$[M_{a\,2'2'}] = \frac{F_{3a}}{EI\lambda F_{5a}}$$

whereas, the mobility at point 2 in translation owing to a pure force at point 2 would be:

$[M_{a\,22}] = 0$ (no translation possible when end is pinned).

Substituting the mobility terms in the natural frequency equation, Eq. (3b), from Table 1, and cancelling out the quantities EI - because they are the same for each frame member (we have assumed uniform cross section in the frame), we resolve the equation to

$$\frac{F_{3a}}{F_{1a}} + \frac{2F_{3b}}{F_{5b}} + \frac{2F_{3c}}{F_{5c}} = 0 \qquad (4)$$

where the functions F are given (that is,

TABLE 1

Tip Receptances for Beams with Different Nature of End Support (excerpt from Ref. [1])

	Type of Beam		Receptance										
	Nature of Support	End	a_{00}	$a_{00'}$ / $a_{0'0}$	a_{0f} / a_{f0}	$a_{0f'}$ / $a_{f'0}$	$a_{0'0'}$	$a_{0'f}$ / $a_{f0'}$	$a_{0'f'}$ / $a_{f'0}$	a_{ff}	$a_{ff'}$ / $a_{f'f}$	$a_{f'f'}$	
1	Free	$x = 0$	$\frac{-F_3}{EI\lambda^3 F_3}$	$\frac{-F_1}{EI\lambda^3 F_3}$	$\frac{F_8}{EI\lambda^3 F_3}$	$\frac{F_{10}}{EI\lambda^3 F_3}$	$\frac{F_6}{EI\lambda F_3}$	$\frac{-F_{10}}{EI\lambda^2 F_3}$	$\frac{F_7}{EI\lambda F_3}$	$\frac{-F_3}{EI\lambda^3 F_3}$	$\frac{F_1}{EI\lambda^2 F_3}$	$\frac{F_6}{EI\lambda F_3}$	1
	Free	$x = \ell$											
2	Clamped	$x = 0$								$\frac{-F_3}{EI\lambda^3 F_4}$	$\frac{F_1}{EI\lambda^2 F_4}$	$\frac{F_6}{EI\lambda F_4}$	2
	Free	$x = \ell$											
3	Clamped	$x = 0$										$\frac{F_1}{EI\lambda F_5}$	3
	Pinned	$x = \ell$											
4	Free	$x = 0$	$\frac{2F_1}{EI\lambda^3 F_5}$	$\frac{-F_6}{EI\lambda^3 F_5}$		$\frac{-F_7}{EI\lambda^2 F_5}$	$\frac{2F_3}{EI\lambda F_5}$		$\frac{F_9}{EI\lambda F_5}$			$\frac{F_1}{EI\lambda F_5}$	4
	Pinned	$x = \ell$											
5	Free	$x = 0$	$\frac{-2F_2}{EI\lambda^3 F_6}$	$\frac{F_5}{EI\lambda^2 F_6}$	$\frac{-F_9}{EI\lambda^2 F_6}$		$\frac{2F_1}{EI\lambda F_6}$	$\frac{-F_8}{EI\lambda^2 F_6}$		$\frac{-F_9}{EI\lambda^3 F_6}$			5
	Sliding	$x = \ell$											
6	Pinned	$x = 0$					$\frac{-F_5}{2EI\lambda F_1}$		$\frac{F_8}{2EI\lambda F_1}$			$\frac{-F_5}{2EI\lambda F_1}$	6
	Pinned	$x = \ell$											
7	Sliding	$x = 0$	$\frac{-F_2}{2EI\lambda^3 F_2}$			$\frac{F_{10}}{2EI\lambda^2 F_2}$						$\frac{F_6}{2EI\lambda F_2}$	7
	Pinned	$x = \ell$											
8	Clamped	$x = 0$								$\frac{-F_3}{EI\lambda^3 F_9}$			8
	Sliding	$x = \ell$											
9	Sliding	$x = 0$	$\frac{-F_9}{2EI\lambda^3 F_1}$		$\frac{-F_7}{2EI\lambda^2 F_1}$					$\frac{-F_9}{2EI\lambda^3 F_1}$			9
	Sliding	$x = \ell$											

Notation: $F_1 = \sin\lambda\ell \sinh\lambda\ell$ $\quad F_6 = \cos\lambda\ell \sinh\lambda\ell + \sin\lambda\ell \cosh\lambda\ell$

$F_2 = \cos\lambda\ell \cosh\lambda\ell$ $\quad F_7 = \sin\lambda\ell + \sinh\lambda\ell$

$F_3 = \cos\lambda\ell \cosh\lambda\ell - 1$ $\quad F_8 = \sin\lambda\ell - \sinh\lambda\ell$

$F_4 = \cos\lambda\ell \cosh\lambda\ell + 1$ $\quad F_9 = \cos\lambda\ell + \cosh\lambda\ell$

$F_5 = \cos\lambda\ell \sinh\lambda\ell - \sin\lambda\ell \cosh\lambda\ell$ $\quad F_{10} = \cos\lambda\ell - \cosh\lambda\ell$

$F_1 = \sin \lambda L \sinh \lambda L$). Because the argument is the same for each individual element (beam) of the frame, Eq. (4) can be written as

$$\left(\frac{F_3}{F_1}\right)_a + 2\left(\frac{F_4}{F_1}\right)_b - 2\left(\frac{F_1}{F_2}\right)_c = 0 \qquad (5a)$$

$$\left(\frac{F_3}{F_1}\right)_a - 2\left(\frac{F_4}{F_1}\right)_b + 2\left(\frac{F_1}{F_2}\right)_c = 0 \qquad (5b)$$

This may be solved by taking trial values of λL and plotting the expression of Eq. (5) against λL. The numerical values of the functions F are tabulated in Table 7, 1(d) of Ref. [1], pages 364-373, for λL ranging from 0 to 11. The general method of solution will be described later.

SYMMETRICAL MODE

The symmetrical mode is the predominant mode when the frame is vibrated along its centerline. For the deflection shape to be symmetrical about the centerline, as shown in Fig. 2(a), the slope at the center of the top member must always be horizontal. From this it follows that the intersection of the diagonals must have zero rotation so that the deflection shape is maintained symmetrical. In keeping with the assumption of zero longitudinal deflection in the members, the tops of the vertical legs, points "2" and "3," plus the center of the diagonals, point "0," must also have zero translation. With zero translation and rotation, then point "0" can be considered as a point of fixety as shown in Fig. 4. As in the case of the antisymmetrical mode, here too the frame can be represented by one half frame. The constraints resulting from the other half consist of the clamped support at point "0" and a guide to allow deflection while maintaining zero slope at the center of the top member. Because member "d" joins the rest of the frame at two points that are clamped, it can be ignored in this analysis as long as the clamped supports are maintained. The half frame then is simplified as shown in Fig. 4(b). Point "2" is considered simply supported because, as in the antisymmetrical mode, although it can rotate, it is assumed that it can not translate, owing to the assumption of negligible longitudinal deflection in the frame members.

Joined at point "2," members "a," "b," and "c" can be regarded as three subsystems connected in parallel. The total mobility, then, using the same steps as in the antisymmetrical case, is found to be

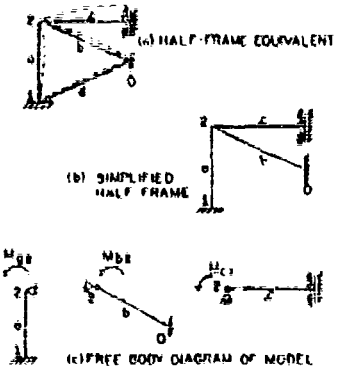

Fig. 4. Vibration modal for symmetrical mode

$$\mathbb{M}_{\text{total}} = \frac{1}{\frac{1}{\mathbb{M}_{a\,2'\,2'}} + \frac{1}{\mathbb{M}_{b\,2'\,2'}} + \frac{1}{\mathbb{M}_{c\,2'\,2'}}} \qquad (6)$$

The overall impedance is the denominator of this overall mobility. As stated above, when the overall impedance is set to equal zero, we have the frequency equation that, when solved, will yield the roots for the natural frequency of the various modes. The frequency equation for the symmetrical mode then is

$$Z_{\text{total}} = \frac{1}{\mathbb{M}_{a\,2'\,2'}} + \frac{1}{\mathbb{M}_{b\,2'\,2'}} + \frac{1}{\mathbb{M}_{c\,2'\,2'}} = 0 . \qquad (7)$$

The mobility for the free body components shown in Fig. 4(c) are from Table 1:

$$\mathbb{M}_{a\,2'\,2'} = \frac{F_{3a}}{(EI\ F_{4a})}$$

$$\mathbb{M}_{b\,2'\,2'} = \frac{F_{3b}}{(EI\ F_{4b})}$$

$$\mathbb{M}_{c\,2'\,2'} = \frac{F_{2c}}{(2EI\ F_{1c})} .$$

With substitution of these functions of mobility into Eq. (7), and with assumption of uniform section and material throughout the frame, the frequency equation becomes

$$\left(\frac{F_3}{F_1}\right)_a + \left(\frac{F_3}{F_1}\right)_b + \left(\frac{F_1}{F_2}\right)_c = 0 \qquad (8)$$

The method of solution of this frequency equation, in terms of the parameter λL and natural frequency, is described next.

SOLVING FOR THE ROOTS TO THE NATURAL FREQUENCY EQUATION

To illustrate the method of solving for the roots to the natural frequency equation, we will apply the procedure to the case of the antisymmetrical mode for a frame configuration ratio of 0.6 as an example. The equation that must be solved then is Eq. (5) because it applies to all antisymmetrical modes. The simplicity of this solution constitutes the main advantage of the mobility method.

From the data in Table 7, 1(d) of Ref. [1], pages 364-373, curves of the quantities F_5/F_3 and $2F_1/F_5$ are plotted in Fig. 5 with respect to the argument, λL. These are the basic curves involved in the antisymmetrical mode. To yield the solution for Eq. (5), these curves must be normalized with respect to the length of one chosen member of the frame and the new curves must then be operated on by the equation.

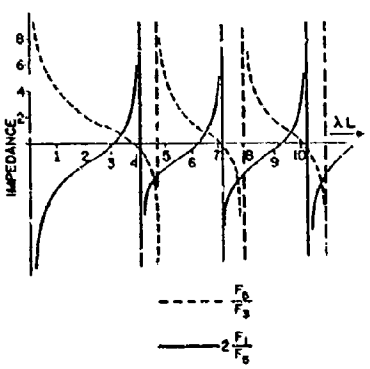

Fig. 5. Basic impedance curves for antisymmetrical modes

In this example, the length of member "a" is chosen arbitrarily and the curves are then stretched or compressed to reflect their relative length with respect to member "a." The curve pertaining to member "a" obviously remains intact. The length of member "b" is practically equal to the length of member "a." Therefore, the curve pertaining to member "b" also remains unchanged. However, for member "c" which is shorter than member "a" by a factor of 1.2 (that is, $L_a/L_c = 1.2$), the basic curve $2F_1/F_5$ in Fig. 5 is stretched out by the same factor along the abscissa when replotted in Fig. 6.

In subsequent steps, the curves $2(F_1/F_5)_b$ and $2(F_1/F_5)_c$ are summed. The intersections

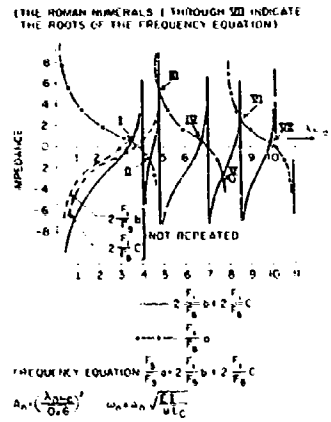

Fig. 6. Impedance curves for antisymmetrical modes for frame ratio = 0.6

of the composite curve with the curves $(F_5/F_3)_a$ are the roots of the frequency equation, Eq. (5b). These roots, indicated by roman numerals in Fig. 6, are $\lambda_n L_a = 3.45, 4.3, 6.7, 7.7, 8.4 \ldots$. Substituting for the beam characteristic, $\lambda_n = (\omega_n^2 \mu/EI)^{1/4}$, we have the expression for the natural frequency at these modes:

$$\omega_n = (\lambda_n L_a)^2 \sqrt{\frac{EI}{\mu L_a^4}}$$

where $(\lambda_n L_a)$ is the root of the frequency equation.

To compare results with those of similar frames, we will express the natural frequency expression in terms of the full length of the horizontal member, L_C:

$$\omega_n = \Lambda_n \sqrt{\frac{EI}{\mu L_C^4}} .$$

The frame ratio, r, is defined as the vertical divided by the horizontal: $r = L_A/L_C = L_a/2L_c$ (member c in the half frame is half of full length).

Then, when the root is found in terms of length for member "a," the frequency coefficient is

$$\Lambda_n = \left(\frac{\lambda_n L_a}{r}\right)^2$$

and when the root is found in terms of the length for the half frame member "c," the coefficient is

$$A_n = (2\pi_n L_c)^2$$

RESULTS OF NATURAL FREQUENCY COEFFICIENTS

For the purpose of comparison, the natural frequency coefficients of the double diagonally braced portal frame analyzed in this paper have been tabulated in Table 2, together with those of the single diagonal brace and simple (unbraced) portal frame. The analyses of the latter two have not been discussed in this paper although they are quite similar. The tabulation conveniently demonstrates the increase in natural frequency of the double brace frame over the single brace and over the simple (unbraced) frame. For instance, for a frame ratio of one, the fundamental antisymmetrical natural frequency has a coefficient of 19.0 for the double brace frame, 9.6 for the single brace frame, and 3.2 for the unbraced frame. The increase gained in the symmetrical mode, however, is relatively small.

Tests were conducted using a frame model of cold rolled steel, 0.020 in. thick, 1 in. wide in cross section, 7.5 in. high, and 12.5 in. long (0.6 frame ratio). The fundamental frequencies for both the symmetrical and antisummetrical modes were found to be within 2 percent of their calculated values. Higher resonances were detected, but, unfortunately, their deflection shapes were not very clear under the stroboscopic light as a result of the imperfections in the model plus the relative inability for large deflections in higher modes.

DEFLECTION SHAPES

For each natural frequency, a corresponding deflection shape exists. The mobility curves for the frame components, Figs. 6 through 10, are very helpful in determining the deflection shapes. It has been found desirable to use, as an example, the case of 0.2 frame ratio (Fig. 9) because this ratio involves essentially only two subsystems or two curves at any given value of

TABLE 2
Tabulation of Calculated Coefficients of Natural Frequencies — A_n

$$\left(\omega_n = A_n \sqrt{\frac{EI}{\mu L_c^4}}\right)$$

Mode \ L_A L_C	1.0	0.6	0.2	0.0	1.0	0.6	0.2	1.0	0.6	0.2
I	14.5	19.8	21	22	3.2	7.2	19.5	9.6	14	18.8
II	19	33	52	61.7	12.9	16.1	30.7	14.4	18	21.4
III	30	50	81	121	21	43	60	19.8	39	53
IV	42.5	51	120	196	23	52.6	108	22.8	47	59
V	51	64	180	296	46	66	180	30	55.6	107
VI	60	106	202	410	—	—	—	—	—	—
VII	64	124	352	-	—	—	—	—	—	—
VIII	92	154	520	—	—	—	—	—	—	—
IX	100	165	—	—	—	—	—	—	—	—
	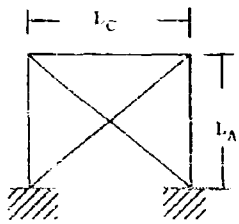				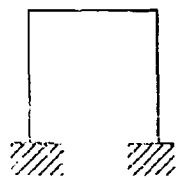			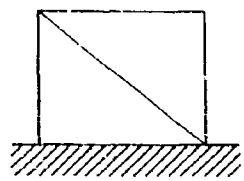		
	Double Brace Frame				Simple Frame			Single Brace Frame		

Note: Symmetric modes are indicated by line under coefficient.

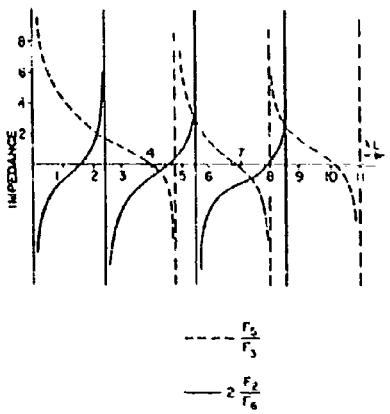

Fig. 7. Basic impedance curves for symmetrical modes

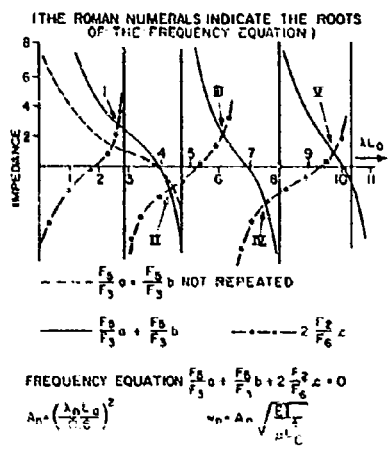

Fig. 8. Impedance curves for symmetrical modes for frame ratio = 0.6

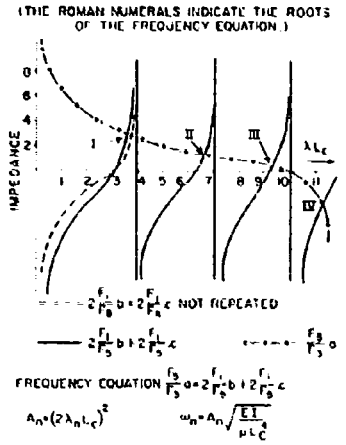

Fig. 9. Impedance curves for antisymmetrical modes for frame ratio = 0.2

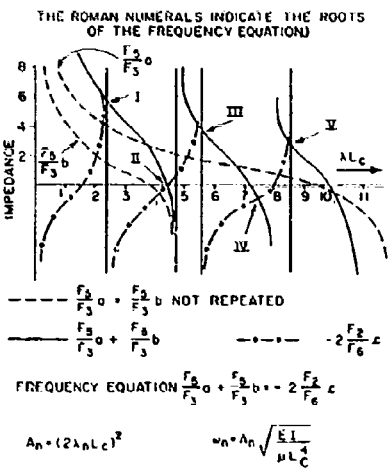

Fig. 10. Impedance curves for symmetrical modes for frame ratio = 0.2

the abscissa, one for member "a" and one for the dynamically similar members "b" and "c." With only two subsystems involved, the deflection shapes should be more apparent.

In Fig. 9, the length of the half-frame member "c" is used in the abscissa. The member "a" is shorter by a factor of 2.5 (that is, $L_a/L_c = 1/2.5$); hence, its curve is stretched out by the same factor. Members "b" and "c" are assumed equal in length; therefore, one curve for both of them, their composite curve, is shown in Fig. 9. The resulting mode shapes for both symmetrical and antisymmetrical cases are shown in Fig. 11.

The stiffness in member "a" is easily recognized by the fact that its first mode curve intersects four consecutive mode curves of members "b" and "c." The first root occurs at $\lambda L_c = 3.6$ where the first curve of members "b" and "c" intersects the initial part of the curve for the stiff member "a." The deflection shape for this root is one without any inflection points

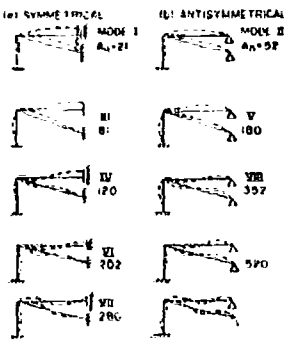

Fig. 11. Deflection mode shapes for frame ratio = 0.2

(see Fig. 11, Mode II). Mode I, the fundamental, occurs in the symmetrical mode which for the 0.2 frame ratio is obviously more compliant.

The second root in Fig. 9, at $\lambda L_c = 6.7$, is the intersection of the same curve of members "b" and "c." Therefore, the deflection shape consists of the next higher mode for members "b" and "c" in compatibility with, but out of phase with, the major deflection in member "a." Each mode is characterized by a change in phase from the previous mode between the member "a" and the two members "b" and "c" which, having equal length and end support, are dynamically identical. The third and fourth roots ($\lambda L_c = 9.4, 11.5$) occur at the intersections of the first curve pertaining to member "a," and the third and fourth curve for members "b" and "c." Consequently, the stiff member "a" is again subject to its first mode shape while the other two members, longer and more flexible, are subject to higher mode shapes with inflection points.

It is plain to see by extrapolation that the next root should occur at the intersection of the second curve for member "a" and the fourth for members "b" and "c." Thus, as the frequency increases, for the first time the short stiff member "a" is deflected in the next higher mode shape with an inflection point. These deflection shapes for frame ratio of 0.2 apply only to the antisymmetrical mode. Using the same technique, with Fig. 10, the deflection shapes for the symmetrical mode, shown also in Fig. 11, are determined.

CONDITION OF ZERO FRAME HEIGHT, $L_A/L_C = 0$

As the length of the vertical member approaches zero, the frame reduces to just the top member "c" clamped at both ends, and its solution is, obviously, identical to that of the fixed end beam.

Theoretically, the member "a" can still be considered as a beam of zero length and infinite rigidity. Its curve, then plotted with respect to λL_c, gets stretched out to infinity. Hence, for all values of the quantity λL_c the ordinate of the curve $(F_3/F_3)_c$ is equal to infinity. Consequently, referring to the antisymmetric case of 0.2 frame ratio in Fig. 9, the frequency equation can be satisfied only at the asymptotes of the curve $2F_1/F_3$. The values of λL_c at these asymptotes constitute the roots of the case of zero frame ratio. The corresponding natural frequency coefficients, λ_n, are 61.7, 196, 410, . . . , equal to the antisymmetric modes of the fixed end beam.

The shape with translation but no slope at the midpoint is found from the curves of the symmetrical mode in Fig. 10. Using the same reasoning as in the above case, the roots must be the asymptotes of the curve $2(F_2/F_6)_c$. The natural frequency coefficients for these roots are 22, 121, 292, . . . , equal to the symmetrical modes of the fixed end beam.

Because these coefficients as found from this analysis are equal to those published in textbooks for the fixed end and the cantilever beams, the comparison can be used as proof of the accuracy of the application of the mobility method.

CONCLUSIONS

Mobility or receptance is a measure of the ease of motion of a system. The reciprocal is called impedance which naturally is a measure of the system's resistance to motion. The impedance of a system is zero when the system has minimum resistance to motion and this occurs when the system vibrates at a natural frequency. Therefore, the equation of zero impedance represents the natural frequency equation.

In the discussion of the symmetrical and antisymmetrical mode, it has been shown how this frequency equation has been produced for each mode in terms of mathematical functions of each member of the frame. The mobility (or

impedance) method of solving these equations has been illustrated. This method is basically a graphical one and it gives us, in essence, a graphical picture of the vibration characteristic of the system. From Fig. 6, for instance, one can easily find the natural frequency roots for the antisymmetrical mode of the braced portal frame with a 0.6 configuration ratio; also, one can determine the deflection shape of each mode. This has been illustrated for the case of the 0.2 frame configuration ratio. Using the mobility curves, the analyst can also study the effect resulting from changes in the rigidity of any one member. For instance, a separate set of impedance curves was not required to solve for the limit case where the length of the vertical member approaches zero. This condition reduced the frame to a fixed beam (the top member fixed at both ends).

It has been shown that the vibration characteristics of a frame composed of two or more members may be found by interrelating the mobility of the individual members. It must be noted that as the number of members increases, and as the number of ways in which they may be oriented relative to each other thereby increase, more and more terms have to be included in the overall mobility equation. This can raise severe practical limitations on the extent to which this method of analysis may be applied to systems that have a large number of members. The analyst, however, by virtue of judgment can eliminate members that have minimum effect upon the behavior of the remaining frame. This was implemented in the analysis. The half-frame was simplified by the elimination of member "d," thereby reducing the vibration model from one having two joints to one having one.

ACKNOWLEDGMENT

The author expresses his gratitude to Professor John R. Currert, Polytechnic Institute of Brooklyn, for his invaluable instructions during a school project on the same subject as this paper.

REFERENCE

1. R. E. D. Bishop and D. C. Johnson, The Mechanics of Vibration (Cambridge Univ. Press, New York), pp. 359, 363-373

BIBLIOGRAPHY

1. Mac Duff, J. N., and Currert, J. R., Vibration Control (McGraw-Hill, Inc., New York), 1958

2. Plunkett, R., "Measurement of Mobility," J. Appl. Mech., pp. 250-256 (Sept. 1954)

DISCUSSION

Mr. Dobson (Gen. Elec. Co.): We use normal mode theory in the evaluation of frames such as you are talking about. Could you tell me briefly the advantage of the impedance method that you have discussed over normal mode theory? Do you use computer programs to actually solve your problems?

Mr. Verga: I can not tell you right now what the advantages of the impedance method would be over the normal mode theory. Although so far we have not used computers, we can do so by taking the data in Bishop and Johnson's "The Mechanics of Vibration" and putting it in the memory of a computer. In that case we can analyze systems with much greater complexity and without the need of trying to reduce the frame by making assumptions based on good judgment, as we did here in eliminating member "d." If member "d" could not have been eliminated, the curves would have become much more complicated. The mobility functions would have included many more terms and it would have been much more difficult to do. The computer would have been much more effective if we had not been able to eliminate member "d."

Mr. Dobson: Do you have any feeling for the accuracy of your method?

Mr. Verga: We have not calculated accuracy. I guess the accuracy in this method is a function of the illustrator or the draftsman in plotting out the equations.

Mr. Manning (Bolt Beranek, & Newman, Inc.): You eliminated member "d" by assuming that the junction of the cross members did not move. I wonder if this is a good assumption when the angle between them is very small?

Mr. Verga: You were referring to joint "0" I take it — the node? We know it did move and therefore we know that the assumption is not 100 percent correct. But because the motion at point "0" will induce kinetic and strain energy in the member, and because this member is so remote from point "2" upon which we hinged our equations, we decided that the overall effect of those two quantities upon the rest of the frame would be a minimum. I guess the answer to your question is that the relative deflection in that member, because of the fixity at the bottom, would be much less than the deflections at the members up above. I suppose this is why the test produced numbers which bore out these assumptions.

Mr. Manning: I think I am asking a different question. I am thinking that you have neglected at point "2" any motion other than moment because you have three beams joined at right angles. I think this is valid.

Mr. Verga: That is right. At point "2" we have assumed zero translation. This is because point "2" is interconnected by diagonal members which are fixed at the other end to the fixture. Therefore, if we must maintain our assumption of neglecting the longitudinal deflections in these members, then we must say that point "2" does not translate. For point "2" to translate, the diagonal members would undergo longitudinal deflections.

Mr. Manning: But this would not be true at point "0," the center point.

Mr. Verga: Point "0" [illegible] in to the four diagonal members. Therefore, for point "0" to move in translation, the diagonal members too must move longitudinally.

Mr. Manning: Yes, but if you have a very shallow angle, point "0" could move in vertical translation without causing much compression in the diagonal element. Go to the case of zero height; then you have the cross members lying flat in the plane and you can picture a mode in which the center point moves up and down and is the antinode of a vibration.

Mr. Verga: This would be much more effective in the symmetrical mode shape, where the vibration is up and down, which we did not discuss here. But you are correct. In the vertical sense that factor would be more predominant and probably would have to be considered.

Mr. McConnell (Iowa State Univ.): In removing the member, I gathered that you said that point "0" was a rigid connection between the cross diagonals?

Mr. Verga: Point "0" was a rigid connection. The joints are rigid, but not rigid with respect to the ground.

Mr. McConnell: No, but rigid with respect to each member. Then, in removing this member, you have removed a constraint as far as moment is concerned on the other diagonal.

Mr. Verga: Yes. The only thing that would make member "d" move would be a moment transmitted through this rigid joint but the effect of member "d" was to create a hinged condition at point "0" which we did not remove. If member "d" were not there, then point "0" would be allowed to deflect up, down, and sideways and not only in the limit condition that the gentlemen from Bolt, Beranek, & Newman brought out earlier.

Mr. McConnell: The rotation at point "0" is not the rotation of a simple support?

Mr. Verga: The rotation at point "0" would still take place and that would be carried out to member "d."

Mr. McConnell: Member "d" influences the amount of rotation. I was wondering if you have any comparison or if you have made a study of the comparison of how much the frequency of that member has been changed by removing the torsional stiffness.

Mr. Verga: We were not hunting for the frequency in member "d." We were hunting for the frequency in the frame. I did run tests which showed that the fundamentals were hardly affected. I do not have a number here for the percentage difference between the natural frequency of the fundamental from tests and that calculated, but I think it is in the paper. The percentage turns out to be very small.

Mr. Putman (Westinghouse Research Lab.): There seems to be in the last two questions some concern about moving member "d." This also concerns me. It seems to me that this is a valid approximation, as long as the natural frequency of that member happens to correspond to the natural frequency of the total structure. Only under these conditions will there be moment transferred between member "d" and, I guess, "c" that it adjoins. Do you believe this is so?

Mr. Verga: I think you are partly right but let me also say that, if member "d" were maintained, then the impedance curves would have shown an additional curve. It would have increased the number of modes from the five

which we were able to see in that graph to six. I am not interested at this point in that additional mode. The overall frame is not influenced very much by the fact that the kinetic and strain energies of "d" have been removed. As far as I am concerned, "d" is still there because I am maintaining the constraint that "d" has produced. I am assuming that its kinetic strain energies have a small net effect upon the three members or upon the rest of the frame.

Mr. Putman: How would you solve the problem if you were to take "d" into account? It seems to me that one of the things which enables you to do the problem is the fact that you have this text book which gives you driving point impedances of beams with certain sorts of end conditions. If you put member "d" in, then member "c" is no longer pivoted there.

Mr. Verga: Member "c" is still pivoted. We have not changed the boundary conditions. I am justifying the elimination of "d" because the effect that "d" has had upon the frame is still being maintained.

Mr. Putman: It is if they rotate about that point, but it is not a free rotation as you assumed. It has another moment coming from member "d."

Mr. Verga: Right. There is at point "0," where "d" has been removed, some resistance to rotation owing to the strain energy. At the same time there is some effect in opposition to resistance owing to the kinetic energy that has also been removed.

Mr. Putman: You are saying that resistance is small, right?

Mr. Verga: Yes. I am saying that the overall effect is small. To avoid going into a computer and to illustrate this as quickly as possible, I have been able to remove it.

Mr. Putman: I think the subject of discussion is whether it is or is not small.

Mr. Verga: I will add that the tests have shown that it is small. I guess without those tests I would have the same doubts which you are displaying.

* * *

APPLICABILITY OF MECHANICAL ADMITTANCE TECHNIQUES*

D. U. Noiseux and E. B. Meyer
Bolt, Beranek, & Newman, Inc.
Cambridge, Massachusetts

This paper reviews the conditions under which mechanical admittance techniques can be used to calculate vibration transmission. An example of random vibration transmission illustrates the range of errors which can be anticipated within the present state-of the-art.

INTRODUCTION

The applicability of mechanical admittance techniques to the solution of vibration transmission in real structures is reviewed in this paper. By techniques we mean the measurement of the admittances and the calculation of transmission based on the measured admittances. We shall use admittances because it is a more convenient format from an experimental point of view than the equivalent impedance format.

We will assume that the reader is already familiar with the admittance or impedance formats for harmonic and random vibration transmission [1-3].

The structures considered are those typical of aerospace vehicles: A composite of beams and panels in a gas medium. The structures can thus be viewed as waveguides where the gas-solid interfaces of the structure guide the different types of waves that the structures allow: Extensional waves, flexural waves, torsional waves, and so forth. The electrical analogy is then seen to be with microwaves rather than with electric circuit theory based on lumped parameters.

The mechanical admittance formulation relates the excitation and responses of a set of points of a linear structure. When all the degrees of freedom of each point are included, the formulation is a complete one. It is a statement of linearity. From the experimental point of view the admittance formulation is deceptively simple. It says that any information as to what types of waves are propagated in the structure is irrelevant provided one obtains the complete set of admittances at the selected points; wave information is traded for a vast amount of experimental evidence at specific points.

Experimentally we cannot obtain a complete set of admittances, and those experimental values that we can measure contain inherent experimental errors. The incomplete admittances require the selection of a simplified model of the vibration transmission which is compatible with the quantities that can be measured. This model can be chosen only with a good understanding of the principal modes of vibration transmission in the structure. The experimental errors further limit the size of the model because the propagation of errors in the calculations is such that errors in the results grow very rapidly with the complexity of the model.

For periodic and transient excitations the admittance format relating excitations and responses is a rather simple one. For random vibration the format becomes much more involved. In the harmonic case the excitation and response are column matrices; in the random case they are square matrices of spectral densities. The calculation format also becomes more complicated. Because these calculations involve more experimental elements than in the harmonic case, the calculations will also yield larger errors.

*The work reported herein was performed under USAF Contract No. AF 33(615)-5117

It is interesting to compare the limitations of two very different approaches to the vibration transmission problem: The admittance technique and the simulation of the structure by a digital computer. The computer simulation consists of taking a model of the structure as a set of differential equations with boundary conditions and of performing accurate calculations based on this model. The variables and the operators of the differential equations and the boundary conditions are precise and consistent statements about the model, although the model is necessarily only an approximation of the real structure. From these precise statements the computer can make very precise calculations, limited only by the number of bits of each word.

In the admittance technique the structure solves its own differential equations and boundary conditions whatever they may be. However, the experimental errors restrict the accuracy of the calculations that can be made.

Both the computer simulation and the admittance technique are deterministic approaches to a problem that is not absolutely definite: The dimensions of the structure, the boundaries or interfaces of built-up elements, the damping mechanism, and so forth, are not accurately known for a given structure; furthermore, they vary from unit to unit of the same design. Either approach should choose approximations that are compatible with the present uncertainties in the structures.

The state-of-the-art of mechanical admittance techniques is still far from a level of sophistication approaching the domain of uncertainty of a structure. This is why rather crude approximations are often justified because more refined ones include greater experimental errors which defeat the greater potential accuracy in the end result.

APPLICATIONS

The admittance technique is an experimental technique; the admittances in the vibration transmission formulas are obtained experimentally. This technique requires that the structures be available, at least separately.

The format of admittance for vibration transmission has only limited applications in design work because it deals with information at the terminals – the admittances of a set of points. For design, more insight into the mode of transmission is needed.

Although the excitation of a structure appears as a set of effective force or velocity sources in the impedance or admittance formulation, it need not be of mechanical origin. Acoustical excitation, for example, falls within the scope of mechanical admittance techniques provided the acoustical coupling with the acoustical field is invariant to the perturbations caused by the connection of additional structural elements. In practice this requires that the acoustic excitation area be sufficiently removed from the connection area so that the impedance of the connection reflected onto the excitation area is negligible.

There are two rather broad categories of vibration transmission problems where the admittance technique has been applied with some success. The first category consists of cases where the excitation is harmonic and of relatively low frequency. In the second category the excitation is random having a relatively broad frequency spectrum.

Both categories are limited to vibration transmission across a small set of contact points between two structures, each point having very few significant degrees of freedom. (In most cases we consider only one degree of freedom per point.)

This restriction to contact points instead of line or area contacts is inherent in the admittance formulation. Although a line or surface admittance could be approximated by an ensemble of point admittances, and the problem carried on a point admittance basis, it is clear that the number of points selected would be rather large for high frequencies. Then the accuracy of calculations degenerates rapidly with the order of the matrices.

We are limiting the applicability of admittance technique to a connection of only two structures, the connection or interface being a set of points. Only one structure is active, that is, has vibration sources; the other structure is passive.

Formally, the admittance technique is neither restricted to a single interface nor to a single active structure. In the category of low-frequency harmonic excitation, linear superposition of the responses obtained when only one structure is assumed active can be used; we then have essentially two separate vibration problems. The difficulty is in the superposition, because each calculated response has errors that are usually much greater than the individual experimental errors; thus in frequency regions where the responses are almost equal and nearly out of phase, very large errors result in their superposition. If the excitations of each structure, although individually

harmonic, are independent, this difficulty is not present.

In the category of random excitation with broad frequency spectra, we generally cannot superimpose the responses obtained from one active structure to those obtained from the second structure when active. In fact there is formally no superposition theorem for such case, all the excitations with their combined cross power spectral density must be applied simultaneously. However, when the excitations are independent, either because they come from independent processes or because they originate from the same process and the time delays and dispersion in the two active structures are such as to render each excitation independent, a superposition of the power-like quantities in the responses is then permissible. This is often the case. It follows that consideration of two connected active structures often amounts to the solution of two independent problems

Limiting vibration transmission to one interface is again for the practical reason of experimental errors. Formally, the vibration transmission across one interface can be iterated with the addition of another structure and interface. However, the experimental errors render this iteration impractical. We might make an exception for two interfaces when the structure between them is rather simple, for example a set of shock mounts; even here some caution is necessary at high frequencies.

Finally, it is important to detect and make use of any symmetry that exists. The point to make is that symmetry should be introduced in the formulation of the transmission rather than letting symmetry find its own way in matrices of large order.

With these remarks in mind we can discuss each of the two categories of applications.

Low Frequency Harmonic Excitation

Consider two structures, one passive and the other active, to be joined at one interface consisting of a few points, each having very few – one or two degrees of freedom. Symmetry of the structures is introduced in the formulation of vibration transmission. The excitation is harmonic, having a line spectrum with only a few lines

This type of problem has been solved successfully in the past, with admittance techniques, as in the case of machinery mounted resiliently on a base, where either the base or the machinery is active. Many such cases are reported in the literature.

At frequencies up to the first few resonances of the structures, the admittance technique could yield fairly accurate results because experimental errors like transducer constraints on the structures can be minimized, and the model of transmission could be a fairly simple one. At intermediate and high frequencies, one has to resort to much simplified models of transmission and accept fairly large uncertainties in the calculated result.

Broadband Random Vibration

We are still restricting our problem to that of two structures, one active and the other passive, to be connected by a few points, each point having one or at most two degrees of freedom. Again, symmetry of the structures, if it exists, is introduced directly in the formulation of the vibration transmission.

The formulation of the random transmission is generally taken as an approximate one, because the full formulation in terms of the complete power spectral densities has unmanageable proportions. The approximations are those of assuming independence of the excitation at each point, and of working with relatively broad frequency bands, such that only the mean values of the impedances, and the mean square values of the excitations are required. It is a rather rough approximation. Some refinements [3] like the use of average admittances with correlation coefficients could be made

Calculations of Vibration Transmission

In view of the many approximations used, it is quite important to select a simple but realistic transmission model on which to base the calculations of transmission. By model we mean the number of points, their degrees of freedom, the symmetry of the coupling between points, and so forth. Once the model is chosen and some measurements made, the model should be checked against these measurements to see if further simplifications are possible. One important simplification to look for is the following one.

The vibration transmission across the interface of two connected structures requires that the free velocities of the face of the active

structure be known and that the admittance matrices of the two faces be known. When the admittances of one face, say, that of the second structure, are much greater than those of the first structure, the face of the first structure becomes a velocity source. If the reverse situation is true, where the admittances of the first structure are much greater than those of the second structure, the first structure becomes a force source. In practice, one or the other situation will be true in many frequency ranges. This information makes the calculations much simpler. It follows that even a crude approximation of the admittance of the faces of the two structures could be very useful in vibration transmission.

Examples of such cases where admittance technique could be very useful are found in aerospace structures, to which a secondary structure, like an instrument package, is to be attached. If the interface of the aerospace structure is specified only by accelerations, an important modifier of the transmission is missed – that of the interaction between the impedance matrices of the interfaces. The specified free acceleration of the source amounts to assuming an infinite source impedance. This assumption is often a very unrealistic one. If, in addition to the free accelerations, the impedances of the two interfaces are obtained, a much better estimate of vibration transmission could be calculated.

Often the source admittance, for one degree of freedom, of only one typical point of the interface is very valuable information; that, along with the free acceleration at that point and of course with the admittance of the load, could be used to yield rather good estimates of vibration transmission. This admittance could be specified only in magnitude and averaged over each frequency band. It is interesting that this kind of rough estimate is useful for the random vibration but would not be useful for the harmonic case which requires much more detailed information.

Vibration Testing

An important application of admittance techniques is in the simulation of the vibration environment. Unfortunately many of the vibration tests for acceptance of an instrument package disregard the admittances of the sources, retaining only their free velocities (or accelerations). A more realistic test is obtained if both the source admittances and the spectrum of the free velocities are simulated, and the instrument package is mounted on this simulator. This would allow modes of transmission, for example moment coupling, that are not at present simulated by the conventional lineal shakers. The source and load admittances are permitted to interact to give a more realistic vibration level at the base of the instrument package. Admittance technique in this case is used to verify that the simulator has the correct source admittances. There are difficulties, however, in simulating low frequency admittances; high frequency admittances are more easily simulated because they become the driving point admittances of the infinite extension of the source structure in the immediate vicinity of the source points.

In practice, it may be necessary to perform the vibration test in two steps if the shakers cannot supply enough excitation through the simulated source admittance. In the first step, the simulated source admittance is excited at some level and the resulting acceleration spectrum noted at the connection points, but without the test package; then the test package is connected and the resultant change in acceleration spectrum of these points noted. The same change in spectrum is applied to the original specifications of free accelerations giving the modified acceleration levels to be used in the second step. In the second step the test package is tested directly by the shakers without the simulated source admittance.

This two-step approach is not as realistic as the single-step approach because the test points are more constrained by the shaker connection than with the simulated source admittance.

EXAMPLE OF RANDOM VIBRATION TRANSMISSION

We consider a cylindrical shell as the first structure and a "black box" as the second structure. The shell represents an aerospace structure vibrating in response to rocket noise or similar excitation that creates a vibration field. The black box represents an instrument package that contains some vibration sensitive components. The black box is tied to the shell by two points which are the interface.

The measured overall transmission obtained when the two structures are tied together will be compared with the calculation of transmission using the measured admittances. Realizing that only an incomplete set of admittances can be obtained experimentally because we cannot measure moment admittances, and that experimental errors are present in the measurement of each admittance element, the

challenge is one of approximations. We will try to use in our calculations the least number of measurements that permits a reasonable prediction of the vibration transmission.

Description

Cylindrical Shell – The cylinder is a thin aluminum shell reinforced with three rings and five longitudinal aluminum beams. The rings and beams are cemented to the shell with epoxy. We have the following dimensions:

Diameter	25 in.
Length	6 ft
Skin thickness	1/16 in., Al.
Cross section of rings and beams	1/2 × 3/4 in

The skin of the shell has damping tape to increase the loss factor of the shell to approximately 5×10^{-3} above a few hundred Hz.

The cylinder is set vertically, supported at three points on the floor; at these three points the base ring is clamped to the floor.

The vibration field is induced by one Goodmans type V-50 shaker which is attached to one longitudinal beam at approximately 2-1/2 ft from the floor. The shaker applies random vibrations to the shell in the form of individual third octave bands of noise. The excitation voltage at the shaker will be kept at a constant value for the set of third octave bands during all the active tests – both those giving the free velocities at the attachment points of the black box and those giving the overall transmission.

The two points of the interface between the shell and the black box are located on adjacent longitudinal beams of the shell and on the same circumference.

Black Box – The black box is represented by an aluminum beam carrying an aluminum plate. The plate has damping tape to bring its loss factor to approximately 10^{-2} at frequencies above a few hundred Hz. The two ends of the beam are the two points of the interface which connects to the cylindrical shell. The output point is near one edge of the plate. This model of the black box was chosen to include the constituents of a box (beam and plate) and yet to be simple enough to permit some analysis.

Photographs of the cylinder, load and vibration source of the cylinder are shown in Fig. 1. The load is seen on the left hand side; the exciting shaker is on the right hand side. A closeup view of the load connected to the cylinder is given in Fig. 2; the miniature accelerometer is at the output point, 3.

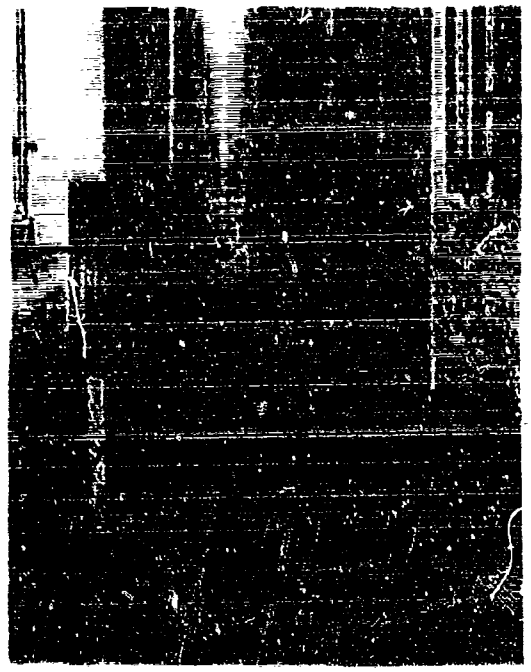

Fig. 1. Photograph of the cylinder, exciting shaker and load

Calculations

Following the block diagram of Fig. 3, and assuming harmonic excitation, the output velocity V_3 at point 3 is given by the matrix equation

$$V_3 = Y_3' Y \cdot Y'^{-1} V \qquad (1)$$

where V is the free velocity vector at points 1 and 2, Y and Y' are the admittance matrices of points 1 and 2 and points 1' and 2', and Y_3' is the transfer admittance from points 1' and 2' to point 3.

In terms of accelerations aV_3 and aV we can rewrite the same equation as

$$aV_3 = aY_3' \cdot Y \cdot Y'^{-1} \cdot aV \qquad (2)$$

For random excitation, we consider a set of frequency bands and write the transmission

Fig. 2. Photograph of the load attached to the cylinder

in terms of average admittances over each frequency band:

$$\overline{\Delta V_3} = \overline{\Delta Y_3'} \left[\overline{\Delta Y} + \overline{\Delta Y'} \right]^{-1} \overline{\Delta V_1} \,. \qquad (3)$$

This is an approximate formulation which has been justified elsewhere [3]. The bar over each quantity expresses the average character of each term. Each element of average admittance, times ω, takes the form

$$\overline{\omega y} = \overline{\omega y_i} \left[1 + e^{i\theta} + (1 - \gamma^2)^{1/2} \right] \qquad (4)$$

where γ is the correlation coefficient of the envelope of the band of noise that we have called the coherence coefficient:

$$\gamma = |\gamma| e^{i\theta} \,. \qquad (5)$$

The first term $e^{i\theta}$ is a phasor; the second term $(1 - \gamma^2)^{1/2}$ is treated as a random independent quantity.

The measurements with an impedance head and an accelerometer have been set up to obtain directly the quantities in Eq. (3); there are altogether 10 quantities to be measured in Eq. (3),

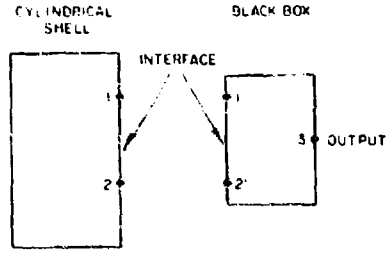

Fig. 3. Two-point interface between two structures

and each quantity has a magnitude and correlation coefficient that is the equivalent of a phase angle.

The calculation of the transmitted acceleration $\overline{\Delta V_3}$ is shown in Fig. 4 and compared with the measured overall acceleration. The difference between the two curves of Fig. 4 is the error which we now discuss.

CONCLUSIONS

The result of Fig. 4 shows a fair agreement between the transmission calculated by admittance technique and the actual overall transmission. However, there are significant errors in each frequency level, sometimes exceeding 10 db. The errors can be divided into the following kinds: Errors associated with the model of transmission assumed for the calculations, errors related to the approximate format of Eq. (3) for random vibration, and experimental errors.

The model of transmission assumes that only the force coupling (or transverse acceleration on the beam of the cylinder) is significant between the shell and the black box. This model gives 2×2 matrices for the admittances Y and Y' of the interface. Moment coupling plays an essential role in beams and plates and should be included. Then each point of the interface would have two degrees of freedom and the admittance matrices Y and Y' would become 4×4 matrices. However, better this new model would be, we cannot measure conveniently the moment impedance elements of the matrix. Specifically, if the matrix Y is so organized that the force components of admittance are listed first, followed by the moment components, we would have

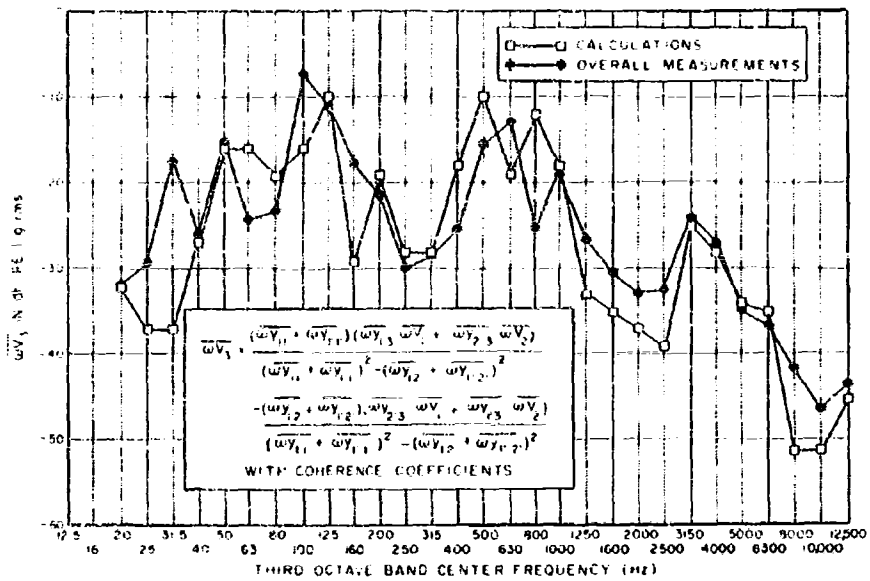

Fig. 4. Calculated and measured acceleration response $\overline{\omega V_3}$ of the load on the cylinder

$$Y = \begin{bmatrix} y_{11}^{VF} & y_{12}^{VF} & y_{13}^{VM} & y_{14}^{VM} \\ y_{21}^{VF} & y_{22}^{VF} & y_{23}^{VM} & y_{24}^{VM} \\ y_{31}^{rF} & y_{32}^{rF} & y_{33}^{rM} & y_{34}^{rM} \\ y_{41}^{rF} & y_{42}^{rF} & y_{43}^{rM} & y_{44}^{rM} \end{bmatrix}.$$

Because $y_{ij} = y_{ji}$ by reciprocity, there are 10 independent elements. The superscripts V and r refer to lineal and angular velocity. The superscripts F,M refer to force and moment. Assuming that we can measure angular velocity r but not the moment M it follows that there are three elements: y_{33}, $y_{34} = y_{43}$, and y_{44} (that cannot be measured conveniently within the present state-of-the-art). In some cases it may be possible to relate force admittances to moment admittances [3] using for example the relations found in semi-infinite beams or plates. This approximation should be investigated further.

Reconsidering the model used for the calculations, we may question the relevance of the coupling between the two points of the interface. If these two points were assumed to be independent, an even simpler model would result where each matrix becomes a single element. This was used for the basis of a calculation which is shown in Fig. 5. The result is almost as good as the result of Fig. 4. This result should be viewed with caution. It is caused by the high degree of symmetry of the cylinder and of the black box, with respect to a line midway along and perpendicular to a line joining the two contact points.

The format of Eq. (3), where the excitation and response are column matrices, is an approximation of the more rigorous format in terms of power spectral densities. The format of Eq. (3) introduces systematic errors. Whether the more rigorous format would yield more accurate calculations is questionable in view of experimental errors. Because the average admittances in Eq. (3) have a smaller range of values as a result of the averaging process, the calculations involving inverse matrices are less likely to become unstable; the growth of errors in the calculations is restricted. This would not be the case with the power spectral density formulation where the harmonic admittances have a very large dynamic range and the resultant admittance matrix may become "ill conditioned" because of experimental errors.

In conclusion we can say that admittance techniques are usefull for the calculations of

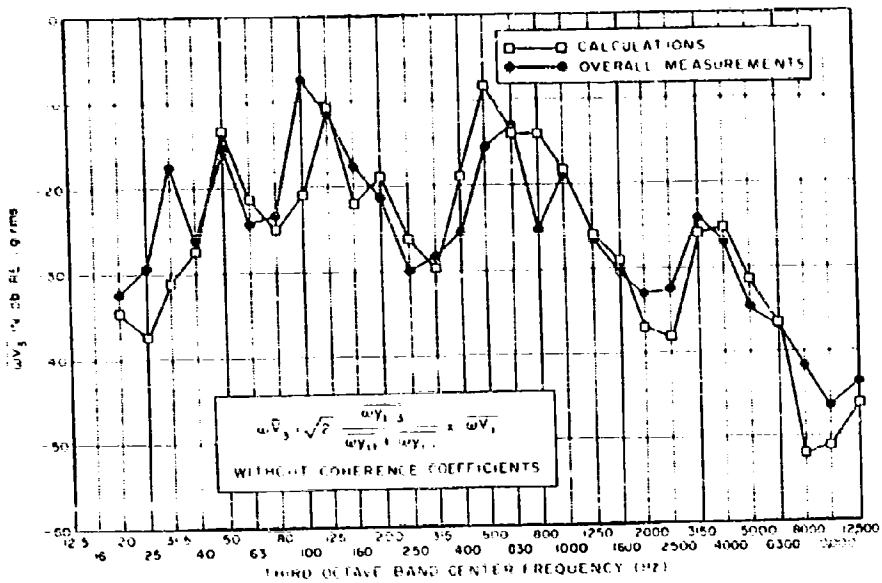

Fig. 5. Calculated and measured acceleration response $\overline{V_3}$ of the load on the cylinder

vibration transmission of many relatively simple cases. Indeed, we do not know of other techniques that could yield results like those of Fig. 4 or 5.

Further work in the development of techniques to measure moment admittances is needed. Also a more systematic balance between the effects of experimental errors on the calculations of random vibration, the approximate model of transmission, and the approximate formulation of random vibration should be sought.

REFERENCES

1. S. Robinson, "Transmission Matrices for Vibration and Their Relation to Admittance and Impedance," J. Eng. for Industry, Trans. ASME, 86:Series B, No. 1 (1964)
2. J. D. Robson, An Introduction to Random Vibration (Edinburgh Univ. Press, Edinburgh), 1964
3. D. U. Noiseux and E. B. Meyer, "Application of Impedance Theory and Measurements to Structural Vibration," Tech. Rept. AFFDL-TR-67-182

* * *

APPLICATION OF THE MECHANICAL RECEPTANCE COUPLING PRINCIPLE TO SPACECRAFT SYSTEMS*

Ewald Heer
Jet Propulsion Laboratory
California Institute of Technology
Pasadena, California

and

Loren D. Lutes
Rice University
Houston, Texas

This paper explores the use of mechanical receptances (frequency response functions) in determining the dynamic response of a system from subsystem characteristics, where the basic problem is considered to be that of joining together and determining the dynamic response of a number of components that may, for example, simulate space vehicle subsystems. A brief theoretical discussion is given which includes the problem of component resonance and a short description of the Receptance Coupling Program (RECEP). The particular problem of eliminating the effects of the measuring equipment from experimentally determined receptances is treated. In an example of a beam excited simultaneously at two points, comparison of the measured and corrected results shows considerable influence of the experimental equipment.

INTRODUCTION

During recent years attention has been directed to the analysis and evaluation of the general dynamical and vibrational behavior of structural systems with ever increasing complexity. While it is desirable to consider the complete system, a direct dynamic analysis of a large spacecraft system may not be practicable even with the most powerful computer presently available. Similarly, it is frequently not feasible to conduct dynamic tests of spacecraft systems in one piece because of their size, or because different parts of these systems are fabricated and assembled at different geographical locations. A method of first dividing the system into suitable subsystems and then determining the system response from the subsystem characteristics has, therefore, definite advantages, particularly when some subsystems already have flight qualification and are to be combined with different, new subsystems, as, for example, in the Apollo and Mariner space programs.

In this paper the method of determining the dynamic response of a system from the subsystem characteristics is explored for application to large space vehicle systems. The basic problem is considered to be that of joining together and determining the dynamic response of a number of subsystems that may simulate a launch vehicle, a spacecraft, an entry capsule, and a lander system.

Presently employed practices in analysis and dynamic testing of spacecraft subsystems usually oversimplify spacecraft interaction with the launch vehicle. In Refs. [1-3], among others, it has been pointed out that it is important to consider the spacecraft as an integral part of the space vehicle system. Such considerations become particularly important for the later stages of a mission, when a number of subsystems of comparable mass dynamically interact. An example of such systems is a planetary lander subsystem attached to an entry capsule that in turn is mounted to a fly by or orbiting spacecraft. Another, but similar, situation

*This paper presents the results of one phase of research carried out at the Jet Propulsion Lab., Calif. Inst. Tech., under Contract No. NAS 7-100, sponsored by NASA.

exists in the Apollo program, where the space vehicle system consists of the three stages, S-IC, S-II, S-IV B, and the Apollo spacecraft, which includes a command/service module and a lunar excursion module. The launch vehicle and/or spacecraft is thus composed of two or more subsystems that can be large by themselves and that can be designed, built, and tested by different manufacturers. Furthermore, the same subsystem can be used in different missions. A method of determining the dynamic response of a system from subsystem characteristics that are determined experimentally and/or analytically has, therefore, a wide application in the development of space vehicles.

The method of analyzing dynamic systems based on subsystem characteristics has been advocated in one form or another by a number of authors [4-10]. In addition, a digital computer program has been developed in Ref. [11] based on the developments in Ref. [7].

If the subsystem characteristics are determined analytically using a modal analysis approach, the developments in Refs. [7] and [11] are, in most cases, suitable for the analysis of the coupled system. However, if the subsystem characteristics are determined experimentally on actual structural systems, it is convenient to use the concept of transfer function (frequency response function) for the response analysis of the coupled system, as advocated in Ref. [10]. Of course, the concept of transfer function is not restricted to the use of experimental data, because the transfer functions can be generated from modal analyses; this then opens the interesting and practically useful possibility of designing new subsystems (for example, spacecraft) coupled to already qualified and tested subsystems (for example, boosters) that are characterized by their transfer functions at the interface points.

Within the broad concept of transfer function, the concept of receptance has been found to be somewhat more convenient than the concept of impedance, mobility, or the like, and is therefore adopted here. Nevertheless, the developments in this paper are, with slight modifications, also valid for these other concepts, as is indicated in the example discussed later in this paper under Elimination of Instrumentation Effects. Unless stated to the contrary, the derivations are in the frequency domain and all matrix manipulations are valid at a particular frequency. All receptances and inputs are complex functions of frequency so that damping is allowed for as long as linearity is preserved.

THEORY OF RECEPTANCE COUPLING

A system is considered composed of N arbitrarily interconnected subsystems (Fig. 1). For

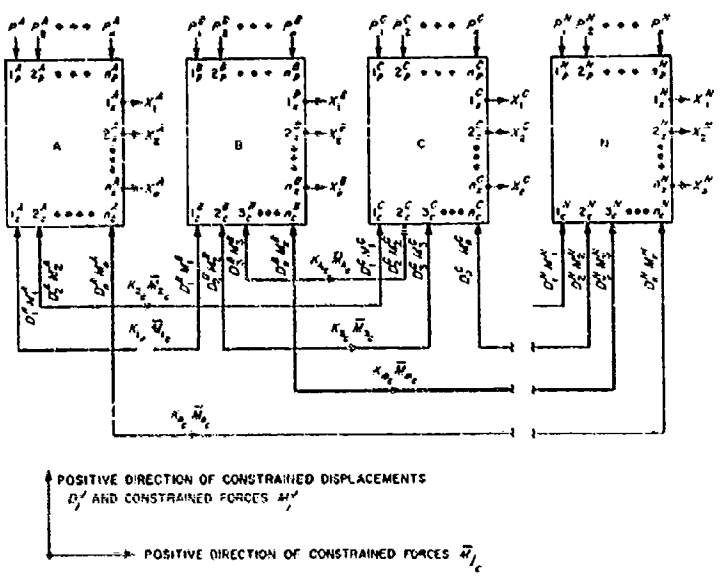

Fig 1. Representation of system consisting of N coupled subsystems

practical reasons, which in most cases require deformable rather than rigid connections between the subsystem's coupling points, it is assumed that the interconnections consist of discrete massless coupling units (Fig. 2), with generally typical, frequency-dependent compliances $K_{m_i}(\omega)$ [10].

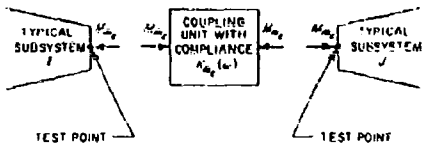

Fig. 2. Typical coupling unit

In the frequency domain the vector of constrained displacements of the typical subsystem J for a particular frequency ω can be written

$$\{D^J\} = [\bar{\mathcal{F}}^J]\{M^J\} + [\bar{\mathcal{F}}^J]\{P^J\} \qquad (1)$$

and for the entire system,

$$\{D\} = [\bar{\mathcal{F}}]\{M\} + [\bar{\mathcal{F}}]\{P\} \qquad (2)$$

where $[\bar{\mathcal{F}}^J]$ and $[\bar{\mathcal{F}}^J]$ are the receptance matrices in the Jth subsystem involving only coupling points and one coupling and one excitation point, respectively; while $\{M^J\}$ and $\{P^J\}$ are the vectors of constrained forces and external excitations, respectively. The matrices in Eq. (1) are submatrices in Eq. (2) and determine the partitioning pattern of the latter. The excitation vector in the frequency domain $\{P\}$ in Eq. (2) is related to the excitation vector in the time domain by the following Fourier transform relation:

$$\{P(\omega)\} = \int_{-\infty}^{\infty} \{p(t)\} e^{-i\omega t}\, dt . \qquad (3)$$

The conditions of compatibility at the coupling points can be written with the help of Fig. 1 as

$$[C]\{D\} = \left[K\right]\{M\} . \qquad (4)$$

The equilibrium conditions across the coupling units become

$$[C]^T\{M\} = \{M\} \qquad (5)$$

where $[C]$ is a real rectangular matrix having only two nonzero elements in each row, (-1) and (+1). $[C]$ can be partitioned as determined by $\{D\}$ as follows:

$$[C] = \left[[C^A] \ \ldots\ [C^J] \ \ldots\ [C^N]\right] \qquad (6)$$

where each submatrix has at most one nonzero element in a row. $[K]$ is the diagonal compliance matrix of the coupling units.

Using Eqs. (2), (4), and (5), the vector of the unknown constrained forces can be written

$$\{M\} = [C]\,[A]\,[C]^T[\bar{\mathcal{F}}]\{P\} \qquad (7)$$

where

$$[A] = \left[\left[K\right] - [C]^T[\bar{\mathcal{F}}][C]\right]^{-1} . \qquad (8)$$

The frequency response vector resulting from the external excitations and constrained forces in subsystem I is

$$\{X^I\} = [\mathcal{F}^I]\{P^I\} + [*\mathcal{F}^I]\{M^I\} \qquad (9)$$

and the frequency response vector for the entire system is

$$\{X\} = [\mathcal{F}]\{P\} + [*\mathcal{F}]\{M\} \qquad (10)$$

where $[\mathcal{F}]$ is the matrix of receptances between response and excitation points, while $[*\mathcal{F}]$ is the matrix of receptances between response and coupling points; $[\mathcal{F}^I]$ and $[*\mathcal{F}^I]$ are the respective submatrices and determine the partitioning patterns of the matrices $[\mathcal{F}]$ and $[*\mathcal{F}]$, respectively. Substituting Eq. (7) in Eq. (8) gives

$$\{X(\omega)\} = [H(\omega)]\{P(\omega)\} \qquad (11)$$

where the system receptance matrix is

$$[H] = \left[[\mathcal{F}] + [*\mathcal{F}][C]^T[A][C][\mathcal{F}]\right] . \qquad (12)$$

Owing to the partitioning pattern determined by the submatrices, the system receptance matrix can be partitioned in the following manner:

$$[H^{IJ}] = [\mathcal{F}^{IJ}] + [*\mathcal{F}^I][C^I]^T[A][C^J][\mathcal{F}^J] \qquad (13)$$

where

$$[\mathcal{F}^{IJ}] = [0] \quad \text{for } I \neq J$$
$$= [\mathcal{F}^I] \quad \text{for } I = J . \qquad (14)$$

The time response vector is obtained from Eq. (11) using the Fourier transform relation as follows:

$$\{x(t)\} = \frac{1}{2\pi}\int_{-\infty}^{\infty} \{X(\omega)\}e^{i\omega t}\,d\omega \qquad (15)$$

Equations (11) and (15) give, respectively, the response in the frequency and time domain owing to the deterministic excitations $\{p(t)\}$. If the system is subjected to stationary random excitations, the excitation crosscorrelation functions and the excitation cross-power spectral densities between points ℓ in subsystem L and points m in subsystem M are obtained, respectively, as shown in Ref. [10]:

$${}_pR^{LM}_{\ell m}(\tau) = \lim_{T\to\infty}\frac{1}{T}\int_{-T/2}^{T/2} p_\ell^L(t)\,p_m^M(t+\tau)\,dt \qquad (16)$$

and

$${}_pS^{LM}_{\ell m}(\omega) = \int_{-\infty}^{\infty} {}_pR^{LM}_{\ell m}(\tau)\,e^{-i\omega\tau}\,d\tau. \qquad (17)$$

The response cross-power spectral densities between points j in subsystem J and points k in subsystem K are then obtained from Eqs. (12) and (17) as

$${}_pS^{JK}_{jk}(\omega) = \sum_{\ell=1}^{\ell_p}\sum_{m=1}^{m_p}\sum_{L=A}^{N}\sum_{M=A}^{N} H^{JL*}_{j\ell}(\omega)\,H^{KM}_{km}(\omega)\,{}_pS^{LM}_{\ell m}(\omega) \qquad (18)$$

where the first two right-hand terms are the complex conjugates of the receptance between point j in subsystem J and points ℓ in subsystem L and the receptance between points k in subsystem K and points m in subsystem M.

COMPONENT RESONANCE

The analysis in the frequency domain of general coupled configurations can be accomplished using Eq. (11) or (18), where the system receptance matrix is determined by Eq (12) or (13). However, in practice certain computational difficulties may arise at certain frequencies which are resonance frequencies for one or more of the uncoupled subsystems. Close to or at these frequencies the receptances of the respective subsystems become very large as compared with those subsystems not at resonance. Because in general the subsystem resonance frequencies do not coincide with those of the coupled system, the receptances of the former will also be large as compared with the latter. Thus, it is often necessary to compute "normal size" receptances (reflecting no resonance) by taking differences between very large terms that reflect subsystem resonance. In Ref. [12], it is shown how the computational accuracy near a subsystem resonance can be greatly improved.

Equation (3) can be written as

$$[H^{IJ}] = [\bar{H}^{IJ}] + [\alpha^I][A][\alpha^J] \qquad (19)$$

where

$$[\alpha^I] = [\bar{H}^{IJ}][C^J]^T \qquad (20)$$

and

$$[\psi] = [C^J][\bar{H}^{JJ}]. \qquad (21)$$

Near a resonance frequency of some subsystems there will be large receptance terms in Eq. (19). Let these large receptance terms be $O(\lambda)$, where $O\lambda \gg 1$, and nonresonance receptances are $O(\ell)$. It is shown that the $O(\cdot)$ parts of each matrix in Eq. (19) are parallel in the sense of parallel vectors in multidimensional space. Noting that for a nonresonance frequency of the entire system each coupled receptance matrix $[H^{IJ}]$ is $O(\ell)$, it is shown that for subsystem resonance of subsystem R, $[H^{IR}]$ and $[H^{RJ}]$ are computed as differences of $O(\lambda)$ terms and $[H^{RR}]$ is computed as differences of $O(\lambda^2)$ terms. By a new formulation of the problem the large parallel parts are removed from the matrices of Eq. (19), giving an entirely equivalent receptance matrix formulation,

$$[H^{IJ}] = [\gamma^{IJ}] + [\alpha^I][B][\alpha^J] \qquad (22)$$

without, however, the component resonance computational difficulties.

THE RECEPTANCE COUPLING PROGRAM (RECEP)

The RECEP program is divided into four basic links, each of which is capable of filling the core. As shown in the functional flow diagram in Fig. 3, the first link computes the matrix [B] in Eq. (22) and the second link computes the system receptance matrix $[H^{IJ}]$, that is, [H]. If the system is subject to determinate excitations, the third link computes the frequency response vector $\{X\}$ in Eq. (11) and the time response vector $\{x\}$ in Eq. (15). For stationary

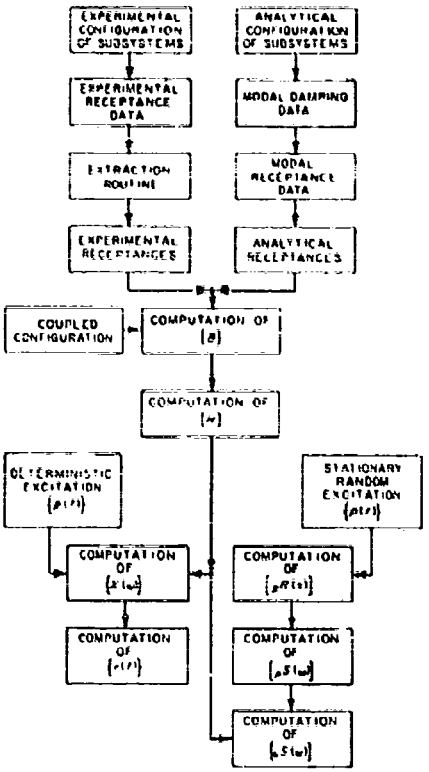

Fig. 3. Functional flow diagram of the Receptance Coupling Program (RECEP)

random inputs, the fourth link computes the excitation crosscorrelation matrix in Eq. (16), the excitation cross-power spectral densities in Eq. (17), and selected elements of the response cross-power spectral densities in Eq. (18).

The present design of the RECEP program is such that up to 35 coupling units (a total number of 70 coupling points) can be handled. Therefore, if there are 2 subsystems, each one may have up to 35 coupling points, or, if there are 35 subsystems, each one may have 2 coupling points.

The maximum number of excitation points in the entire system may be up to 120. These may be distributed unevenly among the subsystems such that no subsystem has more than 80 excitation points. Similarly, the maximum number of response points may be up to 120, with not more than 80 response points in any one subsystem. With these limitations, the maximum sizes of all matrices discussed earlier under Theory of Receptance Coupling and Component Resonance are determined.

In addition to user specified input, such as the coupling matrix [C], the constrained matrix [K], the excitations, and the frequency ranges of interest, the RECEP program has as input the subsystem receptances that are functions of frequency and, in general, are complex because of damping. The subsystem receptances may be generated analytically through a subsystem modal analysis or they may be measured through a subsystem vibration test consisting of sinusoidal excitations, deterministic excitations, or random excitations. In any case, the input data must be available and must be read for each frequency of interest. If the data are continuously changing with frequency, which, indeed, is most often the case, the readings must be taken at sufficiently close intervals. This requires a large volume of input data to be handled, and an automatic transfer of data becomes necessary.

Analytical data for the determination of subsystem receptances $\alpha_{ij}(\omega)$ are usually obtainable as the normal modes V_{ik} giving the response of the kth mode at point i, the modal frequencies ω_k, and the modal masses m_k. These data are on cards, tape, or disks and are read automatically into the computer. The receptances at each frequency ω are then computed by the modal receptance routine in RECEP as

$$\alpha_{ij}(\omega) = \sum_k \frac{V_{ik} V_{jk}}{m_k \left[(\omega_k^2 - \omega^2) + 2i\zeta_k \omega_k \omega\right]} \qquad (23)$$

where ζ_k is the assumed or measured modal damping factor.

The experimentally measured receptances are translated into digital data on cards, magnetic tape, or disks before being entered into the RECEP program. These data are then used directly for further computations, if it can be assumed that the experimental measuring equipment has not substantially influenced the results. Otherwise the influence of the measuring equipment can be eliminated by the "extraction routine" in RECEP as shown below.

ELIMINATION OF INSTRUMENTATION EFFECTS

When the receptances of a structural system are measured, there are necessarily moving parts such as transducers, forge gages, and so forth, attached at the test points (Fig. 4). If

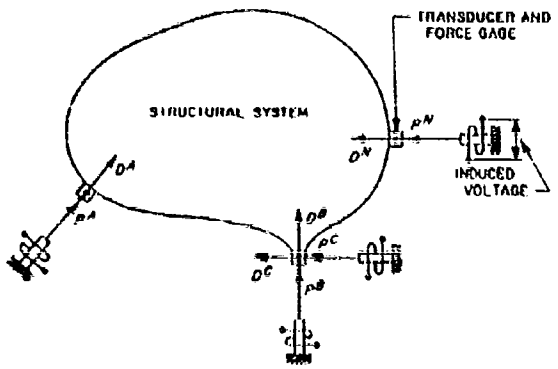

Fig. 4. Multishaker excitation of structural system

the number of moving parts and/or their mass is large enough, the measured results are often considerably distorted from their true values. Using the receptance coupling technique, it is shown in this section how the true receptances of the structure can be obtained from the measured ones and from knowledge of the equipment receptances.

To begin with, it is assumed that the structure is supported by soft springs so that the lowest frequency of the springs-structure system is far below the lowest frequency of interest, or that the structure is supported directly by the shakers (Fig. 4). If the structure is excited, the attached transducers, force gages, and so forth, are moving with the structure at the attachment points, while the base of the shaker may or may not be fixed to the ground. Without loss of generality, it is assumed here that the bases of the shakers are fixed to the ground as shown in Fig. 4. The most general case is that, at each shaker, between shaker base and transducer, force gages measure the transmitted forces $P^A \ldots P^N$, and the transducers measure the respective motions $D^A \ldots D^N$. It is assumed that the receptances of the attached moving parts are known and that relative compliances between transducers and attachment points can be estimated by specifying suitable coupling units K_{m_r}. One shaker at a time is then excited, and all forces and motions are simultaneously measured and recorded.

In Fig. 5, a system representation is given, delineating the coupling of N shakers to the typical subsystem Q. If the shaker A is excited by an induced voltage, the force $P^{AA} \ldots P^{NA}$ and the displacements $D_1^{QA} \ldots D_\rho^{QA}$ are measured and recorded as functions of frequency. With the help of Eqs. (2), (4), and (5), the following matrix equation can then be written:

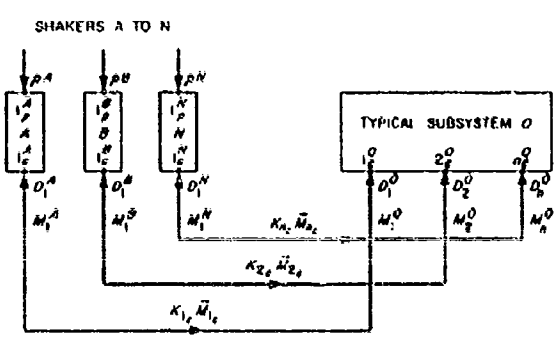

Fig. 5. Systems representation of multishaker excitation of subsystem Q

$$\begin{Bmatrix} \begin{Bmatrix} D_f^{QA} \\ \vdots \\ D_n^{QA} \end{Bmatrix} \\ \begin{Bmatrix} D_f^{QA} \\ \vdots \\ D_n^{QA} \end{Bmatrix} \end{Bmatrix} = \begin{bmatrix} [\quad - K_f] & & \\ & [\quad - K_n] & \\ & & [\quad] \end{bmatrix} \begin{Bmatrix} \begin{Bmatrix} -M_f^A \\ \vdots \\ -M_n^A \end{Bmatrix} \\ \begin{Bmatrix} M_f^A \\ \vdots \\ M_n^A \end{Bmatrix} \end{Bmatrix} + \begin{bmatrix} [\quad] \\ [\quad] \end{bmatrix} \begin{Bmatrix} P^{AA} \\ \vdots \\ P^{NA} \end{Bmatrix} \tag{24}$$

where the second superscript A indicates that the data were obtained while shaker A was excited. The [illegible] are the n known coupling point receptances of the N shakers, and the [illegible] are the n known cross receptances between coupling and excitation points of the shakers. The [illegible] are the unknown receptances of the typical subsystem Q.

By exciting all N shakers, one at a time, a set of n equations similar to Eq. (24) can be written. These equations can be combined as follows:

$$\begin{bmatrix} [D^{QA}] \\ [D^{QB}] \end{bmatrix} = \begin{bmatrix} [\quad - K] & \\ & [\quad - K] \end{bmatrix} \begin{bmatrix} [-M] \\ [\quad] \end{bmatrix} + \begin{bmatrix} [\quad] \\ [\quad] \end{bmatrix} [P^{\quad}] \tag{25}$$

Eliminating [illegible] and solving for [illegible], one obtains the subsystem receptances as

$$[\quad] = [D^{Q}] \left\{ [\quad - K] \right\}^{-1} \left\{ [\quad] [P^{\quad}] - [D^{Q}] \right\}^{-1} \tag{26}$$

where the measured displacements and forces are, respectively,

$$D^{Q} = \begin{bmatrix} D_f^{QA} & \cdots & D_f^{QN} \\ \vdots & & \vdots \\ D_n^{QA} & \cdots & D_n^{QN} \end{bmatrix} \qquad P^{\quad} = \begin{bmatrix} P^{AA} & \cdots & P^{AN} \\ \vdots & & \vdots \\ P^{NA} & \cdots & P^{NN} \end{bmatrix} \tag{27}$$

For an application of Eq. (26), a free-free beam with two shaker mountings as shown in Fig. 6 has been chosen. The moving parts of the shakers, that is, the accelerometers and force gage parts moving with the beam during excitation at each point, weigh 0.2 lb, while the beam itself weighs 3.33 lb. The measured responses D^A and D^B are accelerations and were recorded in terms of g's, while the forces P^A and P^B were recorded in terms of grams. The assumption that [illegible] and [illegible] in Eq. (26) implies that the moving parts of the experimental equipment are rigidly attached masses at the points 1 and 2 and that one can work in this case with the accelerations for D^A and D^B rather than displacements.

Both the measured and the corrected acceleration transfer function amplitudes are recorded in Figs. 7 through 10 for comparison. The corrected amplitudes were determined using Eq. (26).

CONCLUSIONS

After developing the theory of receptance coupling earlier in this paper, following essentially the more detailed developments in Ref. [10], the problem of component resonance [12] has been discussed and some overall characteristics of the Receptance Coupling Program (RECEP) have been indicated.

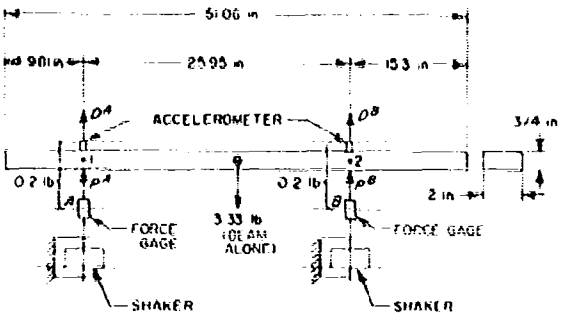

Fig. 6 Free-free beam and shaker configuration for transfer function measurement

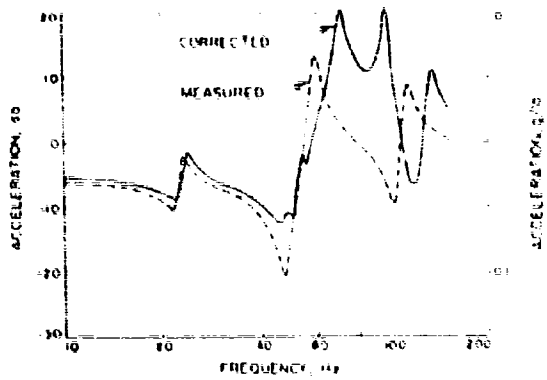

Fig. 7. Comparison of measured receptance and corrected receptance α_{11}

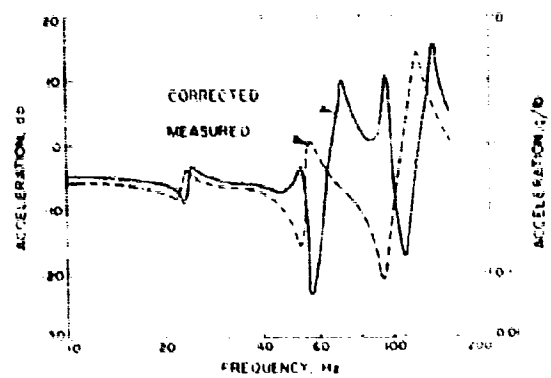

Fig. 8. Comparison of measured receptance and corrected receptance α_{22}

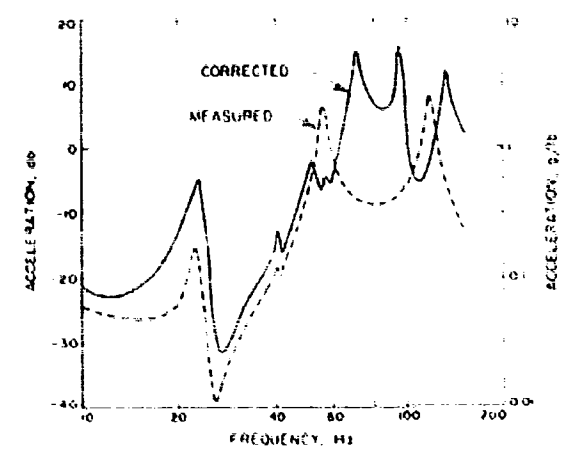

Fig. 9. Comparison of measured receptance and corrected receptance α_{12}

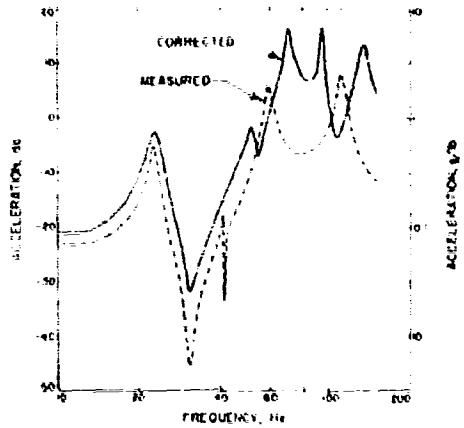

Fig. 10. Comparison of measured receptance and corrected receptance $\bar{\theta}_{21}$

The particular problem of eliminating the effects of the measuring equipment from experimentally determined receptances was treated in some detail. For the experimental configuration of Fig. 6, the comparison (Figs. 7 through 10) of the experimental receptances (acceleration transfer functions) with the corresponding corrected receptances, using Eq. (36), shows that, in this case, the experimental equipment has considerably influenced the results even though the total moving mass of the experimental equipment is little more than 10 percent of that of the beam. It is concluded that in experimental work careful attention should be given to the elimination of the distortions of the results owing to equipment effects.

Because of the reciprocity requirement for linear systems, the receptances $\bar{\theta}_{12}$ and $\bar{\theta}_{21}$ should be equal. The plots in Fig. 11 give a comparison of the amplitudes of these two independently measured and computed receptance functions. While the frequencies of the peak responses agree quite well, there are many discrepancies in the amplitudes and frequencies at the point of antiresonance between 25 and 35 Hz. This may be a result of noise level effects, which can be quite disturbing at these low levels of response.

From the results of this example, which still has been treated somewhat crudely, it is tentatively concluded that the judicious use of the "extraction routine" in RECEP offers a means of eliminating at least coarse effects of measuring equipment, thus improving the experimental data and hence the response analysis.

ACKNOWLEDGMENT

The authors would like to thank M. R. Trubert for developing the measured data in Figs. 7 through 10.

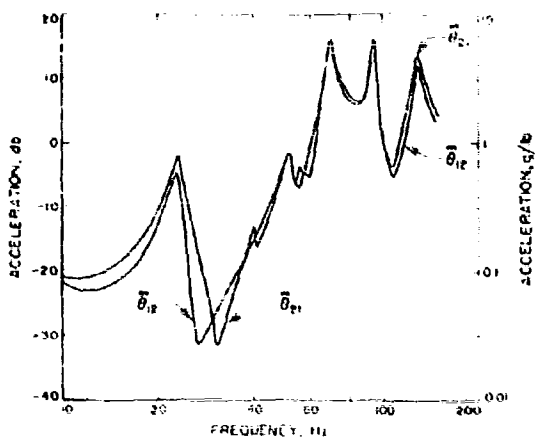

Fig. 11. Comparison of the corrected (computed) receptances $\bar{\theta}_{12}$ and $\bar{\theta}_{21}$

REFERENCES

1. H. J. Runyan and A. G. Rainey, "Launch-Vehicle Dynamics," NASA TM X-607, Dec. 1961

2. W. H. Gayman, "A Note on Boundary-Condition Simulation in the Dynamic Testing of Spacecraft Structures," TR-32-938, Apr. 1966

3. M. R. Trubert, "Use of Ranger Flight Data in the Synthesis of a Torsional Acceleration Transient for Surveyor Vibration Qualification Testing," TM 33-237, Jet Propulsion Lab., Pasadena, Calif., Apr. 1966

4. H. Holzer, Die Berechnung der Drehschwingungen (Springer, Berlin), 1921

5. N. O. Myklstad, Vibration Analysis (McGraw-Hill, New York), 1944

6. C. E. Pestel and [illegible]. Leckie, Matrix Methods in Elasto Mechanics (McGraw-Hill, New York), 1963

7. W. C. Hurty, "Dynamic Analysis of Structural Systems Using Component Modes," J. AIAA, 3:678 (1965)

8. W. J. Duncan, "Mechanical Admittances and Their Applications to Oscillation Problems," H.M.S.O. (Aeronautical Research Council), Repts. and Memos., No. 2000, London, 1947

9. R. E. D. Bishop and D. C. Johnson, The Mechanics of Vibration (Cambridge Univ Press), 1960

10. E. Heer, "Coupled Systems Subjected to Determinate and Random Input," Int. J. Solids Structures, 3:155-166 (1967)

11. R. M. Bamford, "A Modal Combination Program for Dynamic Analysis of Structures," TM 33-290, Rev. 1, Jet Propulsion Lab., Pasadena, Calif., July 1967

12. L. D. Lutes and E. Heer, Receptance Coupling of Structural Components Near Component Resonance (in press)

DISCUSSION

Mr. Smith (Bell Aerosystems Co.): I think you said that your program had a capability of handling 35 couplings, 130 inputs not greater than 60 on each subsystem. You have demonstrated good correlation between the cross receptances on a very simple beam. How ambitious do you expect to be in attempting to use the capacity of your program on a more complex structure? How many of these inputs would you expect to use? It appears to me that you have thought it worthwhile writing a program where you may have a matrix of receptances which is extremely large. I foresee trouble if you try to be too ambitious.

Mr. Heer: If I understand the question correctly, you are saying that, in using more and more receptances the computation inaccuracy may increase, and that it may become unfeasible to get accurate results for such large arrays of receptances. In developing the computer program we actually went up to the limit of the core capacity of the computer. It may be quite true that, using 130 points as inputs and consequently large arrays, the computation inaccuracy may become questionable. All I can say at this time is that we have not run the computer program using 130 input points. I could not make an accurate statement as to what the accuracy is when using that large amount of data.

* * *

A VERIFICATION OF THE PRACTICALITY OF PREDICTING INTERFACE DYNAMICAL ENVIRONMENTS BY THE USE OF IMPEDANCE CONCEPTS

Frank J. On
NASA, Goddard Space Flight Center
Greenbelt, Maryland

The results of a study on the verification of the practicality of predicting interface dynamical environments through the use of mechanical impedance theory and measured "in-service" data are presented. The investigation was carried through two parallel paths using one-dimensional, multidegree of freedom lumped parameter models. A series of digital computer simulated models of varying degrees of freedom was treated to illustrate the theoretical procedural requirements. Laboratory tests using equivalent experimental models were conducted to demonstrate the practical application of the technique. A comparative study was performed on the measured and predicted results. In general, the results of the prediction based on in-service data are in good agreement with measured results. Error analysis in measurements and computations indicates that interpretation of absolute accuracy of the predictions requires caution. As the "exact" impedance of an actual structure is, in general, unknown, success in the predictions may be enhanced by the combined use of measured and computed impedance results and by a sound program of error analysis.

INTRODUCTION

In recent years, the problem of predicting the true interface dynamical environment of a complex aerospace structure during its launch phase has been of much interest. Frequently vibration tests are conducted that poorly simulate the environmental conditions. One of the basic reasons for unrealistic vibration tests lies in the methods used in deriving motion-input specifications. Specifications derived from field data often consider only peak responses and neglect the characteristic differences that may exist between the item being tested and the one previously used in the field. When combined in a vibration test, this practice can result in high overtests at some frequencies, while at other frequencies the test item may be undertested.

It has been suggested that a solution lies in the incorporation of mechanical impedance concepts. Unfortunately, there are factors that may prevent this concept's immediate practical application. Some of these factors are the lack of field data to derive test specifications, the practical inexperience in applying the concept, and perhaps the complexity of the concept itself.

The primary purpose of this study is to verify the aspect of the application of the impedance concepts to the prediction of interface environments. Effort is devoted specifically to the demonstration of the prediction of interface velocity of a new system configuration from the interface velocity information previously determined on another configuration. The treatment of velocity is selected for convenience because impedance and mobility quantities are considered. The task requires that the interface driving point impedance of the constituent systems be known a priori. To achieve the most severe test of the prediction technique, steady-state sinusoidal vibrations are treated because amplitude sensitivity is greatest for this case. Theoretically, this technique is applicable to all processes that satisfy Fourier transformation. A summary of the theoretical background required for this phase of study is presented in this paper. The underlying theoretical basis for additional development work may be found in Refs [1] through [3].

This study was carried through two parallel paths of developments using one-dimensional, multidegree of freedom lumped parameter models. Digital computer simulated models were

treated to demonstrate the theoretical procedural requirements. Laboratory measurements of equivalent experimental models were obtained for use in the prediction technique. For convenience, the models were considered arbitrary representations of launch vehicle (L/V) and spacecraft (S/C) structural systems of 5 and 2 degrees of freedom, respectively.

THEORETICAL BACKGROUND

Consider a one-dimensional structure that is otherwise separated into two component structures at some terminal. A general representation of such a system is shown in Fig. 1, where for convenience its component structures are identified by the vehicle V_a and the spacecraft P_b. In connection with this system, a problem of major interest is how does one analyze and define the dynamic environment at the input to the spacecraft.

In accordance with the equation of interconnection for one-dimensional structures, the steady-state sinusoidal velocity response at the interface terminal of the vehicle and spacecraft system, denoted by subscript I, is given in Ref. [1] as

$$V_{I(\omega)} = \frac{-F^{b}_{V_a}(\omega)}{Z_{V_a}(\omega) + Z_{P_b}(\omega)} \qquad (1)$$

where F^b represents the Fourier transform of $f(t)$ measured at the interface terminal when that terminal is blocked so that no motion occurs; Z_{V_a} and Z_{P_b} are the mechanical impedance of the vehicle and spacecraft looking back from the interface, respectively.

Alternatively, in terms of mechanical mobility Y (inverse of impedance), and "free" velocity, denoted by subscript f,

$$V_{f(\omega)} = \frac{-F^{b}_{V_a}(\omega)}{Z_{V_a}(\omega)} ; \qquad (2)$$

Eq. (1) becomes

$$V_{I(\omega)} = \frac{Y_{P_b}(\omega)}{Y_{P_b}(\omega) + Y_{V_a}(\omega)} \cdot V_{f(\omega)} ; \qquad (3)$$

V_f represents the transform of the velocity at the interface terminal when that terminal is unrestrained.

In cases where either the vehicle or the spacecraft is replaced by some other structure, new interface response characteristics may be predicted. Suppose that the interface velocity characteristic corresponding to a new spacecraft P_r on the same vehicle V_a is desired; then using Eq. (1), the new velocity is

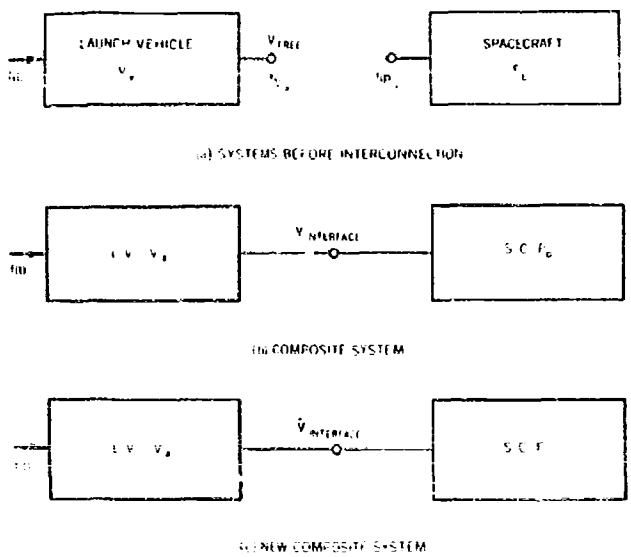

Fig. 1. Block diagrams of (a) subsystems, (b) composite system, and (c) new composite system

$$\bar{V}_I(\omega) = \frac{Z_{V_A}(\omega) + Z_{P_b}(\omega)}{Z_{V_a}(\omega) + Z_{P_r}(\omega)} \times V_I(\omega) \qquad (4)$$

when Z_{P_r} is the mechanical impedance of the new spacecraft. Alternatively, using Eq. (3), in terms of mobility Eq. (4) becomes

$$\bar{V}_I(\omega) = \frac{Y_{P_r}(\omega)}{Y_{P_b}(\omega)} \times \frac{Y_{V_a}(\omega) + Y_{P_b}(\omega)}{Y_{V_a}(\omega) + Y_{P_r}(\omega)} \times V_I(\omega) \qquad (5)$$

TEST CONFIGURATIONS AND PROCEDURES

For convenience in this study, the prediction is identified as the prediction of interface environment of system B from that of system A.

The constituent models of test configuration A are shown in Fig. 2. Configuration B differs from A only in the payload model. The lumped parameters of these two models are given in Table 1. A typical test setup is shown in Fig. 3. The inner frame permitted accurate alinement of the models through adjustment of the radially positioned coil springs. The outer frame provided vibration isolation from extraneous sources. In accordance with the program outline of Fig. 4, series of tests were conducted to determine mobility, free velocity, and interface velocity data for subsequent application to the prediction technique under discussion.

For convenience, a Ling 227L shaker simulated the L/V thrust motor. The source of vibration was assumed as a constant amplitude force of varying frequencies generated by perturbations in the thrust vector. Experimentally, this assumption was satisfied by servo controlling the force developed at the shaker armature mass. This was accomplished by servo controlling a sine swept input current to the armature using an amplitude servo/monitor in the feedback loop as shown in Fig. 5. The amplitude and frequency linearity of this control for the force setting used (F_2 = 30 lb) across the frequency band (50 Hz - 2 kHz) was better than ± 1 db. The phase shift referenced to the armature current was about ±7 degrees. This force level was selected because of the necessity of having an adequate signal-to-noise ratio and to remain below the fatigue characteristics of the spring-damper elements of the models.

The technique of calibrating the force level that was to be applied in the test in terms of input armature current consisted of multiplying the moving element mass of the Ling shaker, in a no table-load condition, by the measured acceleration of the moving element

(a) SPACECRAFT STRUCTURE MODEL

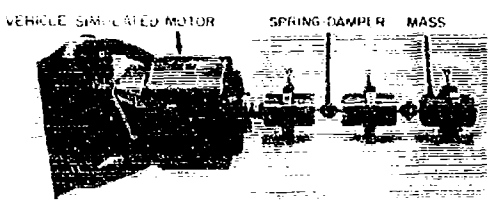

(b) LAUNCH VEHICLE STRUCTURE MODEL

(c) LAUNCH VEHICLE/SPACECRAFT SYSTEM MODEL

Fig. 2. Description of test configuration A

TABLE 1
Properties of Test Models

Test Configuration A								
i = [a]	S/C Model			L/V Model				
	1	2	3	1	2	3	4	5
M_i (lb m)	1.2	22.5	21.2	1.0	1.5	22.0	22.5	21.2
K_i (10^5 lb/in.)	9.3	0.8	–	28.0	200.0	9.3	0.8	–
C_i (lb/in./sec)	0.9	1.9	–	3.6	248.0	0.9	1.9	–
Test Configuration B								
i = [a]	S/C Model			L/V Model				
	1	2	3	1	2	3	4	5
M_i (lb m)	1.2	42.5	41.2	1.0	1.5	22.0	22.5	21.2
K_i (10^5 lb/in.)	0.8	9.3	–	28.0	200.0	9.3	0.8	–
C_i (lb/in./sec)	1.9	0.9	–	3.6	248.0	0.9	1.9	–

[a] i indices from left to right of Fig. 2.

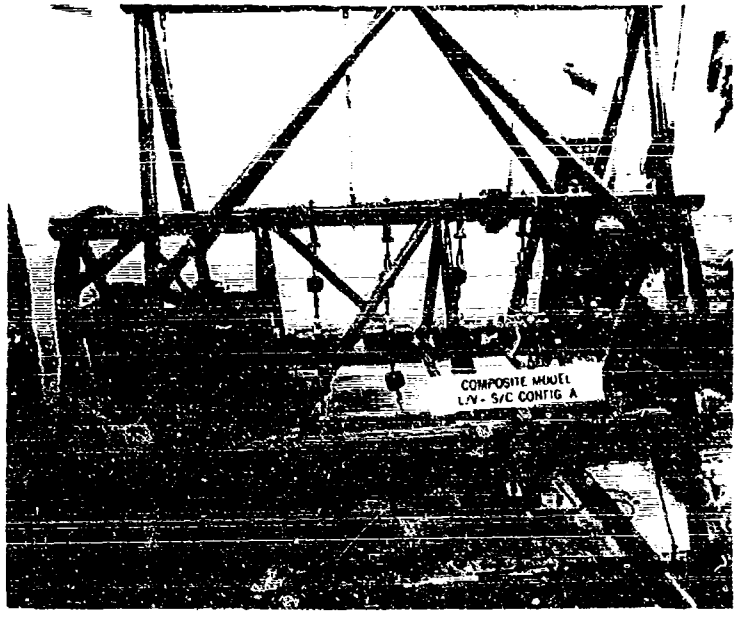

Fig. 3 Test setup for interface velocity measurements -- test configuration A

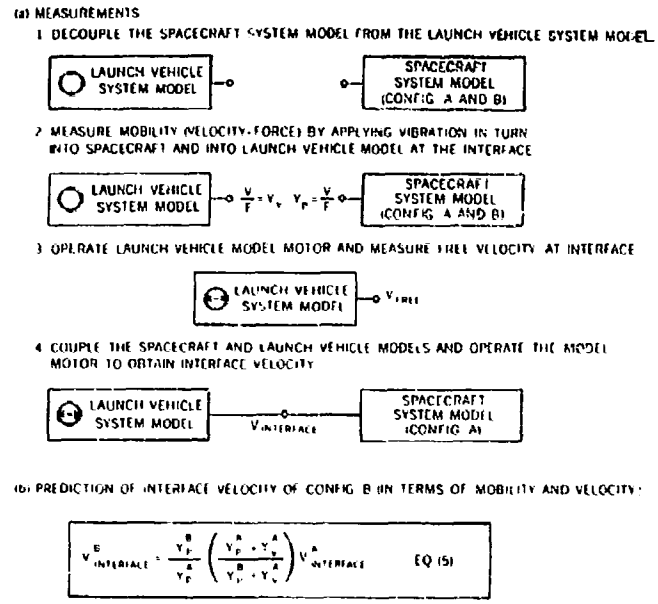

Fig. 4. Program outline of (a) measurements and (b) prediction

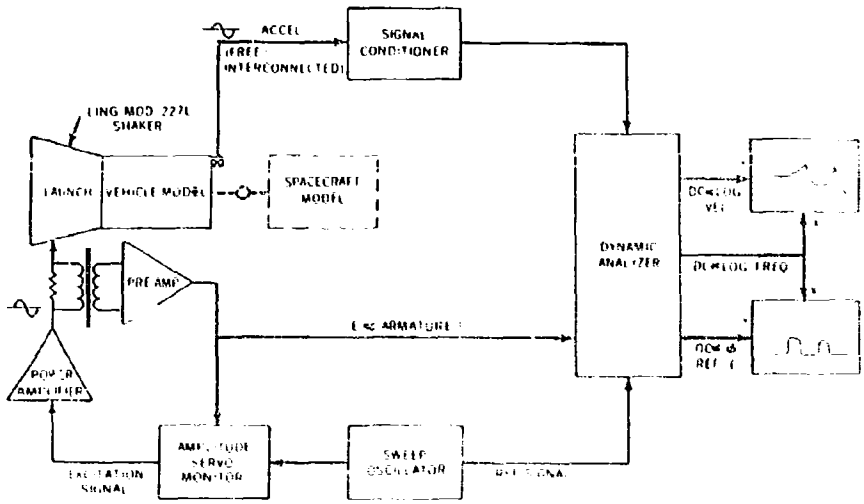

Fig. 5. Block diagram of velocity measurement and force control instrumentation

and relating it to the measured current. The mass-like characteristic of the moving element from 50 Hz to 2 kHz was verified within ±1 db. Although testing was conducted to 5 kHz for possible frequency analysis, the validity of any amplitude measurement at greater than 2 kHz is questionable. The frequency band was swept at the rate of 0.4 decades/min which was verified to be sufficiently slow to reproduce accurate resonant and antiresonant peaks, and consequently, a good simulation of the sinusoidal dwell phenomenon. An Endevco accelerometer Model 2235-C was mounted at required locations for free and interface velocity measurements.

A Pye-Ling Type V.50 Mk 1 vibration generator was used to supply the 10 to 20 lb sinusoidal force required in the measurement of interface driving point mobility shown in Fig. 6. An Endevco Model 2110 impedance head was used in these measurements. During mobility measurements, the cancellation of mass effect of the impedance head and adaptor was only partially successful. As a result of the relatively light mass of the impedance head-adaptor, this did not significantly degrade the test results.

DESCRIPTION OF COMPUTATIONAL PROGRAMS

Digital computer simulation of the models and Fortran programs embodying the equations of Ref. [2] were constructed for processing on a CDC 3100 computer to illustrate the computational procedural requirements. Acceptable input data consisted of the mass, stiffness, and damping parameters for the L/V and S/C models, the force amplitude at each mass station, and a set of discrete frequency parameters. In this study, the input parameters were experimentally determined to an estimated error of ±1 db. The interface driving point impedance of the L/V and S/C models was first computed. The inverse of this impedance was printed as mobility. Free velocity outputs were computed next. By means of the program embodying Eq. (5), the velocity at the interface of the combined L/V and S/C system was obtained. The various results obtained by this program are identified as "theoretical" results as opposed to prediction and measurement or test results.

A shorter and simpler Fortran program was written for processing only Eq. (5) for the prediction of interface velocity of configuration B using measured mobilities and interface velocity of configuration A. Data inputs for this program were generated from the actual plots of the measured results.

DESCRIPTION OF PREDICTION TECHNIQUE

The prediction of the interface velocity of configuration B was achieved through the use of the digital computer program for processing Eq. (5). The input data consisted of interpolated data from graphical curves of the measured mobility magnitude and phase angle of the L/V model, the S/C model of configurations A and B, and the interface velocity data of configuration A. In this technique the L/V system was identical for both configurations. Only the S/C systems were structurally different. In essence,

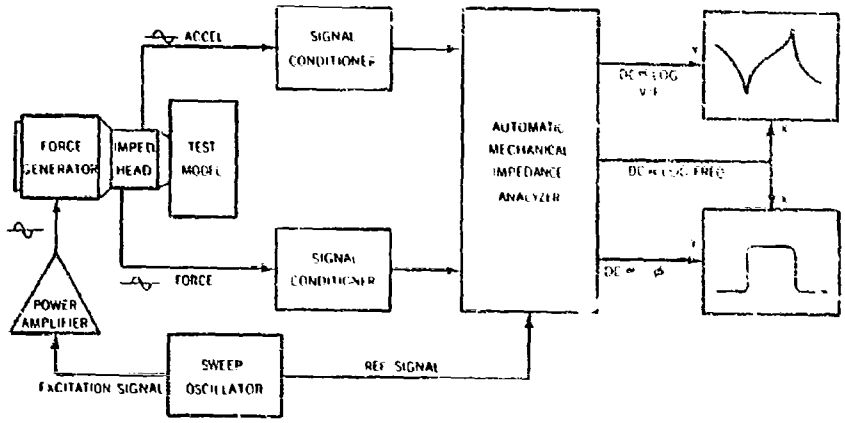

Fig. 6. Block diagram of mobility measurement instrumentation

this technique treats the situation that simulates the practice of using a standard L/V system to launch a variety of S/C configurations.

It should be noted that in the above prediction technique of Eq. (5), the measured mobility data could have been substituted by mobility data generated from the mathematical model of the constituent systems.

CONSIDERATIONS

The overall results of this investigation for the two system configurations presented in this paper are depicted in Figs. 7 through 15.

The intermediate results of interest are shown in Figs. 7 through 12 where the theoretical results are shown as discrete points while those of measurements are shown as continuous plots. The probable errors in various measurements, as determined in Ref. [3], are summarized in Table 2. The absolute decibel difference between test and theoretical results for the different quantities is presented respectively in Fig. 13(a), (b), and (c), where the shaded points correspond to the decibel difference at or near a resonance or antiresonance. The noted large differences at some of these critical frequencies primarily result from the high sensitivity to small frequency shifts as well as from the possible high amplitude sensitivity owing to the effect of damping.

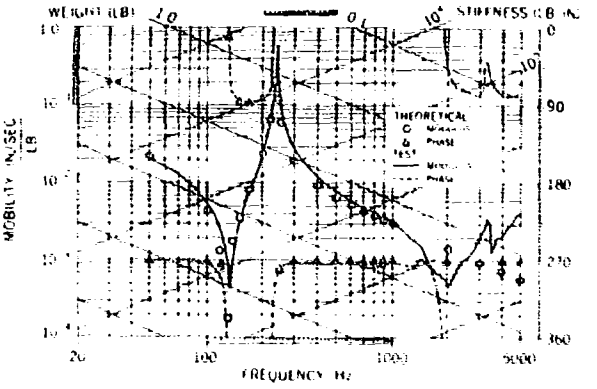

Fig. 7. Interface driving point mobility of L/V model of configurations A and B (theoretical vs test)

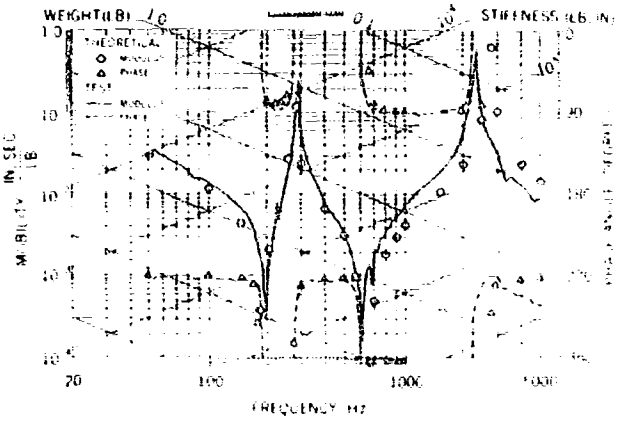

Fig. 8. Interface driving point mobility of S/C model of configuration A (theoretical vs test)

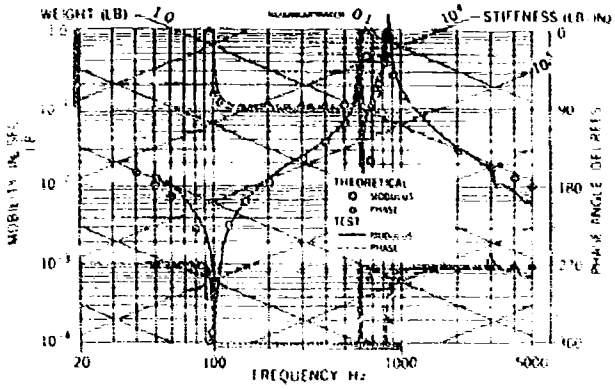

Fig. 9. Interface driving point mobility of S/C model of configuration B (theoretical vs test)

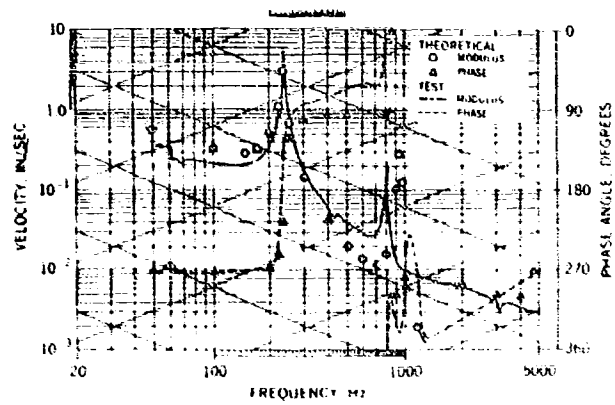

Fig. 10. Free velocity of L/V model of configurations A and B (50-lb-force input, theoretical vs test)

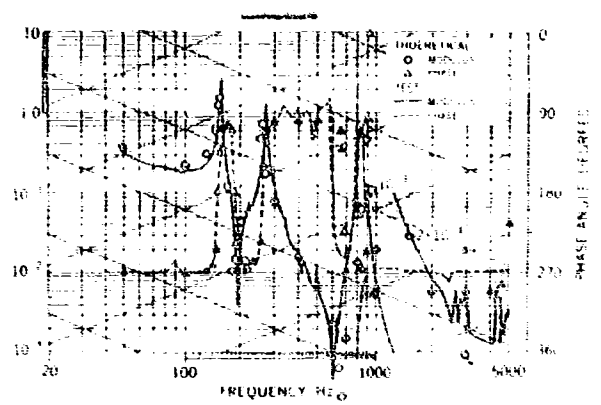

Fig. 11. Interface velocity of configuration A (theoretical vs test)

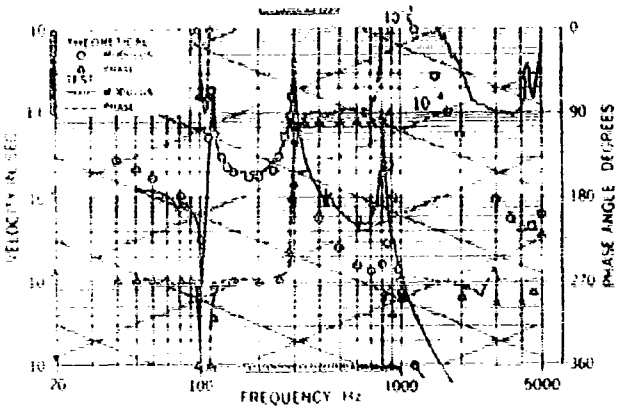

Fig. 12. Interface velocity of configuration B (theoretical vs test)

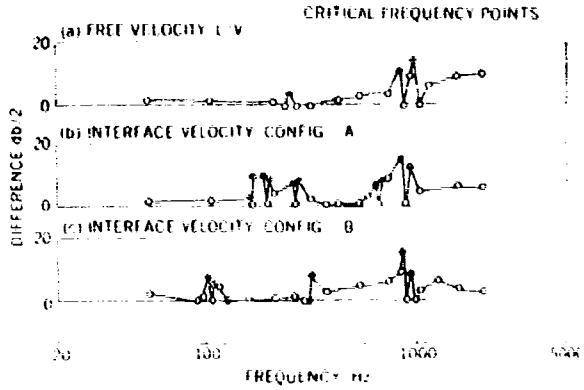

Fig. 13. Decibel difference between test and theoretical results in modulus of (a) free velocity, (b) interface velocity, configuration A, and (c) interface velocity, configuration B

The prediction of the interface motions for configuration B using Eq (5) is presented and compared to the results obtained by test and by theoretical computations in Figs. 14(a) and 14(b). In Fig. 15(a), the absolute decibel differences between the predicted results and those of test measurements and theoretical computations are shown. The excellent comparisons in critical frequencies, determined by peaks and notches between the individual results of Fig. 14(a), are shown in Fig. 15(b) expressed in decibel difference. In Fig. 15(a), the large differences between predicted results and test results at some of the critical frequencies were primarily attributed to small errors in the input parameters of Eq. (5) resulting in an out-of-proportion effect on the predicted interface velocity. The small errors are the results of the accumulated effect of measurement data errors and errors from graphical interpolations of magnitudes and phase angles of the pertinent input parameters.

The application of the foregoing prediction technique to practical field and test laboratory environments will require several additional considerations. Frequently the desired mobility characteristic of an aerospace structure, such as a L/V and S/C system, is time dependent as well as frequency dependent and may even be nonlinear. Moreover, the interface between a L/V system and S/C system may also be

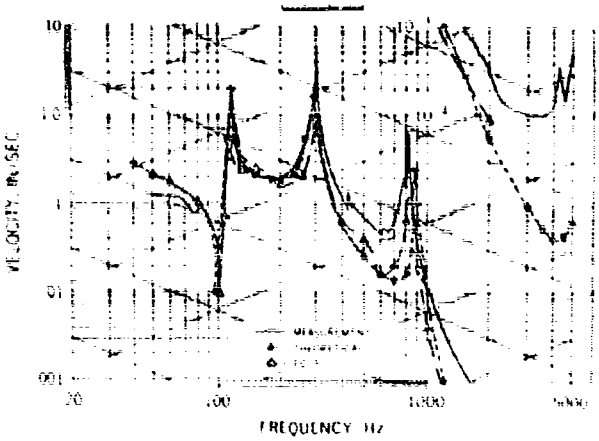

Fig. 14(a). Magnitude of interface velocity of configuration B predicted by Eq. (5) and compared to measurement and theoretical results

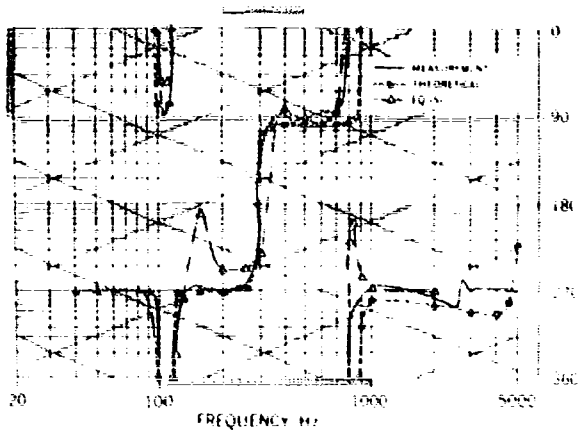

Fig. 14(b). Phase angle of interface velocity of configuration B predicted by Eq. (5) and compared to measurement and theoretical results

unusually large so that the multidimensional aspects of the systems need to be treated.

CONCLUSIONS

The results of this study indicate that the impedance technique of predicting interface dynamical environments through the use of measured "in-service" data is practical within certain limitations. The interpretation of the absolute accuracy of the predicted results should be made with caution, particularly near resonances and antiresonances. The accumulative nature of the probable errors inherent in Eq. (5) of the prediction technique can be greatly suppressed through improved accuracy and precision in the generation of the pertinent impedance data. The effect of errors in in-service motion measurements is found to be of a lesser degree. Because the "exact" impedance of actual structures is in general unknown, the success in predictions will be further enhanced by the combined use of measured and computed impedance results, together with a sound program of error analysis.

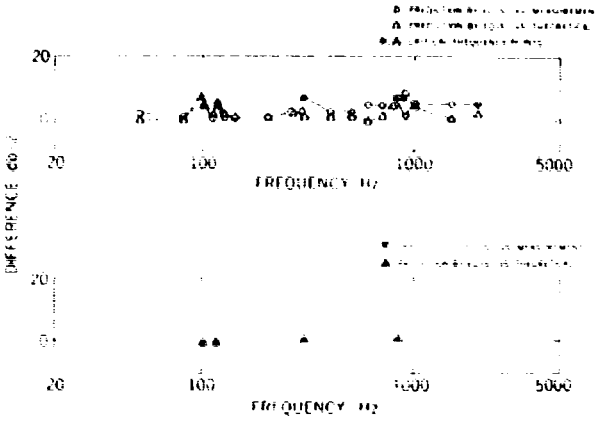

Fig. 15(a). Decibel difference in magnitude of velocity between prediction by Eq. (5) and (a) measurement and (b) theoretical results, and 15(b) decibel difference in critical frequency between prediction by Eq. (5) and (a) measurement and (b) theoretical results

TABLE 2
Measurement Errors

Type	Modulus	Phase	Frequency
Complex mobility (50 Hz - 5 kHz)	±1.2 db	±3.0 deg.	±3.5%
Free interface velocity (50 Hz - 2 kHz)[a]	±1.0 db	±3.0 deg.	±3.5%

[a]Constant force servo-control system characteristic precluded accurate velocity test results above 2 kHz. Test conducted to 5 kHz for frequency analysis only.

As this study was restricted to one-dimensional applications, the conclusions should not be construed to hold with equal validity for multidimensional applications without further studies. The case of sinusoidal dwell vibration treated in this study probably subjected the prediction technique to the worst possible conditions. This was partially substantiated by the largest decibel difference between prediction and test magnitudes of velocity occurring at resonances and antiresonances where sensitivity to damping is greatest. To evaluate the performance of the prediction technique for transient and random environments, further studies are required.

ACKNOWLEDGMENTS

The author wishes to express his sincere appreciation to Mr. Joseph Young, Structural Research and Technology Section, for his most helpful suggestions during the preparation of this paper; to Mr. Gary K. Jones for his assistance in the computer programming; and to Mr. Edward McCloskey for his support in the experimental instrumentation area.